THE UNIVERSITY OF
WARWICK

University of Warwick institutional repository: http://go.warwick.ac.uk/wrap

A Thesis Submitted for the Degree of PhD at the University of Warwick

http://go.warwick.ac.uk/wrap/66341

This thesis is made available online and is protected by original copyright.

Please scroll down to view the document itself.

Please refer to the repository record for this item for information to help you to cite it. Our policy information is available from the repository home page.

Thermodynamic and heat transfer analysis of a carbon – ammonia adsorption heat pump

by

Ángeles María Rivero Pacho

A thesis submitted in partial fulfilment of the requirements for the degree of Doctor of Philosophy

University of Warwick, School of Engineering

April 2014

Contents

Appendices

List of figures

List of tables

Nomenclature

Variables

A	Cross section area	m^2
A	Heat transfer area	m^2
c_p	Specific heat capacity at constant pressure	J/(kgK)
c_v	Specific heat capacity at constant volume	J/(kgK)
C	Slope of saturated ammonia line in a Clapeyron diagram	-
d	Density	kg/m^3
D	Diameter	m
F	Reference thermal resistance	$(m^2K)/W$
h	Heat transfer coefficient	$W/(m^2K)$
H	Enthalpy	J/kg
H_g	Enthalpy of saturated ammonia gas	J/kg
H_f	Enthalpy of saturated ammonia liquid	J/kg
I	Electrical current	A
k	Effective thermal conductivity	W/(mK)
k_{check}	Check valve proportionality constant	-
K	Constant in the modified Dubinin-Astakhov equation	-
l	Length	m
L	Latent heat of vaporisation	J/kg
$LMTD$	Log mean temperature difference	K
$\dot{m}$	Mass flow rate	kg/s
M	Mass	kg
n	Exponent in the modified Dubinin-Astakhov equation	-
N	Number of longitudinal divisions of adsorption bed	-
NTU	Number of transfer units	-
Nu	Nusselt number	-

p	Pressure	bar
Q	Heat flux	J/m^2
$\dot{Q}$	Heating power	W
R_{gas}	Gas constant	J/(kgK)
R_E	Electrical resistance	Ω
R_T	Thermal resistance	$(m^2K)/W$
t	Thickness	m
$time$	Time	s
Δt	Time step	s
T	Temperature	K
T'	Temperature in future time step	K
UA	Overall heat transfer coefficient	W/K
v	Velocity	m/s
V	Voltage	V
x	Concentration	kg/kg
x_0	Limiting (maximum) concentration	kg/kg

Greek symbols

α	Temperature coefficient	Ω/K
ε	Effectiveness	-
ρ	Electrical resistivity	Ωm
λ	Intrinsic thermal conductivity	W/(mK)
μ	Dynamic viscosity	kg/(ms)
ν	Kinematic viscosity	m^2/s

Subscripts

0	Initial
ads	Adsorption
air	Air
amm	Ammonia
bed	Adsorption bed
c	Carbon
check	Check valve
cond	Condenser
cooler	Cooler
desup	Desuperheat
ev	Evaporator
f	Heat transfer fluid
h	Hydraulic
in	Inlet
int	Interfacial
l	Anter Quickline-10^{TM} lower plate
liq	Liquid
LEAD	Electrical lead resistances
M	Electrical lead resistance and resistance under test
out	Outlet
r	Anter Quickline-10^{TM} reference calorimeter
rec	Receiver
R	Electrical resistance under test
s	Sample
sat	Saturation
sink	Anter Quickline-10^{TM} heat sink
sup	Superheated ammonia gas
u	Anter Quickline-10^{TM} upper plate
w	Sorption generator wall

Acknowledgements

I would like to express my sincere gratitude to my supervisor Professor Critoph for the continuous support of my Ph.D study and research, for his patience, motivation and immense knowledge. His guidance helped me in all the time of research and writing of this thesis. I could not have imagined having a better supervisor and mentor for my Ph.D study.

My sincere thanks also go to Dr. Metcalf for all his help and advice.

A special thanks to my family. Words cannot express how grateful I am to my mother and father for all of the sacrifices that they have made on my behalf.

Abstract

The modelling, design, construction and experimental testing of a carbon-ammonia adsorption heat pump is presented. The main objective of the research was to computer simulate and test a 4-beds thermal wave adsorption cycle and to improve the heat transfer rate in an existing shell and tube generator.

The existing generators were shell and tube type and were made of nickel brazed stainless steel but their heat transfer performance was poor. New heat exchangers with same design but larger in size were manufactured.

The sorbent material, active carbon, was tested in order to characterise its thermal properties and a new generator filling technique was developed and presented.

Computational modelling was carried out to evaluate the performance of the 4-beds thermal wave adsorption cycle. The proposed system was an air source heat pump that could deliver an output heating power of 7 kW and a seasonal heating COP of 1.47.

The adsorption generators were tested in a 4-bed thermal wave air-source heat pump system and achieved heating output powers between 4.5 to 5.20 kW if taking into account the system heat losses (4.30 to 4.90 kW without heat losses) and heating COP's of between 1.26 and 1.31 if taking into account the system heat losses (1.13 to 1.18 kW without heat losses).

These values were significantly lower than the predicted performance of the simulation. The main cause of this discrepancy was the water distributors located at the end of the generators that distorted during the testing stage and blocked the tubes of the generators.

Chapter 1

Introduction

1.1. Background

In the UK, 44% of the total consumed energy is used for any form of heating, being the 52% of the 906 TWh of natural gas in 2011 used to provide heating for buildings and industry. Heating within the domestic sector currently accounts for 23% of UK energy demand [1].

The Carbon Plan and the Strategic Framework stated that meeting the 80% CO_2 reduction targets will need emissions from buildings to fall near zero by 2050. This will need promoting a more efficient use of gas heating in the short to medium term, with gas use reduced to close to zero by 2050 [1].

One way of helping to reduce the emissions of CO_2 is to develop a more efficient heat pump or refrigeration technology for domestic use.

1.2. Aims and objectives

The aim of this project was to develop a commercially viable heat driven carbon-ammonia heat pump system with a high efficiency (heating COP) and specific heating power (output power per kilo of adsorbent) using a shell and tube heat exchanger, an appropriate choice of adsorbent material and a four-bed thermal wave cycle.

A heat driven heat pump was chosen to be developed over a mechanically driven vapour compression system as it uses primary energy sources more efficiently and can use energy from renewable sources such as solar collectors or waste heat from other sources.

An adsorption system was used over an absorption one because of their low operational cost and maintenance, higher reliability, simple and continuous operations and no crystallisation, corrosion or chemical disposal issues.

A carbon-ammonia pair was chosen because of the following reason:

- Ammonia is a great refrigerant because of its high latent heat and small and polar molecules which improve its adsorption by the adsorbent. Its high operating pressure enables ammonia leakage to be produced from the system to the environment, which avoids deterioration of the heat pump system performance. Its high operating pressures avoid mass transfer effects in the adsorption generators. Ammonia does not harm the ozone layer nor has global warming potential. The disadvantages of the ammonia are its toxicity, that it is corrosive to copper and its alloys and that needs costly pressurised systems (up to 20 bar).
- Active carbons are relatively inexpensive, have a high density, can adsorb high quantities of ammonia and their activation can be tailored to their application. Other reason that favoured the selection of active carbon as the adsorbent material is the experience that the researchers at the University of Warwick have to work with it and ammonia.

The objectives of the project were:

- To carry out the computational modelling of a four-bed thermal wave heat pump cycle.
- To carry out a heat transfer study of the active carbon available for the heat pump in order to identify the best sorbent sample.
- To develop an efficient way of filling the sorption bed with the chosen carbon sample.
- To design, manufacture and test the modelled heat pump cycle in order to validate the computational modelling.

1.3. Conclusions

In this project a carbon-ammonia adsorption heat pump was theoretically evaluated, designed and tested and heat transfer experiments on different carbon samples were conducted in order to identify the best sample to use in the system.

The project started with the simulation modelling development of the four-bed thermal wave cycle with generators that were previously used in another project. Once the simulation was done, the experimental set up was carried out and the complete system was tested. The results obtained were not satisfactory and it was identified that the heat transfer rate in the sorption generators was very poor due to the adsorbent material characteristics. Due to the low power output of the existing generators it was decided that new adsorption generators of larger size and with a different adsorbent material were needed.

In order to characterise the adsorbent material, a complete study on the heat transfer properties of different grain sizes and binary mixtures of active carbon was done. After the experiment analysis, a chosen carbon grain size and binary mixture were used to fill the generators with.

Finally, the complete system with the new larger adsorption generators and new adsorbent material was tested.

The order of the chapters are: introduction, theory, literature review, generator description and sorption material specifications, heat pump system design and simulation, simulation results, heat transfer in adsorbent beds, construction of prototype system, instrumentation and control, experimental results and analysis and conclusions and further work.

References

[1] Department of Energy and Climate Change (DECC), The future of heating: meeting the challenge, 2013.

Chapter 2

Literature review

2.1. Introduction

In this chapter firstly, an overview of heat pumps and the context where the development of the heat driven heat pump takes place are studied.

Secondly, the work carried out by the researchers in the adsorption heat pump field is presented. That includes methods investigated to improve heat transfer in adsorbent beds, methods developed in order to achieve heat recovery to increase the COP (Coefficient of Performance, explained in Chapter 3) and finally, adsorption machines available in the market or under development are presented.

2.2. Overview of heat pumps

A heat pump is described as a device that moves energy in the form of heat from a source of heat to a destination. They are designed to transfer thermal energy in the opposite direction of the spontaneous heat flow by absorbing heat from a cold space and releasing it to a warmer one.

In order to accomplish this heat transferral the heat pump uses some amount of external power.

Heat pump systems can be divided into two categories, engine-driven or sorption devices.

The engine driven systems comprise conventional gas fuelled engines driving conventional vapour compression heat pumps and as well novel engine types that could be combined with novel heat pump cycles.

The sorption systems use the ability of a solid sorbent or liquid to adsorb/absorb and desorb refrigerant in order to be used as a thermal compressor, analogous to the mechanical compressor in an electric heat pump.

In a sorption cycle the refrigerant is adsorbed/absorbed at a low temperature and pressure in the thermal compressor, then when the sorbent is heated the temperature and pressure increase and the refrigerant is desorbed (driven out of the compressor). The same fundamental thermodynamics are applied to both types of sorption systems, solid sorbents and liquids, and there are engineering advantages and disadvantages in using either one of them but the choice for a particular application depends on the implementation, size, efficiency and cost of the system.

2.2.1. Advantages of heat driven heat pumps

The major advantage and reason for the interest in heat driven heat pumps is the better utilisation of primary energy that they offer.

Conventional vapour compression or engine driven systems used in heat pumping applications need electricity to drive their mechanical compressor and they are able to reach high efficiency of conversion from mechanical work to heating.

For example, the COP of a heat pump application can be 3. However, the conversion of primary fuel to electricity at the power station and then the transmission losses of the electricity grid to the consumer may be 25% efficient. As a result, the overall conversion of primary energy to heating is only 75% efficient.

On the other hand, a heat driven heat pump powered by gas can achieve a COP of 1.3 and it represents the overall conversion efficiency from primary energy. It can be observed that a heat driven heat pump can perform considerably better than a conventional electrically driven machine.

The factor to take into account for the economic interest in heat driven cycles is the cost of the primary fuels that are currently 35% of the cost of electricity.

Other advantages of the heat driven heat pumps are the use of primary energy, fuel, at the point of demand that can reduce CO_2 and other emissions to the environment, the ability to produce heat at higher temperatures than the vapour compression cycles, little mechanical work input and the lack of moving parts in their systems which makes them particularly attractive for small applications.

2.3. Context and background

A reduction of 80% based on 1990 levels of the overall UK greenhouse gas emissions by 2050 was established in the Climate Change Act [1]. These emission reductions have to come from all main sectors of energy usage. Heat alone currently emits more greenhouse gas emissions than would be allowed for all three heat, electricity and transport combined sectors in 2050. Another target established in the National Renewable Energy Action Plan for the United Kingdom was to increase to 15% the amount of energy used that is produced by renewable sources by 2020 [2].

Heating within the domestic sector currently accounts for 23% of UK energy demand [3], being 71% of it used for space heating and 29% used for hot water production.

Another important data is that more than 40% of fossil fuels are burnt for low temperature heating purposes [4] (where the domestic sector is included) which produces more than 24% [5] of UK CO_2 emissions.

Even if major efforts to reduce the heating demand were put into practise (user behaviour change, optimised industrial processes, improved insulation and reduced infiltration in buildings) a major increase in heating energy efficiency through new and improved technology will be needed if the 2050 target is to be met.

The direct combustion of fuels for the production of heat at temperatures below 200°C it is not efficient. A good range of heat pumping and storage systems could be used instead dramatically reducing CO_2 emissions.

Current electric heat pump systems perform poorly, below their potential, although 50% efficiency improvement and higher delivery temperatures are achievable.

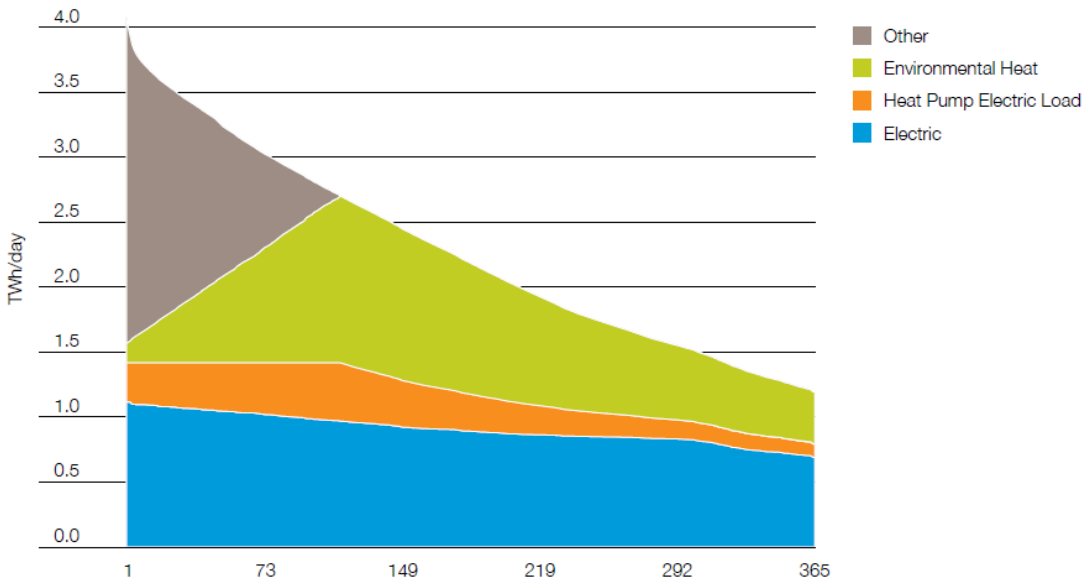

Figure 2.1 – Electricity and heat load duration curves [6]

In Figure 2.1 is possible to observe that the demand for domestic heat is much 'peakier' than the demand for electricity. The blue series represents the demand for electricity (excluding heating) and the remaining series represent heating load. The 'other' series includes gas and biomass and for houses not connected to the gas network, oil [6].

Electric heat pumps could supply a significant amount of the heat demand (orange and green series in Figure 2.1) with little requirement for extra electricity generation capacity.

In order to satisfy the entire load (including the grey series) building between 100 GW and 150 GW of new capacity will be necessary, most of which will run for less than half the year, with correspondingly unfavourable economics.

If electric heat pumps were chosen to satisfy the entire load, the electrical grid would need more power stations to cope with the electric heat pumps demand and the capacity needed would exceed 3 times the current one. More over the electric network would need to be increased between 4 and 7 times the actual one, rewiring 250,000 km of grid in the next 15 to 30 years [7].

Taking into account that 90% of homes (which are responsible for 80% of carbon emissions from UK housing) are connected to the gas grid, gas driven heat pumps could play a key role in the challenge of reducing the emission of CO_2 in the UK. They currently produce 30% less emissions compared to a fossil fuel boiler (heat pumps typically have a COP of 1.3 or above compared to a 0.9 efficiency for a high performing boiler) but those saving could grow up to 65% with achievable technology

development. The higher efficiency also leads to lower running costs, saving at least £300 per year based on a typical UK old suburban semi-detached home (thermal demand of 18,000 kWh) [8].

In the UK in the short term gas heat pumps must compete with condensing gas boilers rather than electric heat pumps in the market. The main type of gas driven heat pump to be commercialised would be the air source one due to the market size of the retrofit market, although ground source heat pumps may be important future niche markets.

The world domestic boiler market is estimated at between 10 and 12 million units per annum, the UK being the biggest share in terms of volume and value. The size of the UK market is around 1.5 million domestic boilers units per annum becoming the largest potential market for gas heat pumps [9, 10].

Private new build and retrofit homes are best target markets for gas driven heat pumps. Retrofit is by far the largest market and essential if gas heat pumps are to become mass market.

When installed in private new-build (around 150,000 units per annum) gas heat pumps will be most efficient with lower temperature water output which requires a well-insulated home with modern radiators or underfloor heating.

The payback time of the extra cost of a heat pump, which is determined by its fuel savings if compared to a conventional boiler, is the consumer's main concern and it depends on the size of house and comfort standards since in the domestic range the capital cost of the heat pump is not strongly dependent on the nominal power output. Assuming economies of scale in production, payback times of 3 years seem feasible for larger houses and 5 years in smaller ones.

National Grid [11] has looked at scenarios for 2050 and beyond that encompass a role for both gas and electric heat pumps. One of them is the Gone Green scenario, a UK future energy scenario, which is constructed in such a fashion that the renewable energy and carbon emissions targets are always achieved. In this scenario important reductions have been made in fossil fuel use for electricity generation and smart grids control the supply and demand. The primary energy consumption has been significantly reduced due to improvements in insulation and the increasing use of heat pumps and hybrid devices for space and water heating [11].

Figure 2.2 represents the Gone Green scenario prediction for the domestic and commercial heating market.

By 2030 most of the more cost effective refurbishments of the UK's buildings being done and the cost reduction of ground source heat pumps makes them become a good option for domestic heating.

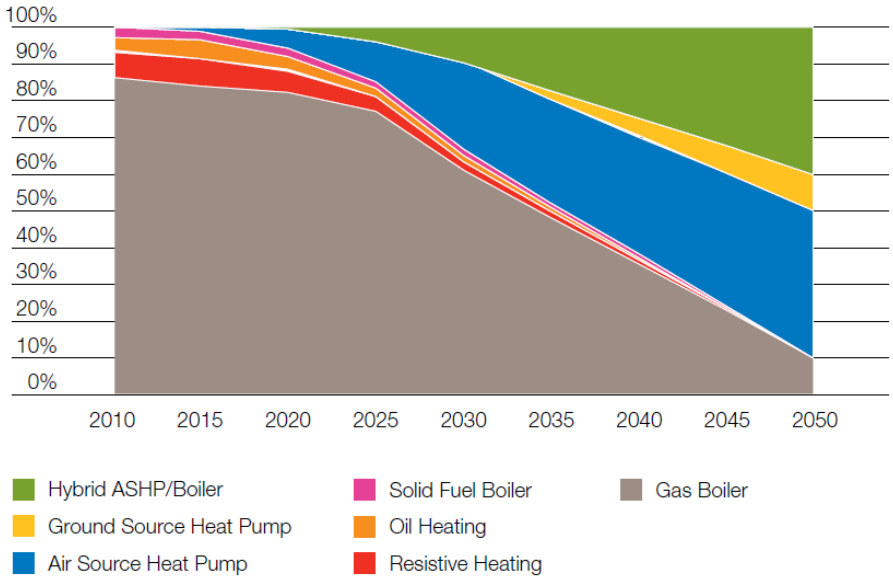

Figure 2.2 – Breakdown of the domestic and commercial heating market [6]

Between 2030 and 2050 most efficiency gains are made by the changing way heat is supplied in buildings with a shift to heat pumps for well insulated new properties with hybrid heat pump (gas or electric) and boiler systems being used in buildings in which the difference in seasonal heat requirements makes them less suited to be supplied by heat pumps alone.

By 2050 gas boilers will still represent 10% of the heating market and they will also be used in hybrid heat pump/boiler systems and in heat pump systems.

2.4. Heat transfer in heat pumps

The main problem associated with solid adsorbents used in adsorption refrigeration or heat pump systems is their low thermal conductivity, which affects the performance (COP) and the power output of the system. During a refrigeration cycle, the adsorbent has to be heated (desorbing refrigerant) and cooled (adsorbing refrigerant) in order to complete a thermodynamic cycle.

The aim of the adsorption system development is to achieve a low capital cost by reducing the adsorption generator size and reducing the cycle time. In order to achieve this, high rates of heat and mass transfer in and out of the adsorbent are critical. To improve the heat transfer and as a

consequence, the sorption process of the adsorbent, it is important to increase its thermal conductivity and reduce its thermal contact resistance with the walls of the heat exchanger without increasing the thermal capacity of the generator or reducing its mass transfer.

2.4.1. Adsorbent thermal conductivity

The intrinsic thermal conductivity of the adsorbent and the contact resistance between wall and sorption material are important factors to take into account in order to achieve a good heat transfer in adsorption beds.

Due to the porosity of the adsorbents their thermal conductivity usually is very low. Granular adsorbents have a thermal conductivity of around 0.1 W/(mK) and a wall contact resistance with the walls of the heat exchanger of 20 W/(m^2K) [12].

Experimental tests show that for beds of granular active carbon and ammonia the typical density achieved is 500 kg/m^3 and the thermal conductivity is 0.165 W/(mK) (with minor changes due to concentration). This value contrasts with the individual carbon grains thermal conductivity, at least five times higher, 0.85 W/(mK), depending on the adsorbate concentration [13].

Many approaches have been developed in order to improve the global heat transfer within the solid adsorbent and between the generator wall and the adsorbent.

One of them is the addition to the adsorbent of a material with higher thermal conductivity.

The addition of expanded natural graphite (ENG) to the adsorbent grains followed by the compression of the mixture in order to create a matrix that intensifies the heat transfer around the adsorbent is a very common technique due to the ENG high thermal conductivity and diffusivity, 10 times higher than aluminium. One disadvantage of this technique is the high percentage of ENG that has to be added to the adsorbent to achieve good thermal conduction paths.

A mixture of 70 % NaX zeolite powder and 30% of a highly conductive matrix of ENG was studied by Guilleminot [14]. The experiments carried out with this mixture show thermal conductivities of between 2 and 10 W/(mK), about 100 times higher than packed bed zeolite adsorbent, 0.09 W/(mK).

In order to obtain a low contact resistance between the zeolite grains and the graphite a good consolidation is very important. Other experiments carried out by Pons [P] show thermal conductivity values of between 5 and 15 W/(mK) [15].

When the ENG was used along with silica gel it was reported an achieved thermal conductivity value of 10 W/(mK) [16] and when used with granular carbon a thermal conductivity of 2.5 W/(mK) was reported [17].

Other technique used to increase the thermal conductivity in the adsorbent is to coat metallic foams with adsorbent materials. Bonaccorsi et al [18] reported thermal conductivities of 24 W/mK for a 85% porosity of graphite foam (better than for aluminium foams) with SAPO zeolite coated on top. This technique achieves low thermal contact resistance between the adsorbent and the foam as the adsorbent is directly synthetised on the foam.

Similarly, copper foams of 70% porosity where as well compactly coated by zeolite synthesis treatments achieving a low wall contact resistance as the zeolite was bonded to the substrate [19].

Another improvement in the heat transfer rate can be achieved with the introduction of fins in the generators. Critoph [20] presented a laboratory monolithic carbon-ammonia aluminium finned prototype that could achieve an effective thermal conductivity of 20 W/(mK)). The carbon aluminium laminate was compressed inside the retaining vessel up to 150 MPa in order to achieve good thermal contact between the fins, the vessel walls and the carbon.

Tamainot-Telto [21] and Critoph [22] reported an increase in the density and thermal conductivity by compacting adsorbent powder (active carbon) with a binder. This monolithic carbon was manufactured based on 208C carbon precursor, mixed with an organic binder, compressed at high pressures and fired. The thermal conductivity values obtained could be as high as 0.44 W/(mK).

Finally, last method presented that enhances the thermal conductivity of the adsorbent is the convective thermal wave concept developed by Critoph [23]. This concept uses the refrigerant itself to transfer the heat through forced convection in the adsorption bed although it only can be applied to high pressure systems.

2.4.2. Generator design

The adsorbent bed or adsorption generator is described as a heat exchanger that transfers heat between the heat transfer fluid and the adsorbent. The higher the transfer rate and the lower the thermal mass of the bed will improve the efficiency of the refrigerator or heat pump machine.

The type of proposed heat exchanger geometries are listed below:

- Shell and tube, where the heat transfer fluid flows through the tubes and the adsorbent is located in the shell.
- Plate type heat exchanger.
- Tubes, where the adsorbent is located in the inside of the tube and the heat transfer fluid flows around the tubes.

A shell and tube adsorption generator used in an adsorption ammonia-carbon heat pump was presented by Critoph [24]. As the theoretical modelling suggested, the shell and micro-tube construction could have less thermal mass and equivalent heat transfer, achieving an output power of 7 kW and a seasonal heating COP of 1.35.

A slim thin-wall shell-tube adsorber prototype of activated carbon and methanol was built and tested by Gui [25] who obtained a specific heating power of 487 W/kg and a COP of 1.47.

A plate shim design presented by Tamainot-Telto [26] consisted in 29 layers of 4 mm thick of active carbon. These stainless steel shims were designed in order to cope with differential pressures of up to 20 bar. It achieved an averaging cooling power of 1.6 kW and a cooling COP of 0.22.

Other plate type heat exchangers were proposed by Tchernev and Emerson [27] and by Cacciola and Restuccia [28]. The main advantage of this type of heat exchangers is the reduced conduction path length through the adsorption material which enables a shorter cycle time and a higher specific heating/cooling power.

Critoph [29] presented a multiple bed adsorption cycle that used monolithic carbon and ammonia. The design of the beds consisted on 12.7 mm outer diameter stainless steel tubes with an internal lined layer of 3mm of monolithic carbon. Computational simulations of the cycle predicted a cooling COP of 0.6 and a specific cooling power of 142 W/kg.

2.5. Heat recovery in heat pumps

In order to increase the efficiency of the adsorption cycles obtaining a good rate between adsorption and desorption, many regeneration techniques have been formulated and developed. The most important is the one that allows the rejected heat to be transferred efficiently from an adsorption

compressor to another one. I.e. the heat of the adsorption output can be used to preheat the desorbing bed when the temperature difference between them allows it.

In order to achieve heat regeneration, two main options are available. The first one is to use a thermal wave arrangement and the second one is to use multiple bed cycles.

2.5.1. Thermal wave cycles

The concept of a thermal wave cycle was first described by Shelton [30] and Tchernev [31]. The thermal wave cycle comprises 2-beds and is the simpler method of achieving heat recovery between the beds, increasing the COP of the system. Shelton predicted a heating COP of 1.8 and a cooling COP of 0.8 for the charcoal-ammonia system.

Jones [32] presented a thermal wave cycle that instead of 2-beds used 4-beds. More beds could be used but the complexity of the system would not make it cost effective. By adding more beds in the system the gradient in the hottest or coldest generator at the end of the cycle will be significantly reduced. The cooling COP presented for a carbon-ammonia pair 4-bed cycle was 1.02, for the 6-bed cycle was 1.06 and for the 12-bed cycle was 1.16 [33].

2.5.2. Multiple bed cycles

In the multiple-bed cycles the heat recovery is carried out between multiple isothermal beds.

Meunier [34] calculated the amount of heat recovery that could be achieved between a two-bed cycle and between an infinite number of beds cycle, which indicates the theoretical maximum COP achieved with an adsorption cycle.

Critoph [35] approached the second law analysis of a carbon-ammonia system based the work of Meunier [34] and calculated the losses that result from all non ideal heat flows by considering the heating (or cooling) effect that they could generate if driving reversible heat pumps (or refrigerators) before reaching ambient temperature.

Metcalf [36] presented a computational analysis of a carbon-ammonia 4-bed multiple bed cycle and it was compared to a 2-bed bed cycle. For specific heating powers lower than 3 kW the 4-bed cycle showed better performance, with heating COP's ranging from 1.4 to 1.65. For specific heating powers higher than 3 kW the 2-bed cycle showed better performance, with heating COP's ranging from 1.4 to 1.25.

The higher the number of beds that take part in the heat recovery process the higher the recovered heat but the more complex the system. A system with more than 4-beds is very difficult to set up due to the amount of pumps and valves required.

2.6. Adsorbent pair

The preferred refrigerant and adsorbent pairs due to their efficiency in adsorption refrigeration cycles are water-zeolite, methanol-carbon, ammonia-carbon and ammonia-salts. Besides the above mentioned gases, other alternatives are R32 and butane that have been studied with porosity tests in order to possibly use them as refrigerants with monolithic active carbon adsorbents.

The main characteristics that a gas should have in order to work well with active carbon are being polar, having a high enthalpy of vaporisation per unit volume of liquid and a low molecular weight. Having a high enthalpy of vaporisation ensures that the maximum possible proportion of the heat input is used for desorption and the maximum possible is wasted on sensible heating of the adsorbent [37].

The preferred refrigerant to be used as a pair with active carbon is ammonia as it has good heat transfer and thermodynamics properties which enables the use of more compact system components that have smaller heat transfer areas. It is the most environmental refrigerant, being ozone friendly, it can work well in a wide range of temperatures and has a relatively low price (if compared to HFCs). On the other hand it has the disadvantage of being extremely toxic, flammable at certain concentrations and incompatible with copper or its alloys.

2.7. Adsorption cycle machines

In this section some of the adsorption machines that are currently being commercialised or in development process are presented.

The German company Viessmann commercialised in Germany the Vitosorp 200-F machine, a zeolite-water gas adsorption ground source heat pump that is sold combined with a conventional condensing boiler. It provides a nominal heat output of 11 kW and it was designed for a single family building. It has a seasonal efficiency of 124% based on upper gas calorific values [38].

Another German company,Vaillaint is currently developing a gas powered heat pump that uses a 2-bed zeolite-water cycle. It provides a heating output power of 10 kW at a high efficiency level of 135%. It has been designed to be used in detached and semidetached homes [39].

The Japanese company Mayekawa Mycom manufactures a zeolite-water refrigerator that chills water down to 10-15 °C and uses a low temperature heat source (around 68 °C). Its cooling power ranges from 50 to 430 kW [40].

References

[1] Climate Change Act 2008, Chapter 27, http://www.legislation.gov.uk/ukpga/2008/27/pdfs/ukpga_20080027_en.pdf on 27/08/2014.

[2] National Renewable Energy Action Plan for the United Kingdom, Article 4 of the Renewable Energy Directive 2009/28/EC, https://www.gov.uk/government/uploads/system/uploads/attachment_data/file/47871/25-nat-ren-energy-action-plan.pdf on 27/08/2014.

[3] Department of Energy and Climate Change (DECC), The future of heating: meeting the challenge, 2013.

[4] Nera Economic Consulting, Renewable Heat Technologies for Carbon Abatement: Characteristics and Potential, Final Report to the Committee on Climate Change July 2009.

[5] The Future of Heating: A strategic framework for low carbon heat in the UK, DECC, March 2012.

[6] UK Future Energy Scenarios, UK gas and electricity transmission, National Grid, September 2012.

[7] Why hybrids and gas heat pumps?, Stephen Marland, National Grid.

[8] Gas-driven heat pumps: Opening opportunities in the UK retrofit sector?, Delta-ee whitepaper, September 2012.

[9] Market Assessment in the Field of Domestic Heating, Optimat, June 2009.

[10] Market assessment for Sorption Energy, Angle Technology, December 2010.

[11] UK Future Energy Scenarios, UK gas and electricity transmission, National Grid, November 2011, http://www.nationalgrid.com/NR/rdonlyres/86C815F5-0EAD-46B5-A580-A0A516562B3E/50819/10312_1_NG_Futureenergyscenarios_WEB1.pdf on 27/08/2014.

[12] Critoph, R. E., Zhong, Y., Review of trends in solid sorption refrigeration and heat pumping technology, Proceedings of the institution of mechanical engineers part e-journal of process mechanical engineering, 219, pp. 285-300. ISBN 0954-4089.

[13] Critoph, R. E., Turner, L., Heat transfer in granular activated carbon beds in the presence of adsorbable gases, Internationl. Journal of Heat and Mass Transfer, 38, pp. 1577-1585, 1995.

[14] Guilleminot, J. J., Chalfen, J. B., Choisier,A., Heat and mass transfer characteristics of composites for adsorption heat pumps, Proceedings of the international absorption heat pump conference, ASME, pp. 401–406, 1994.

[15] Pons, M., Laurent, D., Meunier, F., Experimental temperature fronts for adsorptive heat pump application, Applied thermal engineering, 16, pp. 395-404, 1996.

[16] Eun, T. H., Song, H. K., Han, J. H., Lee, K. H., Kim, J. N., Enhancement of heat and mass transferrin silica-graphite composite blocks for adsorption heat pumps: Part I. Characterization of the composite blocks, International Journal of Refrigeration, 23, pp. 64-73, 2000.

[17] Wang, L. W., Tamainot-Telto, Z., Thorpe, R., Critoph, R. E., Metcalf, S. J., Wang, R. Z., Study of thermal conductivity, permeability and adsorption performance of consolidated composite activated carbon adsorbent for refrigeration, Renewable energy, 36, pp. 2062-2066, 2011.

[18] Bonaccorsi, L., Bruzzaniti, P., Calabresea, L., Freni, A., Synthesis of SAPO-34 on graphite foams for adsorber heat exchangers, Applied Thermal Engineering, 61, pp. 848-852, 2013.

[19] Bonaccorsi, L., Freni, A., Proverbio, E., Restuccia, G., Russo, F., Zeolite coated copper foams for heat pumping applications, Microporous and Mesoporous materials, 91, pp. 7-14, 2006.

[20] Critoph, R.E. Tamainot-Telto, Z., Davies, G.N.L., Prototype of a fast cycle adsorption refrigerator utilizing a novel carbon-aluminium laminate. Proceedings of the institution of mechanical engineers, part A, Journal of Power Energy, 214, pp. 439-448, 2000.

[21] Tamainot-Telto, Z., Critoph, R. E., Adsorption refrigerator using monolithic carbon-ammonia pair, International Journal of Refrigeration, 20, pp. 146-155, 1997.

[22] Critoph, R. E., Evaluation of alternative refrigerant–adsorbent pairs for refrigeration cycles, Applied Thermal Engineering, 16, pp. 891-900, 1996.

[23] Critoph, R. E., Forced convection adsorption cycles, Applied thermal engineering, 18, pp. 799-807 1998.

[24] Critoph, R. E., Metcalf, S. J., Progress in the development of a carbon-ammonia adsorption gas-fired domestic heat pump, International sorption heat pump conference, Padua, 2011.

[25] Gui, Y. B., Wang, R. Z., Wang, W., Wu, J. Y., Xu, . X., Performance modelling and testing on a heat-regenerative adsorptive reversible heat pump, Applied Thermal Engineering, 22, pp. 309-320, 2002.

[26] Tamainot-Telto, Z., Metcalf, S. J., Critoph, R. E., Novel compact sorption generators for car air conditioning, International journal of refrigeration, 32, pp. 727-733, 2009.

[27] Tchernev, D. I., Emerson, D. T., High efficiency regenerative zeolite heat pump, ASHRAE Trans, 94, 1988.

[28] Cacciola, G., Restuccia, G., Progress on adsorption heat pumps, Heat recovery systems & CHP, 14, pp. 409-420, 1994.

[29] Critoph, R. E., Multiple bed regenerative adsorption cycle using the monolithic carbon-ammonia pair, Applied thermal engineering, 22, pp. 667-677, 2002.

[30] Shelton, S. V., Solid adsorbent heat pump system, US patent 4,610,148, 1986.

[31] Tchernev, D. I., Heat pump energized by low-grade heat source, US patent 4,637,218, 1987.

[32] Jones, J. A., Sorption refrigeration research at JPL/NASA, eat recovery systems & CHP, 13, pp. 363-371, 1993.

[33] Jones, J. A., Carbon-ammonia regenerative adsorption heat pump, AES-Vol 31, International absorption heat pump conference, ASME 1993.

[34] Meunier, F., Second law analysis of a solid adsorption heat pump operating on reversible cascade cycles: application to zeolite-water pair, Heat recovery systems, 5, pp. 133-141, 1985.

[35] Critoph, R. E., An Approach to Second Law Analysis of Adsorption Heat Pumps, International sorption heat pump conference, Maryland University, 2014.

[36] Metcalf, S. J., Critoph, R. E., Tamainot-Telto, Z., Optimal cycle selection in carbon-ammonia cycles, Intrnational journal of refrigeration, 35, pp. 571-580, 2012.

[37] Critoph, R.E., Evaluation of alternative refrigerant-adsorbent pairs for refrigeration cycles, Applied Thermal Engineering, 16, pp. 891-900, 1996.

[38] Vissmann, Vitosorp 200-F: Innovative gas adsorption heat pump for high-efficiency heating URL: http://www.viessmann.com/com/content/dam/internet-global/pressetexte/com_2013/pr-Vitosorp_200-F.pdf on 27/04/2014.

[39] Vaillant, Development – The future, zeolite heating appliance, URL: http://www.vaillant-export.com/homeowners/renewable-energy/development on 27/04/2014.

[40] Mayekawa Mycom, AdRef – Noa Adsorption chiller with zeolite, URL: http://www.mayekawausa.com/brochures/pdf/AdRef-Noa_brochure.pdf on 27/04/2014.

Chapter 3

Theory

3.1. Introduction

In this chapter, the basic adsorption cycle is described and presented along with the description of the thermal wave cycle developed in this project.

The adsorption equation of state and thermodynamic relationships used in the generator design and simulation modelling are presented.

3.2. Adsorption cycle

3.2.1. Cycle operation

The most basic adsorption refrigeration cycle is shown in Figure 2.1 where two linked vessels are presented. The vessel on the left hand side acts as the generator, containing the solid adsorbent and adsorbed refrigerant, whilst the vessel on the right hand side acts as a receiver, condenser and evaporator during the cycle, containing refrigerant gas.

In the Stage (a) of the cycle the system is at low pressure and ambient temperature. The adsorbent contains a high concentration of adsorbed refrigerant whilst the right hand vessel contains refrigerant gas.

When the vessel on the left is heated, the adsorbed refrigerant gets driven out and the pressure of the system increases. In Stage (b) the pressure of the system is high enough so that the refrigerant gas starts to condense in the right hand vessel whilst rejecting heat. After that the generator is cooled back to the initial low temperature readsorbing the refrigerant in the adsorbent material

which creates a drop in the pressure of the system. When the pressure drops, the liquid refrigerant boils and produces the cooling effect, absorbing heat. In Stage (c) the system returns back to the initial state and the cycle is completed.

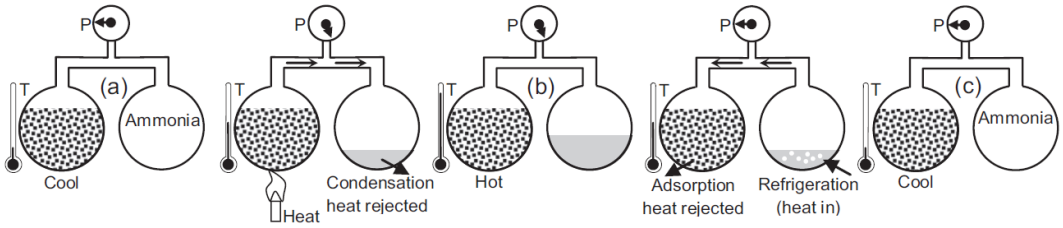

Figure 3.1 – Simple adsorption cycle schematic [1]

The cycle provides heating/cooling discontinuously for approximately half of the cycle time. If two or more generators are operated out of phase the heating/cooling could be produced continuously.

When continuous heating/cooling is produced the right hand vessel mentioned above is usually split into two separate components: a condenser and evaporator. Each generator of the system is connected to the condenser and to the evaporator via separate automatic check valves as shown in Figure 3.2.

Once the refrigerant is desorbed from the generator, it is condensed in the condenser and it passes through an expansion valve to reduce its pressure. After that the refrigerant evaporates in the evaporator and finally it can be adsorbed in the generator completing a cycle.

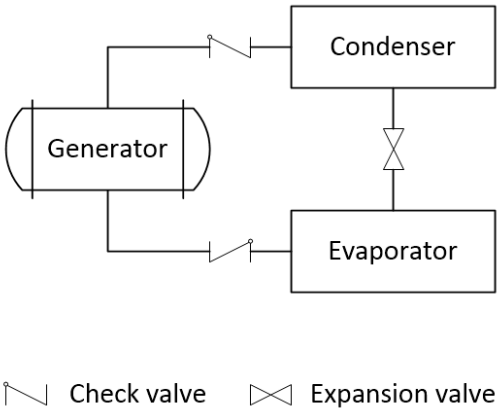

Figure 3.2 – Refrigerant circuit for one sorption generator

3.2.2. Basic ideal adsorption cycle

The basic adsorption refrigeration cycle is plotted in Figure 3.3 in a Clapeyron diagram (pressure - Temperature - concentration).

The ideal adsorption cycle assumes that the condensation and evporation occur at constant pressures and that the void volume in the bed is zero so that the pressurisation and depressurisation are isosteric processes.

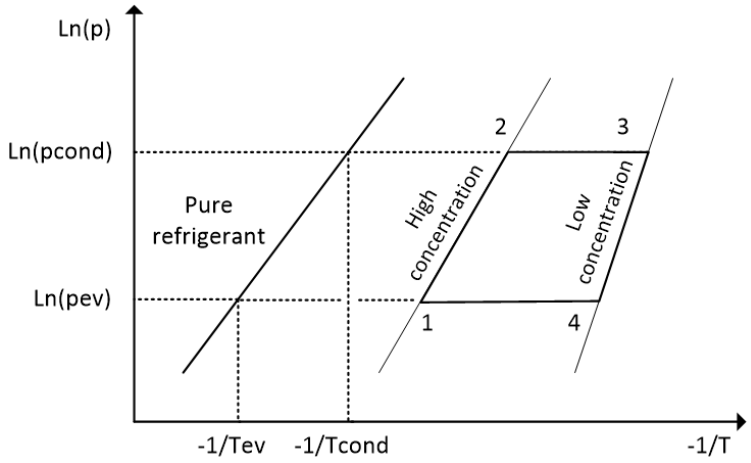

Figure 3.3 – p-T-x (Clapeyron) diagram for a single adsorption cycle

The adsorption cycle can be described in four stages:

- Stage 1 → 2 – isosteric pressurisation: The adsorbent in the bed is heated and its pressure rises from evaporating to condensing pressure. If the void volume in the bed is zero, the process will be isosteric. If some volume exists in the bed, some refrigerant will be desorbed.
- Stage 2 → 3 – isobaric desorption: The adsorbent continues to be heated and starts desorbing refrigerant at the condensing pressure while the refrigerant condenses in the condenser.
- Stage 3 → 4 – isosteric depressurisation: The adsorbent in the bed is cooled and its pressure decreases from condensing to evaporating pressure. If the void volume in the bed is zero, the process will be isosteric. If some volume exists in the bed, some refrigerant will be adsorbed.
- Stage 4 → 1 – isobaric desorption: The adsorbent continues to be cooled and starts adsorbing refrigerant at the evaporating pressure while the refrigerant evporates in the evporator.

3.2.3. Coefficient of performance (COP)

The coefficient of performance of a heat pump or refrigerator is defined as the ratio of heating or cooling provided to input energy in the process.

In the case of adsorption heat pump or refrigeration cycles (heat driven heat pumps or refrigerators) the heating and the cooling COP's are defined by equations 3.1 and 3.2.

$$COP_{heating} = \frac{Q_{cond}+Q_{cooler}}{Q_{boiler}} \quad (3.1)$$

$$COP_{cooling} = \frac{Q_{ev}}{Q_{boiler}} \quad (3.2)$$

where

Q_{cond} is the heat released in the condenser

Q_{cooler} is the heat released in the cooler

Q_{boiler} is the heat provided by the boiler (input energy in the process)

Qev is the heat absorbed by the evaporator

3.2.4. Thermal wave cycles

The COP of the basic adsorption cycle presented above is quite low. In order to increase it, heat regeneration techniques that allow efficient heat transfer from one adsorption generator to another should be used.

Mutiple bed and thermal wave cycles are two ways of achieving heat recovery but thermal waves approach the performance of a multiple bed system in a simpler way by only using two beds (patented by Shelton and Tchernev) [2,3].

In Figure 3.4 the basic thermal wave cycle is shown, where a heat transfer fluid is pumped by a reversible pump through two beds, a heater and a cooler in a closed loop.

At the beginning of the cycle Generator 1 is cold (maximum adsorbent concentration) and Generator 2 is hot (minimum adsorbent concentration). In Stage 1, if the pump is pumping clockwise, the heat transfer fluid flows through Generator 2 recovering heat from it, then receives more heat from the heater and finally flows through Generator 1 heating it and desorbing refrigerant to the condenser. At the same time in the other part of the cycle, the heat transfer fluid is passing thrugh Generator 1 releasing heat to it, then reduces its temperature in the cooler and finally flows through Generator 2 cooling it and adsorbing refigerant from the evaporator.

The thermal wave front velocity in the beds is much lower than the one of the heat transfer fluid.

Once the heat transfer fluid front reaches the end of the bed and its temperature changes rapidly the pump is reversed and the thermal wave front passes back down the bed in the opposite direction.

This type of cycle enables simple but limited heat recovery between the generators. A combination of good heat transfer design in the Generators and a low heat transfer fluid flow rate are needed to achieve a good performance.

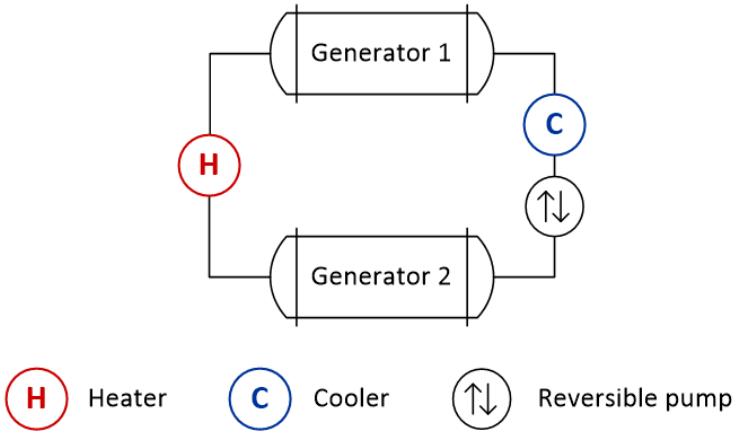

Figure 3.4 – Basic 2 bed thermal wave cycle

This project carried out the development of a 4 bed thermal wave cycle first proposed by Jones [4]. The cycle schematic is shown in Figure 3.5. The fluid stream flows clockwise during the whole cycle and consecutively through the four generators.

The cycle starts in Stage 1 when the hot fluid, after being heated in the heater, flows through Generator 1 increasing its temperature and desorbing refrigerant. The same fluid, when leaving Generator 1 at a slight lower temperature, enters Generator 2 preheating it. After Generator 2, the fluid is cooled in the cooler and then it flows through Generator 3, reducing its temperature and adsorbing refrigerant. After Generator 3 the fluid at a slight higher temperature enters Generator 4 precooling it.

In Stage 2 the Generator 2, that was preheated in Stage 1, is heated with fluid coming directly from the heater. Similarly, the Generator 4 that was precooled in Stage 1 gets cooled in Stage 2. Generators 1 and 3 are precooled and preheated respectively in Stage 2.

At any time of the cycle there is at least one generator desorbing refrigerant and at least other one adsorbing refrigerant so that the heating/cooling effect is continuos.

In Figure 2.5 it is possible to observe how the heater and cooler (and the fluid pump) virtually move around the generators, heating and cooling them accordingly to the stage.

During a complete cycle each generator of the system is preheated, heated, precooled and cooled providing continuos cooling or heating.

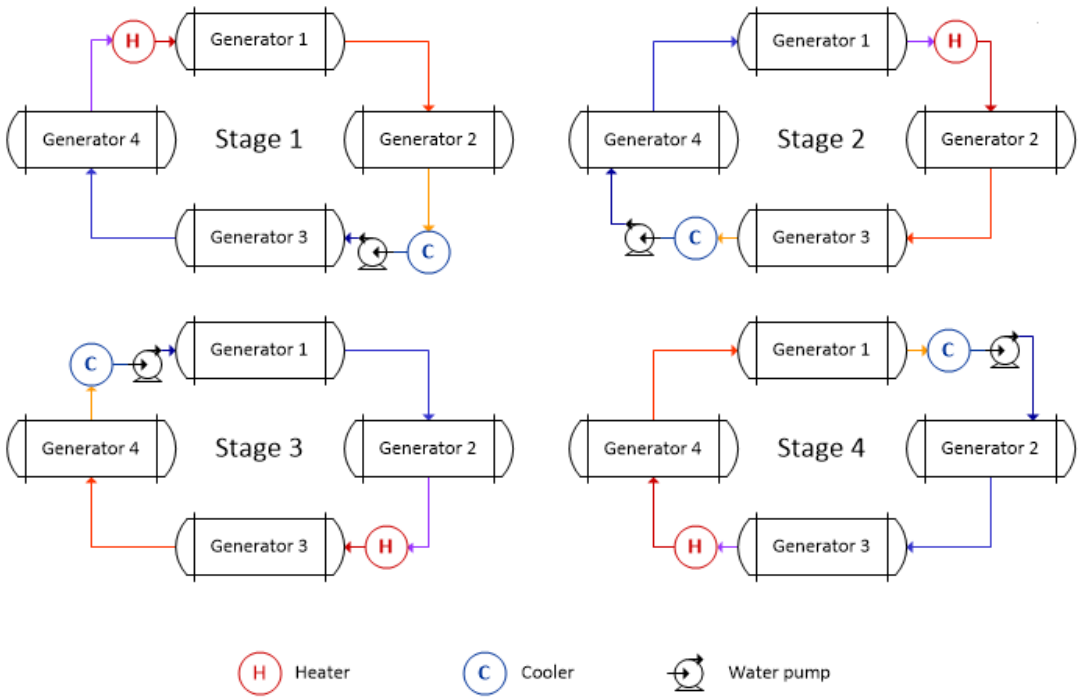

Figure 3.5 – 4 beds thermal wave cycle

Increasing the number of generators in the cycle would reduce the thermal gradient of the hottest and coldest generator at the end of the cycle (irreversibility reduction) which as a consequence would result in an increase of the overall COP of the system. Due to space and complexity the number of beds was limited to 4 in this project.

In order to implement the four-bed thermal wave cycle four adsorption generators, a heater, a cooler, a pump and two 4-pole 4 way heat transfer fluid valves are needed.

3.3. Adsorption equation of state

The mass of refrigerant (ammonia) adsorbed in the beds depends on the temperature and pressure of the system. The ammonia concentration is calculated with the modified Dubinin-Astakhov equation presented by Critoph [5].

$$x = x_0 \, e^{-K\left(T/T_{sat}-1\right)^n} \tag{3.3}$$

where

T is the refrigerant/adsorbent temperature (K)

T_{sat} is the saturation temperature (K)

x is the adsorbed refrigerant concentration (kg/kg)

x_0 is the maximum (limiting) concentration (kg/kg)

K and n are constants

3.4. Thermodynamic relationships

3.4.1. Saturation temperature

Equation 3.4 presents the relationship between pressure and saturation temperature for ammonia.

$$\ln p_{sat} = A - \frac{C}{T_{sat}} = 11.515 - \frac{2748.3}{T_{sat}} \tag{3.4}$$

p_{sat} is the saturation pressure (bar)

T_{sat} is the saturation temperature (K)

A and C are constants

3.4.2. Heat of adsorption

The calculation of the isosteric enthalpy of adsorption is presented by Hill [6]

$$\left(\frac{\partial p}{\partial T}\right)_x = \frac{H_{ads}}{T(v_g - v_s)} \tag{3.5}$$

where

H_{ads} is the isosteric heat of adsorption (J/kg)

P is the pressure (Pa)

x is the concentration (kg/kg)

v_g is the specific volume of the unadsorbed gas (m^3/kg)

v_s is the specific volume of the adsorbed gas (m^3/kg)

It is assumed that $v_s << v_g$ so that the heat of adsorption can be calculate as

$$H_{ads} \cong \left(\frac{\partial p}{\partial T}\right)_x T v_g \tag{3.6}$$

The pressure partial derivative is calculated with equations 3.3 and 3.5 and can be substituted with

$$H_{ads} \cong \frac{C\,p}{T_{sat}} v_g \tag{3.7}$$

References

[1] Metcalf, S. J., Critoph, R. E., Tamainot-Telto, Z., Optimal cycle selection in carbon-ammonia adsorption cycles, International journal of refrigeration, 35, pp. 571-580. 2012.

[2] Shelton, S. V., Solid adsorbent heat pump system, US patent 4,610,148, 1986.

[3] Tchernev, D. I., Heat pump energized by low-grade heat source, US patent 4,637,218, 1987.

[4] Jones, J. A., Sorption refrigeration research at JPL/NASA, Heat recovery systems & CHP, 13, pp. 363-371, 1993.

[5] Critoph, R. E., Adsorption refrigerators and heat pumps, Carbon materials for advanced technologies, Elsevier, Chapter 10, ISBN 0-08-042683-2.

[6] Hill, T. L., Statistical mechanics of adsorption. IX. Adsorption thermodynamics and solution thermodynamics, Journal of chemical physics, 18, pp. 246-256, 1950.

Chapter 4

Generator description and sorption material specifications

4.1. Introduction

In this chapter the design and manufacturing of the sorption generators used in the heat pump machine and their sorption material are explained and discussed.

4.2. Sorption generators

The generators or sorption beds are heat exchangers that transfer heat between the sorption material (active carbon) and the heat transfer fluid (water). The type of heat exchanger used in this project was a shell and tube.

Two different size generators were used and their specifications are explained in the following sections. Both small and large generators were made of stainless steel 304 and their tubes had an outer diameter of 1.2 mm and an inner diameter of 0.8 mm.

4.2.1. Small generators

The small generators, pictured in Figure 4.1, were designed for and used in a previous project by the researchers of the University of Warwick.

They had an end plate diameter of 95.5 mm and had 766 holes where tubes of 297 mm length were inserted. The end plates and the tubes were nickel brazed together, creating a core, then this core

was introduced in the shell of the generator (similar to Figure 4.4) and everything was nickel brazed. The generator assembly was finished when two flanges were attached one at each end of the shell.

The shell had three openings (similar to Figure 4.4), one of them was used both as an ammonia inlet from the evaporator or as an outlet to the condenser, the second one was connected to an ammonia relief valve, and the third opening had a pressure transmitter and the ammonia feed connector fitting connected.

One disadvantage of this generator was that when all the assembly is brazed together it can only be filled once with the sorption material and could not be reused.

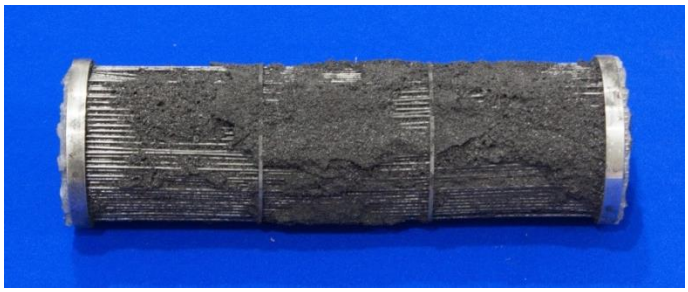

Figure 4.1 – Small generator removed from shell

In order to remove the generator shown in Figure 4.1 from its shell, the shell had to be cut and the generator and the shell were no longer usable. In order to avoid this, when a larger generator was needed to be manufactured it was designed so that the beds could be refilled and tested with different sorption materials.

Another disadvantage of this generator was that not all the volume enclosed in the shell had good heat transfer with the tubes. Around 19% of the carbon inside the shell was located at the periphery of the core (chunks of carbon can be observed in Figure 4.1). This negatively affected the coefficient of performance and the heating power as a considerable amount of carbon is not being heated or cooled and no ammonia is desorbed or adsorbed.

4.2.2. Large generators

The large generators design and manufacturing process was slightly different from the small ones so that the core could be refilled and tested with different sorption materials or mixtures.

These generators were three times larger than the small ones because when the latter were tested their poor performance lead to low output power and increasing their size would increase the output power.

Figure 4.2 – Large generator

The end plates of the generators had a diameter of 144.5 mm and 1777 holes where the tubes of 396 mm length were inserted (Figure 4.2 and 4.3). When the generators were manufactured, first the end plates were tack welded together with 6 rods to serve as a jig. After this, the 1777 tubes were inserted through both end plates and were nickel brazed together creating the core of the generator.

Figure 4.3 – End plate of large generator

After the core was filled with sorption material (see section 4), it was slid inside the shell and instead of being nickel brazed all together, two o-rings at each end of the shell sealed the core avoiding any refrigerant leaving the core or any heat transfer fluid flowing into the core.

The shell had three openings (Figure 4.4), one of them was used both as an ammonia inlet from the evaporator or as an ammonia outlet to the condenser, the second one had an ammonia relief valve connected, and the third opening had a pressure sensor and the ammonia feed connector fitting connected.

In Figure 4.4 it is possible to see the o-ring grooves at the end of the shell.

Figure 4.4 – (a, b) Large generator shell

Once the generator is placed in the shell two spiral water distributors, as pictured in Figure 4.5, are placed at both ends of the core. These water distributors were manufactured by a rapid prototyping machine and were made of ULTEM™ 9085, a high performance thermoplastic with a glass transition temperature of 186 °C.

They were used to distribute the heat transfer fluid (water) evenly among all the generator tubes and create a uniform temperature fluid front.

Figure 4.5 – Rapid prototype spiral distributor (a) Front, (b) Back

Finally, two flanges were attached at the ends of the shell completing the generator assembly.

4.3. Sorption material

The sorption material used in both small and large generators is active carbon type 208C based on coconut shell precursor manufactured by Chemviron Carbon Ltd. The active carbon can be obtained in different sizes with grains ranging from millimetres (Figure 4.6a) to microns (Figure 4.6b) long.

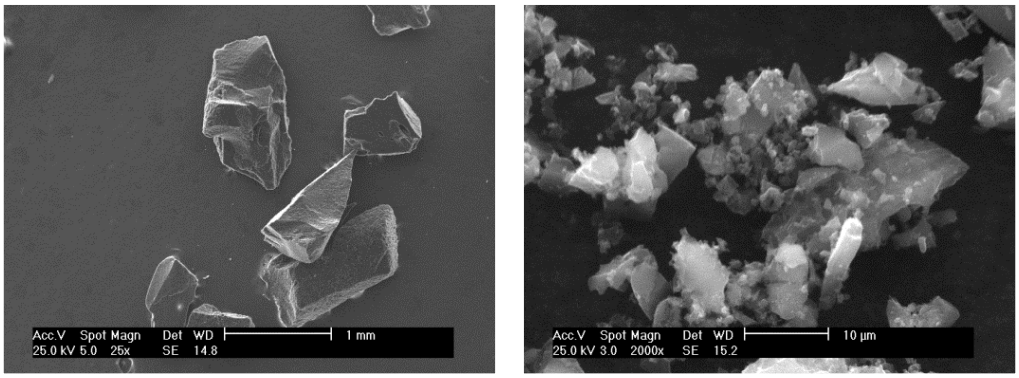

Figure 4.6 – (a) Carbon grains size 12x30, (b) Carbon powder

The grain sizes are classified according to the US standards mesh numbers and their relationships are shown in Table 4.1.

US standard Mesh No.	Sieve opening
100	0.150 mm
80	0.180 mm
70	0.212 mm
60	0.250 mm
50	0.300 mm
45	0.355 mm
40	0.425 mm
35	0.500 mm
30	0.600 mm
25	0.710 mm
20	0.850 mm
18	1.00 mm
16	1.18 mm
14	1.40 mm
12	1.70 mm

Table 4.1 – Relationship between US mesh grade and sieve opening

During this project, five different carbon sizes were used in heat pumping applications and in heat transfer experiments. Their sizes are shown in Table 4.2.

Mesh number	Sieve opening (mm)
12 x 30	1.70 x 0.60
20 x 40	0.85 x 0.425
30 x 70	0.60 x 0.212
50 x 100	0.30 x 0.15
Powder	< 0.18

Table 4.2 – Carbons 12x30, 20x40, 30x70, 50x100 and powder sieve analysis

The grain size distribution of the grades 20x40, 30x70 and 50x100 is shown in Table 4.3. The sieve analyses were done to the batches that the University of Warwick received from the manufacturers as they vary from batch to batch.

Mesh number	Sieve opening (mm)	17th Nov 2010	26th June 2012	3rd July 2012
		20x40	30x70	50x100
18 x 20	1.00 x 0.85	1	-	-
20 x 30	0.85 x 0.60	95.8	1.6	-
30 x 35	0.60 x 0.50		22.1	-
35 x 40	0.50 x 0.425		30.6	-
40 x 45	0.425 x 0.355	3.1	28.9	-
45 x 50	0.355 x 0.300	0.1	13	12.0
50 x 60	0.300 x 0.250	-	3.5	7.3
60 x 70	0.250 x 0.212	-	0.3	19.9
70 x 80	0.212 x 0.180	-	-	22.9
80 x 100	0.180 x 0.150	-	-	29.8
-100	< 0.150	-	-	8.1

Table 4.3 – Carbon 20x40, 30x70 and 50x100 sieve analysis

The powder was also analysed. The results are shown in Figure 4.7.

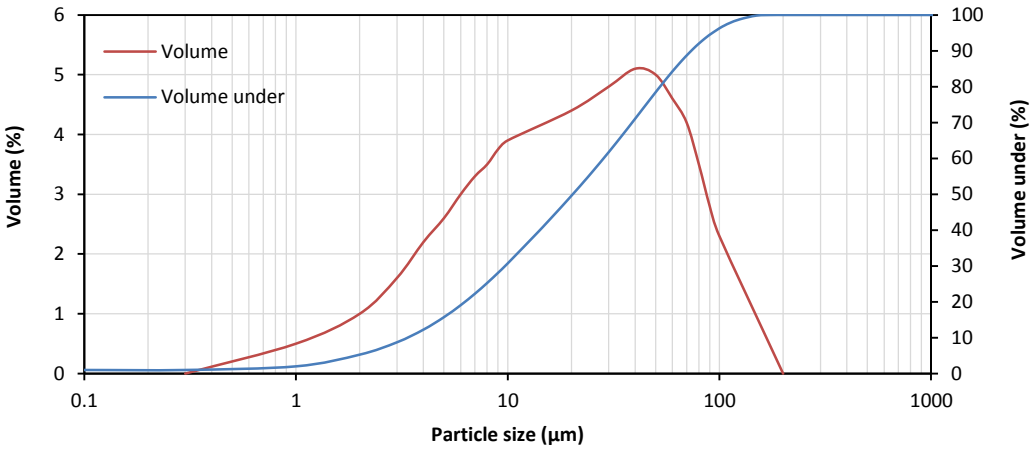

Figure 4.7 – Particle size distribution of powder

This type of carbon 208C is especially good for heat pumping applications. The carbon, prior to its use in the heat pump, was tested in a Rubotherm^{TM} magnetic balance to determine its adsorptive characteristics. The values obtained are shown in Table 4.4.

Limiting concentration	x_0	0.2551 kg/kg
Constant in D-A equation	K	3.9615
Exponent constant in D-A equation	n	1.227

Table 4.4 – Thermodynamic properties of carbon 208C

The heat transfer properties of the carbon are analysed in Chapter 7.

4.4. Generator filling process

The filling process of the generator was different for the small and the large generators as their manufacturing processes were different. In the following sections both filling processes are explained.

4.4.1. Small generators

The small generators were filled with a mixture of carbon grains, powder and binder (proprietary material, supplied by Chemviron) and its specifications are shown in Table 4.5. Water was added to the mixture to dissolve the binder so that it could help to create bridges between the carbon particles in order to increase the thermal conductivity of the sorbent.

Parameter	**Value**
Carbon type	Chemviron 208C
Mixture type	58% 20x40 grains, 29% powder and 13% binder
Carbon mass	0.985 kg
Sorption material volume	1.87 l
Packed density	527 kg/m^3

Table 4.5 – Properties of the carbon used in the small generators

The mixture was poured through the connectors of the shell and the generator was vibrated during the process. After this, the generators were heated at 100-200 °C in order to remove the water and then pyrolysed at 400-500 °C in order to transform the carbon binder into charcoal.

4.4.2. Large generators

The filling process of the large generators was different from the small ones. The large generators were designed as a two-part system, the core (end plates and tubes) and the shell so that they could be refilled and tested with different sorption materials.

In order to fill the cores with carbon, they were half-wrapped first with two layers of stainless steel gauze of different aperture size and one of borosilicate glass microfiber filter to prevent the fine carbon powder escaping from the generator. Their specifications can be found in Tables 4.6, 4.7 and 4.8.

Parameter	Value
Manufacturer	Locker wire wavers ltd
Model number	500 plain twill
Material	Stainless steel
Aperture size	0.026 mm
Wire diameter	0.025 mm

Table 4.6 – Fine gauze specifications

Parameter	Value
Manufacturer	Locker wire wavers ltd
Model number	300 plain twill
Material	Stainless steel
Aperture size	0.049 mm
Wire diameter	0.036 mm

Table 4.7 – Coarse gauze specifications

Parameter	Value
Manufacturer	Whatman
Model	28418398 (US reference), 1822-915
Thickness	0.26 mm
Pore size	1.2 µm

Table 4.8 – Glass filter specifications

The wrapping order was firstly the finest gauze in direct contact with the carbon and tubes, then the glass filter and finally the coarse gauze.

With half generator wrapped, it could be then filled with the carbon mixture. On this ocassion no binder was used in the mixture for a few reasons. The first reason is that once it is pyrolysed it creates a hard conglomerate of carbon that is very difficult to break if the core is wanted to be refilled with other sorption material. Another reason is that when the small generators were tested in the heat pump machine, low performance was recorded and it was suspected that the binder does not adhere the carbon to the steel tubes resulting in a low heat transfer coefficient.

The mixture chosen to fill the generator was made of grains and powder and its specifications are shown in Table 4.9.

Parameter	**Value**
Carbon type	Chemviron 208C
Mixture type	2/3 20x40 grains and 1/3 powder
Carbon mass	3 kg
Sorption material volume	4.7 l
Packed density	640 kg/m^3

Table 4.9 – Properties of the carbon used in the large generators

Once the generator was filled up with carbon the other half of it was wrapped with the gauze and glass filter and an epoxy adhesive (DP 760) manufactured by 3M was used to adhere the gauzes to the generator's rods and end plates. A picture of the finished generator can be seen in Figure 4.8.

Figure 4.8 – Large generator filled with carbon and wrapped in glass filter and gauze

4.5. Conclusion

The design and manufacturing process of two low thermal mass and high density power sorption shell and tube heat exchangers has been discussed. Both were made of nickel brazed stainless steel and had tubes of 1.2 mm outer and 0.8 inner diameters. The small generator had an end plate

diameter of 95.5 mm, length of 297 mm and 766 tubes and could contain roughly 1 kg of active carbon. The large generator had an end plate diameter of 144.5 mm, length of 396 mm and 1777 tubes and could contain up to 3 kg of active carbon.

The sorbent material, active carbon, characteristics were measured and characterised and filling techniques developed.

Chapter 5

Heat pump system design and simulation

5.1. Introduction

In this chapter the specifications of the 4 bed thermal wave cycle heat pump are outlined and the computational modelling of the system is carried out to in order to obtain the COP-SHP relationship.

5.2. System specifications

The heat pump design in this project was aimed to be used in a domestic environment (space and water heating), replacing the gas condensing boiler, the most widespread product used for domestic space heating in the UK. The domestic market has potential for significant reductions in energy usage and therefore carbon dioxide emissions.

For space heating of a typical family home in the UK, a three bedroom semi detached house, which is required to be maintained at an internal temperature of 18 °C, the heat pump should supply a heating power of 7 kW [1].

5.3. System design

An overview of the system design is shown in Figure 5.1. The machine was driven by the heat supplied by a gas burner and used pressurised water as heat transfer fluid. The water used in the heating system of the house is passed through the ammonia condenser and then through the cooler (fluid to fluid heat exchanger) where it increases its temperature.

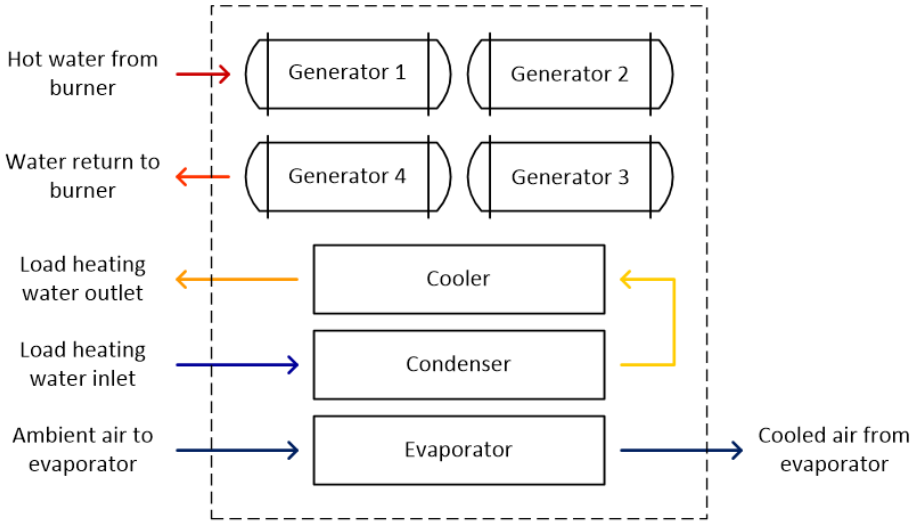

Figure 5.1 – Heat pump system diagram

The prototype of the heat pump designed and modelled was an air source heat pump, although it could have been a ground source if desired. Air source was chosen over ground source as the latter requires a suitable portion of land for bore-holes or coils and has a much higer cost.

5.3.1. Gas burner

A diagram of the gas burner arrangement that drives the heat pump is shown in Figure 5.2. The cycle starts with fresh air input to the burner, once the air passes through the burner it becomes exhaust gas at high temperature that heats the heat transfer fluid used to drive the heat pump. After this, the exhaust gas at a lower temperature is used to supply more heat to the load water system with an air to water heat exchanger before being exhausted.

The burner was not modelled in the simulation of the heat pump. It was assumed a constant temperature input to the machine. During the testing of the heat pump the driving heat was supplied by an electric heater in order to simplify the rig.

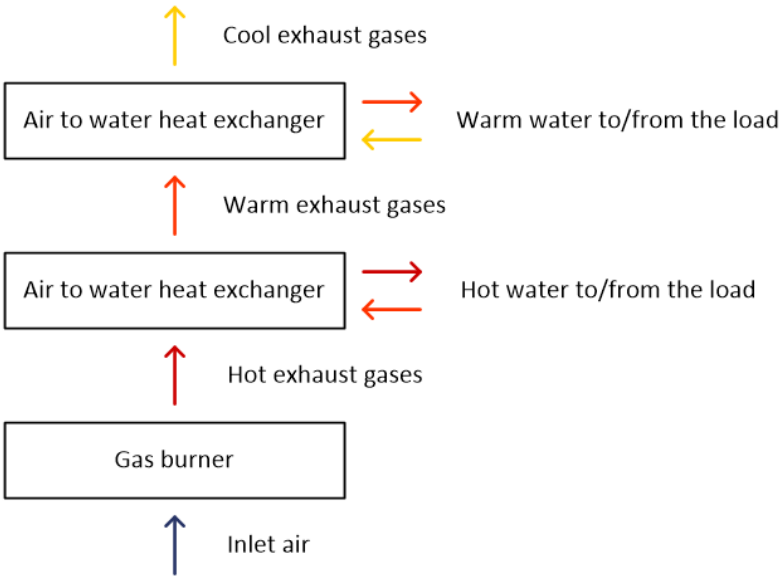

Figure 5.2 – Gas burner diagram

5.3.2. Generators

The specifications of the generator used in the following modelling description correspond to the large generators described in Chapter 4 and are listed in Table 5.1.

Parameter	Value and units
Carbon type	208C
Carbon mass, M_c	3 kg
Tube wall thickness, t_w	0.2 mm
Wall material	AISI 304L
Wall mass, M_w	4.98 kg
Fluid channel diameter, D_f	0.8 mm
Heat transfer area, A	1.77 m^2
Heat transfer coefficient fluid-wall, UA_{fw}	5497.5 W/K
Heat transfer coefficient wall-carbon, UA_{wc}	1169.5 W/K

Table 5.1 – Modelled generator specifications

5.3.3. Cooler, condenser and evaporator

Three of the components presented above are heat exchangers that needed to be specified in the model. Plate heat exchangers were used as the cooler and the condenser due to its compactness. A stainless steel tubes and aluminium fins fan coil was used as evaporator.

5.4. Material properties

5.4.1. Wall properties

The material used in the tube walls of the generator is stainless steel AISI 304L and its properties are listed in the Table 5.2. Stainless steel was selected as the wall material due to its compatibility with ammonia, corrosion resistance and high fatigue limit. Although the thermal conductivity of the steel is not very high it does not affect the overall heat transfer as the wall thickness is very low.

Property	Value and units
Specific heat, $c_{p,w}$	460 J/(kgK)
Thermal conductivity, k_w	16 W/(mK)
Density, d_w	8000 kg/m^3
Outer wall diameter, D_w	1.2 mm
Wall thickness, t_w	0.2 mm

Table 5.2 – Wall material properties [2]

5.4.2. Heat transfer fluid properties

The heat transfer fluid is water and its properties at a cycle average temperature of 100 °C are listed in Table 5.3. As the working temperature of the heat transfer fluid needs to be higher than 100 °C to achieve a good efficiency and power output the water lines are pressurised previously to testing. One disadvantage is that due to the pressure (up to 8 bars) the manifolds of the generators are quite bulky and increase the thermal mass of the system. On the other side, the main advantage is that it has a relatively high thermal conductivity (five times higher than oil).

Property	Value and units
Specific heat, $c_{p,f}$	4219 J/(kgK)
Thermal conductivity, k_f	0.68 W/(mK)
Density, d_f	958 kg/m^3
Fluid channel diameter, D_f	0.8 mm

Table 5.3 – Heat transfer fluid properties [3]

5.4.3. Sorption material properties

The sorption material used in this system is carbon type 208C based on coconut shell precursor manufactured by Chemviron Carbon Ltd, its specifications are listed in Table 5.4. The generators were filled with a binary mixture of grains and powder and were vibrated in order to obtain a high

carbon density. More information regarding carbon characteristics and generator filling can be obtained in Chapter 4.

The carbon 208C was also chosen for its good ammonia sorption characteristics.

Property	**Value and units**
Carbon type	208C
Specific heat (function of the temperature in Kelvin), $c_{p,c}$	$175+2.245 \cdot T_c$ J/(kgK)
Thermal conductivity (solid carbon), k_c	0.85 W/(mK)
Density (solid carbon), d_c	1000 kg/m^3
Limiting (maximum) concentration, x_0	0.255 kg/kg
Constant in the modified Dubinin-Astakhov equation, K	3.962
Exponent in the modified Dubinin-Astakhov equation, n	1.227

Table 5.4 – Sorption material properties

5.4.4. Refrigerant properties

The refrigerant used in the heat pump system is ammonia and its specifications are listed in Table 5.5.

Property	**Value and units**
Specific heat of liquid, c_{pamm}	6677 J/(kgK)
Thermal conductivity, k_{amm} (at 100 °C)	0.06 W/(mK)
Slope of saturated ammonia line on Clapeyron diagram, C	2823.4

Table 5.5 – Refrigerant properties [3]

5.5. Model assumptions and governing equations

5.5.1. Generator model

A computational model using a two-dimensional finite difference grid was written in order to analyse the heat pump cycle.

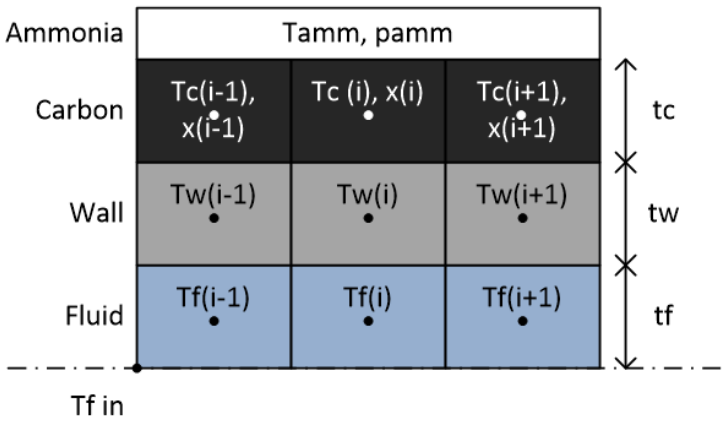

Figure 5.3 – Schematic diagram of the modelled generator

The generator model is a lumped finite difference model in which the heat transfer fluid, the wall and the sorption material are represented by single elements, as shown in Figure 5.3.

The generator model contains two heat transfer coefficients, one between the fluid and the wall and other between the wall and the carbon. In the case of the wall-carbon heat transfer coefficient it can be assumed that there is perfect contact between them or that there exists a wall contact resistance. The thermal resistance of the steel wall was considered negligible due to its low thickness and relatively high thermal conductivity (if compared to the water and carbon).

As a thermal wave is being modelled, conduction along the wall and the carbon has been taken into account.

The flow in the beds was investigated to ensure that the flow was laminar in all cases. Equation 5.1 was used to calculate the Reynolds number:

$$Re = \frac{d_f \, v \, D_h}{\mu} = \frac{\dot{m}_f \, D_h}{d_f \, v \, A} \tag{5.1}$$

where

d_f is the fluid density (kg/m^3)

v is the mean velocity of the fluid (m/s)

D_h is the hydraulic diameter of the pipe (m)

μ is the dynamic viscosity of the fluid (kg/(ms))

$\dot{m}_f$ is the water mass flow (kg/s)

v is the kinematic viscosity (m^2/s)

A is the cross section area of the pipe (m^2)

It was confirmed that the flow was laminar in all cases investigated, achieving a maximum Reynolds number of 310.

The heat transfer coefficient between the fluid and the wall was calculated with the Equation 5.2 and with values of Nusselt number for fully developed laminar flow in circular pipes. *Nu* numbers were provided under the following conditions:

- Uniform surface heat flux: *Nu* = 4.36
- Uniform surface temperature *Nu* = 3.66

Neither of these two extreme conditions match those in the beds so an average of *Nu* = 4 was used in the model.

$$Nu = \frac{h_{fw} D_h}{k_f} \tag{5.2}$$

Nu is the Nusselt number

h_{fw} is the heat transfer coefficient between fluid and wall (W/(m^{2}K))

k_f is the fluid thermal conductivity (W/(mK))

The fluid-wall heat transfer coefficient was calculated as:

$$h_{fw} = \frac{4\, k_f}{D_f} \tag{5.3}$$

where

D_f is the fluid channel diameter (inner diameter of the pipe) (m)

The overall heat transfer coefficient between the wall and the carbon was calculated both considering a perfect contact between the wall and the carbon and as well considering the resistance effect of a thin layer of ammonia around the wall.

For the perfect contact case, the heat transfer coefficient is described in Equation 5.4.

$$h_{wc} = \frac{2\, k_c}{D_w \ln\left(\frac{D'}{D_w}\right)} \tag{5.4}$$

where

h_{wc} is the heat transfer coefficient between wall and carbon (W/(m^{2}K))

k_c is the carbon effective thermal conductivity (W/(mK))

D_w is the outer diameter of the pipe (m)

D' is the diameter that divides the carbon control area (hexagon) in two equal areas (m) (see Figure 5.4) (m)

For the surface resistance effect case, the wall-carbon heat transfer coefficient previously described is combined with the wall-ammonia heat transfer coefficient, described in Equation 5.5.

$$h_{wamm} = \frac{2\,k_{amm}}{D_w \ln\left(\frac{D_w + 2\,t_{amm}}{D_w}\right)} \tag{5.5}$$

where

h_{wamm} is the heat transfer coefficient between wall and ammonia (W/(m^{2}K))

k_{amm} is the ammonia thermal conductivity (W/(mK))

t_{amm} is the thickness of the ammonia layer surrounding the wall (m)

The total heat transfer coefficient wall-ammonia-carbon (h_{wcamm}) is calculated with Equation 5.6.

$$h_{wcamm} = \frac{1}{\frac{1}{h_{wc}} + \frac{1}{h_{wamm}}} \tag{5.6}$$

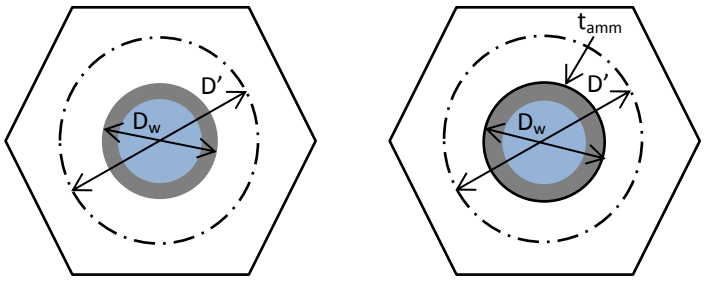

Figure 5.4 – Cross section area of a generator's tube (a) Case with perfect contact between wall and carbon, (b) Case with convective effect of ammonia on the tube.

One of the equations used in the simulation that calculates the heat transfer between the fluid and the wall of the generator is a log mean temperature difference, Equation 5.7.

$$LMTD_{fw} = \frac{(T_{f,in} - T_w) - (T_{f,out} - T_w)}{\ln\left(\frac{T_{f,in} - T_w}{T_{f,out} - T_w}\right)} \tag{5.7}$$

where

$LMTD_{fw}$ is the log mean temperature difference between the fluid and the wall (K)

$T_{f,in}$ is the fluid inlet temperature (K)

$T_{f,out}$ is the fluid outlet temperature (K)

T_w is the wall temperature (K)

The governing equations of the model are shown below:

Energy balance equation of the fluid:

$$\frac{UA_{fw}}{N}\left(T_{w,(i,j)} - T_{f,(i,j)}\right) - \frac{\dot{m}_f\, c_{p,f}}{2}\left(T_{f,(i+1,j)} - T_{f,(i-1,j)}\right) = \frac{M_f\, c_{v,f}}{N\,\Delta t}\left(T_{f,(i,j+1)} - T_{f,(i,j)}\right) \quad (5.8)$$

Energy balance equation of the wall:

$$\frac{UA_{wc}}{N}\left(T_{c,(i,j)} - T_{w,(i,j)}\right) + \frac{UA_{fw}}{N}\left(T_{f,(i,j)} - T_{w,(i,j)}\right) + \frac{k_w\, A_w}{2\,\Delta l}\left(T_{w,(i+1,j)} + T_{w,(i-1,j)} - 2\,T_{w,(i,j)}\right) =$$

$$\frac{M_w\, c_{pw}}{N\,\Delta t}\left(T_{w,(i,j+1)} - T_{w,(i,j)}\right) \quad (5.9)$$

Energy balance equation of the carbon:

$$\frac{k_c\, A_c}{2\,\Delta l}\left(T_{c,(i+1,j)} + T_{c,(i-1,j)} - 2\,T_{c,(i,j)}\right) + \frac{UA_{wc}}{N}\left(T_{w,(i,j)} - T_{c,(i,j)}\right) = \frac{M_c}{\Delta t}\left(c_{p,c} + x\, c_{p,amm}\right)\left(T_{c,(i,j+1)} - T_{c,(i,j)}\right) - M_c\, H_{ads}\frac{x_{(i,j+1)} - x_{(i,j)}}{\Delta t} \quad (5.10)$$

where

i and *j* indicate longitudinal position in the bed and time respectively (-)

UA_{fw} is the overall fluid-wall heat transfer coefficient (W/K)

UA_{wc} is the overall wall-carbon heat transfer coefficient (W/K)

T_f is the fluid temperature (K)

T_w is the wall temperature (K)

T_c is the carbon temperature (K)

$\dot{m}_f$ is the fluid mass flow rate (kg/s)

$c_{p,f}$ is the specific heat capacity at constant pressure of the fluid (J/(kgK))

$c_{p,w}$ is the specific heat capacity at constant pressure of the wall (J/(kgK))

$c_{p,c}$ is the specific heat capacity at constant pressure of the carbon (J/(kgK))

$c_{p,amm}$ is the specific heat capacity at constant pressure of the ammonia (J/(kgK))

$c_{v,f}$ is the specific heat capacity at constant volume of the fluid (J/(kgK))

M_f is the fluid mass in the control volume (kg)

M_w is the wall mass in the control volume (kg)

M_c is the carbon mass in the control volume (kg)

k_w is the wall thermal conductivity (W/(mK))

k_c is the carbon effective thermal conductivity (W/(mK))

A_w is the cross section area of the wall (m^2)

A_c is the cross section area of the carbon (m^2)

N is the number of longitudinal divisions of the bed (-)

Δt is the time step (s)

Δl is the longitudinal length step (m)

As a thermal wave was modelled, conduction along the wall and carbon was taken into account.

The model is based on an ideal cycle and it is assumed that the adsorption and desorption stages happen at a constant pressure, i.e. they are isobaric processes. This assumption enables Equation 5.10 to be integrated through time obtaining the following equation:

$$\frac{x_{(i,j+1)}-x_{(i,j)}}{\Delta t}=\frac{\Delta x}{\Delta t}=\left(\frac{\partial x}{\partial T_c}\right)\frac{\Delta T_c}{\Delta t}+\left(\frac{\partial x}{\partial p}\right)\frac{\Delta p}{\Delta t}=\left(\frac{\partial x}{\partial T_c}\right)\frac{\Delta T_c}{\Delta t}+\left(\frac{\partial x}{\partial T_{sat}}\right)\frac{\Delta T_{sat}}{\Delta t} \tag{5.11}$$

The amount of adsorbed ammonia in the carbon is calculated with a modified Dubinin – Astakhov equation presented by Critoph [4].

$$x = x_0\, e^{-K\left(\frac{T_c}{T_{sat}}-1\right)^n} \tag{5.12}$$

where

x refrigerant concentration (kg/kg)

x_0 limiting (maximum) refrigerant concentration (kg/kg)

K is a constant (-)

T_c is the carbon temperature (K)

T_{sat} is the saturation temperature of the ammonia (K)

n is a constant (-)

The partial derivatives of Equation 5.11 can be calculated analytically as:

$$\left(\frac{\partial x}{\partial T_c}\right)_p=\left(\frac{\partial x}{\partial T_c}\right)_{T_{sat}}=-\frac{K\,n\,x}{T_{sat}}\left(\frac{T_c}{T_{sat}}-1\right)^{n-1} \tag{5.13}$$

$$\left(\frac{\partial x}{\partial p}\right)_{T_c}=\left(\frac{\partial x}{\partial T_{sat}}\right)_{T_c}=\frac{K\,n\,x\,T_c}{{T_{sat}}^2}\left(\frac{T_c}{T_{sat}}-1\right)^{n-1} \tag{5.14}$$

Finally obtaining the variation of refrigerant concentration over time:

$$\frac{\Delta x}{\Delta t}=\frac{K\,n\,x}{\Delta t\,T_{sat}}\left(\frac{T_c}{T_{sat}}-1\right)^{n-1}\left(\frac{\Delta T_{sat}\,T_c}{T_{sat}}-\Delta T_c\right) \tag{5.15}$$

Equation 5.10 is rewritten as:

$$\frac{k_c\,A_c}{2\,\Delta l}\left(T_c(i+1,j)+T_c(i-1,j)-2\,T_c(i,j)\right)+\frac{UA_{wc}}{N}\left(T_w(i,j)-T_c(i,j)\right)=M_c\left(c_{p,c}+x\,c_{p,amm}\right)\frac{\Delta T_c}{\Delta t}-$$

$$M_c\,H_{ads}\,\frac{K\,n\,x}{\Delta t\,T_{sat}}\left(\frac{T_c}{T_{sat}}-1\right)^{n-1}\left(\frac{\Delta T_{sat}\,T_c}{T_{sat}}-\Delta T_c\right) \tag{5.16}$$

The enthalpy of adsorption or isosteric heat of adsorption was calculated from Equation 5.17.

$$H_{ads} \cong \frac{C\, R_{gas}\, T_{amm}}{T_{sat}} \tag{5.17}$$

where

H_{ads} is the ammonia enthalpy of adsorption (J/kg)

C is the slope of saturated ammonia on a Clapeyron diagram (-)

R_{gas} is the ammonia gas constant (J/(kgK))

T_{amm} is the ammonia temperature (K)

The specific heat capacity of the carbon is variable and depends on its temperature. It can be calculated with Equation 5.18 which provides a linear relationship between heat capacity and temperature, obtained by Turner [5] from experimental data.

$$c_{p,c} = 175 + 2.245\, T_c \tag{5.18}$$

The specific heat capacity of the ammonia is assumed to have a constant value of 4734 J/(kgK) as suggested by Critoph [6].

5.5.2. Condenser model

The ammonia gas desorbed from the carbon leaves the beds and goes into the condenser in a superheated state. In the condenser, at a constant pressure, the ammonia gas releases heat in order to be desuperheated and be transformed into liquid. The rate of heat release in the condenser is calculated as a function of the desorbed ammonia by the beds with Equation 5.19.

$$\dot{Q}_{cond} = M_c \frac{\partial x}{\partial time}\left(H_{sup}(p_{cond}, T_c) - H_f(p_{cond})\right) \tag{5.19}$$

where

$\dot{Q}_{cond}$ is the heating power produced in the condenser (W)

p_{cond} is the condensing pressure (bar)

H_{sup} is the enthalpy of the superheated ammonia gas (J/kg)

H_f is the enthalpy of the saturated ammonia liquid (J/kg)

Due to the fact that the heat pump has 4 beds, it is possible that more than one bed desorbs ammonia at the same time therefore the total amount of ammonia going into the condenser is calculated by adding the partial desorptions of each bed. The heat released by the condenser can be calculated with its heat transfer coefficient and logarithm mean temperature difference or with the heat transfer fluid mass flow and its increase in temperature.

$$\dot{Q}_{cond} = UA_{cond}\ LMTD_{cond} = \dot{m}_{cond}\ c_{p,fcond}(T_{fcond,in} - T_{fcond,out}) \quad (5.20)$$

where

$\dot{Q}_{cond}$ is the heating power produced in the condenser (W)

UA_{cond} is the heat transfer coefficient of the condenser (W/K)

$T_{fcond,in}$ is the inlet water temperature to the condenser (K)

$T_{fcond,out}$ is the outlet water temperature from the condenser (K)

T_{cond} is the condensing temperature (K)

$\dot{m}_{cond}$ is the mass flow of fluid through the condenser (kg/s)

$c_{p,fcond}$ is the specific heat capacity of the condenser fluid (J/(kg K))

Equation 5.20 can be rearranged using the equivalent ***ε-NTU*** method

$$\dot{Q}_{cond} = \varepsilon_{cond}\ C_{min}\left(T_{fcond,in} - T_{cond}\right) = UA_{cond}\ \varepsilon_{cond}\left(T_{fcond,in} - T_{cond}\right) \quad (5.21)$$

The effectiveness of the condenser, ε_{cond}, is defined as

$$\varepsilon_{cond} = 1 - e^{-NTU_{cond}} \quad (5.22)$$

And the number of transfer units, NTU_{cond}, is defined as

$$NTU_{cond} = \frac{UA_{cond}}{C_{min}} \quad (5.23)$$

C_{min} is the lowest heat capacity rate (mass flow multiplied by specific heat) of the two streams flowing through the condenser (in this case it is the heat transfer fluid stream) (W/K).

The heat transfer,$\dot{Q}_{cond}$, is given by

$$\dot{Q}_{cond} = \frac{UA_{cond}}{NTU}\left(T_{fcond,in} - T_{cond}\right)(1 - e^{-NTU}) \quad (5.24)$$

The energy balance equation for the condenser, taking into account the losses due to the superheated state of the ammonia entering the condenser and the thermal mass of the condenser, is given by

$$\dot{Q}_{cond}\ \Delta t = M_{amm,liq}\ L - M_{cond}\ c_{p,cond}(T_{amm} - T_{cond}) + \Delta Q_{desup} \quad (5.25)$$

where

Δt is the model time step (s)

$M_{amm,liq}$ amount of ammonia condensed in the model time step (kg)

L is the ammonia latent heat (J/kg)

M_{cond} is the condenser mass (kg)

$c_{p,cond}$ is the specific heat capacity of the condenser (J/(kgK))

T_{amm} is the temperature of ammonia entering the condenser (K)

ΔQ_{desup} is the heat used to desuperheat the ammonia entering the condenser (J)

It is assumed that the entire mass of the condenser, M_{cond}, is at condensing temperature, T_{cond}.

The desuperheating energy is defined by the following equation

$$\Delta Q_{desup} = \sum \dot{m}_{check} \left(H_{sup}(p_{cond}, T_c) - H_g(p_{cond}) \right) \Delta t \tag{5.26}$$

where

H_g is the enthalpy of the saturated ammonia gas (J/kg)

$\dot{m}_{check}$ is the refrigerant mass flow through the check valve in this case entering the condenser (kg/s)

The desuperheating process takes into account the ammonia desorbed from more than one bed.

5.5.3. Evaporator model

The ammonia that enters the evaporators after passing through the expansion valves is a mixture of liquid and gas. In the evaporators, at a constant pressure, all the ammonia liquid becomes saturated gas by absorbing heat. The heat absorbed in the evaporator, power input, is calculated as a function of the adsorbed ammonia by the beds with Equation 5.27.

$$\dot{Q}_{ev} = M_c \frac{\partial x}{\partial time} \left(H_g(p_{ev}) - H_f(p_{cond}) \right) \tag{5.27}$$

where

$\dot{Q}_{ev}$ is the cooling power produced in the evaporator (W)

p_{ev} is the evaporating pressure (bar)

Due to the fact that the heat pump has 4 beds, it is possible that more than one bed desorbs ammonia at the same time therefore the total amount of ammonia going from the evaporators to the beds is calculated by adding the partial adsorption of each bed.

$$\dot{Q}_{ev} = \dot{m}_{ev}\, c_{p,air} \left(T_{air,in} - T_{air,out} \right) = UA_{ev}\, \varepsilon_{ev} \left(T_{air,in} - T_{ev} \right) \tag{5.28}$$

where

$\dot{m}_{ev}$ is the mass flow of air through the evaporators (kg/s)

$c_{p,air}$ is the specific heat capacity at constant pressure of the air flowing through the evaporators (J/(kgK))

$T_{air,in}$ is the inlet air temperature to the evaporators (K)

$T_{air,out}$ is the outlet air temperature from the evaporators (K)

UA_{ev} is the overall heat transfer coefficient of the evaporator (W/K)

ε_{ev} is the effectiveness of the evaporator (-)

T_{ev} is the evaporating temperature (K)

The effectiveness of the evaporator, ε_{ev}, is defined as

$$\varepsilon_{ev} = 1 - e^{-NTU_{ev}} \tag{5.29}$$

And the number of transfer units, NTU_{ev}, is defined as

$$NTU_{ev} = \frac{UA_{ev}}{\dot{m}_{air}\, c_{p,air}} \tag{5.30}$$

The energy balance equation for the evaporator is given by

$$\dot{Q}_{ev}\, \Delta t = M_{amm,liq}\, L - M_{ev}\, c_{p,ev}(T_{amm} - T_{ev}) \tag{5.31}$$

where

$M_{amm,liq}$ amount of ammonia evaporated in the model time step (kg)

M_{ev} is the evaporator mass (kg)

$c_{p,ev}$ is the specific heat capacity of the evaporator (J/(kgK))

T_{amm} is the temperature of ammonia leaving the evaporator (K)

T_{ev} is the temperature of the evaporator (K)

It is assumed that the entire mass of the evaporator, M_{ev}, is at evaporating temperature, T_{ev}.

5.5.4. Check valve model

The check valve controls the amount of refrigerant (ammonia) that goes from beds to condenser or from the evaporator to the beds. Each bed has two check valves:

- One check valve controls the flow of desorbed ammonia that leaves the bed and goes into the condenser when the pressure of the bed is higher than the pressure in the condenser (condenser check valve).
- The other check valve controls the flow of ammonia that is adsorbed in the bed and that comes from the evaporators when the pressure in the bed is lower than the pressure in the evaporators (evaporator check valve).

For the case of the condenser check valve the mass flow that leaves the bed is calculated by Equation 5.32.

$$\dot{m}_{check} = k_{check}\sqrt{p_{bed} - p_{cond}} \tag{5.32}$$

when $p_{bed} > p_{cond}$. If $p_{bed} \leq p_{cond}$ then $\dot{m}_{check} = 0$.

For the case of the evaporator check valve the mass flow that leaves the bed is calculated by Equation 5.33.

$$\dot{m}_{check} = k_{check}\sqrt{p_{ev} - p_{bed}} \tag{5.33}$$

when $p_{ev} > p_{bed}$. If $p_{ev} \leq p_{bed}$ then $\dot{m}_{check} = 0$.

where

k_{check} is the check valve proportionality constant (-)

p_{bed} is the pressure in the bed (bar)

p_{cond} is the pressure in the condenser (bar)

p_{ev} is the pressure in the evaporator (bar)

The value of k_{check} was chosen so that it produces a low pressure drop and stable results.

These equations do not take into account the cracking pressure of the check valves but it can be easily introduced by applying an offset to the pressure differences.

5.5.5. Receiver model

The condensed ammonia in the condenser passes to the receiver where it is stored and mixed completely with the previous stored ammonia creating a homogeneous liquid. It is assumed that the receiver is at the same temperature than the liquid ammonia stored in it, that the expansion valves are ideal, and that the amount of ammonia that is adsorbed in the beds is equal to the amount of ammonia that leaves the receiver. The temperature of the liquid ammonia in the receiver and the receiver are given by

$$T'_{rec} = \frac{T_{rec}\left(M_{liq,rec} - \Delta M_{liq,ev}\right) + T_{cond}\Delta M_{liq,cond}}{M_{liq,rec} + \Delta M_{liq,cond} - \Delta M_{liq,ev}} \tag{5.34}$$

T'_{rec} is the temperature of the receiver and liquid ammonia in the future time step (K)

T_{rec} is the temperature of the receiver at the present time step (K)

$M_{liq,rec}$ is the amount of ammonia liquid in the receiver (kg)

$\Delta M_{liq,ev}$ is the amount of ammonia liquid that leaves the receiver and enters the evaporator in a time step (kg)

$\Delta M_{liq,cond}$ is the amount of ammonia liquid that leaves the condenser and enters the receiver in a time step (kg)

5.5.6. Cooler model

The cooler transfers heat between the bed's fluid and the load's fluid. It is modelled with the effectiveness method and it is assumed that there are no heat losses.

$$\dot{Q}_{cooler} = \dot{m}_f c_{p,f} \Delta t \left(T_{f,in\ cooler} - T_{f,out\ cooler}\right) = \varepsilon_{cooler} C_{min} \left(T_{f,in\ cooler} - T_{fcond,in}\right) \quad (5.35)$$

$T_{f,in\ cooler}$ is the temperature inlet to the cooler of the bed heat transfer fluid (K)

$T_{f,out\ cooler}$ is the temperature outlet from the cooler of the bed heat transfer fluid (K)

ε_{cooler} is the effectiveness of the cooler (-) that is defined by Equation 5.36

$$\varepsilon_{cooler} = \frac{1-e^{-NTU_{cooler}(1-C_r)}}{1-C_r e^{-NTU_{cooler}(1-C_r)}} \quad (5.36)$$

The number of transfer units of the cooler, NTU_{cooler}, is defined by

$$NTU_{cooler} = \frac{UA_{cooler}}{\min(\dot{m}_f\, c_{p,f}, \dot{m}_{cond}\, c_{p,fcond})} \quad (5.37)$$

UA_{cooler} is the overall heat transfer coefficient of the cooler (W/K)

The heat capacity ratio, C_r, and the lower and the higher heat capacity rates, C_{min} and C_{max}, are defined by

$$C_r = \frac{C_{min}}{C_{max}} = \frac{\min(\dot{m}_f\, c_{p,f}, \dot{m}_{cond}\, c_{p,fcond})}{\max(\dot{m}_f\, c_{p,f}, \dot{m}_{cond}\, c_{p,fcond})} \quad (5.38)$$

5.6. Implementation technique and programming language

The model equations are solved using an explicit time scheme which is quickly written and easy to modify although this type of method requires small time and length step for stability.

Time steps used in the simulations were 1/10 s and 1/20 s, depending on the fluid flow rate. Higher time steps could have been used but the running time of the cycle made it prohibitive (each case can take up to 4 h to be simulated, depending on cycle time). Length steps used in the simulations were 1 mm . Simulations were run until cyclic behaviour was obtained (usually after ten cycles).

The model was written in Matlab™ and it is included in Appendix A.

References

[1] Metcalf, S. J., Compact, efficient carbon-ammonia adsorption heat pump, Ph.D. Thesis, University of Warwick, UK, 2009.

[2] Callister, W.D., Materials science and engineering an introduction, 5th Edition, Wiley, ISBN 0-471-32013-7, pp. 807-810, 1999.

[3] CRC Handbook of Chemistry and Physics, 93rd Edition edited by William M. Haynes, ISBN 1-61-197198-5, 2012.

[4] Critoph, R. E., Adsorption refrigerators and heat pumps, Carbon materials for advanced technologies, Elsevier, ISBN 0-08-042683-2, Chapter 10.

[5] Turner, L., Improvement of activated charcoal-ammonia adsorption heat pumping/refrigeration cycles. Investigation of porosity and heat/mass transfer characteristics, Ph.D. Thesis, University of Warwick, UK, 1992.

[6] Critoph, R. E., Evaluation of alternative refrigerant-adsorbent pairs for refrigeration cycles, Applied Thermal Engineering, 16, pp. 891-900, 1996.

Chapter 6

Simulation results

6.1. Introduction

Once the heat pump system is modelled different set of conditions and parameters are varied in order to study the effect they have on the machine performance and to obtain the desired trade-off between the heating COP and the specific heating power.

6.2. Modelling results

6.2.1. Detailed analysis of a sample cycle

The first set of results presented depends on the properties of the generators and the cycle parameters for the heat pump cycle. The parameters set for this first simulation are presented in Table 6.1.

Parameter	**Value**
Cycle time	260 s
Heat transfer fluid mass flow	0.0375 kg/s
Hot driving temperature	170 °C
Condensing temperature	40 °C
Evaporating temperature	0 °C
Carbon effective thermal conductivity	0.3 W/(mK)

Table 6.1 – Simulation parameters

With the parameters shown above the power output of the heat pump is 6.77 kW (0.56 kW/kg) with a heating COP of 1.49 and the amount of ammonia cycled in the machine over the cycle is 0.52 kg.

Figures 6.1 and 6.2 show the temperature profile of the water, heat transfer fluid, during one cycle inside one of the generators (number 1). In Figure 6.1 it is possible to observe the water temperature

profile from the water inlet end of the generator (Generator length divisions = 1) whilst in Figure 6.2 it is possible to observe the water temperature profile from the water outlet end of the generator (Generator length divisions = 40).

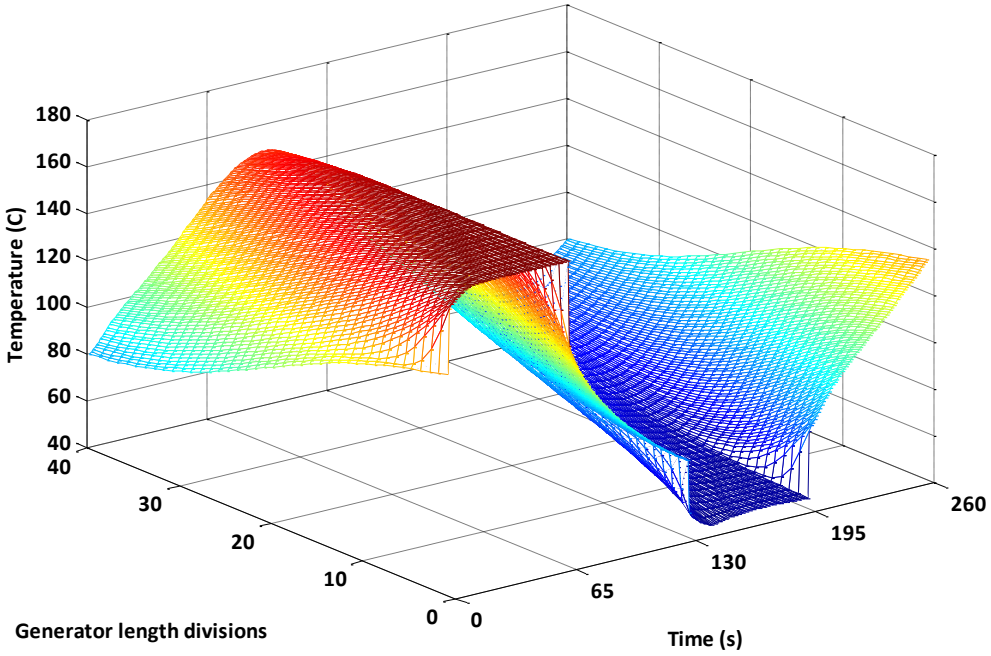

Figure 6.1 – Temperature of water flowing through generator 1 during a complete cycle (inlet side)

From 0 to 65 s the generator is being heated and receives hot water from the electric heater (or gas burner), from 65 to 130 s the generator is being precooled with outlet water coming from other generator that at the same is being cooled. From 130 to 195 s the generator is being cooled with water that comes from the cooler and finally 195 to 260 s the generator is being preheated with outlet water coming from other generator that at the same time is being heated.

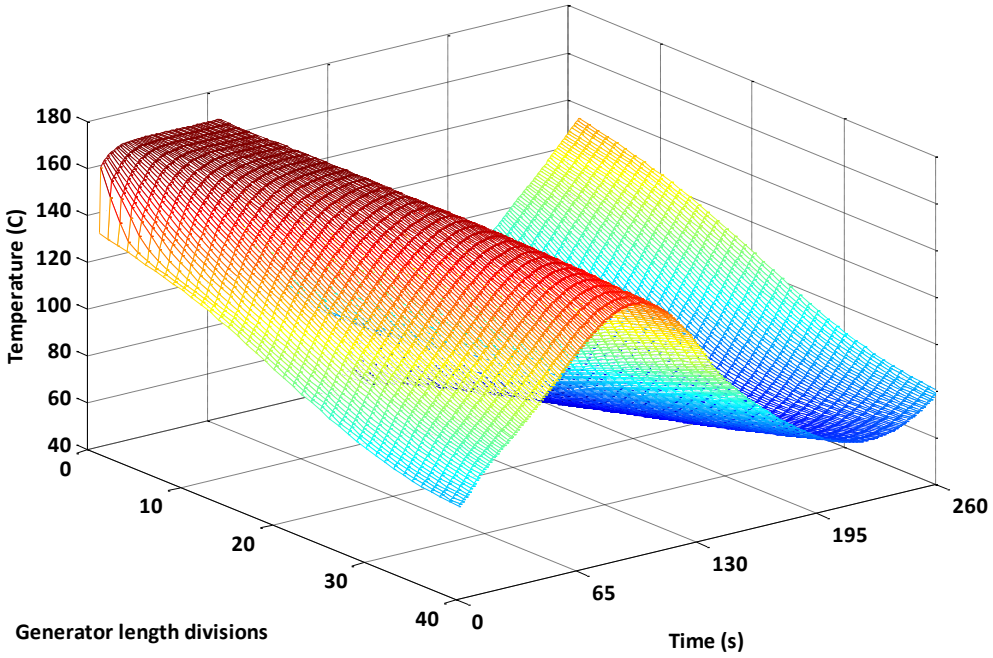

Figure 6.2 – Temperature of water flowing through generator 1 during a complete cycle (outlet side)

Figures 6.3 and 6.4 show the temperature of the carbon, sorption material, during one cycle inside one of the generators (number 1). In Figure 6.3 it is possible to observe the carbon temperature profile from the water inlet end of the generator (Generator length divisions = 1) whilst in Figure 6.4 it is possible to observe carbon temperature profile from the water outlet end of the generator (Generator length divisions = 40).

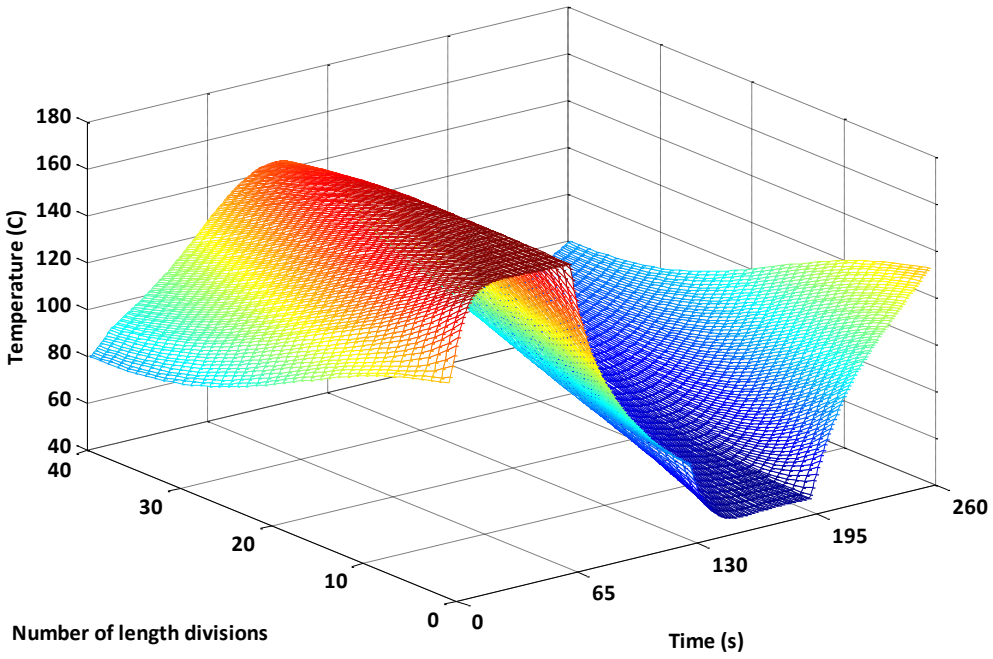

Figure 6.3 – Carbon temperature of generator 1 during a complete cycle (water inlet side)

Both carbon temperature figures show very similar values as the water temperature figures but in this case the temperature change between cycle stages is softened by the heat transfer in the bed.

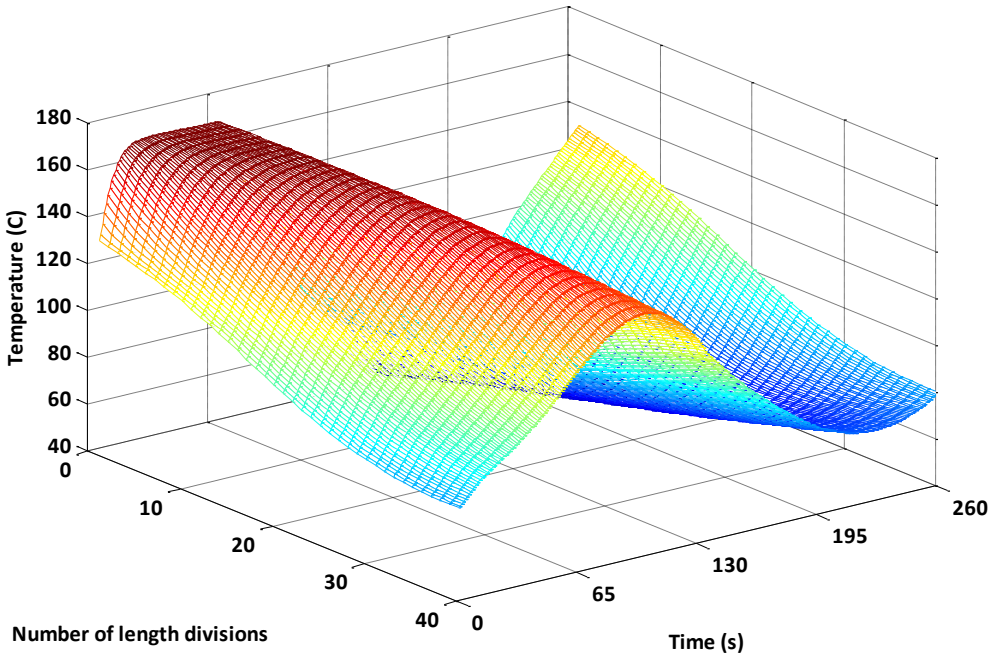

Figure 6.4 – Carbon temperature of generator 1 during a complete cycle (water outlet side)

Figure 6.5 shows the ammonia pressure profile in a generator during a complete cycle. From 0 to 65 s the bed is heated and its pressure increases rapidly until it reaches the condensing pressure whilst the bed desorbs ammonia. From 65 to 130 s the bed is precooled and the pressure of ammonia decreases sharply. From 130 to 195 s the bed is cooled and its pressure reaches the evaporating pressure whilst the bed adsorbs ammonia. Finally from 195 to 260 s the bed is preheated and its pressure increases.

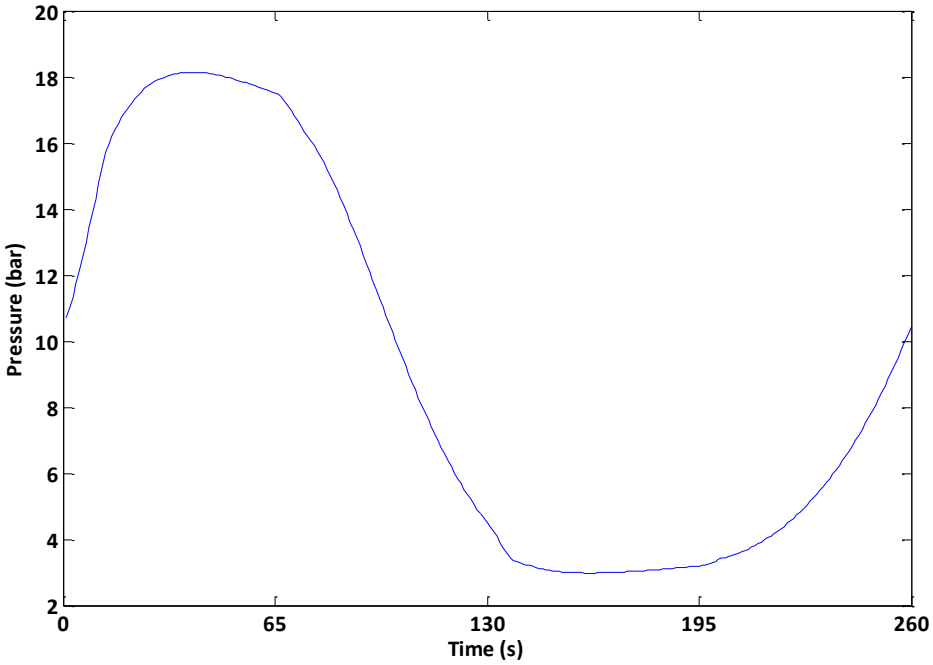

Figure 6.5 – Ammonia pressure in generator 1 during a complete cycle

In Figure 6.6 the pressure of the four generators are plotted over one cycle. The black line indicates the pressure of the condenser as driven by the ammonia desorption pressure of the generators. The grey line represents the pressure of the evaporator that is similarly determined by ammonia adsorption pressure in the generators.

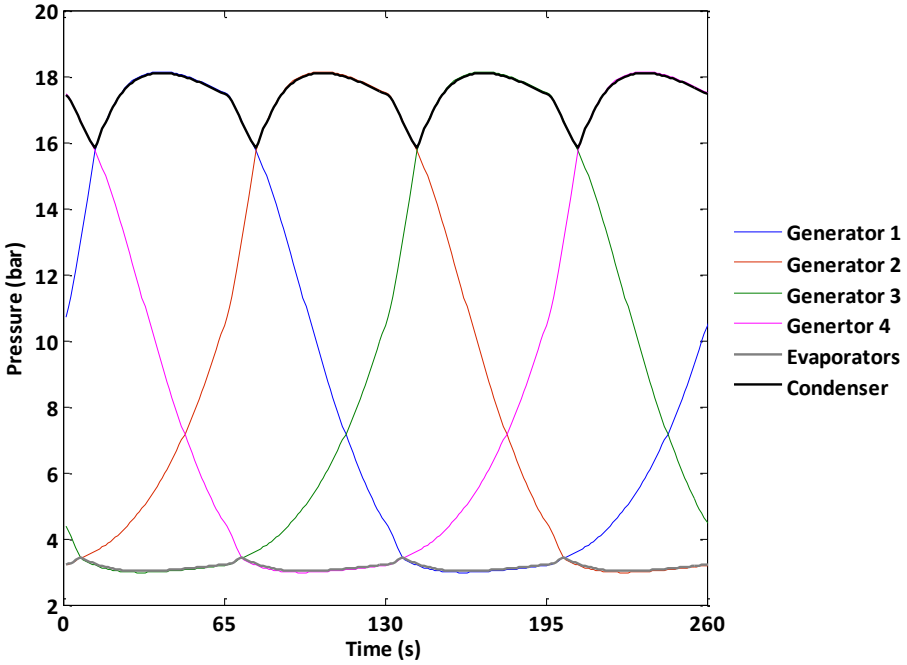

Figure 6.6 – Ammonia pressure of generators 1, 2, 3, 4, condenser and evaporators in a complete cycle

Figures 6.7 and 6.8 show the ammonia concentration in the generator number 1 during a complete cycle. In Figure 6.7 it is possible to observe the bed ammonia concentration from the water inlet end of the generator (Generator length divisions = 1) whilst in Figure 6.8 it is possible to observe the ammonia concentration from the water outlet end of the generator (Generator length divisions = 40).

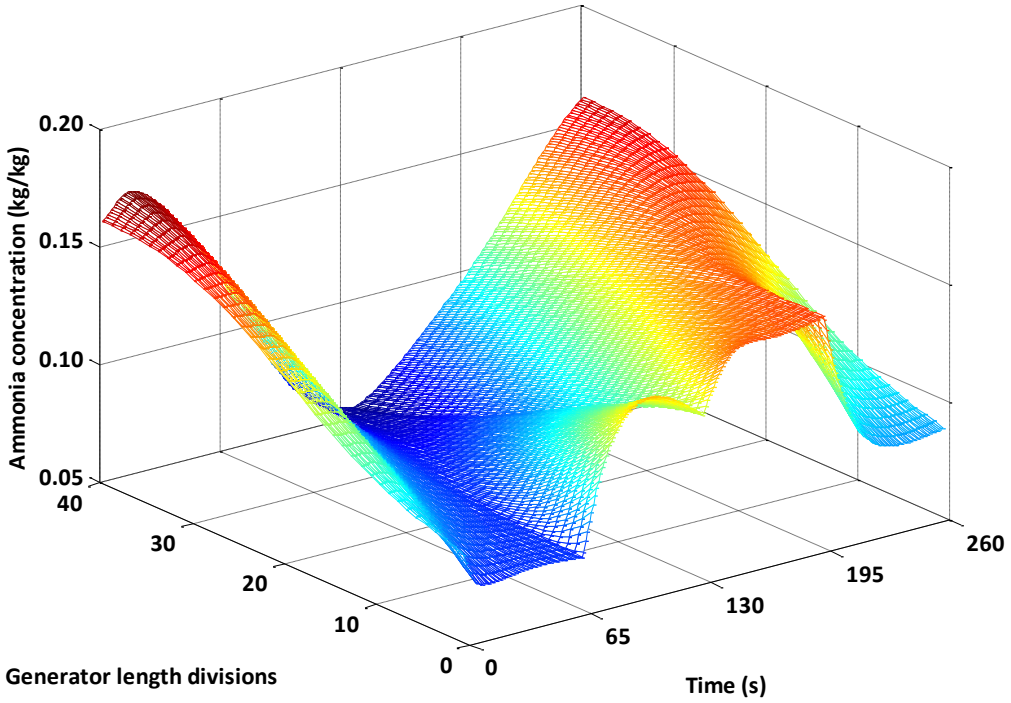

Figure 6.7 – Ammonia concentration in Generator 1 during a complete cycle (water inlet side)

From 0 to 65 s the generator is being heated and it is possible to observe how the ammonia concentration decreases in the inlet water side of the bed. In the outlet water side of the bed at the beginning of the stage an increase in the concentration is observed possible due to slightly colder water from the previous stage of the thermal wave flowing through the generator. Towards the end of the heating stage (65 s) the ammonia concentration decreased in all the beds.

From 65 to 130 s the generator is being precooled and an increase in ammonia concentration is observed only in the water inlet side of the bed. It is possible that the hot water from the previous stage is still travelling through the bed and that is why in the water outlet side of the generator the ammonia concentration is quite low.

From 130 to 195 s the generator is being cooled and a high increase in the ammonia concentration in the water inlet side of the bed is observed. Towards the end of the heating stage (130 s) the ammonia concentration increased in all the bed.

Finally from 195 to 260 s the generator is being preheated and a decrease in ammonia concentration is observed only in the water inlet side of the bed. This is because the cold water from the previous stage is still travelling through the bed and for this reason in the water outlet side of the generator the ammonia concentration is quite high.

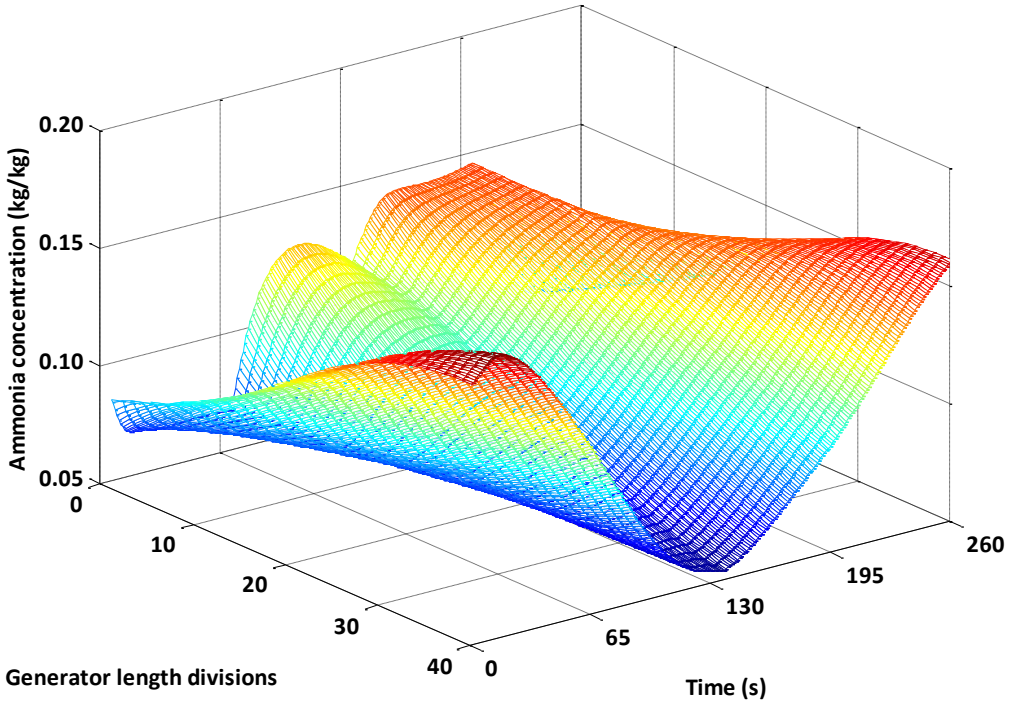

Figure 6.8 – Ammonia concentration in Generator 1 during a complete cycle (water outlet side)

In Figure 6.9 the ammonia swing in a generator (number 1) is plotted during a complete cycle. From 0 to 65 s, heating stage, the amount of ammonia is kept constant at a high level until the generator is pressurised up to the condensing pressure and the check valve opens. Then a sharp drop of ammonia content is observed. From 65 to 130 s, precooling stage, the amount of ammonia is kept constant at a low value for almost all the duration of the stage whilst the pressure of the bed drops. From 130 to 195 s, cooling stage, the amount of ammonia is kept constant at a low level until the generator is depressurised down to the evaporating pressure and the check valve opens. Finally from 195 to 260 s, preheating stage, the amount of ammonia is kept constant at a high level for almost all the duration of the stage whilst the pressure of the bed increases.

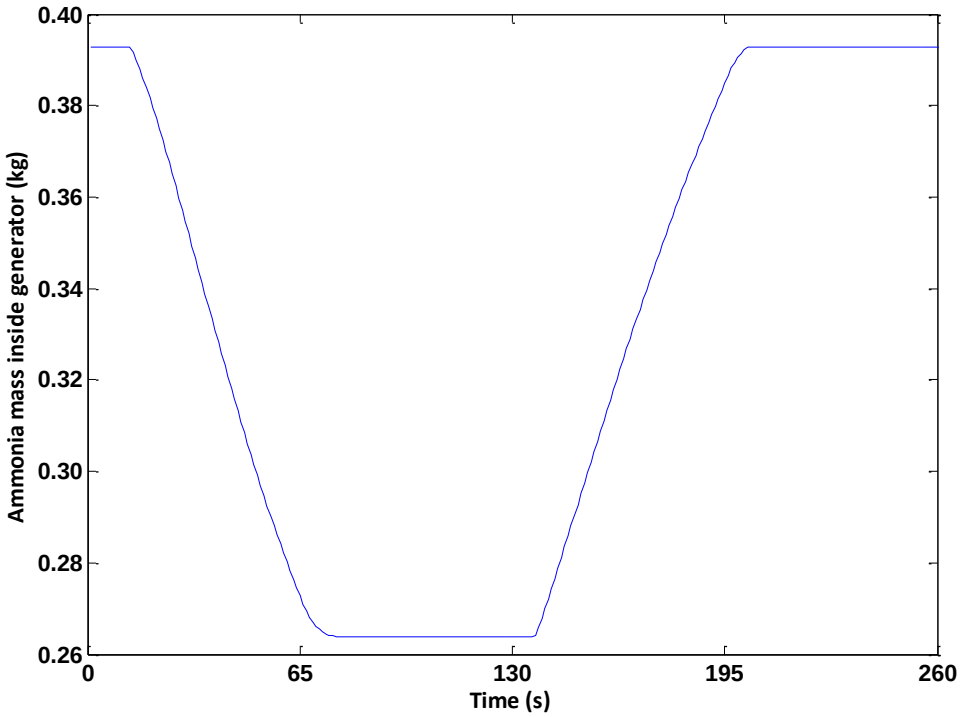

Figure 6.9 – Ammonia swing in Generator 1 during a complete cycle

6.2.2. Performance envelopes

In Figure 6.10 the heating COP is plotted against the specific heating power for the complete set of parameters investigated, varying heating fluid mass flow rates and cycle times whilst keeping the heat driving temperature constant at 170 °C, condensing temperature at 40 °C, evaporating temperature at 0 °C and the effective thermal conductivity at 0.3 W/(mK).

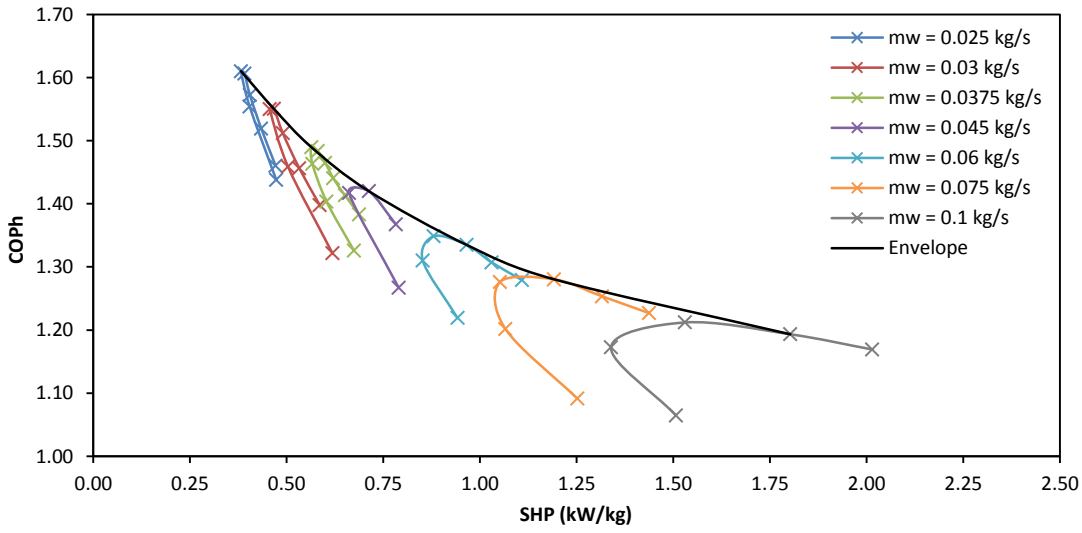

Figure 6.10 – Heat pump operating points and performance envelope (lines of constant flow rate)

The operating points of the heat pump can be plotted for the different mass flow rates, Figure 6.10, and also for different cycle times, Figure 6.11. Both graphs have the same performance envelope. The machine should always be operated at a point that lies on its performance envelope, where there is a trade-off between performance and power output.

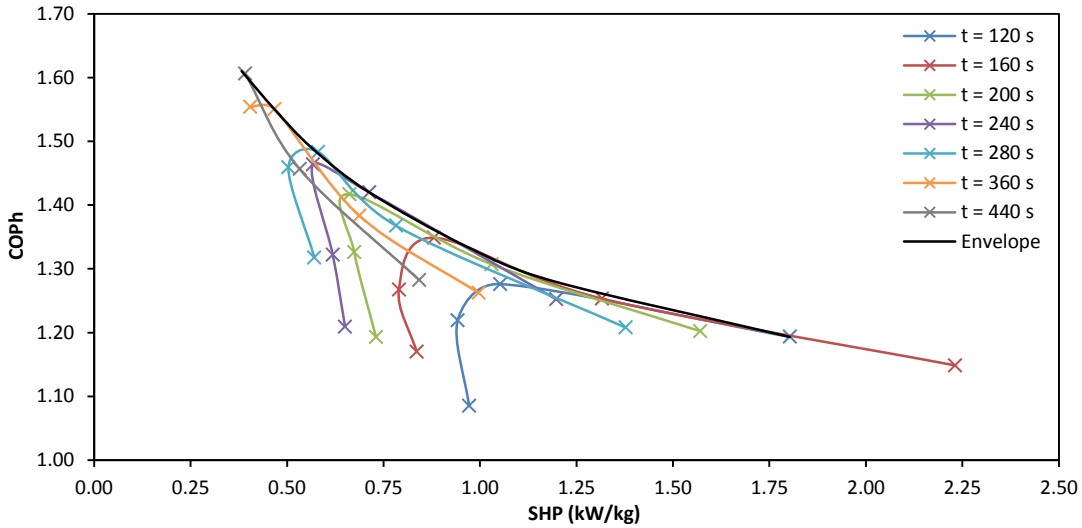

Figure 6.11 - Heat pump operating points and performance envelope (lines of constant cycle time)

The same operating points were plotted in Figure 6.12, heating COP and output power against cycle time for different heat transfer mass flow rates. The axis on the left and the solid lines indicate the heating COP and the axis on the right and the dashed lines indicate the specific output power.

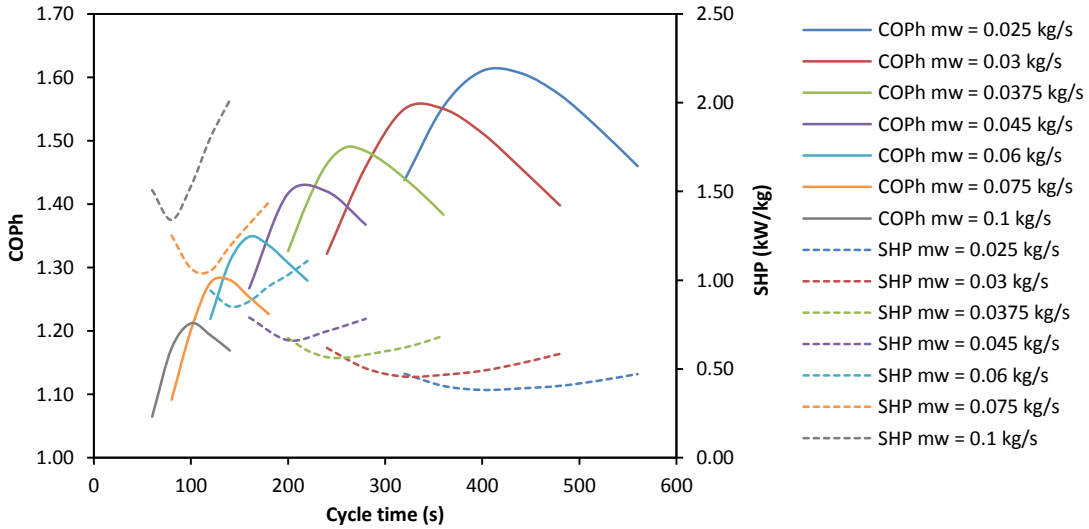

Figure 6.12 – Heating COP and specific heating power trends for simulations at different cycle times and mass flows

Figure 6.13 shows the effect of the heat transfer fluid mass flow rate on heating COP and heat output power for a set cycle time of 260 s and a driving temperature of 170 °C, condensing temperature of 40 °C and evaporating temperature of 0 °C.

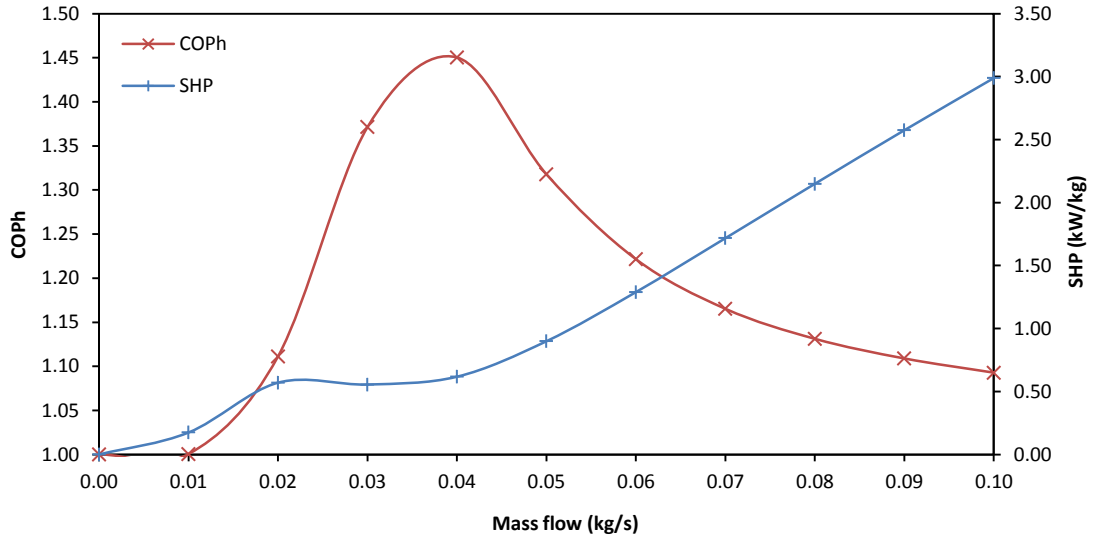

Figure 6.13 – Effect of the heat transfer fluid mass flow on COP and output power for a fixed cycle time of 260 s

From Figure 6.13 it can be seen that when the mass flow tends to zero the SHP tends to zero and the heating COP tends to one. This happens due to the fact that the mass flow is so low that the front of the thermal wave does not have enough time to travel along the bed or that the front of the thermal wave gets distorted and loses sharpness.

At around 0.04 kg/s the performance of the machine reaches a maximum when the heating COP shows a peak.

At higher mas flow rates the heating COP tends to one but the power output increases as the thermal wave does not exists anymore and breaks through the beds transferring heat between the heat driven fluid and the load fluid with very low heat input from the condenser.

6.2.2.1. Driving temperature

The performance envelopes mentioned earlier can be used to compare machine designs or set conditions. In Figure 6.14, three heat pump envelopes that correspond to three different driving water temperatures are plotted. For all cases the condensing temperature is 40 °C, evaporating temperature is 0 °C and the effective thermal conductivity is 0.3 W/(mK).

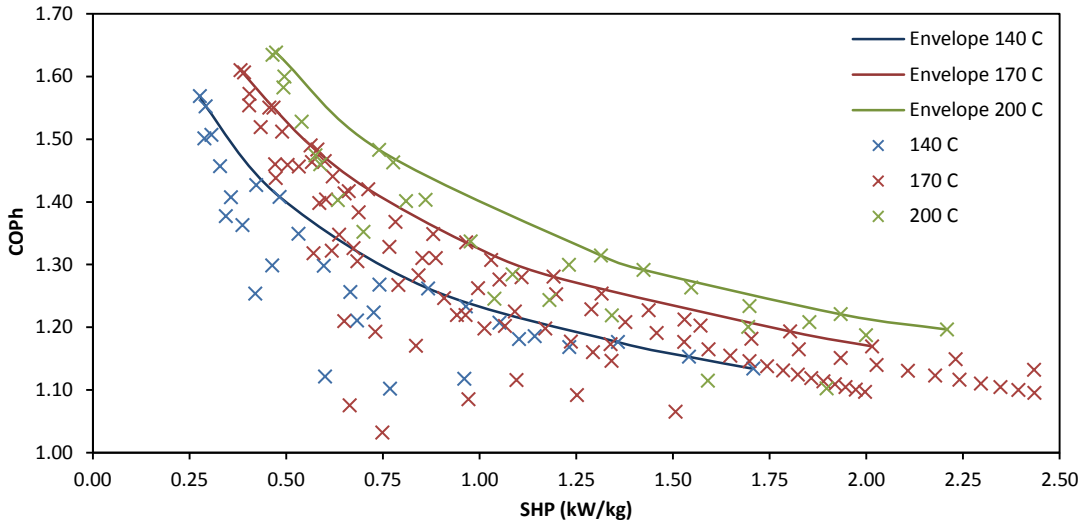

Figure 6.14 – Effect of driving temperature on COP and SHP

From Figure 6.14 it can be observed that the higher the driving temperature the higher the heat pump performance and the output power.

6.2.2.2. Evaporating and condensing temperatures

In Figure 6.15 the performance envelopes of the heat pump run at different evaporating (-5, 0, 5 and 10 °C) and condensing (30, 40 and 50 °C) temperatures are plotted. In all the cases the driving temperature is 170 °C and the effective thermal conductivity is 0.3 W/(mK).

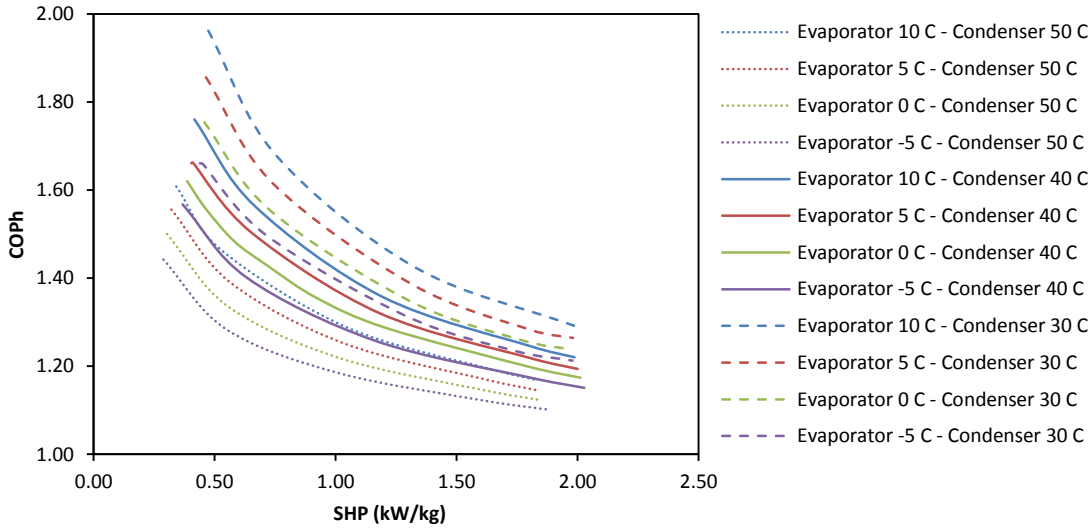

Figure 6.15 – Heating COP comparison of performance envelopes for different evaporating (-5, 0, 5 and 10 °C) and condensing temperatures (30, 40 and 50 °C)

The dashed lines correspond to a condensing temperature of 30 °C, the solid lines correspond to 40 °C and the dotted correspond to 50 °C. The blue lines correspond to an evaporating temperature of

10 °C, the red lines correspond to 5 °C, the green lines correspond to 0 °C and the purple lines correspond to -5 °C.

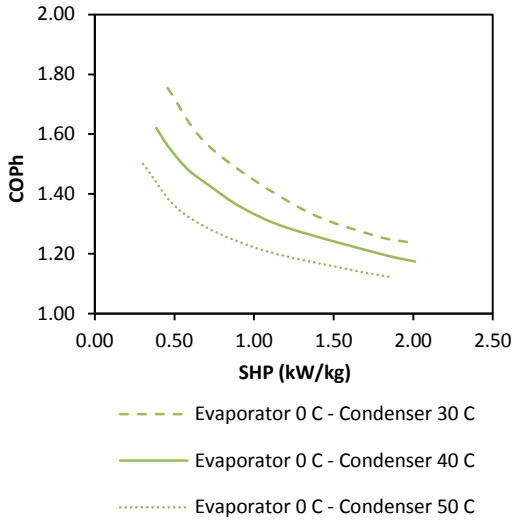

Figure 6.16 – Performance envelopes for an evaporating temperature of 0 °C

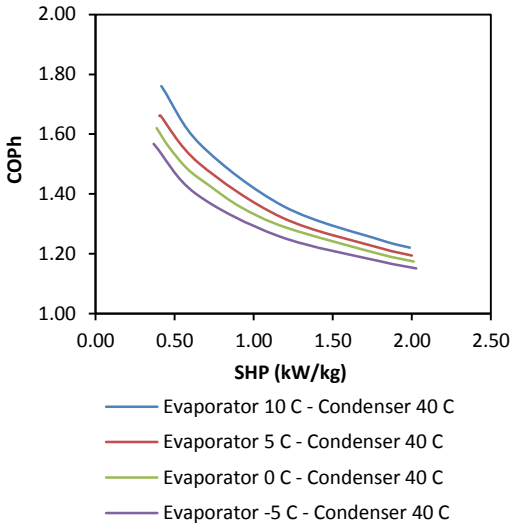

Figure 6.17 – Performance envelope for a condensing temperature of 40 °C

From Figure 6.16 it can be observed that the lower the condensing temperature the higher the heat pump performance and the output power. From Figure 6.17 it can be observed that the higher the evaporating temperature the higher the heat pump performance and the output power.

These trends are as expected from the basic thermodynamics but the graphs quantify the effects.

Figure 6.18 shows the relationship between the heating COP and the output temperature of the water heated by the heat pump at different evaporating temperature conditions when the power output of the heat pump is 7 kW.

As stated above, the higher the evaporating temperature, the higher the performance of the machine. The lower the temperature of the water heated the higher the performance of the machine.

Along with the performance of the heat pump, the efficiency of a condensing boiler was also plotted in order to compare them. As it can be seen in the graph, the boiler can produce hot water in the same range as the heat pump but its efficiency remains constant at 91%, much lower than the performance of the heat pump that for the same conditions it could achieve between 140 or 180% depending on evaporating conditions.

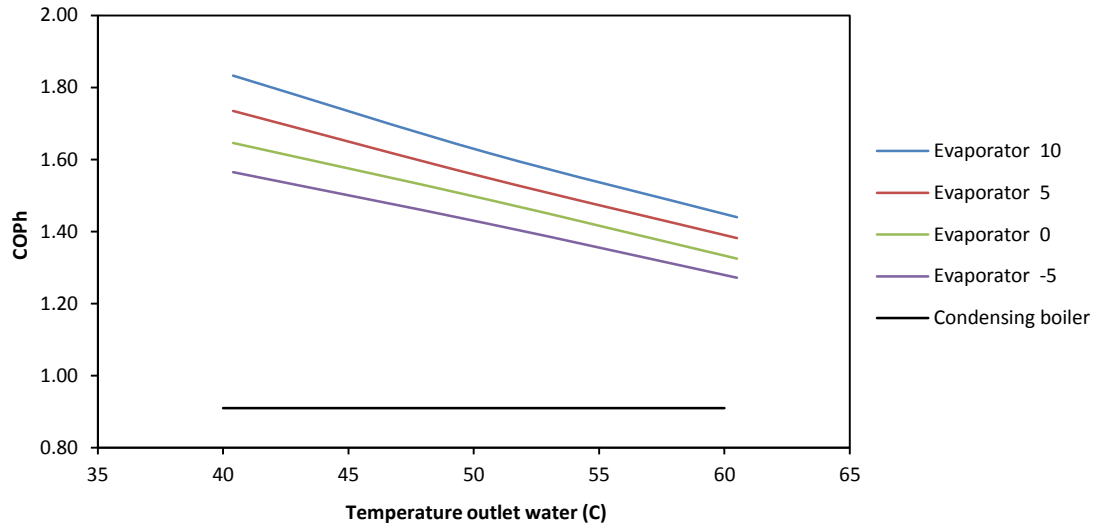

Figure 6.18 – Relationship between the heating COP and the output water temperature for a power output of 7 kW and different evaporating temperatures (comparison a condensing boiler efficiency)

6.2.2.3. Adsorbent thermal conductivity

In Figure 6.19, two heat pump envelopes that correspond to two different effective thermal conductivity of the carbon are plotted. For all cases the condensing temperature is 40 °C, evaporating temperature is 0 °C and driving temperature 170 °C.

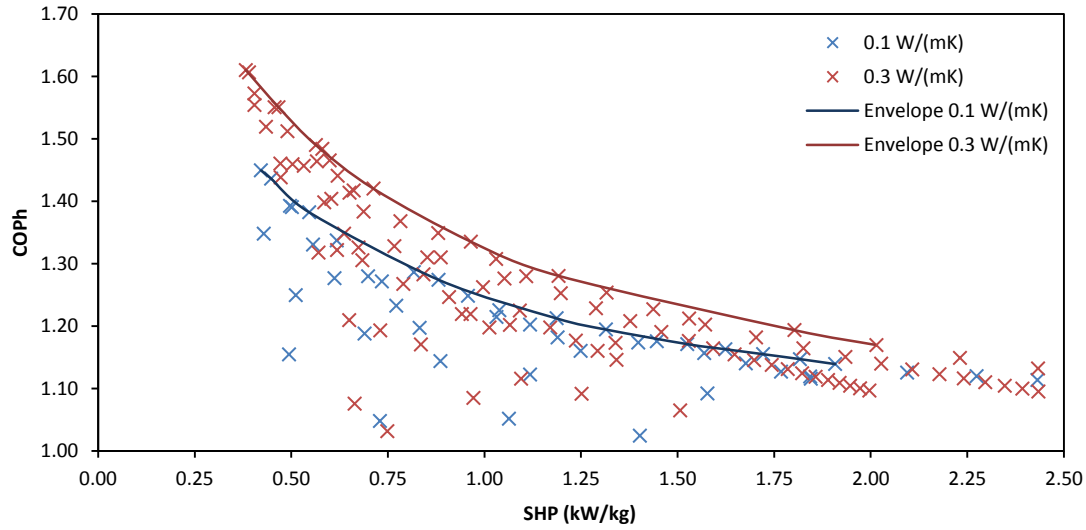

Figure 6.19 – Effect of the carbon thermal conductivity on COP and SHP

From Figure 6.19 it can be observed that the higher the effective thermal conductivity of the carbon the higher the heat pump performance and the output power.

6.2.3. Effect of N (number of length divisions of the generator) in the simulation

The number of longitudinal divisions in which the generators are divided in the model can affect the performance and the power of the heat pump obtained in the simulation. Different tests were run in order to analyse how the chosen N (number of longitudinal divisions) could affect the simulation results. It was found that the greater the N the better for the simulation accuracy of the thermal wave.

Figure 6.20 shows the heating COP and SHP of different ideal simulations that use different N values to see the impact of N. In these simulations the evaporating temperature was 0 °C, the condensing temperature 40 °C, the water driving temperature 170 °C, the effective thermal conductivity of the carbon 0.3 W/(mK), the mass flow 0.0375 kg/s and the cycle time 260 s.

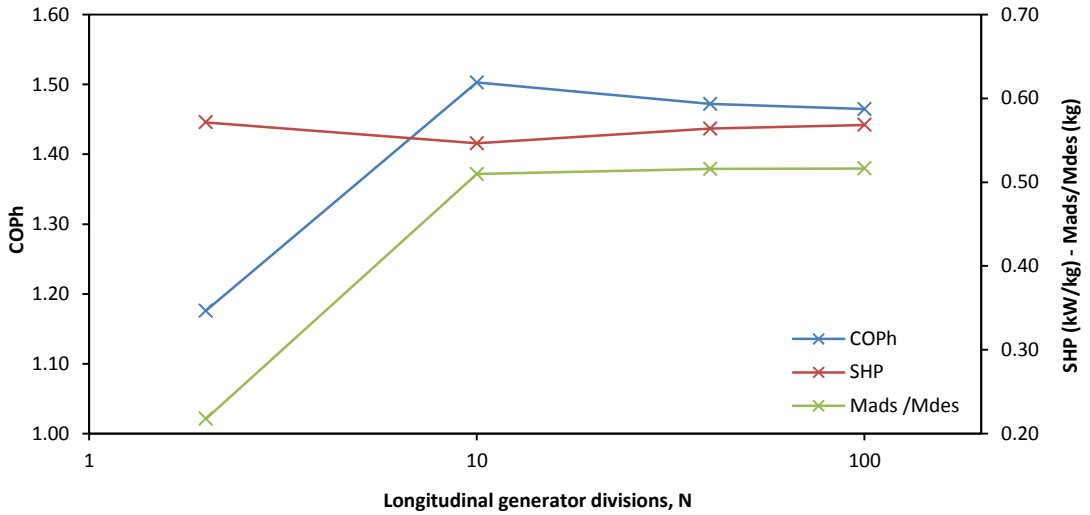

Figure 6.20 – Effect of N on heating COP, output power and mass of ammonia cycled in the system

From Figures 6.21 and 6.22 it can be observed the big differences in the simulated carbon temperature in a generator over a cycle when the N is 2 and 100 respectively.

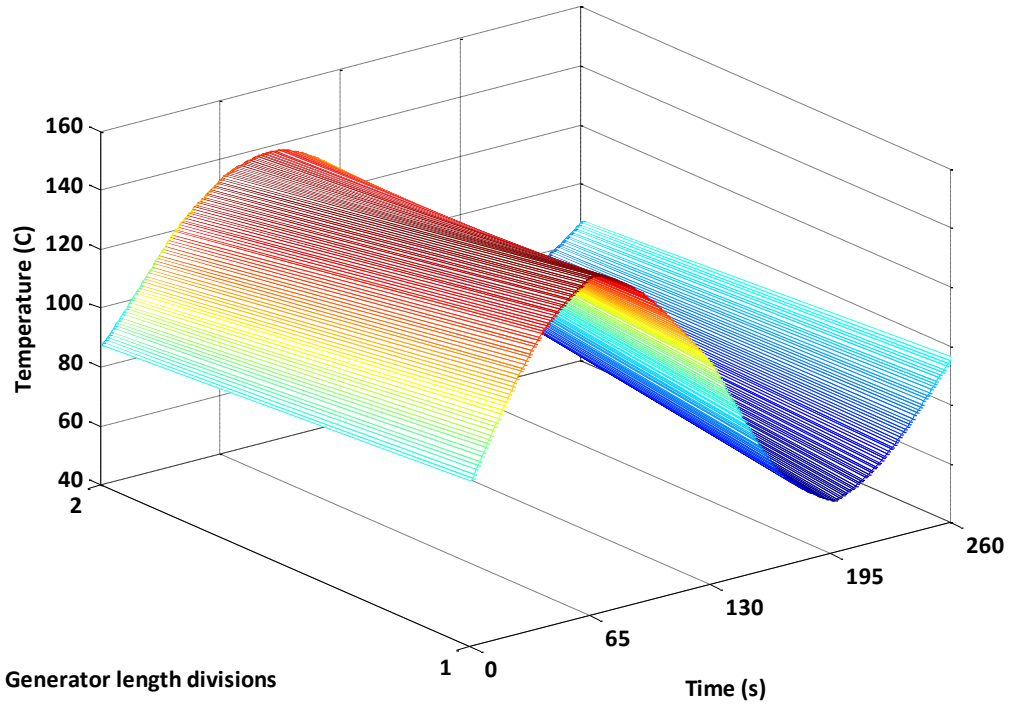

Figure 6.21 – Temperature of carbon of one generator during a complete cycle with N=2 simulation

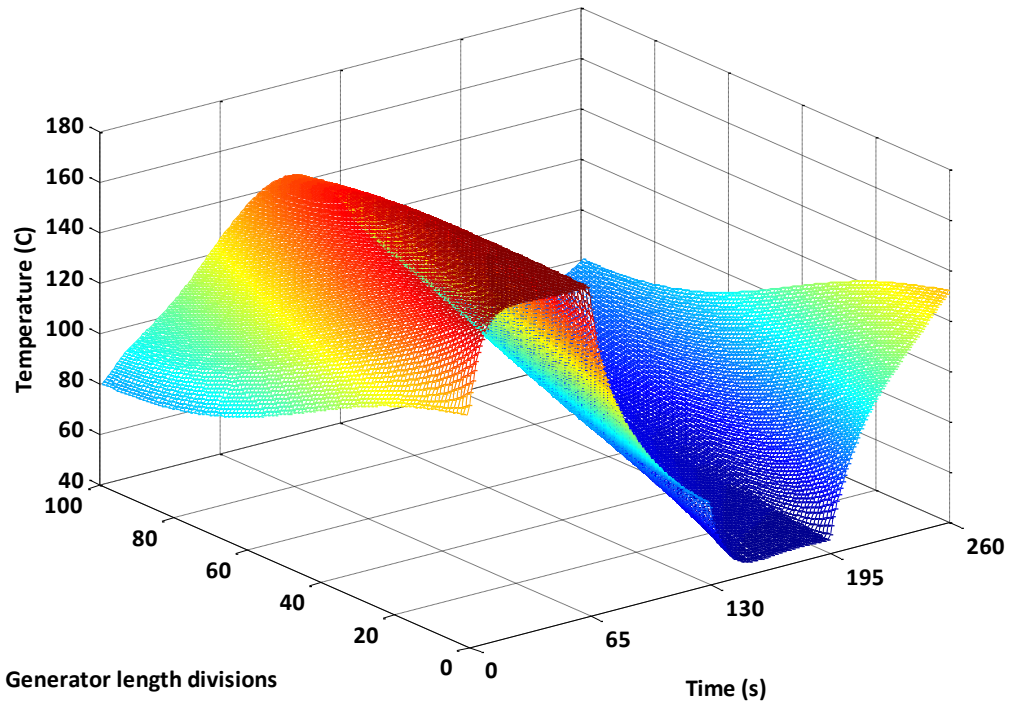

Figure 6.22 – Temperature of carbon of one generator during a complete cycle with N=100 simulation

As the running time of the simulations for N=100 was prohibitively high N=40 was chosen instead which in Figure 6.20 shows very similar performance and power output as the N=100 simulations. With N=40 the sections of the bed in the simulation are approximately 1 mm long.

6.2.4. Modifications to the model simulation

A few modifications were made to the simulation to try to take into account the effects of the experimental set up components:

- Delays in the water circuit: some components such as pipes, valves and water manifolds introduced unwanted water volumes in the system between heater/cooler and valves and between valves and beds.
- Pump speed: the pump installed in the water generators system was stopped for a couple of seconds every time there was a change of stage in the cycle. Once the pump was activated again it took 7 s to reach its nominal speed (ramp).
- Smooth delays in the water circuit: the previously mentioned delays in the water system could be modified to assume that in addition to the delays there existed water mixing in those components. As a result the water inlet (and outlet) profile in the beds was different.
- Convection effect: as explained in Chapter 5, the heat transfer between the tubes of the heat exchanger and the carbon could be modelled using an effective thermal conductivity of the carbon or could be modelled using an intrinsic thermal conductivity of the carbon and a wall contact resistance (modelled as a convection effect).

A cycle with set conditions was run with the different simulation modifications in order to observe their effect in the performance and the change in water profile temperatures and ammonia profile pressure in the system. The set conditions were driving temperature of 170 °C, condensing temperature of 40 °C, evaporating temperature of 0 °C, cycle time of 260 s, heat transfer fluid flow rate of 0.0375 kg/s, carbon thermal conductivity of 0.3 W/(mK) and a wall-carbon contact thickness of 0.026 mm.

The performance, power output and amount of ammonia cycled in the heat pump for the different cycle types are shown in Table 6.2 The cumulative degradation of performance with the increasing number of ‘real’ adjustments can be seen.

Type of cycle	Heating COP	Power output (kW)	Ammonia cycled (kg)
Ideal	1.49	6.77	0.52
Delays	1.43	6.47	0.41
Delays and speed pump effect	1.38	6.65	0.39
Smooth delays and speed pump effect	1.35	6.23	0.47
Smooth delays, speed pump and convective effect	1.33	6.33	0.45

Table 6.2 – Performance of the different modified cycles

Figure 6.23 shows the different water inlet temperatures (solid line) to a generator (number 1) and water outlet temperatures (dashed lines) from the generator for the different modified cycle simulations.

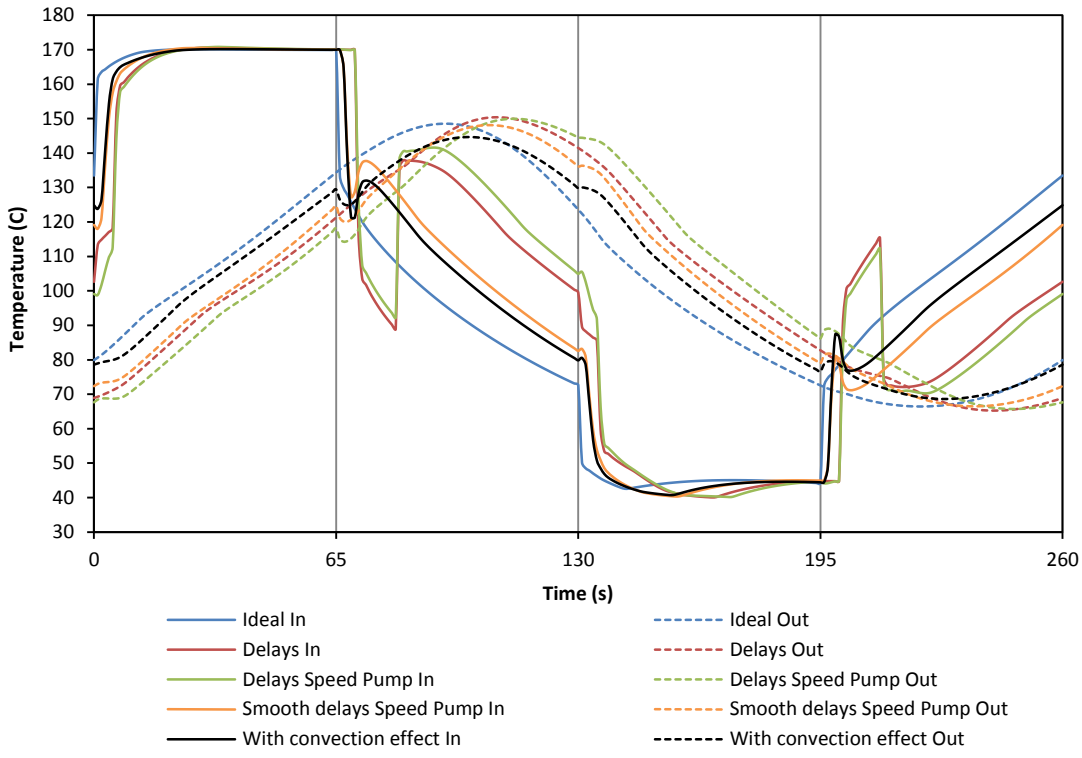

Figure 6.23 – Comparison of temperature profiles of inlet and outlet water to a bed for different modified cycle simulations

Figure 6.24 shows the different ammonia pressure profiles for the different modified cycle simulations.

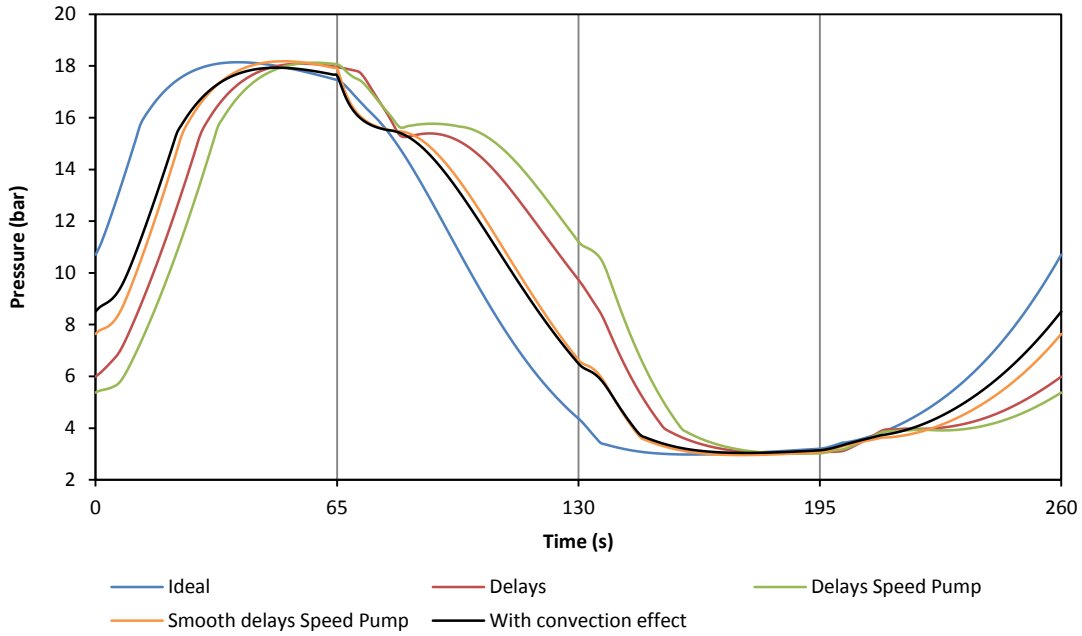

Figure 6.24 – Comparison of bed pressure profiles of ammonia for different modified cycle simulations

Figures 6.25 and 6.26 show for a given set of conditions how the COP and SHP vary with cycle time for different modified cycle simulations. The set conditions are driving temperature of 170 °C, condensing temperature of 40 °C, evaporating temperature of 0 °C, carbon thermal conductivity of 0.3 W/(mK) and a wall-carbon contact thickness of 0.026 mm. In Figure 6.25 the heat transfer fluid flow rate is 0.025 kg/s and in Figure 6.26 the flow rate is 0.1 kg/s.

In both graphs the ideal model simulation is represented by solid line and dots, the smooth delay and speed pump effect model simulation is represented by the dashed line and triangles and the smooth delay, speed pump and convective effect model simulation is represented by the dotted line and crosses.

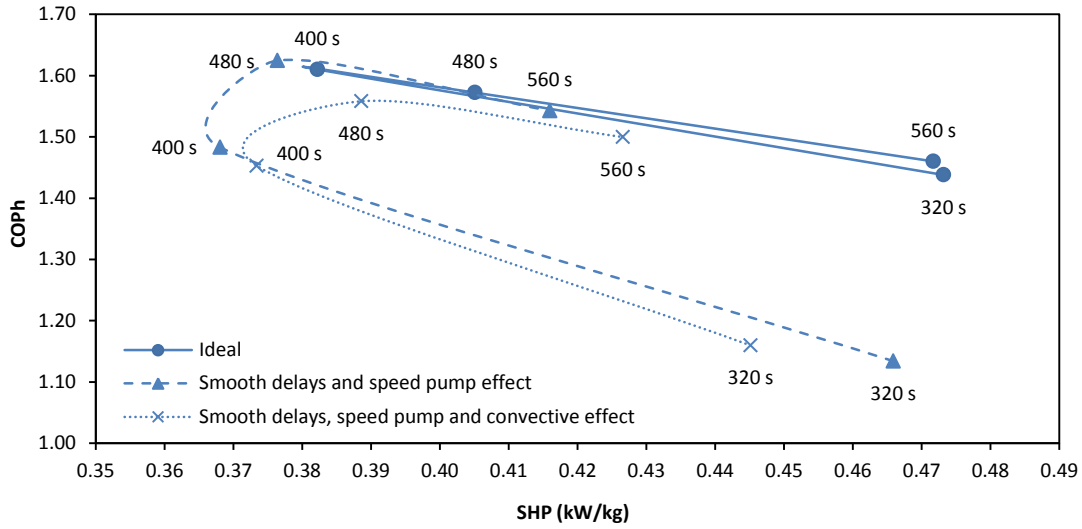

Figure 6.25 – Comparison of heating COP and SHP relationship for different simulations and cycle times for a water mass flow rate of 0.025 kg/s

In both graphs it is possible to observe that the modified model with smooth delays and speed pump effect can achieve similar results to those obtained with the ideal model but with longer cycle times. The model with delays, speed pump effect and increased heat transfer resistance due to the convective effect show much lower performance and cannot achieve the same heating COP values even if the cycle time is higher.

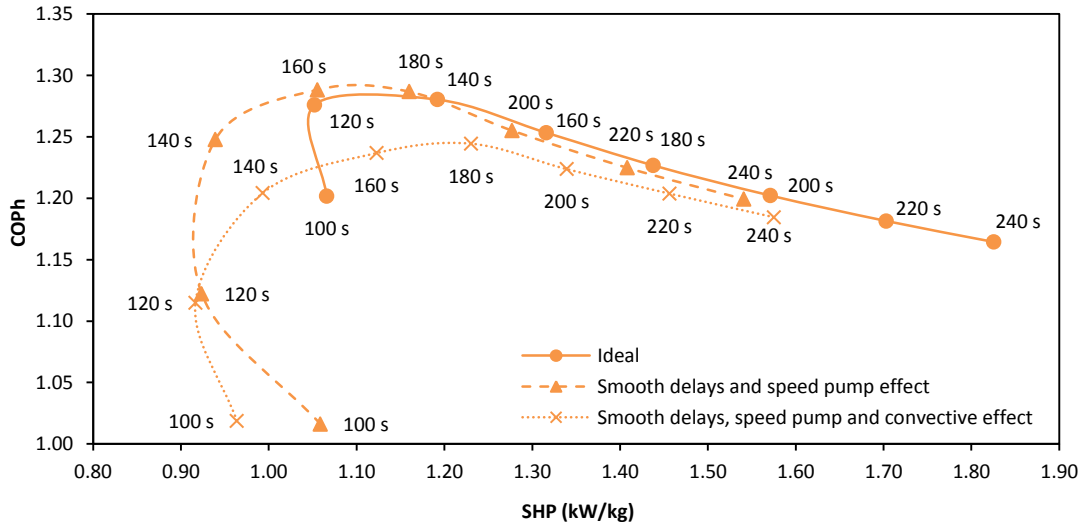

Figure 6.26 – Comparison of heating COP and SHP relationship for different simulations and cycle times for a water mass flow rate of 0.1 kg/s

6.3. Conclusions

The simulation model of the 4 bed thermal wave heat pump has been analysed and compared for many different sets of conditions in order to understand its behaviour and the effect these conditions have on the performance and heat output power.

Firstly a detailed analysis of a sample cycle with set parameters was carried out. The parameters set were cycle time, heat transfer fluid mass flow, hot driving, condensing and evaporating temperatures and carbon effective thermal conductivity. The temperature profiles of the water and carbon, the ammonia concentration, pressure and mass of ammonia cycled during a complete cycle were analysed.

The performance envelope of the heat pump cycle at set driving, condensing and evaporating temperatures and carbon effective thermal conductivity was obtained. The heating COP and specific heating power output for the different heat transfer fluid mass flows and cycle times were plotted in order to obtain their trade-off.

The driving temperature of the cycle was varied and the performance envelopes for different temperatures were obtained. The higher the driving temperature the higher the heating COP and the power output.

The condensing and evaporating temperatures were varied as well and performance envelopes were plotted. The higher the evaporating temperature the higher the heating COP and output power. The higher the condensing temperature the lower the heating COP and the power output.

The performance of the cycle was analysed when the thermal conductivity of the active carbon is varied. The higher the thermal conductivity the higher the heating COP and power output.

Finally, the heat pump simulation model was varied in order to incorporate real effects of the experimental set up of the machine. Different modifications were done such as dead water volumes, water speed pump variation and carbon wall contact resistance inside the generator. Their effects were accumulated in the simulations and the water profiles and ammonia pressures in a generator during a complete cycle were plotted in order to observe the differences. It could be seen that the dead water volumes and water pump variation effect reduce the efficiency and output power of the system but with an increase in the cycle time the same values could be obtained. On the other hand,

when the wall contact resistant effect in the generator is simulated the results obtained are much lower to those of the ideal cycle and an increase in the cycle time could not match them.

Chapter 7

Heat transfer in adsorbent beds

7.1. Introduction

In this chapter, the heat transfer characteristics of different carbon samples suitable for adsorption heat pumping purposes are measured and analysed. The characteristics studied are intrinsic thermal conductivity and wall contact resistance, measured as a contact layer thickness of air or ammonia.

These heat transfer characteristics are measured using two different methods: a steady state method that measures thermal conductivity between flat plates and a transient method that uses a hot tube technique.

The carbon samples studied are a combination of various grain sizes ranging from 1.7 mm to values as small as 1 µm. Apart from measuring grain samples of with a (nominally) single size, binary mixtures of different ratios of grains and powder were also measured and analysed.

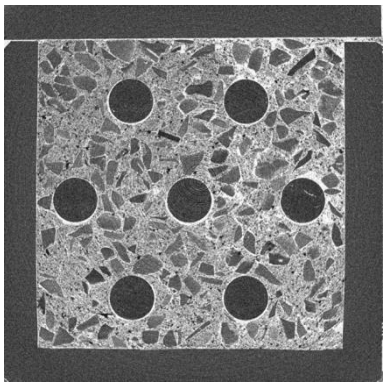

Figure 7.1 – CT scan cross section area of a binary carbon mixture sample filling a scale replica of a shell and tube heat exchanger

Finally, the heat transfer characteristics of the best carbon mixtures obtained in the experiments are evaluated for heat pumping purposes assuming the current shell and tube heat exchanger used by the researchers of the University of Warwick.

7.2. Steady state flat plate measurements

The intrinsic thermal conductivity of the carbon samples was measured with a steady state technique using flat plates. The carbon sample is placed in between the flat plates and the heat flux used in the measurements travels through the sample.

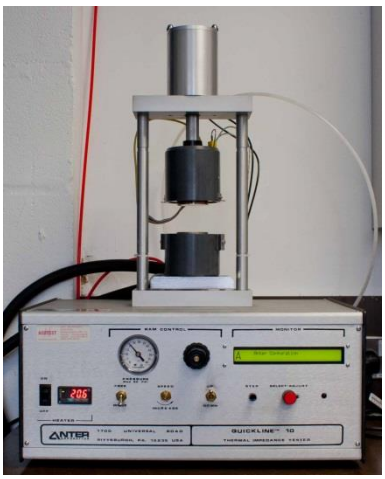

Figure 7.2 - Anter Quickline-10™ machine

The effective thermal conductivity of the carbon samples was directly measured following the ASTM E1530 – 11 Standard Test Method the Guarded Heat Flow Meter Technique [1], using an Anter Quickline-10™ machine, Figure 7.2. Once a complete set of effective thermal conductivity data for all the samples is obtained it is possible to calculate their intrinsic thermal conductivity. The difference between the effective and the intrinsic thermal conductivities is that the first one neglects the effect of the contact resistance between the sample and the sample holders whilst the latter measures the thermal conductivity within the bulk of the material.

7.2.1. Experimental set up description

The Anter Quickline-10™ machine consists of a heater, an upper metal plate (disc of 50.8 mm diameter), a lower metal plate (disc of 50.8 mm diameter), a calorimeter and a heat sink, shown in Figure 7.3. The sample to be measured, that should have parallel 50.8 mm diameter flat surfaces, is

placed between the lower and upper plate. Three thermistors read the temperatures of the upper plate, lower plate and heat sink.

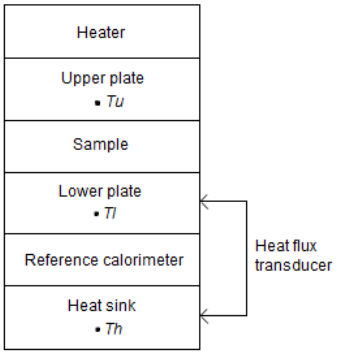

Figure 7.3 - Thermal conductivity principle of the Anter Quickline-10™ machine

The effective thermal conductivity of the samples is calculated using the following equation:

$$k = \frac{t}{R_{T,s}} \tag{7.1}$$

where

k is the effective thermal conductivity (W/(mK))

t is the sample thickness (m)

$R_{T,s}$ is the sample thermal resistance (m^2K/W) that can be obtained from:

$$R_{T,s} = \frac{(T_u - T_l)}{Q} - R_{T,int} = \frac{F \cdot (T_u - T_l)}{(T_l - T_{sink})} - R_{T,int} = F \cdot \left(\frac{\Delta T_s}{\Delta T_r}\right) - R_{T,int} \tag{7.2}$$

where

T_u is the surface temperatures of the upper plate (K)

T_l is the surface temperature of the lower plate (K)

T_{sink} is the heat sink temperature (K)

Q is the thermal flux through the test sample (W/m^2)

$R_{T,int}$ is the total interfacial thermal resistance between the sample and the surface plates (m^2K/W)

F is the reference thermal resistance (m^2K/W)

ΔT_s is the temperature difference across the sample (K)

ΔT_r is the temperature difference across the referenced calorimeter (K)

Before measuring the thermal conductivity of the samples, the Anter Quickline-10™ machine must be calibrated in the samples' range of thermal resistance, so that the values $R_{T,int}$ and F of Equation 7.2 can be obtained.

The thermal conductivity of the carbon samples was measured in both parallel and perpendicular carbon compression directions, but many more samples were tested in the perpendicular direction since due to the arrangement of the sample holder, the density of the sample could be better controlled and also because the orientation of the grains might lead to a higher conductivity result. This would be due to conduction along the longer axis of the grains, rather than perpendicular to them [2].

The samples of carbon compressed in the parallel direction were measured using a sample holder shown in Figure 7.4a consisting of a circular base made of aluminium 6082-T6 and a section of cylinder made of a low conductivity polymer, PVC. The carbon was placed in the holder and once on the lower plate of the machine, the upper plate could compress the sample up to 50 psi (345 kPa) using a pneumatic cylinder.

The samples with carbon compressed in the perpendicular direction were measured with a square cross section sample holder shown in Figure 7.4b that consists of two square blocks of 50.8 mm x 50.8 mm x 10 mm made of aluminium and four walls made of a low conductivity polymer all linked with 24 bolts. With one of the walls removed, the carbon was placed inside the holder and could be compressed by hand using a suitable plunger. In this way the density of the sample could be better controlled. Once the compression process is finished the wall is placed back in the holder and all the attachment is deposited in the machine.

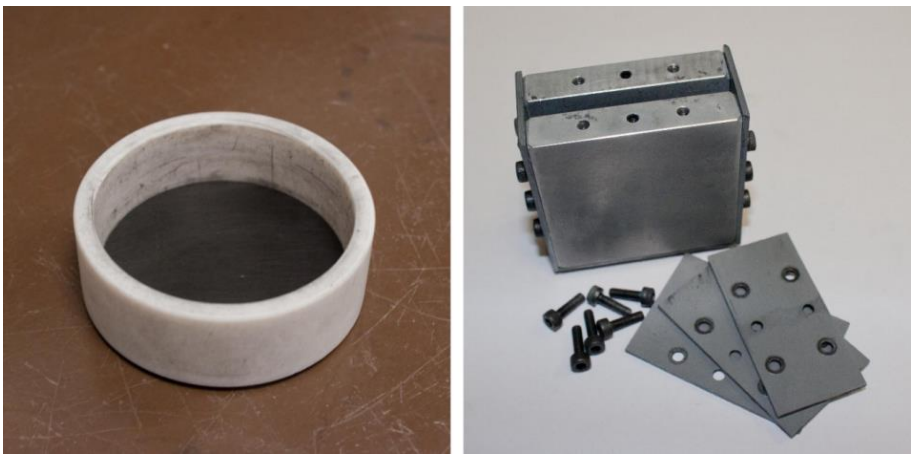

Figure 7.4 - (a) Round sample holder, (b) Square sample holder

The two blocks are made of aluminium 6082-T6 which has a conductivity of 180 W/(mK), three orders of magnitude higher than the carbon samples. The high conductivity of these blocks

effectively transforms the upper and lower surface plates of 50.8 mm diameter into square cross section area surfaces of 50.8 mm side (with the same total heat flux) necessary in order to measure the square carbon samples.

The Quickline-10™ machine is provided with a set of sample disks of known thicknesses and detailed thermal conductivities at different temperatures used to calibrate the machine. A calibration line for round cross section area samples was done with the provided Vespel™ SP-1 (unfilled) samples, two disks of diameter 50.8 mm and thicknesses 3.175 mm and 6.35 mm respectively. The thermal resistance range of the Vespel™ samples was very narrow for the carbon sample experiments and most of them would fall outside this range so a new calibration with another low thermal conductivity material was done.

Four disks of PEEK™ 450G of diameter 50.8 mm and different thicknesses, 2.5 mm, 5 mm, 10 mm and 20 mm respectively, were cut and polished. The thinnest disk was measured in the Quickline-10™ machine and according to the previous Vespel™ calibration line it had a thermal conductivity of 0.30 W/(mK). Once knowing the conductivity of the PEEK™ and the thermal resistance of the other disks, the calibration line used for the carbon experiments was made. The calibration results are shown in Figure 7.5, in which points A, B, C and D are the 2.5 mm, 5 mm, 10 mm and 20 mm thickness PEEK™ disks respectively. From Figure 7.5a and Equation 7.2 the values of F and $R_{T,int}$ were calculated as 0.0024 K/W and 0.001 K/W respectively.

The same procedure was done in order to calibrate the machine for square cross section area samples. Four square blocks of PEEK™ 450G of 50.8 mm side and different thicknesses, 2.5 mm, 5 mm, 10 mm and 20 mm respectively, were cut and polished. The thinnest block was measured in the Quickline-10™ machine along with the two blocks of aluminium on each side that transform the upper and lower surface plates into squares and according to the Vespel™ SP-1 calibration it had a conductivity of 0.29 W/(mK). The calibration results are shown in Figure 7.5b and the values of F and $R_{T,int}$ were calculated as 0.0026 K/W and 0.0001 K/W respectively.

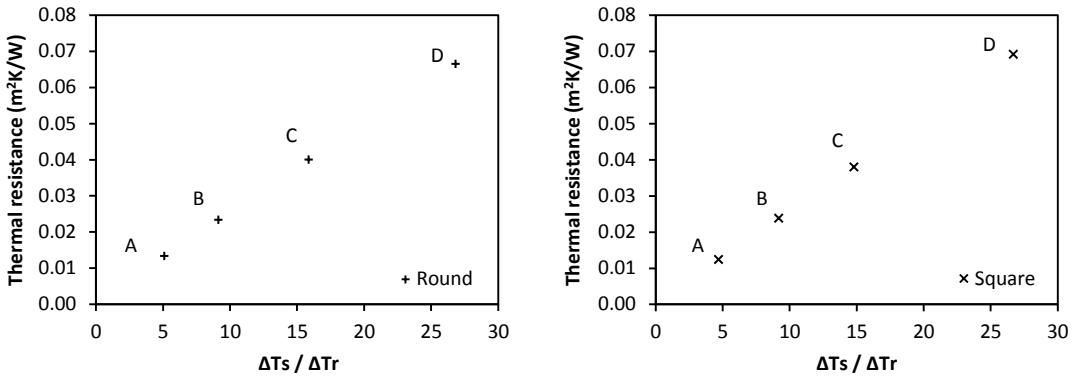

Figure 7.5 - (a) Calibration line made with round PEEK^{TM} samples, (b) Calibration line made with square PEEK^{TM} samples – A, B, C and D correspond to 2.5 mm, 5 mm, 10 mm and 20 mm sample thickness respectively

In order to obtain the thermal conductivity of the carbon samples, measurements of the T_u, T_l and T_h were taken for each sample. For the experiment results to be accurate, each thermal resistance obtained must fall within the corresponding calibration range, which is 0.013 to 0.067 m^2K/W for circular samples and 0.012 to 0.069 m^2K/W for square samples.

To avoid contact resistances between the base of the circular holder and the lower plate of the machine and between the aluminium blocks and the upper and lower plates of the machine the high conductivity grease SG500 (6023) ACC Silicones Ltd (0.77 W/(mK)) was used in all the experiments.

During the process of calibration and measuring samples the Anter Quickline-10^{TM} machine was set and operated at the same boundary temperatures. In this case the machine was set to a high temperature of 55 °C and a low temperature of 10 °C.

The experiment could take up to 3 h to run, depending on the sample thermal conductivity and thickness.

7.2.2. Accuracy of the experiments

The thermal conductivity of the samples is measured with the Anter Quickline-10^{TM} machine with a global error that the manufacturer estimate that can vary between ± 3% and ± 8%, depending on the thermal resistance of the sample. The accuracy improves when the ratio between $R_{T,int}$ and $R_{T,s}$ is small.

In order to obtain the accuracy of the thermal resistance readings it must be taken into account that the Anter Quickline-10^{TM} machine software converts the voltage measured by the three

thermistors in the upper plate, lower plate and heat sink to temperature at a constant 7.045 °C/V rate. The resolution of the voltage meter is 1 mV so the temperature resolution is 0.007 °C. Calculating the reading error with typical values of the carbon samples it is possible to obtain a thermal resistance reading error of 0.179 %.

7.2.3. Flat plates SolidWorks™ validation

In order to have confidence with the tests done with the square flat plate holder, the assembly of aluminium blocks and carbon was drawn in SolidWorks™ and the steady state heat transfer software package within SolidWorks™ was used to simulate each result. The boundary conditions used in each simulation were the upper and lower temperature obtained from the Anter Quickline-10™ machine applied in a circle of 50.8 mm diameter at each side of the sample holder, the rest of the surfaces that during the experiment were in contact with air were treated as adiabatic and the contact between the carbon and the aluminium was treated as a bond.

The simulations show that there is a very low discrepancy, up to 3%, in the effective thermal conductivity value of the 2 mm, 5 mm and 10 mm thickness samples, but the 15 mm thickness samples show a higher error, between 8 and 10%. This indicated that in further experiments the 15 mm holder thickness walls were no longer used.

7.2.4. Analysis of steady state flat plates experiments

As stated above, for every carbon grade and every mixture (1/3 grains, 1/2 grains and 2/3 grains) at least two thermal resistance measurements at different thicknesses were taken for different sample densities.

As an example, the process of obtaining the intrinsic thermal conductivity for the 100% 20x40 grains sample is shown:

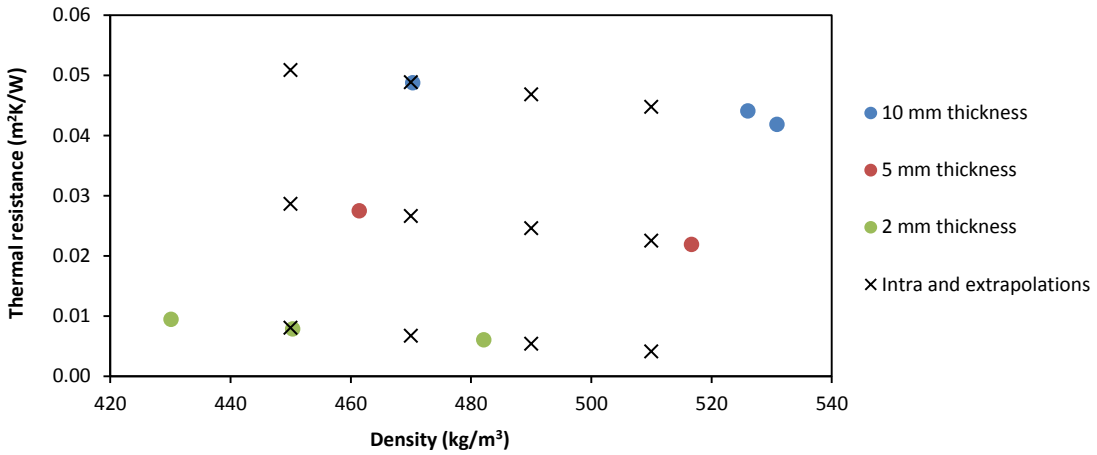

Figure 7.6 – Thermal resistance values of 20x40 100% grains samples at different densities and sample thickness

In Figure 7.6 the results obtained from the Anter Quickline-10™ at different densities and sample thicknesses are plotted (blue, red and green dots). In order to obtain the intrinsic thermal conductivity of the carbon sample at different densities, the thermal resistance at those densities were obtained for every sample thickness using interpolating and extrapolating tools (crosses in Figure 7.6).

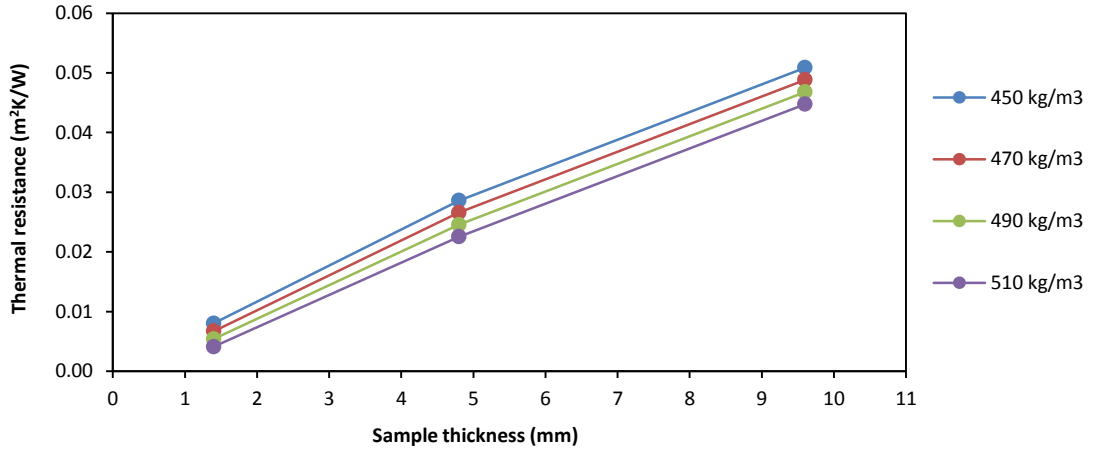

Figure 7.7 – Thermal resistance values of 20x40 100% grains samples at different densities and sample thickness

In Figure 7.7 the crosses from Figure 7.6 are plotted in a different arrangement, relating sample thickness with thermal resistance at different densities. The next step to obtain the intrinsic thermal conductivity of the samples is to obtain the slope of the different density lines.

$$Slope = \frac{\Delta R_T}{\Delta t} = \frac{1}{\lambda} \tag{7.3}$$

Equation 7.3 relates the change in thermal resistance (ΔR_T in m^2K/W) with the change in sample thickness (Δt in m) at a specific density. The slope of each line in Figure 7.7 is the inverse of its intrinsic thermal conductivity (λ in W/(mK))) at that density.

In theory in Figure 7.7 the extrapolation of the lines to zero should give twice the contact resistance between the carbon sample and the aluminium block (positive number) but as seen in the Figure 7.7 this does not happen. It was found that the low thermal conductivity of the samples could cause this inaccuracy but this does not invalidate the fact that the slope of the line between the three points relates to the intrinsic thermal conductivity of the bulk of the sample.

The intrinsic thermal conductivity values of the 100% 20x40 grains sample at 450, 470, 490 and 510 kg/m^3 are plotted in Figure 7.8.

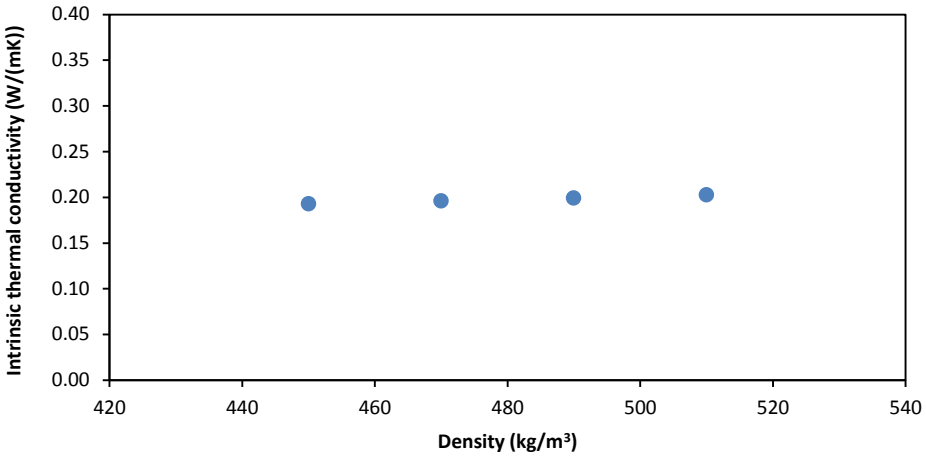

Figure 7.8 – Intrinsic thermal conductivity values of 20x40 100% grains samples at different densities

Another example, same process for 50% 20x40 grains and 50% powder mixture sample is shown:

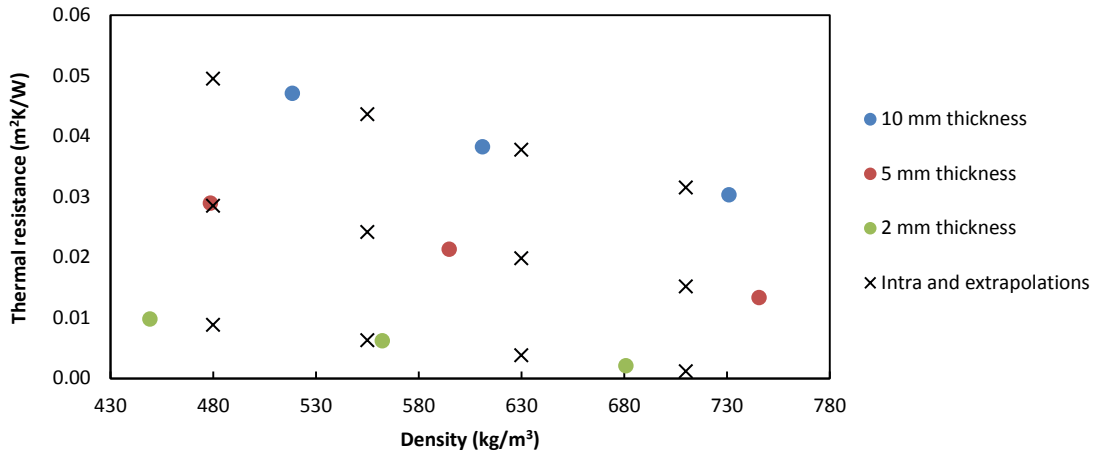

Figure 7.9 – Thermal resistance values of 50% 20x40 grains mixture samples at different densities and sample thicknesses

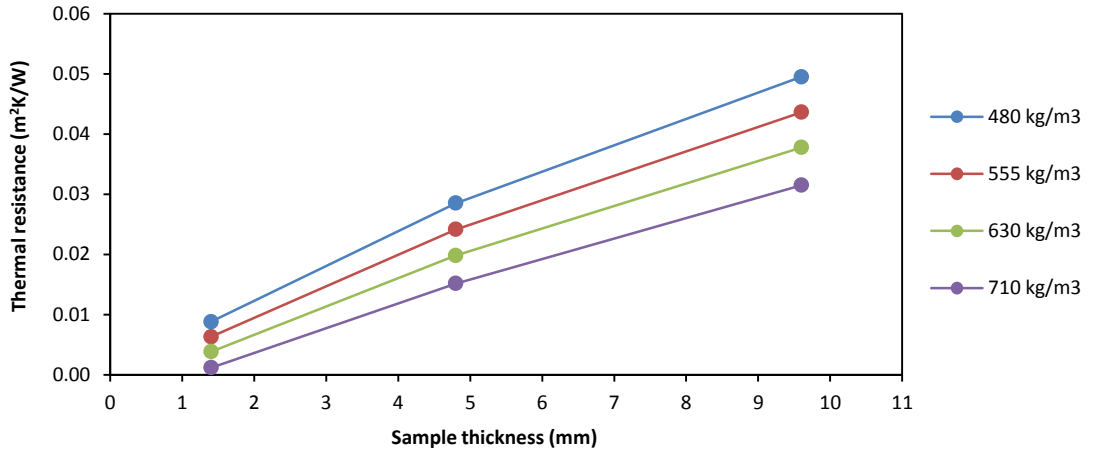

Figure 7.10 – Thermal resistance values of 50% 20x40 grains mixture samples at different densities and sample thicknesses

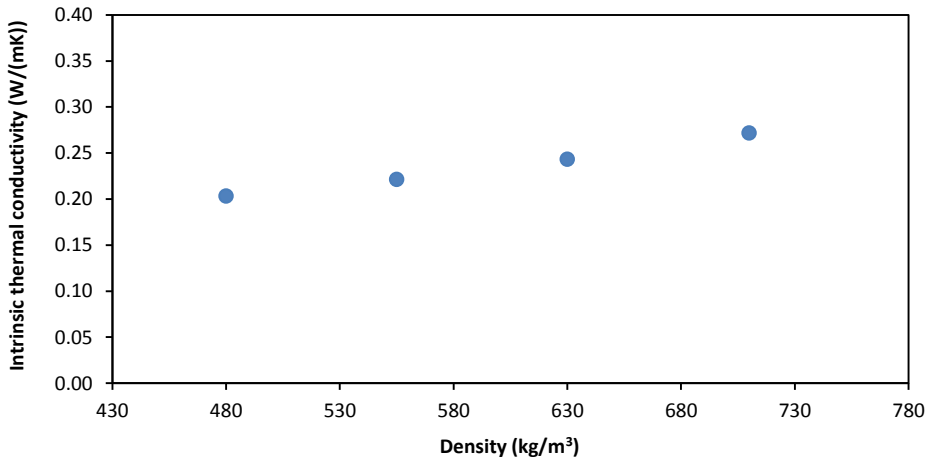

Figure 7.11 – Intrinsic thermal conductivity values of 50% 20x40 grains mixture sample at different densities

7.3. Transient hot tube measurements

The transient hot wire (or in this case, hot tube) technique is well-developed and widely used for measuring the thermal conductivity of fluids and solids. It consists of a tube of a resistive element immersed in the solid sample and the experiment is simply performed by recording the voltage change over the source/sensor element while its temperature is raised by an electrical current. The source element in this case is a stainless steel tube extracted from one of the sorption generators used for heat pumping purposes.

7.3.1. Experimental set up description

The temperature of the hot tube will depend on the electrical properties of the conducting material used and vice versa. The governing equation of the tube electric resistance, R_E (Ω), is:

$$R_E(t) = R_{E,0}\big(1 + \alpha \Delta T(t)\big) \tag{7.4}$$

where

$R_{E,0}$ is the resistance of the tube at the initial temperature (Ω)

α is the temperature coefficient that relates the increase in resistance with the increase in temperature of the material (Ω/K)

ΔT is the temperature difference of the tube between the initial temperature, T_0, and a temperature at given time (K)

t is the time (s)

$R_{E,0}$ depends on the geometry of the hot tube and can be calculated from the following equation:

$$R_{E,0} = \rho_0 \frac{l}{A} \tag{7.5}$$

where

ρ_0 is the electrical resistivity of the stainless steel tube at the initial temperature (Ωm)

l is the length of the hot tube (m)

A is the cross section area of the hot tube (m^2)

When using the hot tube technique it is important to be aware of the influence from the outside of the sample boundaries. According to the hot tube theory it is assumed that the testing sample is infinitely large, is at an initial constant temperature and has no influence from the outside sample surfaces. The hot tube is located in the x axis inside this infinite solid that has an intrinsic thermal

conductivity λ (W/(mK)), a density d (kg/m^3), a specific heat c_p (J/(kgK)) and a heat transfer coefficient between the tube and the solid h (W/(m^{2}K)). With all this data and a simulation program is possible to obtain the temperature increase at any point y, z around the tube and at any time t.

The apparatus used to record the changes of resistance of the hot tube was the SourceMeter™ Line 2430, it is a source measurement unit instrument that provides precision voltage and current sourcing. Its working 4 wire principle is explained in Figure 7.12,

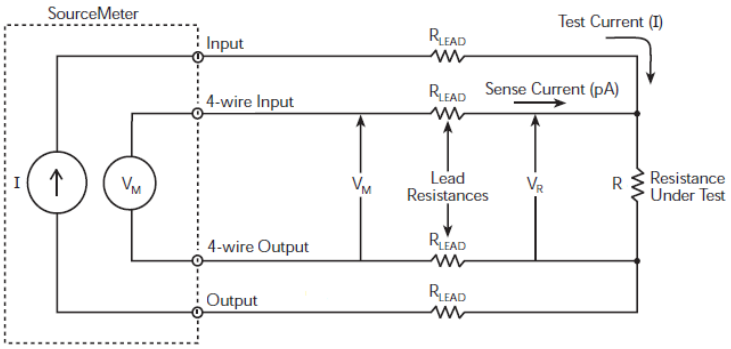

Figure 7.12 - 4 Wire SourceMeter™ resistance sensing diagram

where

I is the applied current from the SourceMeter™ through the hot tube (A)

R_E is the electrical resistance under test (hot tube) (Ω)

$R_{E,LEAD}$ are the electrical resistances of the lead resistances, the connecting wires, (Ω)

V_M is the voltage measured by SourceMeter™ across the hot tube and connecting wires (V)

V_R is the voltage across the hot tube (V)

The main advantage of the 4 wire technique is that it minimizes the effects of lead resistances by measuring the voltage across the resistance under test with a second set of test leads. Since the sense current used is very low (in the order of pA) the lead resistances of the second set are negligible and the measured voltage is essentially the same as the voltage across the resistance under test.

$$R_E = \frac{V_R}{I} \approx \frac{V_M}{I} \tag{7.6}$$

To run this experiment with active carbon, the heating wire and temperature sensor had to be encapsulated or insulated from the testing material as the active carbon is an electrical conductor. In this case the electronic varnish (RS 199-1480) was applied to the surface of the tube by dipping.

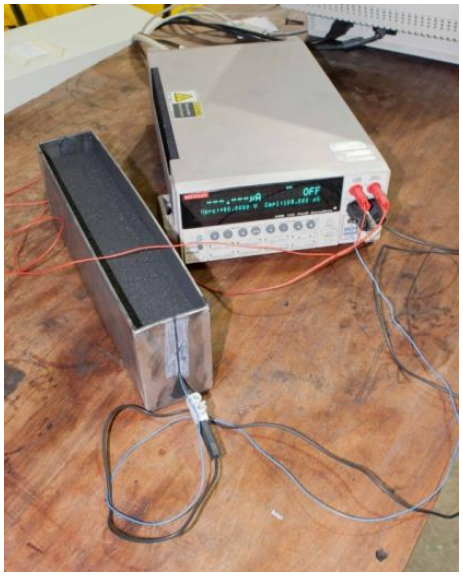

Figure 7.13 – Experimental set up of the transient technique, SourceMeter™ and hot tube buried in the carbon sample

The transient hot tube measurement was carried out using two different sample holders:

- The first one comprises a plastic measurement cylinder (40 mm diameter and 300 mm height) with a 100 mm hot tube place in its axis. This sample holder was used to measure thermal conductivities and thermal resistances of vibrated carbon samples.
- The second one comprises a metallic box (75 mm depth, 150 mm height and 300 mm length) with a 240 mm hot tube placed in longitudinally (see Figure 7.13). This sample holder was used to measure thermal conductivities and thermal resistances of mechanically compressed carbon samples.

For the chosen experiment time (60 s) the heated wave in the carbon never breaks through the boundaries of the samples, otherwise a shorter experiment time would have been chosen.

In all the experiments the applied current on the tube was 3 A and the environmental conditions were 20 °C and atmospheric pressure.

7.3.2. Accuracy of the experiments

The SourceMeter™ unit has detailed information in its manuals about the accuracy of the reading for different currents sources and voltage measurements. The applied current for all the experiments was 3 A with a source resolution of 500 nA, the measured voltages vary from 0.37 to 0.89 V with a measurement resolution of 10 µV and the sampling time was 0.2 s.

The current source accuracy is: $\pm(0.045\% * I + 2\mu)\ A$

The voltage measurement accuracy is: $\pm(0.067\% * V + 300\mu)\ V$

Operating with the known experimental values it is possible to obtain the accuracy of the measured resistances.

In the case of the short hot tube (100 mm) the accuracy is: $\pm 0.150\% * R\ \Omega$

For the long hot tube (240 mm) the accuracy is: $\pm 0.106\% * R\ \Omega$

7.3.3. Analysis of transient hot tube experiments (mathematical modelling)

A computational simulation was written in Matlab™ in order to analyse the resistance results obtained in the transient hot tube experiments. It consists of a one dimensional finite difference model in which the stainless steel tube and the varnish layer are represented by single elements and the active carbon in which the tube is immersed is represented as a grid of concentric layers to the tube axis. The model can be schematically represented in Figure 7.14.

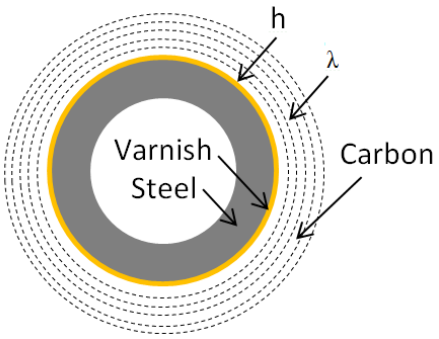

Figure 7.14 - Cross section drawing of the hot tube test

where *h* is the heat transfer coefficient of the air layer that surrounds the hot tube (W/(m^{2}K)) and *λ* is the intrinsic thermal conductivity of the surrounding carbon (W/(mK)).

When modelling the experiment in this way, with a heat transfer coefficient and an intrinsic thermal conductivity, the simulation produces more accurate results and makes it possible to investigate the effect of the wall contact resistance between the different samples and the tube.

The tube wall and air heat transfer coefficient is defined by Equation 7.7.

$$h_{wair} = \frac{k_{air}}{t_{air}} \tag{7.7}$$

where

k_{air} is the air thermal conductivity (W/(mK))

t_{air} is an assumed equivalent air layer thickness that surrounds the hot tube (m)

The stainless steel tube used in the experiments has an outer diameter of 1.2 mm and an inner diameter of 0.8 mm, and the thickness of the varnish layer is 0.05 mm (measured by weighting).

The following table shows the thermo physical properties of the stainless steel and varnish needed to simulate the experiments.

Properties	**Stainless steel**	**Varnish**
Density (kg/m^3)	7873	920
Specific heat (J/(kgK))	485	2090
Thermal conductivity (W/(mK))	16.2	0.12

Table 7.1 - Thermophysical properties of the materials used in the modelling [3, 4, 5]

Before starting the hot tube experiments the resistance of the tube at the initial temperature, R_0, has to be measured. In order to do that, a low electrical current, 10 mA, was applied to the tube and the resistance value was measured to be 1.1982 Ω/m. The resistance temperature coefficient of the stainless steel, α, found from the literature is 0.00112 Ω/m [3].

As the thermal conductivity of the air depends on the temperature and ambient pressure, the value used in the simulations is 0.0321 W/(mK) that corresponds to a temperature of 40 °C (313 K), an average of the tube temperature during the experiments and to atmospheric pressure [6].

The specific heat capacity of the carbon is found to be a function of its temperature in Kelvin is defined in Equation 7.8.

$$c_p = 175 + 2.245 * T(t) \quad (7.8)\ [2]$$

7.4. Active carbon specifications

The granular carbon and the carbon powder used in the experiments were supplied by Chemviron Carbon Ltd., both being type 208C based on coconut shell precursor.

Carbon specifications:

- **12 x 30 USS** (Coarse size, carbon grains can pass through a sieve opening of 1.7 mm but not through an opening of 600 μm): Maximum granular bulk density after vibrating process of 560 kg/m^3.

- **20 x 40 USS** (Medium size, carbon grains can pass through a sieve opening of 850 μm but not through an opening of 425 μm): Maximum granular bulk density after vibrating process of 527 kg/m^3.
- **30 x 70 USS** (Medium size, carbon grains can pass through a sieve opening of 600 μm but not through an opening of 212 μm): Maximum granular bulk density after vibrating process of 553 kg/m^3.
- **50 x 100 USS** (Fine size, carbon grains can pass through a sieve opening of 300 μm but not through an opening of 150 μm): Maximum granular bulk density after vibrating process of 513 kg/m^3.
- **Greater than 80 USS** (Powder, carbon grains that can pass through a sieve opening of 180 μm): Maximum granular bulk density after vibrating process of 544 kg/m^3.

The thermal conductivity and wall contact thermal resistance of the previous five carbon grades were investigated. Every grade was measured on its own and then three binary mixtures of 66.7% grains - 33.3% powder, 50.0% grains - 50.0% powder and lastly 33.3% grains - 66.7% powder (by weight) for each carbon grain were measured.

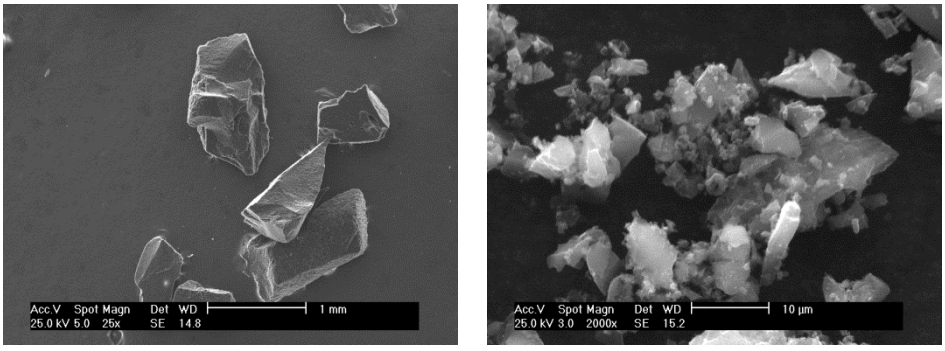

Figure 7.15 – (a) Carbon grains size 12x30, (b) Carbon powder

The round samples (with heat flow parallel to the compression direction) were tested at different thicknesses and densities, depending on the amount carbon placed in the holder and the pressure applied by the upper plate of the Anter Quickline-10^{TM} machine. In the case of the square cross-section area samples (with heat flow perpendicular to the compression direction), four different sample holder's walls were manufactured creating carbon samples of 2 mm, 5 mm, 10 mm and 15 mm thickness. Every carbon mixture of every grain size was measured at least at two different

thicknesses. This was done to investigate the effect of the wall contact thermal resistance and how the bulk density could be affected by the sample thickness.

Before conducting a test the carbon had to be dried to eliminate the moisture that could be adsorbed from the surrounding air. It is sufficient to leave the carbon for 30 min at 150 °C in a furnace.

7.5. Results and discussion

As five different grain sizes and four different gran/powder ratio samples were tested a large amount of data was obtained that can be better analysed separating it in various figures according to grain sizes and grains/powder ratio.

7.5.1. Grain size analysis

The previous data is analysed according to the grain size of the sample mixtures.

7.5.1.1. 12x30 grains samples

In Figure 7.16 it is observed that the intrinsic thermal conductivity of all the samples increases with density at a similar rate. There is a good agreement between the steady state and the transient technique results as observed from the 100% grains and 2/3 grains mixture samples.

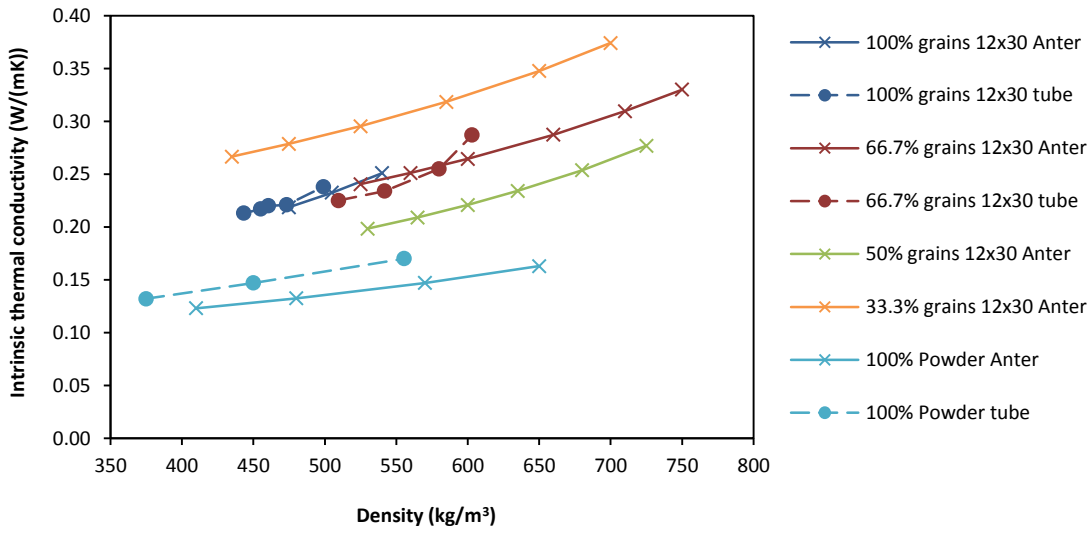

Figure 7.16 – Intrinsic thermal conductivity of various 12x30 grains and powder binary mixtures, 100% grains and 100% powder samples measured by steady state and transient techniques

The mixture that shows the best heat transfer performance is the 2/3 grains mixture, that reaches an intrinsic thermal conductivity of 0.33 W/(mK) at 750 kg/m^3.

The steady state values obtained for the 1/3 grains mixture show a much higher performance than the other two binary mixtures (2/3 and 1/2 grains) and from later analysis done is this chapter it can be stated that these values are not correct.

In Figure 7.17 it is observed that the contact layer thickness of the samples decreases with density. The 100% grain samples show a lower contact air layer thickness than the powder at the same densities. This could be due to the fact that the 100% grain samples provide large grain contact areas (as 12x30 is a large size grain) when the grains are well arranged and their flat sides touch the hot tube creating a good heat transfer path, instead of the point contacts that the 100% powder samples create.

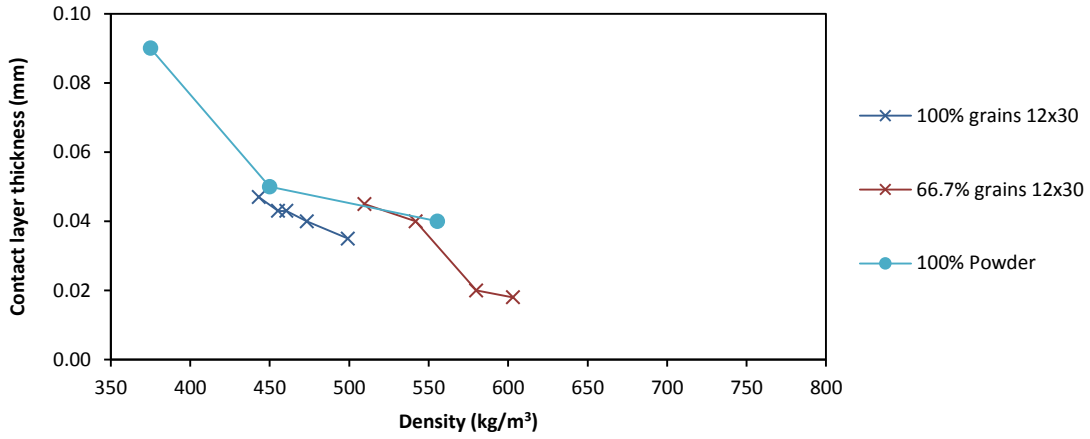

Figure 7.17 – Contact air layer thickness of various 12x30 grains and powder and 100% powder samples measured by transient technique

The contact layer thickness of the 2/3 grains mixture has similar values to the powder samples at low densities (around 0.04 mm at 525 kg/m^3) but at high densities the contact layer thickness decreases sharply (around 0.02 mm at 600 kg/m^3).

7.5.1.2. 20x40 grains samples

In Figure 7.18 it is observed that the intrinsic thermal conductivity of all the samples increases with density at a similarly rate. There is a good agreement between the steady state and the transient technique results except for the 1/3 grains binary mixture sample.

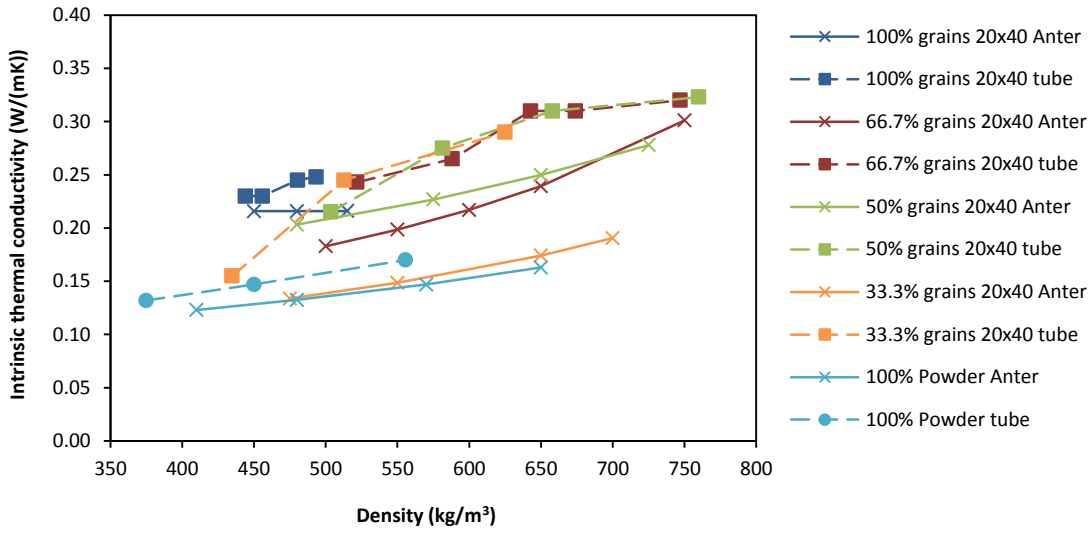

Figure 7.18 – Intrinsic thermal conductivity of various 20x40 grains and powder binary mixtures, 100% grains and 100% powder samples measured by steady state and transient techniques

The mixtures that show the best heat transfer performances are the 2/3 grains and 1/2 grains mixture, that reach an intrinsic thermal conductivity of 0.3 W/(mK) at 750 kg/m^3. The steady state results for the 1/3 grains mixture show a much lower heat transfer performance than the transient results for the same mixture and than the other two binary mixtures.

Samples of binary mixtures show higher densities and higher thermal conductivities than grains or powder on their own. This is achieved because the powder particles fill the air gaps that exist between grains. The better the ratio volume grain/powder and amount grain/powder the higher the density and therefore thermal conductivity.

At low densities he binary samples achieve thermal conductivity values comprised between the powder and grains ones. This occurs as solid grains of carbon are located in the sample bulk and they improve the thermal conductivity.

Figure 7.19 shows the most complete set of data of the relationship between contact layer thickness and density for the 20x40 grain mixtures. It is observed that the contact layer thickness of the samples decreases with density and at high values it tends to stabilise in a certain contact layer thickness.

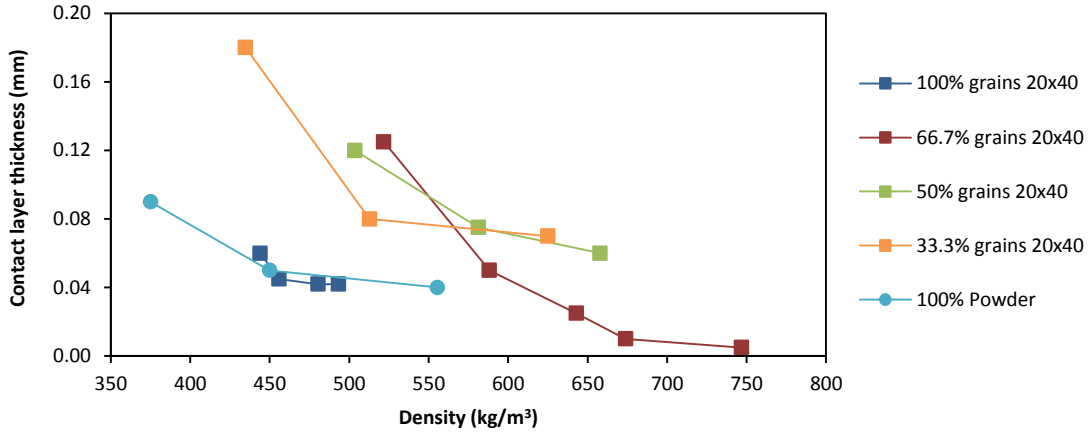

Figure 7.19 – Contact air layer thickness of various 20x40 grains and powder and 100% powder samples measured by transient technique

The 100% powder and 100% grains samples show similar contact air layer thicknesses at the same densities. The lowest contact layer thickness achieved corresponds to the 2/3 grains sample reaching 0.05 mm at 750 kg/m^3.

The contact layer thickness or contact resistance of a sample decreases while its density because while vibrated flat grain surfaces are arranged against other flat grain surfaces or other surfaces such as the hot tube, flat plate or walls of the sample holder.

7.5.1.3. 30x70 grains samples

In Figure 7.20 it is observed that the intrinsic thermal conductivity of all the samples increases with density at a similarly rate except for the 100% grains sample that remains constant and the 2/3 grains mixture sample that increases sharply. There is a good agreement between the steady state and the transient technique results.

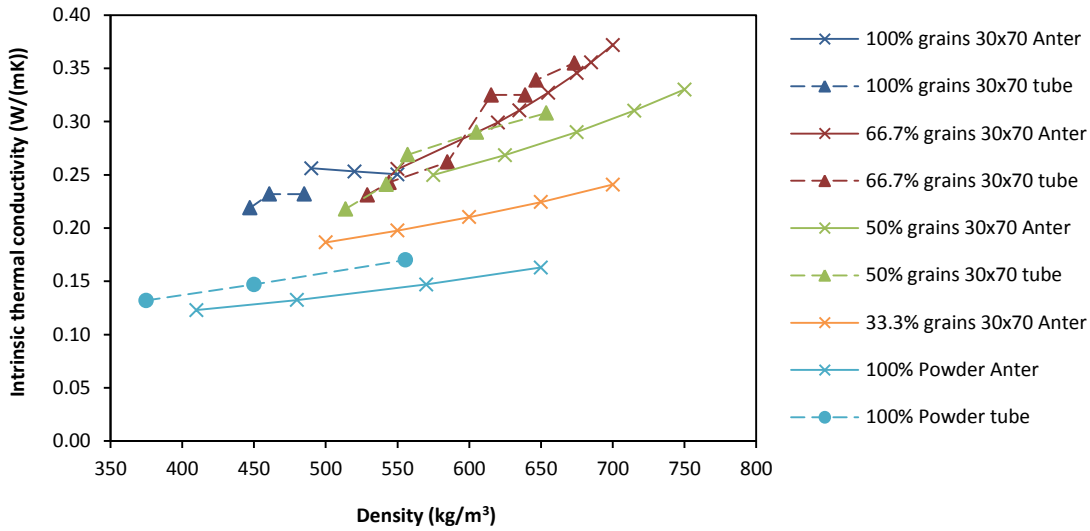

Figure 7.20 – Intrinsic thermal conductivity of various 30x70 grains and powder binary mixtures, 100% grains and 100% powder samples measured by steady state and transient techniques

The mixture that shows the best heat transfer performance is the 2/3 grains mixture, that reaches an intrinsic thermal conductivity of 0.37 W/(mK) at 675 kg/m^3. The 1/2 grains mixture shows similar values to the 2/3 grains mixture at low densities, being lower at higher densities. The 1/3 grains mixture shows the lowest performance of the three binary mixtures but higher than the 100% powder, reaching 0.25 W/(mK) at 700 kg/m^3.

In Figure 7.21 it is observed that the contact layer thickness of the samples decreases with density and at high densities it tends to stabilise in a certain contact layer thickness.

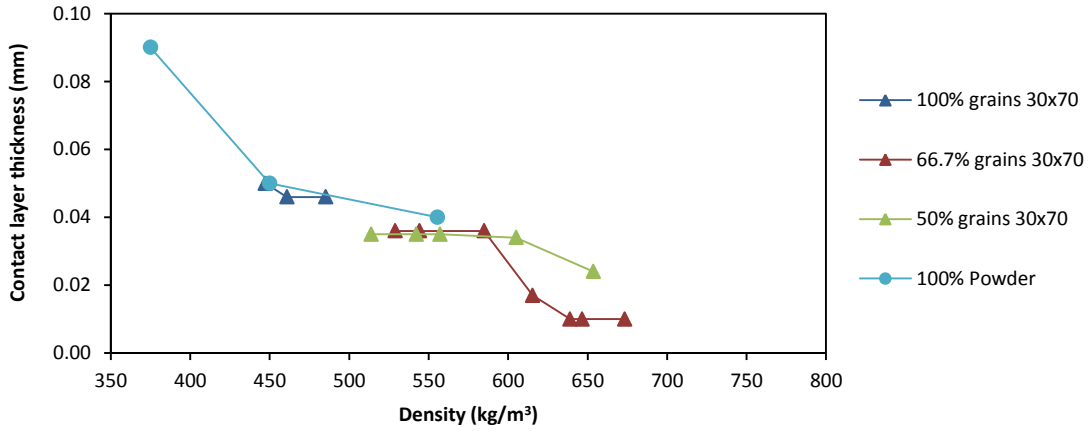

Figure 7.21 – Contact air layer thickness of various 30x70 grains and powder and 100% powder samples measured by transient technique

The 100% grain samples show a similar contact air layer thickness to the powder at the same densities and both samples show higher values than the 2/3 grains and 1/2 grains mixture samples. The 2/3 grains and 1/2 grains mixtures' samples have similar results at low densities but at high densities the 2/3 grains mixture contact layer thickness drops sharply to a thickness of 0.01 mm stabilising at that value.

7.5.1.4. 50x100 grains samples

In Figure 7.22 it is observed that the intrinsic thermal conductivity of all the samples increases with density at a similarly rate except for the 2/3 grains and 1/2 grains samples that have a slightly higher slope. There is a good agreement between the steady state and the transient technique results for the 100% powder sample but in the case of the 2/3 grains sample there is a small difference between the two techniques' results.

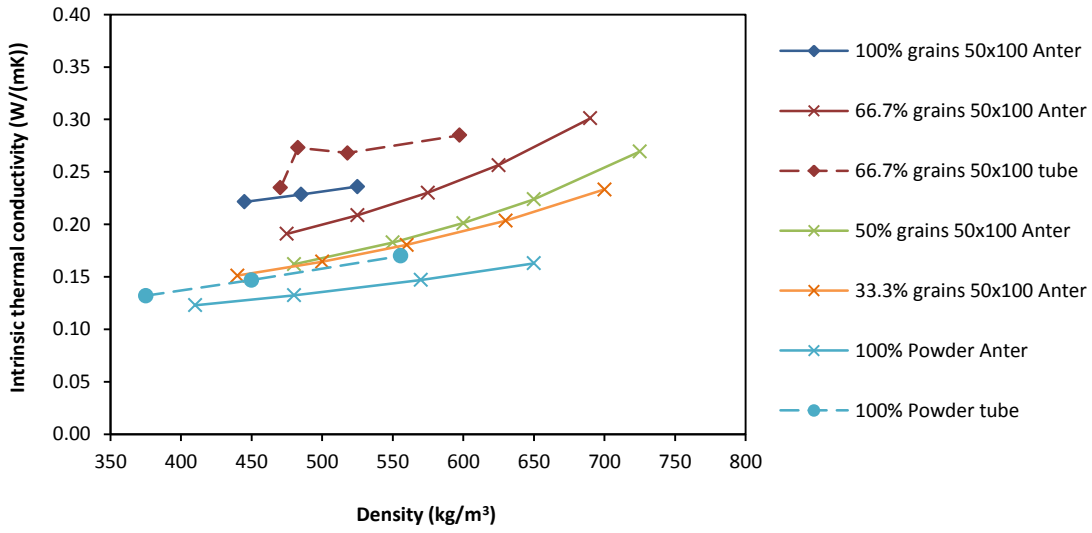

Figure 7.22 – Intrinsic thermal conductivity of various 50x100 grains and powder binary mixtures, 100% grains and 100% powder samples measured by steady state and transient techniques

The mixture that shows the best heat transfer performance is the 2/3 grains mixture, that reaches an intrinsic thermal conductivity of 0.3 W/(mK) at 700 kg/m^3. The 1/2 grains and the 1/3 grains mixtures show similar intrinsic thermal conductivity values at low densities but at higher ones the 1/2 grains sample performs better.

In Figure 7.23 it is observed that the contact layer thickness of the samples decreases with density and at high densities it tends to stabilise in a certain contact layer thickness.

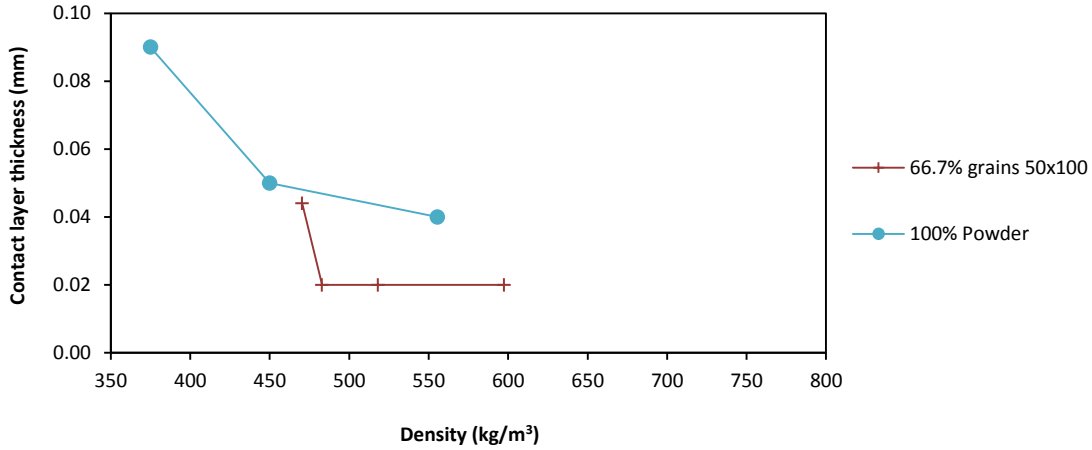

Figure 7.23 – Contact air layer thickness of 2/3 50x100 grains and powder and 100% powder samples measured by transient technique

The 2/3 grains sample shows better contact layer thicknesses than the powder and it stabilises in a contact layer thickness of 0.02 mm at a low density (480 kg/m^3) and remains constant at higher densities.

7.5.2. Grains-powder ratio analysis

The intrinsic thermal conductivity and wall contact resistance data of the carbon is analysed according to the ratio of grains to powder of the sample mixtures.

7.5.2.1. 100% grains and 100% powder samples

In Figure 7.24 it is observed that for all the samples the intrinsic thermal conductivity increases with density. In the case of the 100% grains samples, they fall in a narrow range of density, between 450 and 550 kg/m^3, and their intrinsic thermal conductivity only varies from 0.20 to 0.25 W/(mK). There is not a clear difference in thermal conductivity between the different grain sizes and all the samples show a good agreement when measured with the two techniques, steady state and transient.

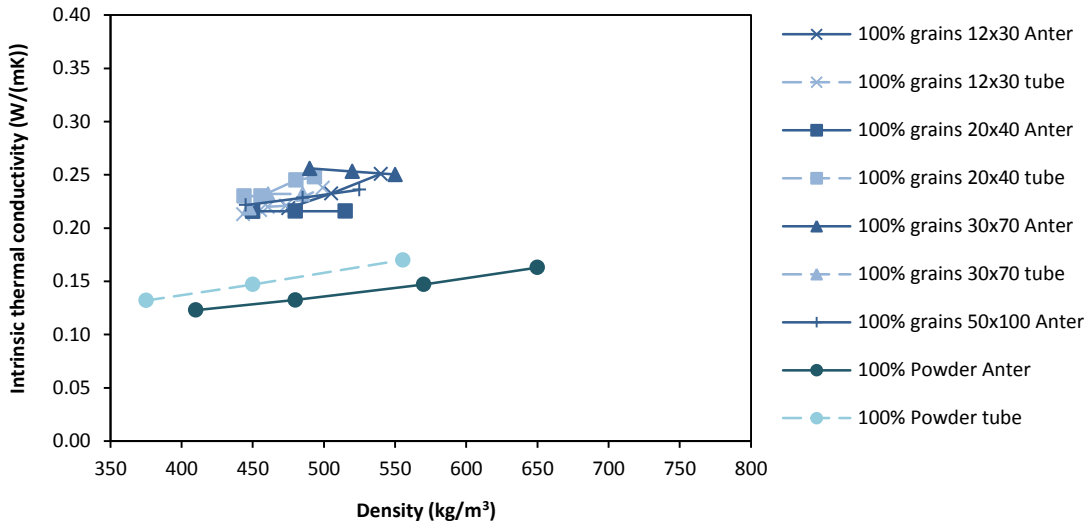

Figure 7.24 – Intrinsic thermal conductivity of 100% various grain sizes (12x30, 20x40, 30x70) and 100% powder samples measured by steady state and transient techniques

The 100% powder samples show a wider density range and lower intrinsic thermal conductivities when compared to the 100% grains ones. The agreement between steady state and transient techniques is quite good showing a small constant off set of 0.05 W/(mK).

At the same densities the powder samples show much lower thermal conductivity than the grain samples. This is due to the high amount of point contacts in the powder samples (contact resistance in the bulk of the sample) and due to the small size of the powder (poor amount of heat travelling through solid carbon).

Very low densities of powder (lower than grain densities) are possible to achieve as the fine carbon particles show electrostatic repulsion force. On the other hand, when compressed, the powder samples can achieve high densities (higher than the grain densities) as due to the small volume of the powder particles they are easily rearranged while vibrated/compressed and increase their packing density.

In Figure 7.25 are plotted the contact layer thickness of 100% grains and 100% powder samples. For all the samples, the contact layer thickness decrease with density.

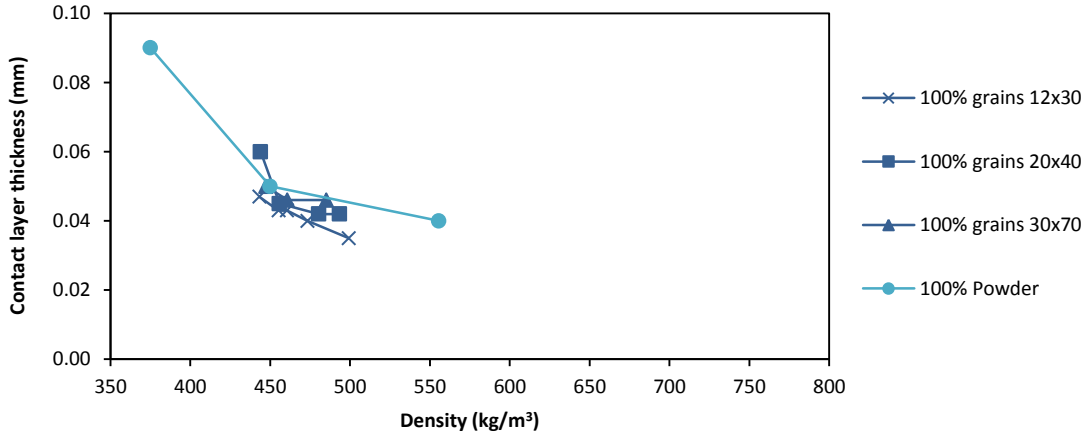

Figure 7.25 – Contact air layer thickness of 100% various grain sizes (12x30, 20x40, 30x70) and 100% powder samples measured by transient technique

The contact air layer thickness of the different grain sizes and the powder show similar results (0.04 to 0.05 mm) at the same densities (450 to 500 kg/m^3).

The contact layer thickness or contact resistance of a sample decreases while its density because while vibrated flat grain surfaces are arranged against other flat grain surfaces or other surfaces such as the hot tube, flat plate or walls of the sample holder.

Although the powder samples can achieve higher densities than the grains, their contact resistance does not reduce significantly due to the high number of point contacts.

7.5.2.2. 66.7% grains and 33.3% powder samples

In Figure 7.26 it is observed that for all the samples the intrinsic thermal conductivity increases with density. This grains/powder ratio mixtures have similar densities and intrinsic thermal conductivity values that range between 500 and 750 kg/m^3 and 0.15 and 0.35 W/(mK) respectively.

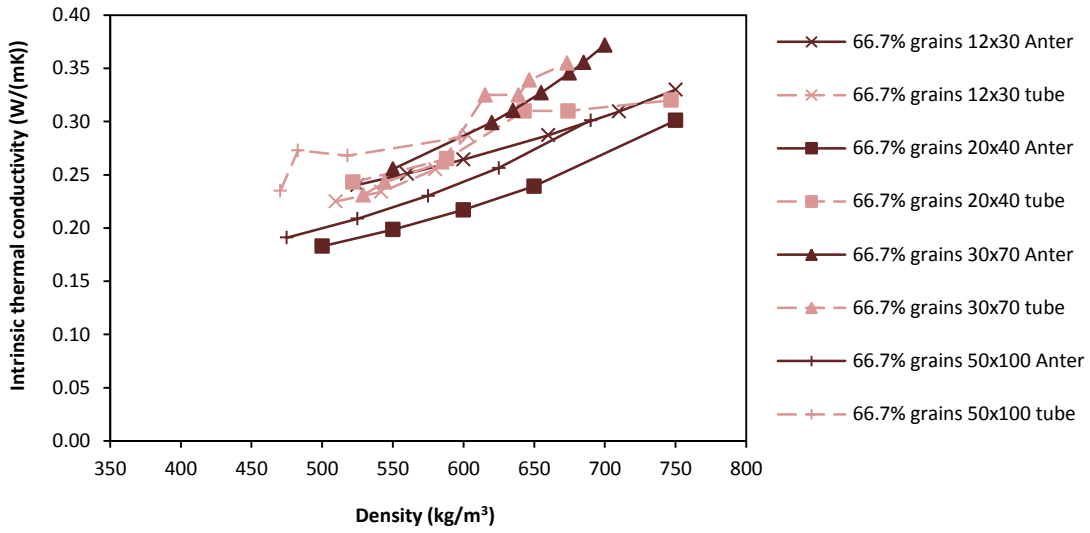

Figure 7.26 – Intrinsic thermal conductivity of 2/3 of various grain sizes (12x30, 20x40, 30x70, 50x100) and 1/3 powder binary mixture measured by steady state and transient techniques

There is a good agreement between the steady state but the transient experiments show slightly higher intrinsic thermal conductivities.

The contact layer thickness of the 2/3 grains samples are plotted in Figure 7.27 and it is observed that the contact layer thickness decrease with density stabilising in a certain value.

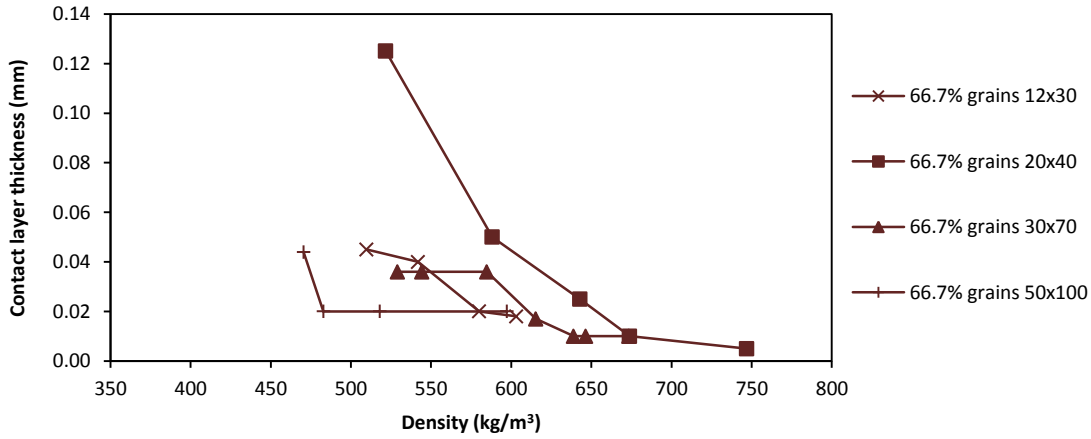

Figure 7.27 – Contact air layer thickness of 2/3 of various grain sizes (12x30, 20x40, 30x70, 50x100) and 1/3 powder binary mixture measured by transient technique

The 2/3 50x100 and 12x30 grains mixture stabilise at around 0.02 mm, the 2/3 30x70 grains mixture stabilises at 0.01 mm and the 2/3 20x40 grains mixture stabilises at a lower value of 0.05 mm. The 2/3 50x100 and 12x30 grains mixtures show poorer performance than the 2/3 30x70 and 20x40

grains mixtures ones and this could be due to the size ratio effect explained previously between grains and powder.

7.5.2.3. 50% grains and 50% powder samples

In Figure 7.28 it is observed that for all the 1/2 grains mixture samples the intrinsic thermal conductivity increases with density at a similar rate. There is a good agreement between the steady state and transient technique measurements although the latter show higher intrinsic thermal conductivity values.

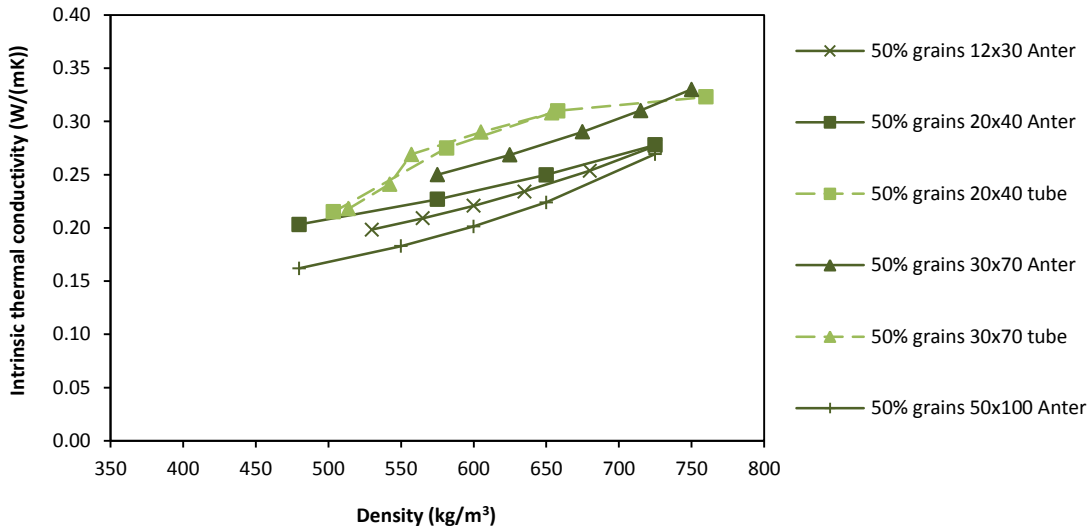

Figure 7.28 – Intrinsic thermal conductivity of 1/2 of various grain sizes (12x30, 20x40, 30x70, 50x100) and 1/2 powder binary mixture measured by steady state and transient techniques

The different grains mixtures samples have similar densities and intrinsic thermal conductivity values that range between 450 and 750 kg/m^3 and 0.15 and 0.35 W/(mK) respectively.

The 1/2 12x30 and 50x100 grains mixtures show poorer intrinsic thermal conductivity characteristics than the 1/2 30x70 and 20x40 grains mixtures that could be due to size ratio effect and number of point contacts, explained previously in the chapter.

The contact layer thickness of the 1/2 grains samples are plotted in Figure 7.29 and it is observed that the contact layer thickness decrease with density. The 1/2 30x70 grains mixture sample shows lower contact layer thickness than the ½ 20x40 grans mixture sample.

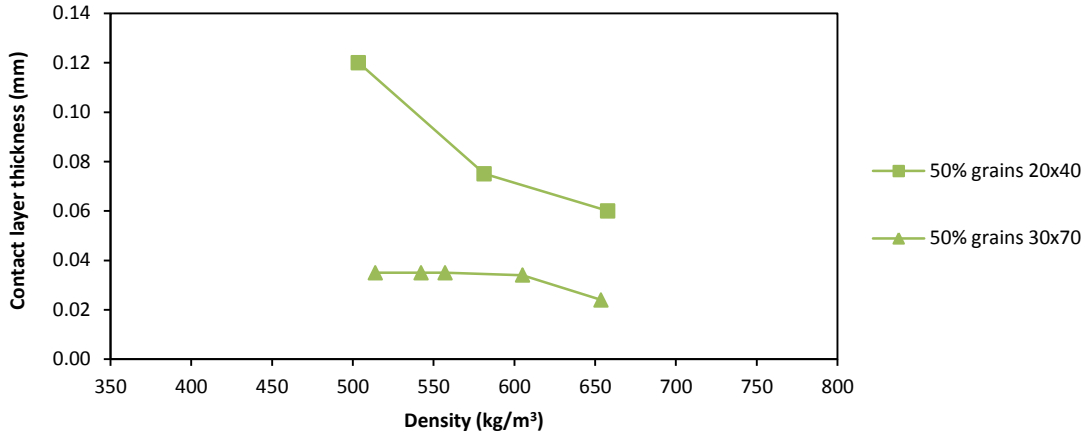

Figure 7.29 – Contact air layer thickness of 1/2 of various grain sizes (20x40, 30x70) and 1/2 powder binary mixture measured by transient technique

7.5.2.4. 33.3% grains and 66.7% powder samples

In Figure 7.30 it is observed that for all the 1/3 grains mixture samples the intrinsic thermal conductivity increases with density at a similar rate. The different grains mixtures samples have similar densities, ranging between 450 and 700 kg/m^3, and similar intrinsic thermal conductivities, ranging from 0.10 to 0.25 W/(mK), except for the 1/3 12x30 grains mixture which shows much higher values than the other samples.

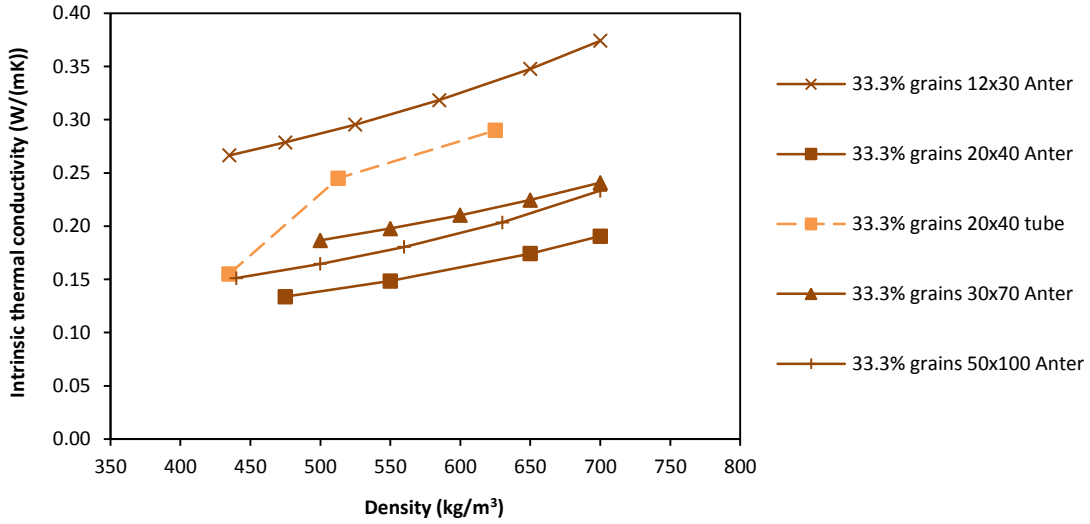

Figure 7.30 – Intrinsic thermal conductivity of 1/3 of various grain sizes (12x30, 20x40, 30x70, 50x100) and 2/3 powder binary mixture measured by steady state and transient techniques

There is a good agreement between the 1/3 20x40 grains mixture results measured by both techniques at low densities but not at medium and high densities.

The contact layer thickness of the 1/3 grains samples are plotted in Figure 7.31 and it is observed that the contact layer thickness decreases with density and stabilises in a certain value, 0.06 mm.

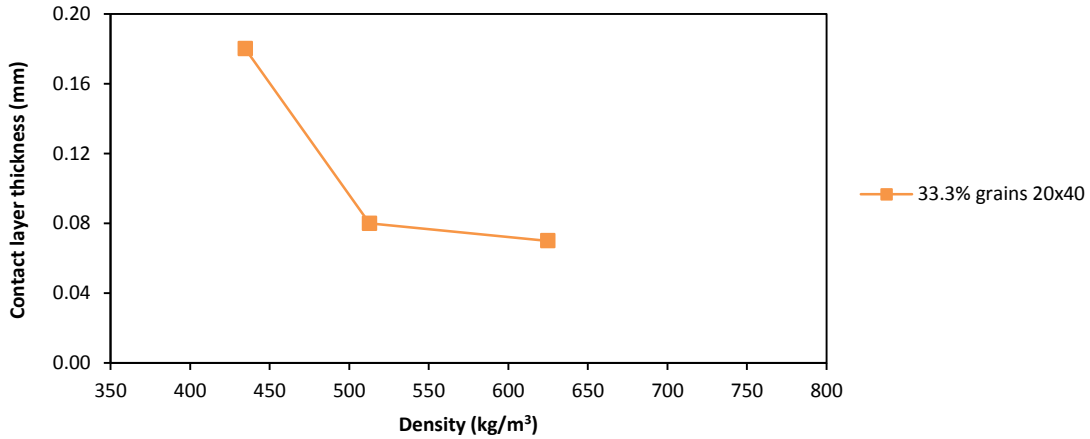

Figure 7.31 – Contact air layer thickness of 1/3 20x40 grains and 2/3 powder binary mixture measured by transient technique

7.6. Carbon samples evaluation for use in current sorption generators

In Figure 7.32 the relationship between the intrinsic carbon thermal conductivity and the ammonia contact layer thickness is plotted for different combinations of three different carbon thickness layers that might surround the generator tubes, 0.25, 0.5, 0.9, 1.5 and 2 mm, and three different U values, 300, 600 and 1200 W/(m^{2}K).

The relationship is calculated by the following equation and is an approximation of conductive radial heat transfer through a thin layer (modelled as a slab) of carbon plus convective heat transfer modelled as a conductive thin layer of gas (ammonia).

$$U = \frac{1}{\frac{d_C}{2\,\lambda_C} + \frac{t_{amm}}{k_{amm}}} \tag{7.9}$$

where

t_{amm} is the ammonia contact layer thickness between tube and carbon (m)

k_{amm} is the thermal conductivity of the ammonia gas at its average working temperature in the heat pump (W/(mK))

d_c is the thickness of the carbon layer that surrounds the generator tube (m)

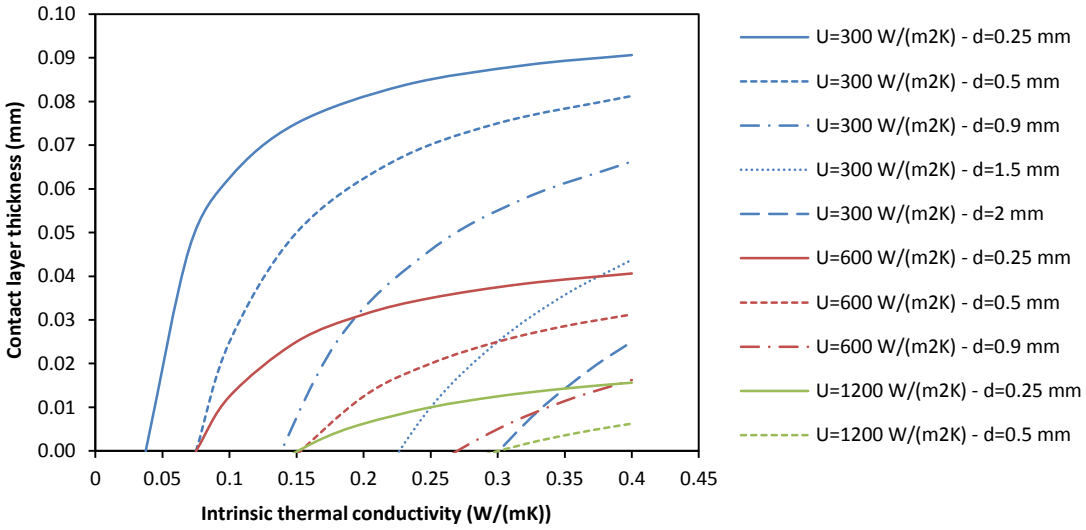

Figure 7.32 – Relationship between carbon intrinsic thermal conductivity and ammonia contact layer thickness for different generator U values and surrounding carbon layer thickness

From Figure 7.32 is possible to see that narrow surrounding carbon layer thickness (0.25 mm) and low U values (300 W/(m^{2}K)) are easier to achieve as the intrinsic thermal conductivity of the carbon can be low and its gas contact layer thickness can be high, low carbon heat transfer performance. When the surrounding layer of carbon gets thicker (2 mm) higher values of carbon intrinsic thermal conductivity and lower values of gas contact layer thickness must be achieved in order to maintain the certain U value, high heat transfer carbon performance.

For a constant surrounding carbon layer thickness its performance must increase if higher values of U want to be achieved.

For the small generator mentioned previously (300 mm long and 150 mm diameter) a UA value of 500 W/K should be achieved in order to perform satisfactorily as a heat pump and generate a power output of around 7 kW. That UA value approximately corresponds to an U value of 600 W/(m^{2}K). In Figure 7.33 the relationship between the specified U value, the carbon intrinsic thermal conductivity and the gas contact layer thickness between the tubes and the carbon are plotted for three different thicknesses of surrounding carbon layers.

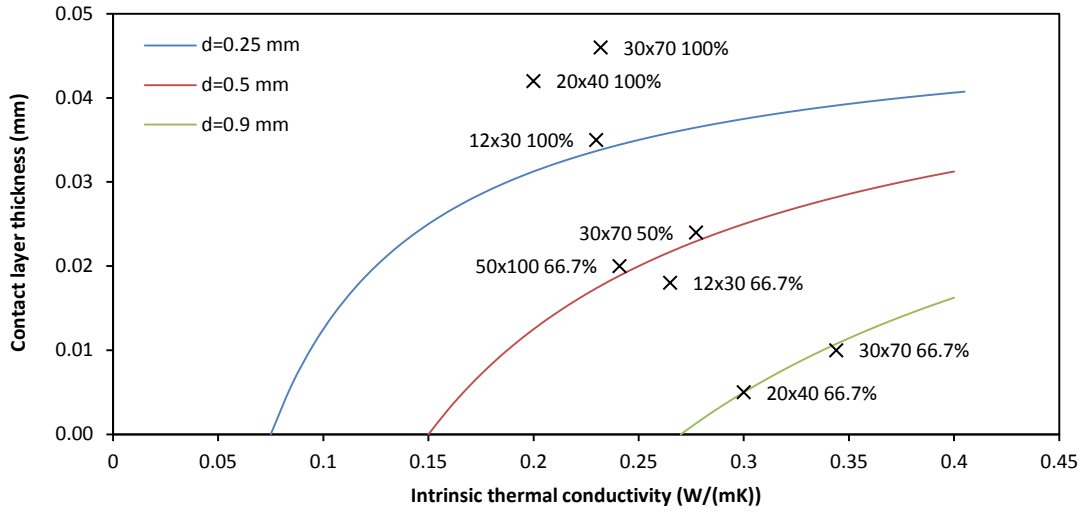

Figure 7.33 – Relationship between carbon intrinsic thermal conductivity and ammonia contact layer thickness for a generator U value of 600 W/(m^{2}K) at different surrounding carbon layer thickness and the best performing experimental values obtained

In addition to the curves, in Figure 7.33, the best heat transfer performing samples values obtained in the experiments are shown as crosses. Table 7.2 contains these best heat transfer performing carbon samples and for each one is indicated the grade of carbon, percentage of grains in the sample, density of the sample, gas layer contact thickness obtained by the transient method, intrinsic thermal conductivities obtained by the two methods and the final column shows the minimum value of the last two mentioned as these intrinsic thermal conductivities can show in some samples discrepancy between the two methods.

Grain size	% of grains in sample	Density (kg/m^3)	t_{air} (mm)	λ_{anter} (W/(mK))	λ_{tube} (W/(mK))	λ_{min} (W/(mK))
12x30	**100%**	499.17	0.035	0.23	0.24	0.23
12x30	**66.7%**	603.09	0.018	0.27	0.29	0.27
20x40	**100%**	493.33	0.042	0.20	0.25	0.20
20x40	**66.7%**	746.85	0.005	0.30	0.32	0.30
30x70	**100%**	485.20	0.046	0.25	0.23	0.23
30x70	**66.7%**	673.33	0.010	0.34	0.36	0.34
30x70	**50.0%**	653.70	0.024	0.28	0.31	0.28
50x100	**66.7%**	597.41	0.020	0.24	0.29	0.25

Table 7.2 – Best heat transfer performing carbon samples tested by the two methods, steady state and transient

In order to better analyse these experimental values in Figure 7.33, they can be divided in three groups. The first group comprises the samples that show the lowest intrinsic thermal conductivity values (around 0.2 W/(mK)) and the highest gas contact layer thickness (around 0.04 mm) correspond to the 100% grains samples of 12x30, 20x40 and 30x70. These samples fall over the 0.25 mm thickness surrounding carbon layer curve which means that in order to achieve a U value of 600 W/(m^2W) in the generator the surrounding carbon layer should decrease, having the tubes of the generator closer. Decreasing the gap between tubes would not be possible as most of the carbon grains would be larger than the gap.

The second group corresponds to samples of 66.7% of 50x100 and 12x30 and 50% of 30x70. They slightly higher intrinsic thermal conductivities (around 0.25 W/(mK)) and lower gas contact layer thickness (around 0.02 mm). These carbon mixtures could achieve the desired U value with a surrounding carbon layer around the tubes of 0.5 mm or higher.

The third group comprises carbon samples of 66.7% of 30x70 and 20x40. They achieve the highest intrinsic thermal conductivities (around 0.325 W/(mK)) and lowest air contact layer thickness (around 0.01 mm) of all the samples tested. According to the previous calculations these samples could achieve the desired U value with a surrounding carbon layer around the tubes of 0.9 mm that corresponds to the current generators' geometry.

According to the experiments and the analysis carried out two carbon mixtures once placed in the generators should have a high heat transfer performance and achieve the desired U value of 600 W/(m^2W). These two mixtures are:

- 2/3 20x40 grains and 1/3 powder at a density of 746.85 kg/m^3.
- 2/3 30x70 grains and 1/3 powder at a density of 673.33 kg/m^3.

The preferred one would be the 2/3 20x40 grains and 1/3 powder mixture as it can achieve the highest density.

7.7. Conclusions

In this Chapter the measurement of the intrinsic thermal conductivity of different carbon samples was carried out by two methods, steady state flat plate and transient hot tube technique, along with the measurement of their wall contact resistance by the transient hot tube technique.

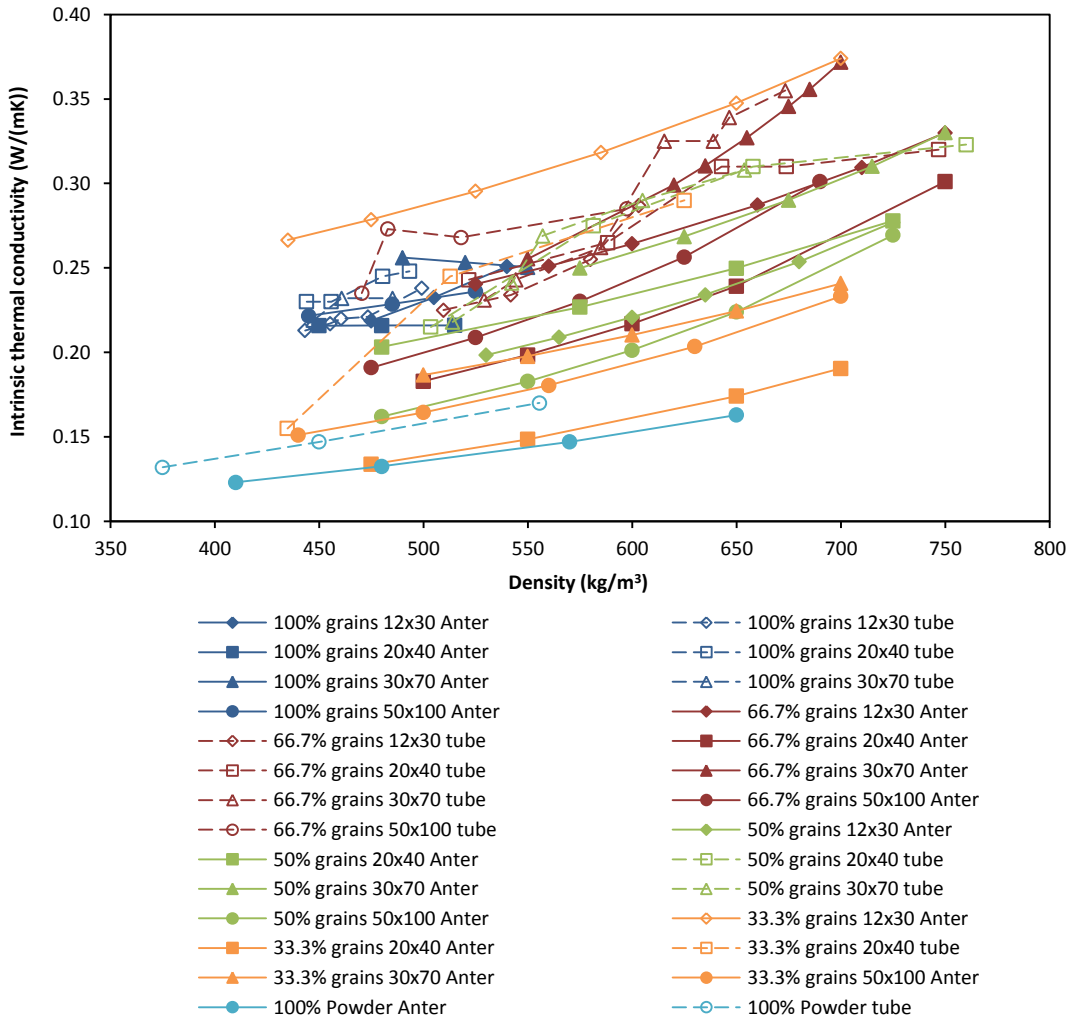

Figure 7.34 - Intrinsic thermal conductivity of various grain sizes (12x30, 20x40, 30x70 and 50x100) and powder mixtures measured by steady state and transient techniques

The Figure 7.34 shows the relationship between density and intrinsic thermal conductivity of binary samples of various grain sizes (12x30, 20x40, 30x70 and 50x100) and powder carbon at different ratios measured by the two techniques explained previously, steady state and transient. Other samples such as 100% grains or powder are plotted as well.

The overall trend that can be observed in Figure 7.34 is that the thermal conductivity of the samples increases with density. Its increasing rate (lines' slope) is similar for any type of sample (different mixtures or grains).

The density range for the different binary mixtures (2/3 grains, 1/2 grains, 1/3 grains) is similar, ranging from 500 up to 750 kg/m^3. Their intrinsic thermal conductivities vary from 0.15 to 0.35 W/(mK) depending on the sample density.

The density range for the different 100% grain samples (12x30, 20x40, 30x70 and 50x100) is similar, going from 450 to 550 kg/m^3. Their intrinsic thermal conductivities vary from 0.2 to 0.25 W/(mK).

The 100% powder samples show the poorest heat transfer performance. Its samples density range from 400 to 650 kg/m^3 and its intrinsic thermal conductivities vary from 0.10 to 0.15 W/(mK).

From Figure 7.34 it can be observed that overall there is a good agreement between the experiment results obtained by both methods, steady state and transient, except some samples such as 1/3 12x30 grains and 2/3 20x40 grains.

In Figure 7.35 the relationship between the contact air layer thickness between the hot tube and the carbon sample obtained by the transient technique and the samples' densities is plotted for the different carbon mixtures.

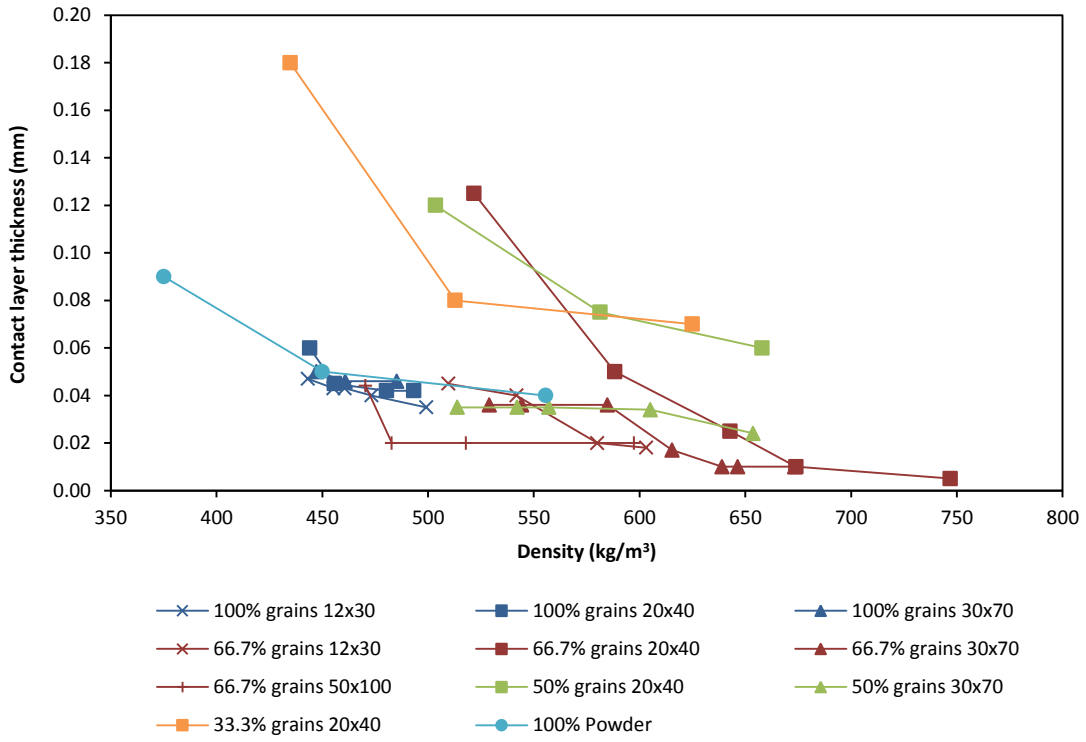

Figure 7.35 – Contact air layer thickness of various grain sizes (12x30, 20x40, 30x70 and 50x100) and powder mixtures measured by transient technique

The general trend that can be observed is that the contact layer thickness decreases with the sample density reaching a stable minimum at high densities.

In the case of the 2/3 50x100 and 12x30 grain mixture samples, they show a slightly poorer heat transfer performance than the 30x70 and 20x40 grain mixtures. This could be due to a size ratio effect between grains and powder and due to the number of point contacts in the mixture. When 12x30 (large) grains are mixed with powder even though there is more conductive heat transfer through the large grains, the gaps between grains are very large compared to the powder size and need lots of powder particles to fill them increasing the point contacts, so that the overall heat transfer characteristics of the mixture are low. When 50x100 (small) grains are mixed with powder even though the gaps between grains can be easily filled with powder, the number of point contacts in the sample increases due to the smaller size of the grains resulting in poor heat transfer performance.

On the other hand, when the 30x70 (medium) and 20x40 (medium) grains are mixed with powder there could is a situation where the trade off between size ratio and number of point contacts is optimum and the thermal characteristics of the mixtures is better than the 12x30 and 50x100 grains. The 100% grains samples show a limited density variation and their contact layer thicknesses do not experience a large variation with density.

Finally, with the data obtained from thermal conductivity and contact resistance experiments it was analysed if the current adsorption generators could achieve the desired U-value of 600 W/(m^2W). Two samples were found to achieve this value: the 2/3 20x40 grains and 1/3 powder sample at a density of 746.85 kg/m^3 and the 2/3 30x70 grains and 1/3 powder sample at a density of 673.33 kg/m^3. The preferred one was the 2/3 20x40 grains and 1/3 powder mixture as it could achieve the highest density and therefore would cycle a higher mass of adsorbent in the heat pump cycle.

References

[1] ASTM E1530 Standard, Standard Test Method for Evaluating the Resistance to Thermal Transmission of Materials by the Guarded Heat Flow Meter Technique, ASTM International, West Conshohocken, PA, 2011.

[2] Tamainot-Telto, Z., Critoph, R. E., Monolithic carbon for sorption refrigeration and heat pump applications, Applied Thermal Engineering, 21, pp.37-52, 2001.

[3] Graves, R. S., Kollie, T. G., McElroy, D. L., and Gilchrist, K. E., The thermal conductivity of AISI 304L Stainless Steel, International Journal of Thermophysics, Vol. 12, No. 2, 1991.

[4] Safety data sheet insulating varnish, CP0247 v2.3 RS 199-1480, Report date: 13/05/2010.

[5] Totten, G. E., Westbrook, S. R., Shah R. J., Fuels and lubricants handbook: technology, properties performance and testing, ASTM International, 2003.

[6] Lemmon, E. W. and Jacobsen, R. T., Viscosity and thermal conductivity equations for nitrogen, oxygen, argon and air, International Journal of Thermophysics, Vol. 25, No. 1, 2004.

Chapter 8

Construction of prototype system, instrumentation and control

8.1. Introduction

In this chapter the construction and design of the laboratory test system is presented. The heat pump prototype was constructed to test the performance of the generator described in Chapter 4 along with the carbon mixture chosen from Chapter 7 and to validate the computational model presented in Chapter 5.

8.2. System design

8.2.1. System Overview

The water schematic of the heat pump is shown in Figure 8.1 and the ammonia pipework is shown in Figure 8.2.

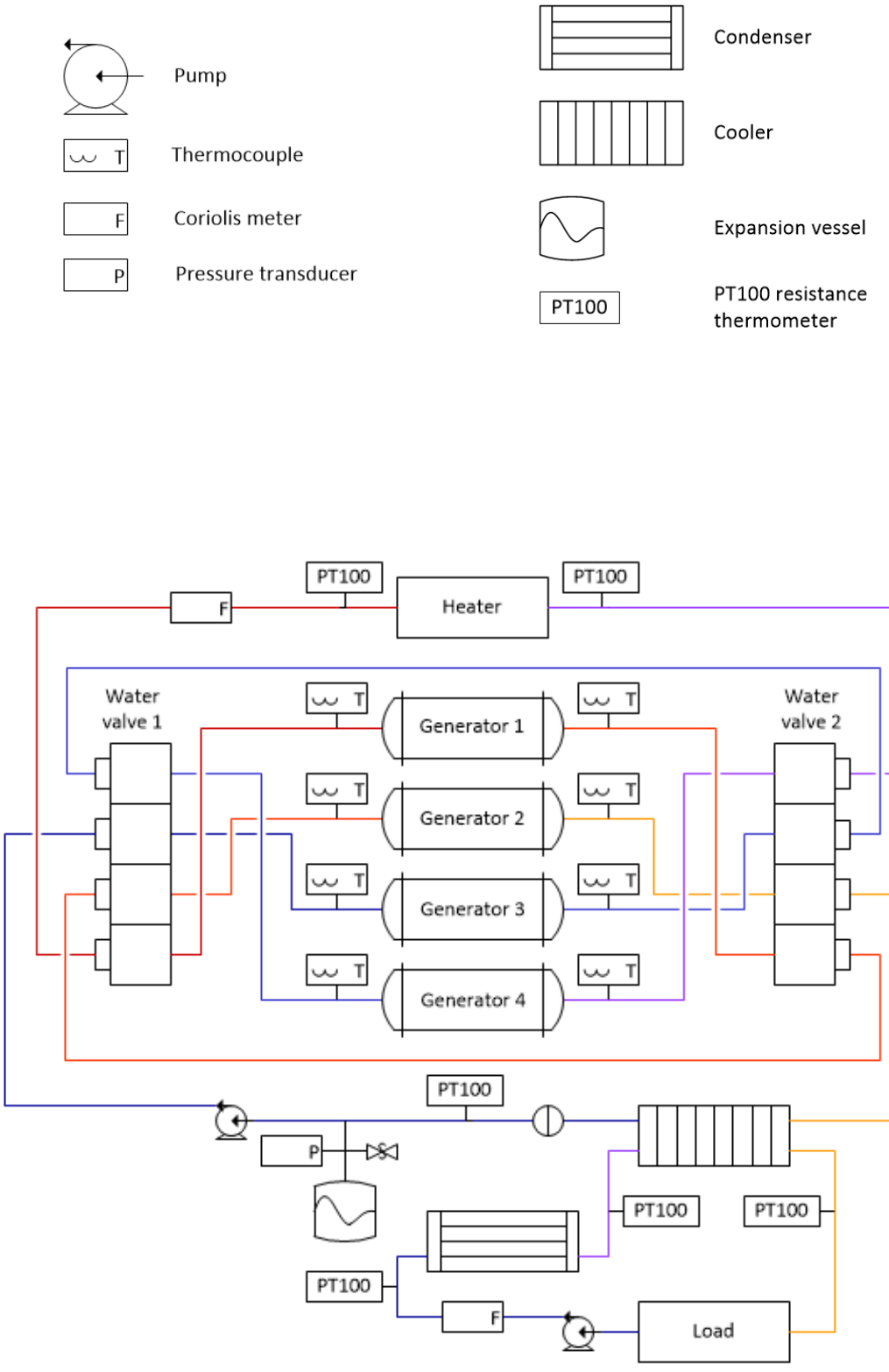

Figure 8.1 – Water pipework circuit

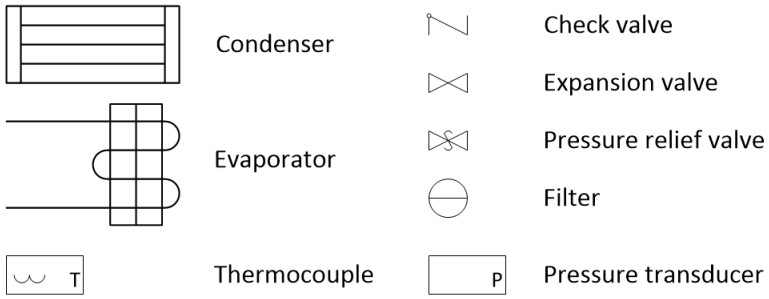

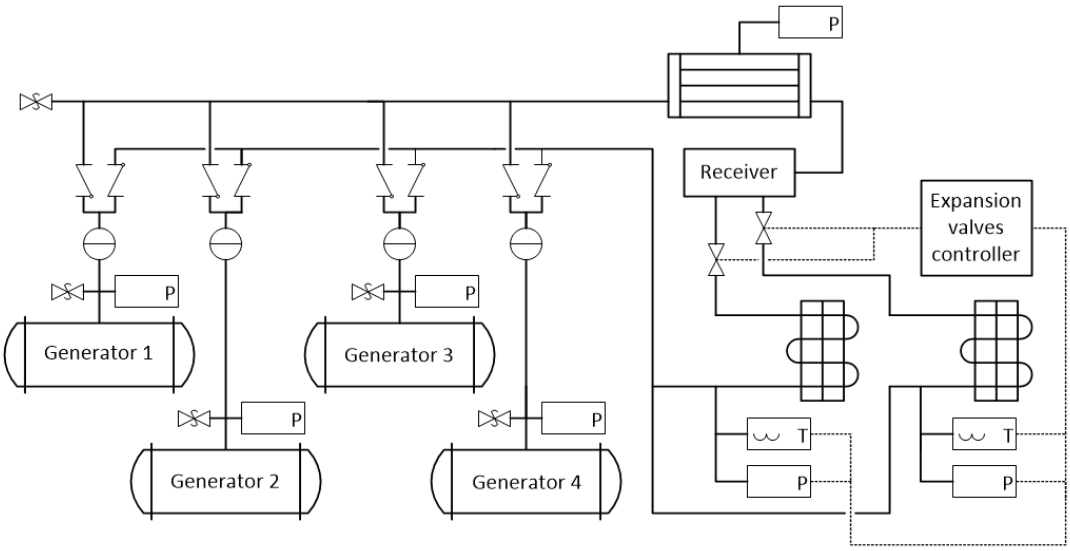

Figure 8.2 – Ammonia pipework circuit

The complete built system with large generators is shown in Figures 8.3 and 8.4.

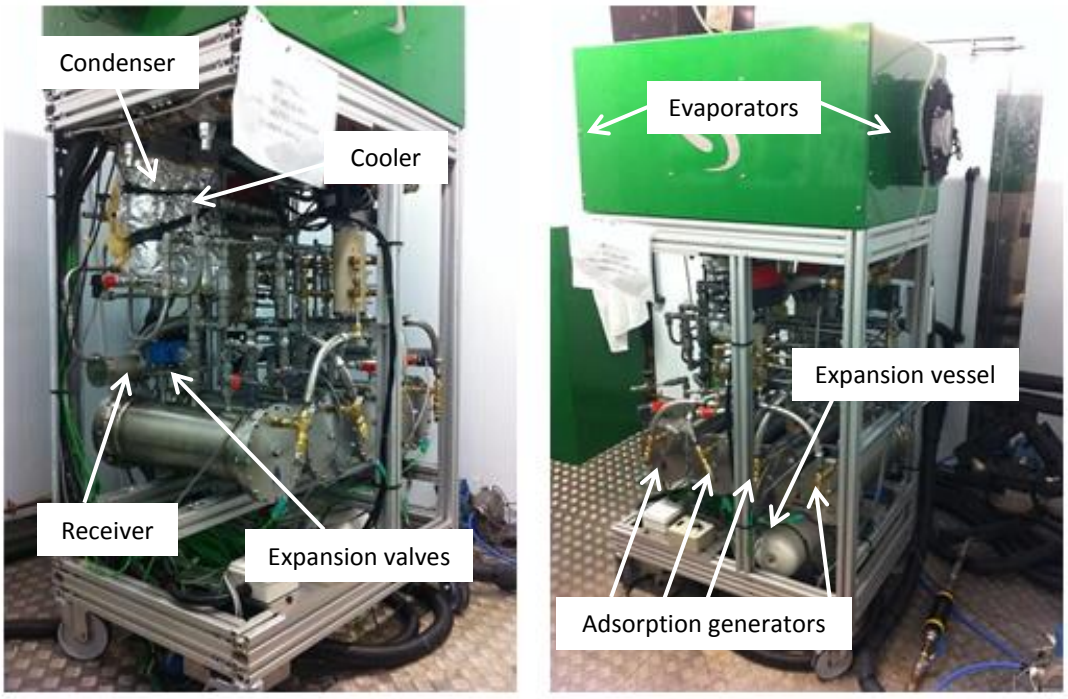

Figure 8.3 – (a, b) General view of laboratory system with large generators (insulation removed)

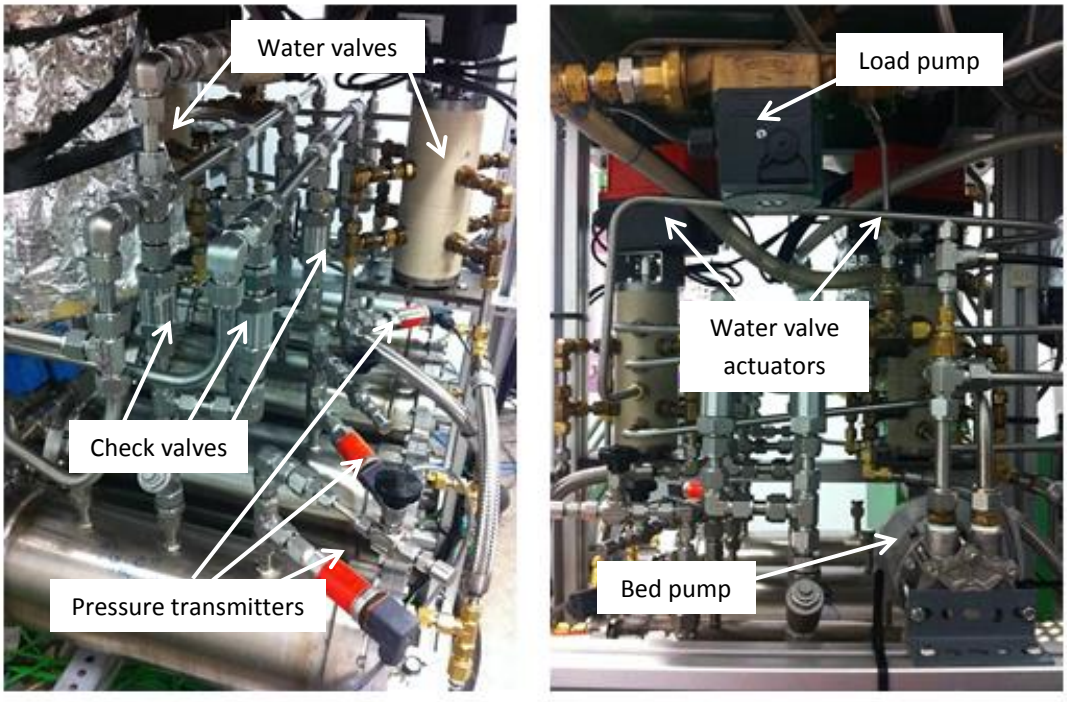

Figure 8.4 – (a, b) Detailed view of laboratory system with large generators (insulation removed)

The previous version of the heat pump machine that used the small generators had a gas burner, instead of an electric heater, and is shown in Figure 8.5.

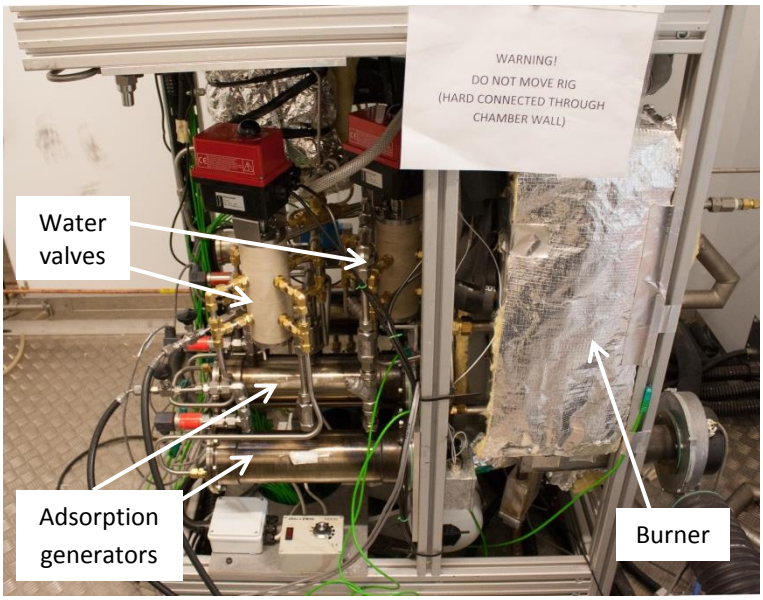

Figure 8.5 – Laboratory system with small generators (insulation removed)

8.2.2. Generators

The four generators used during the testing were described in Chapter 4. Two different size generators were tested at different times, rearranging the system accordingly. The latter ones tripled the size of the first ones in order to increase the heat output and were filled with a different carbon mixture to increase the heat transfer performance.

Tables 8.1 and 8.2 show the properties of the carbon used to fill the small and the large generators respectively.

Parameter	**Value**
Carbon type	Chemviron 208C
Mixture type	58% 20x40 grains, 29% powder and 13% binder
Packed density	527 kg/m^3
Intrinsic thermal conductivity	0.1 W/(mK)
Limiting (maximum) concentration, x_0	0.2551
Constant in the modified Dubinin-Astakhov equation, K	3.9615
Exponent in the modified Dubinin-Astakhov equation, n	1.227

Table 8.1 – Properties of the carbon used in the small generators

Parameter	Value
Carbon type	Chemviron 208C
Mixture type	2/3 20x40 grains and 1/3 powder
Packed density	640 kg/m^3
Intrinsic thermal conductivity	0.29 W/(mK)
Tube contact resistance	0.00087 m^{2}K/W
Limiting (maximum) concentration, x_0	0.2551
Constant in the modified Dubinin-Astakhov equation, K	3.9615
Exponent in the modified Dubinin-Astakhov equation, n	1.227

Table 8.2 – Properties of the carbon used in the large generators

8.2.3. Condenser

The condenser used was a plate heat exchanger and its specifications are shown in Table 8.3. It was manufactured by Alfa Laval, model name AlfaNova HP 27-20H, composed of diffusion bonded stainless steel plates compatible with ammonia.

Parameter	Value
Manufacturer	Alfa Laval
Model	AlfaNova HP27-20H
Number of plates	20
Heat transfer surface area	0.45 m^2
Overall heat transfer coefficient, UA_{cond}	1360.8 W/K

Table 8.3 – Condenser specifications

The manufacturer's data of this heat exchanger is included in Appendix B.

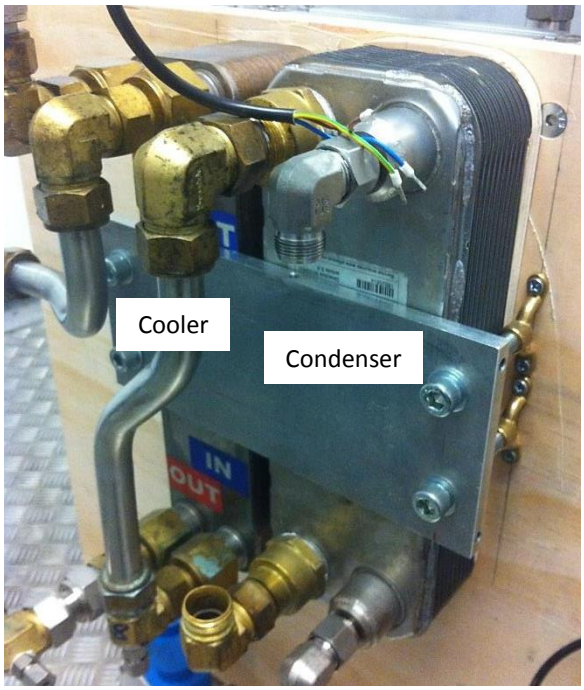

Figure 8.6 – Cooler and condenser

8.2.4. Cooler

The cooler used was a plate heat exchanger and its specifications are shown in Table 8.4. It was a copper brazed heat exchanger manufactured by UK Exchanger Ltd. As the cooler was never in contact with ammonia, copper brazing could be used.

Parameter	**Value**
Manufacturer	UK Exchangers Ltd
Model	SL23TL-AA 30
Number of plates	30
Overall heat transfer coefficient, UA_{cooler}	3467 W/K

Table 8.4 – Cooler specifications

The manufacturer's data of this heat exchanger is included in Appendix B.

8.2.5. Evaporator

Two identical evaporators were installed in the system. Their specifications are shown in Table 8.5 and they are pictured in Figure 8.7.

Parameter	Value
Manufacturer	Lordan
Model	R-717 Heat Pump
Finned height	400 mm
Finned length	450 mm
Air flow rate	1000 m^3/h
Overall heat transfer coefficient, UA_{ev}	369.9 W/K

Table 8.5 – Evaporator specifications

The evaporators were design and manufactured by Lordan. They were fan coils with stainless steel tubes and aluminium fins. They were direct expansion evaporators with one ammonia circuit each fed by a liquid distributor with a total of 64 tubes each in a bank of 4 rows deep.

Each evaporator included a separate defrost unit of 32 tubes in a banks of 2 rows deep.

Figure 8.7 – (a, b) Evaporators

The manufacturer's data of this evaporator is included in Appendix B.

8.2.6. Receiver

The purpose of the receiver is to store the liquid refrigerant that leaves the condenser and ensure that there is always a supply of refrigerant to the expansion valves.

When the system had the small generators installed one receiver was enough for the amount of refrigerant cycled (Figure 8.8a), but with the new larger generators another receiver was needed to store the higher level of refrigerant cycled and it was installed in series with the old one (Figure 8.8b).

Both receivers were made of a cylindrical stainless steel vessel by the University of Warwick workshops.

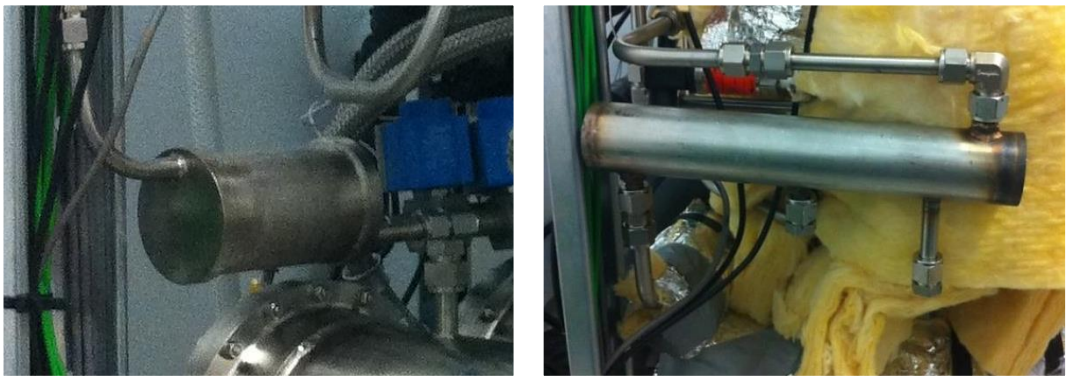

Figure 8.8 – (a, b) Refrigerant liquid receivers

8.2.7. Expansion valve

Due to the variable refrigerant flow rate of the system during a cycle a standard capillary tube could not be used as an expansion valve. Another option was a thermostatic expansion valve but due to its high thermal inertia it would not respond quickly to the refrigerant flow.

Instead, a more sophisticated device was used, an electronic controlled expansion valve especially design for ammonia. The expansion valve, pictured in Figure 8.9, was the model AKVA 10-1. It was actuated by a solenoid valve model 018F6177 and controlled by PID package in LabView. Both expansion valve and solenoid valve were manufactured by Danfoss. Two of these expansion valves (and solenoid valves) were installed in the system as two evaporators were being used.

Figure 8.9 – Expansion valves

The expansion valves actively controlled the evaporator superheat. The superheat of the ammonia leaving the evaporators was calculated by measuring the pressure and the temperature of the gas with a pressure transducer and a thermocouple respectively (specifications of both elements are explained in the Instrumentation section later in this chapter). The valves were operated so that the superheat was around 5 °C

8.2.8. Check valve

The first check valves used in the system were manufactured by Parker Instrumentation, model number 07YP 8Z(A)-C8L-5-T-SS, and are shown in Figure 8.10a. These were poppet type check valves and their cracking pressure was 5 psi (0.345 bar).

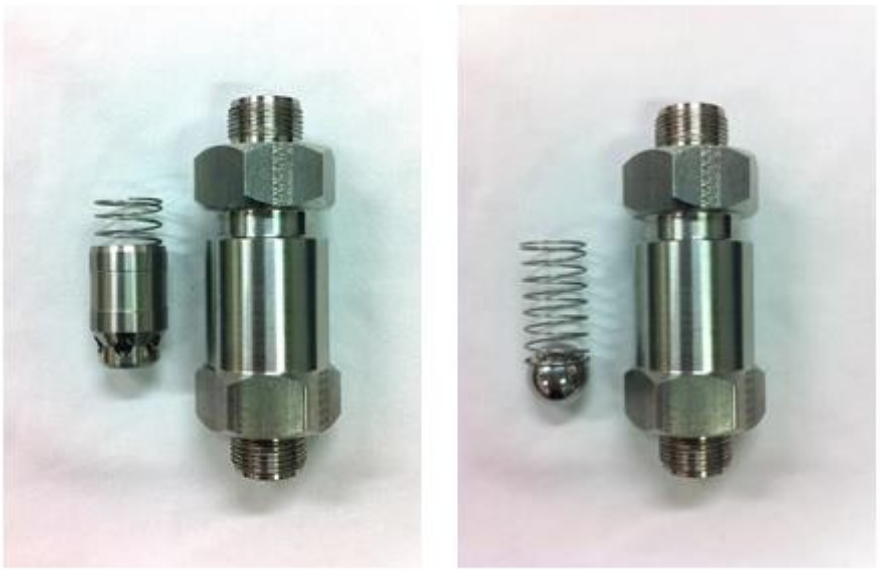

Figure 8.10 – (a) Check valve poppet type, (b) Check valve ball type

Due to the formation of salts in the ammonia circuit, explained in detail in the '5.Challenges' section of this Chapter, the check valves were modified maintaining the same body but changing the poppet for a suitable ball (bearing) and using a stronger spring that increased the cracking pressure to 10 psi (0.689 bar). The size of the ball used (diameter 17 mm) was chosen so that it allowed a good seal with the body gasket. The modified check valve is shown in Figure 8.10b.

A comparison of the internal elements of both check valves are pictured in Figure 8.11.

Figure 8.11 – Comparison of both types of check valves used

8.2.9. Heater

Even though the heat pump was design to be heat driven by gas, during the testing the hot water was supplied by an electric heater rather than a gas burner since it was more convenient and controllable and the aim of the testing was to evaluate the performance of the sorption system. The heater used in the system, pictured in Figure 8.12, was the model Unistat 610w water cooled manufactured by Huber. It specifications are shown in Table 8.6.

The desired temperature was set in the heater's display and the heater regulates the output temperature with a PID controller.

Parameter	**Value**
Manufacturer	Huber
Model	610w
Temperature range	-60 to 200 C
Heating power	6 kW

Table 8.6 – Heater specifications

It took approximately 5 cycles to reach a stable hot water input in the system and the inlet temperature varied a maximum of 3 °C when testing the large generators and 2 °C for the small generators.

Figure 8.12 – Electric heater

The manufacturer's data of this heater is included in Appendix B.

8.2.10. Water supply

The water used in the beds and in the load circuits was supplied from the mains water system. A small volume of corrosion inhibitor manufactured by Rochester Midland, type CLT-545, was added to the water. This corrosion inhibitor contains sodium nitrite and sodium molybdate.

8.2.11. Water valves

The water valves used in the system were specifically designed and manufactured for this project and are as analogous to 4-poles 4-way switches. The overall function of the valve is effectively to switch the relative positions of the beds the heater and the cooler as described in Chapter 2. Two water valves were manufactured and their body is pictured in Figure 8.13. It was made of PEEK^{TM} which can resist high temperatures (up to 250 °C) and has a low thermal conductivity (0.3 W/(mK)) that was needed as in consecutive sections of the valve temperature differences of up to 60 °C were experienced. The discs of the valves were made of brown alumina and were manufactured by a lapping process. In addition to the ceramic discs, other fittings of the valves were made of brass

(torque conductor) and stainless steel (shaft). To ensure a good internal sealing, custom gasket discs were cut and placed between the PEEK™ sections and the ceramic discs.

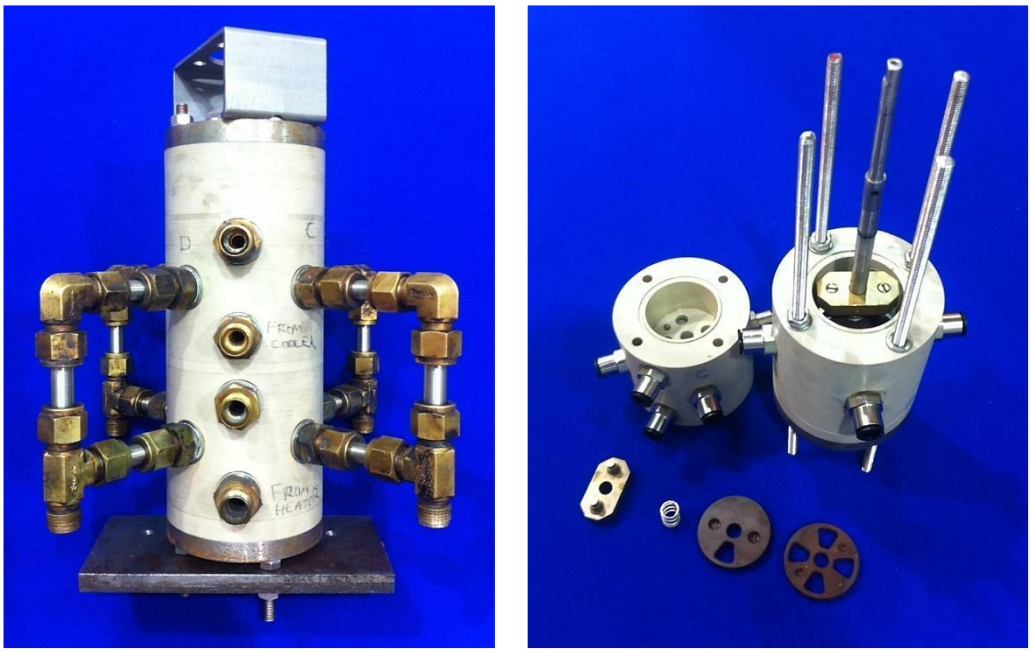

Figure 8.13 – (a) Ceramic discs water valve, (b) Half water valve open with components

The working sequence of the valves is shown in Figure 8.14, where the internal numbers 1, 2, 3 and 4 indicate the stage of the cycle, A, B, C, D refer to each one of the 4 beds and I and o to their inlet and outlet. The two valves could be simplified as a combination of six different valves that can move the four beds in cycles of four stages around the heater and cooler, as it was explained in Chapter 2.

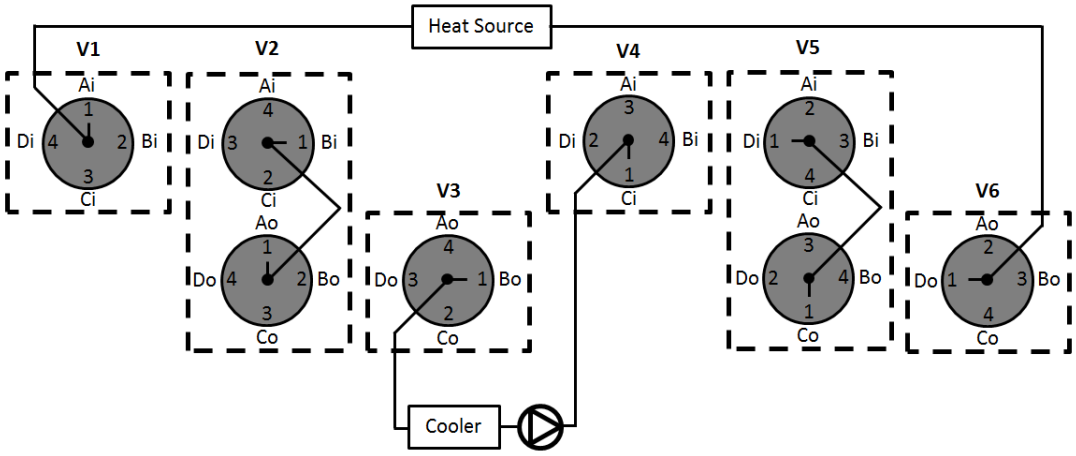

Figure 8.14 – Water valve schematics

8.2.12. Water pumps

One of the main advantages of this thermal wave heat pump cycle compared to other isothermal bed cycles was that only two pumps were needed in the system, pictured in Figure 8.15. One of the pumps used was fitted in the generators' water circuit and the other was fitted in the load's water circuit (as shown in Figure 8.1).

The generators' water pump it is located between the cooler outlet and one of the water valves that directs the water to the inlet of the bed that is being cooled. The load's pump is located between the load's outlet and the inlet to the condenser.

Figure 8.15 – (a) Bed pump, (b) Load pump

The load pump was set to a constant value of 0.16 kg/s for all the experiments whereas the speed of the generator's pump was variable in order to test the heat pump at different speeds and time cycles.

8.2.13. Expansion vessel

As the water used to heat and cool the generators needs to operate at high temperatures (120 to 170 °C), it was pressurised using an expansion vessel. The air side of the vessel is pressurised before the experiments at 6 bars.

8.2.14. Environmental chamber

The environmental chamber (Figure 8.16a) was specially designed for the University of Warwick and meets European standards for heat pumping testing. The two rooms can reach different levels of temperature and humidity ranging from -20 to 50 °C and 0 to 95% respectively.

Figure 8.16 – (a) Environmental chamber general view, (b) Environmental chamber load side

The heat pump machine was located in one room and the load (heaters) was located in the other room. In the first room winter environmental conditions were simulated, 0, 5 or 10 °C and humidity of 50% during testing whilst in the second room a house interior was simulated and the temperature was set to 25, 30 or 35 °C to ensure a constant return water temperature to the condenser.

8.3. Instrumentation

8.3.1. Temperature

The temperature measurements were made with a K-type thermocouple manufactured by TC Ltd and with PT100 thermometers, model PR-11-3-M15-150, manufactured by Omega.

The thermocouples were made of sheathed stainless steel and were 1 mm diameter whist PT100 thermometers were made of sheathed stainless steel and were 1.5 mm diameter.

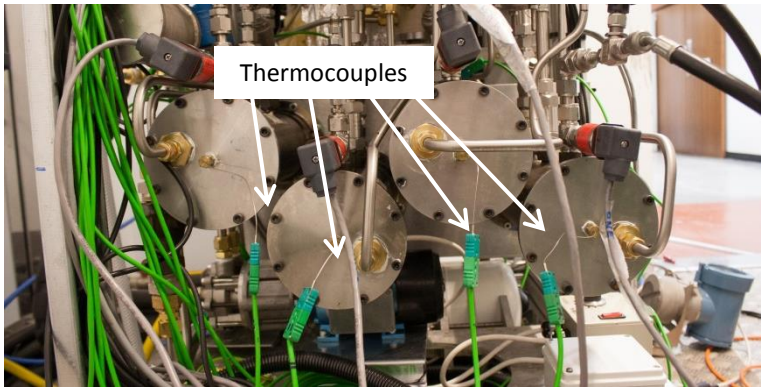

Figure 8.17 – Thermocouples installed in the small generators' end plate

12 thermocouples were installed in the system measuring water, ammonia and air temperatures. The location of each thermocouple is indicated in Table 8.7.

Channel number	Thermocouple location
1	Bed A water inlet
2	Bed A water outlet
3	Bed B water inlet
4	Bed B water outlet
5	Bed C water inlet
6	Bed C water outlet
7	Bed D water inlet
8	Bed D water outlet
9	Evaporator 1 suction
10	Evaporator 2 suction
11	Evaporator 1 air inlet
12	Evaporator 1 air outlet

Table 8.7 – Thermocouple locations

6 PT100 were installed in the system measuring water temperatures with high accuracy. The location of each PT100 is indicated in Table 8.8.

Channel number	PT100 locations
1	Hot water return
2	Hot water flow
3	Condenser inlet (load side)
4	Condenser outlet / Cooler inlet (load side)
5	Cooler outlet (load side)
6	Cooler outlet (bed side)

Table 8.8 – PT100 locations

8.3.2. Ammonia pressure

The ammonia pressure of the four generators, two evporators and condenser was measured using a Danfoss pressure transmitter type AKS 32. It specifications are shown in Table 8.9.

Parameter	Value
Manufacturer	Danfoss
Model	AK 32 060G2080
Pressure range	0 – 40 bar
Accuracy	± 0.3 %
Output signal	0 -10 V

Table 8.9 – Pressure transmitter specifications

8.3.3. Water flow rate

The flow rate of the water circulating in the beds loop and the water circulating in the load loop was measured using two Coriolis meters (Figure 8.18) manufactured by Emerson. Its specifications are shown in Table 8.10.

Figure 8.18 – (a, b) Coriolis meters

Parameter	Value
Manufacturer	Emerson
Model	CMF050M/L
Line size	1/2'' – DN15
Zero stability	0.164 kg/h
Nominal flow rate	3460 kg/h
Maximum flow rate	6800 kg/h
Max. working pressure	103 bar

Table 8.10 – Pressure transmitter specifications

The errors of the measurements vary between 0.144 % estimated for a mass flow of 0.03 kg/s and 0.248 % for a mass flow of 0.01 kg/s.

8.3.4. Data acquisition

The data acquisition was carried out using a PXI-6259 data acquisition card with a SCXI-1102 signal conditioner, pictured in Figure 8.19. The pressure transducers, thermocouples and Coriolis meters were connected to the analogue inputs whereas the expansion valves were monitored using a digital input channel.

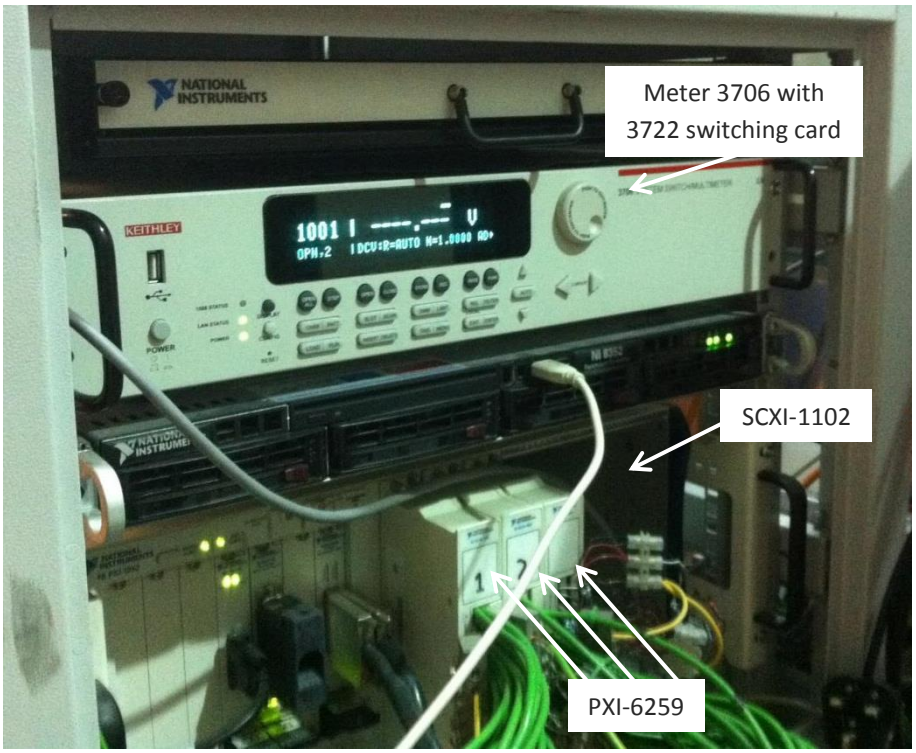

Figure 8.19 – System switch/multimeter, data acquisition card and signal conditioner

The system switch/multimeter, model number 3706 with a 3722 switching card was used for the PT100 thermometers and they were manufactured by Keithley.

The solenoid valves of the expansion valves and the bed's water pump are controlled by the relay rack pictured in Figure 8.20 situated in the controller box, where the actuators power supply and the water pumps power supply are as well situated.

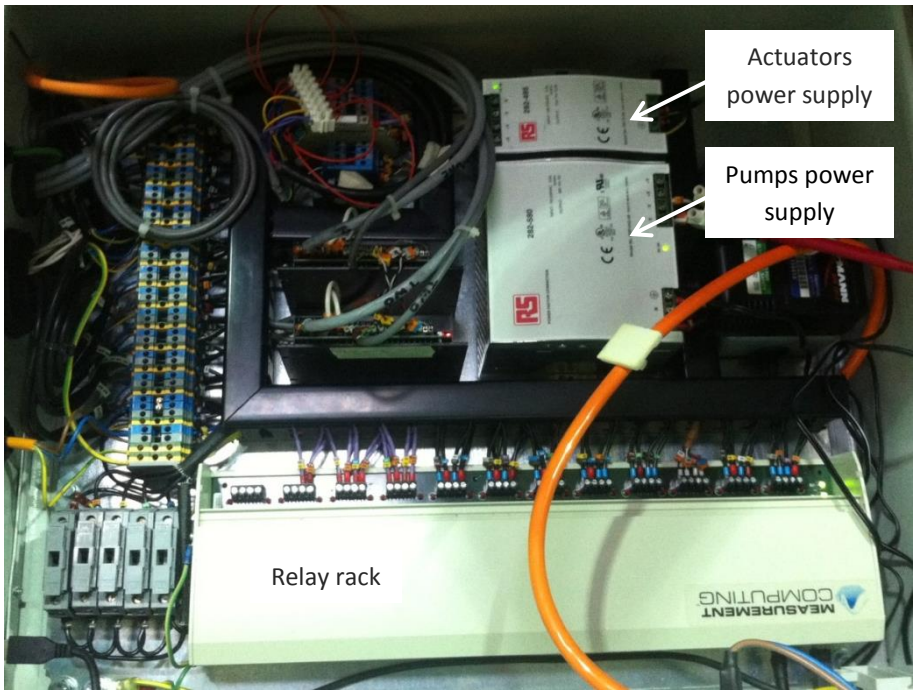

Figure 8.20 – Controller box

The temperature measurement accuracy using a K-type thermocouple is ± 1.8 °C and using a PT100 varies from ± 0.21 to ± 0.49 °C depending on the measured temperature (30 to 170 °C respectively).

The data acquisition equipment was interfaced to a PC with a Windows XP operating system and LabVIEW data acquisition software. The data obtained in the experiments was stored in a .lvm file on the hard drive at approximately 1.5 second intervals.

8.4. Control

8.4.1. Hardware

The control of the machine was carried out through actuators that switched the water valves and an electronic control that switched the water pumps.

8.4.2. Software

The data acquisition and control of the machine was performed using LabVIEW software. While the machine was running one graph showed the pressures in the beds, condenser and evaporators and other graph showed the condenser power and the total output power. Other data such as water mass flows, water temperatures and stage of the cycle are displayed on the monitor while the machine was operating.

The cycle was automatically operated following this sequence (see Figure 8.21):

1. In the stage 1 the hot water from the heater flows through Generator 1 (heating), the water that leaves Generator 1 flows through Generator 2 (preheating), the water that leaves Generator 2 flows throw the cooler reducing its temperature, after this cold water that leaves the cooler flows through Generator 3 (cooling) and the water that leaves Generator 3 flows through Generator 4 (precooling). This stage of the cycle is maintained for a quarter of a cycle time.
2. After this time, the beds' pump stops (for 2 or 3 seconds) while the water valves switch to the next cycle stage. After the water valves have switched the beds' pump starts again and after 9 seconds it reaches the nominal set mass flow.
3. Stage 2 of the cycle will follow but in this case Generator 2 will be heated, Generator 3 preheated, Generator 4 cooled and Generator 1 precooled.
4. Stage 3 of the cycle will follow but in this case Generator 3 will be heated, Generator 4 preheated, Generator 1 cooled and Generator 2 precooled.
5. Stage 4 of the cycle will follow but in this case Generator 4 will be heated, Generator 1 preheated, Generator 2 cooled and Generator 3 precooled.
6. Once all the beds have been preheated, heated, precooled and cooled the cycle finishes and another cycle will start.

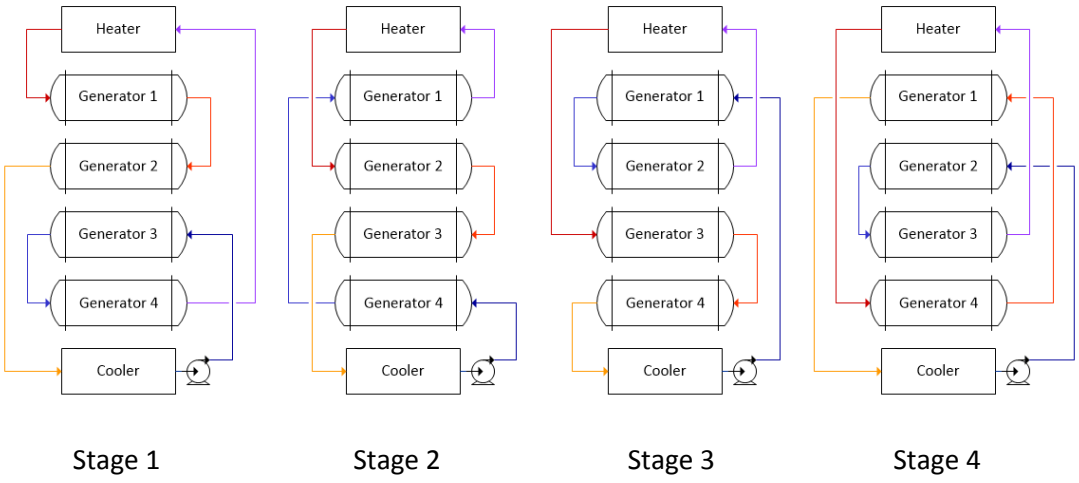

Figure 8.21 – Cycle stages

Simulation results were used to estimate the best mass flow and time cycle conditions to test the machine.

8.5. Challenges

The main challenge of the experimetal tests was the formation of salts inside the system. These salts were formed when the active carbon was in contact with ammonia at high pressure and temperature. The salts could create relatively large, sticky and hard crystals (Figure 8.22b) that stack to every component in the refrigerant circuit, jamming check valves and obstructing and completely blocking pipes and hoses.

When possible, with some components, the salts could be eliminated by dissolving them in water. Another characteristic of these salts is that they sublime at room temperature.

Figure 8.22 – (a) Salts adhered on check valve components, (b) Salt crystals found obstructing and blocking check valves

In order to try to eliminate them, the system was filled and emptied with ammonia 5 times but still some salts were formed that jammed the poppet type check valves (Figure 8.22a) making really challenging to test the system for a long time. To avoid this, the poppet of the check valves, that had a tight tolerance with the body and could easily be jammed with a salt crystal, was replaced by a stainless steel precision ball that perfectly sealed with the existing gasket but had less chance of getting jammed by the salts (Figure 8.22b).

When the ball type check valves were tested there was still jamming occurring (Figure 8.23a) and the system experiments could not be carried out.

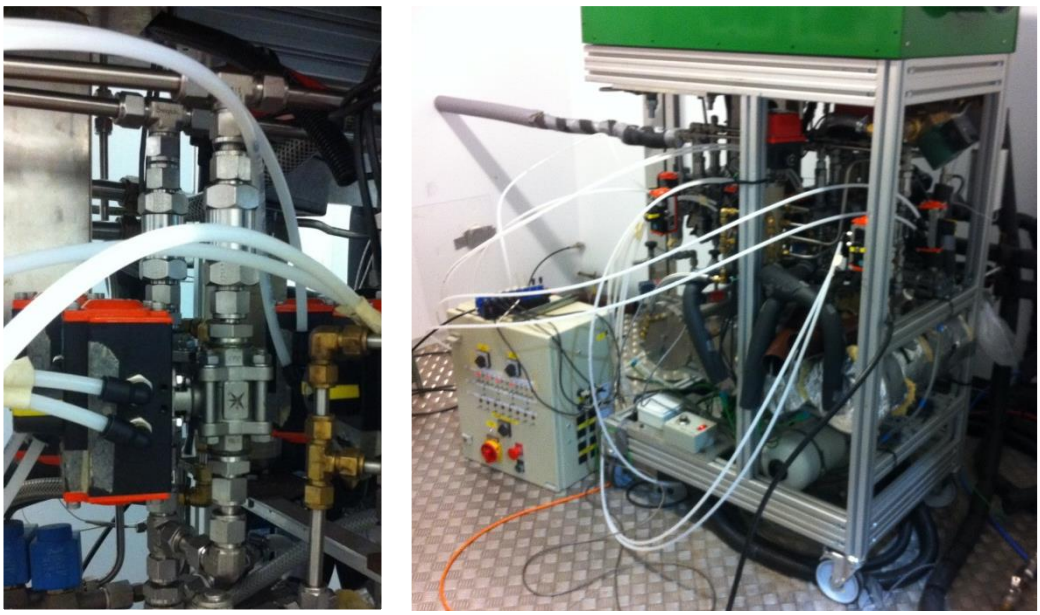

Figure 8.23 – (a) Ball valve installed in series with check valve, (b) System with ball valves and pneumatic control box

As a last resort the body of the check valves was emptied and regular pneumatic ball valves were connected in series (Figure 8.23a). A pneumatic control box was installed and connected to the valves and the correspondent routine control programme was written in Labview. If the pressure of the beds was higher than the condenser one or lower than the evaporators one the ball valves would open for 6 s. After this time the valves would close for 2 s and the beds would be evaluated again.

By doing this the working performance of the valves could be controlled and some test could be run but the ball valves could not seal properly due to the constant switching and the high working temperatures and pressure and ammonia was leaking from the system.

The ventilation of the environmental chamber where the machine was tested was improved because of this leakage and some final tests could be run.

Another challenge encountered was leakage of the water valves. It was discovered that even though the surface finish of the mating surfaces of the ceramic discs was very fine (lapped) the non-mating surfaces were not parallel. This caused water leaks in certain positions of the valves. Once this leakage was discovered the discs were lapped on all surfaces achieving a good parallelism and the leakage was fixed.

8.6. Conclusions

The laboratory heat pump system was designed and constructed to test the adsorption generators and cycle. The machine was expected to achieve a power output of 7 kW and a heating COP of 1.49 with a driving temperature of 170 °C and a condensing and evaporating temperature of 40 and 0 °C respectively.

Chapter 9

Experimental results and analysis

9.1. Introduction

In this chapter, the results obtained from the experimental testing of the heat pump are presented and analysed.

9.2. Steady state performance tests

9.2.1. Insulation and heat loss test

Previously to testing, the complete heat pump assembly (except for the evaporators) was insulated with polyethylene foam and glass fiber. It was insulated internally to avoid heat transfer between the high and low temperature water circuits and externally to avoid heat losses to the environmental chamber that during the testing was set to approximately 11 °C. In Figure 9.1 the insulated heat pump is shown. Some openings were made to the external insulation in order to keep the presure transducers at a low temperature.

Figure 9.1 – Insulated heat pump during testing

Once the machine was insulated a heat loss test was carried out (only in the large generators heat pump system) in order to calibrate the losses of the machine.

The chamber room was set to 11 °C and driving water at 94 °C was delivered by the electric heater and flowing through the machine until steady state was reached. The heat loss measured corresponded to 520 W at an average machine temperature of 94 °C. Depending on the running conditions of the machine (hot driving temperature and condensing temperature) the heat loss could vary but it would do it proportionally.

9.2.2. Tests of small generators

The small generators described in Chapter 4 were tested in a heat pump system in an early stage of this project as they were already manufactured and used in a previous project to this one.

Several tests were performed with different cycle times (from 240 to 600 s) and mass flow rates (from 0.01 to 0.019 kg/s). The machine driving temperature was controlled by the electric heater and was set to 155 °C, the evaporating temperature was controlled by the side of the environmental chamber where the machine was located and it was set to 10.5 °C, the condensing temperatures were controlled by the other side of the environmental chamber where the radiators that simulate the load were installed and they were varied from 35 and 50 °C in different tests.

For each condition the machine was run for at least 5 cycles until equilibrium and repeatability was reached.

The heating COP's and output powers obtained were much lower to the values expected from the computer simulations.

The water temperature profiles in and out of the beds (Bed A, B, C and D), the hot driving temperature (hot flow), its return to the electric heater (hot return), the cold driving temperature (cooler out) and the pressure of the beds during the testing can be observed for different sets of conditions in the following sections as well as a comparison graph of them with the computer simulation results.

9.2.2.1. Test 1 – Experimental results

In the first case (Figure 9.2) the hot driving temperature was 153 °C, the condensing temperature 35 °C, the evaporating temperature 10.5 °C, the heat pump mass flow rate 0.01 kg/s and the cycle time 480 s. The cycle time indicated in the graph is 488 s due to the fact that every time the stage of the cycle changes the water pump is stopped and the water valves change position. This takes approximately 2 s per cycle stage, 8 s in total in a cycle.

With these conditions the heating COP obtained was 1.06 (no heat losses were taken into account for the small generator testing results as there is no data available for them) and the power output was 1.7 kW without heat losses. These values are lower to those obtained by the simulation, where the heating COP was 1.75 and the output power was 2.14 kW.

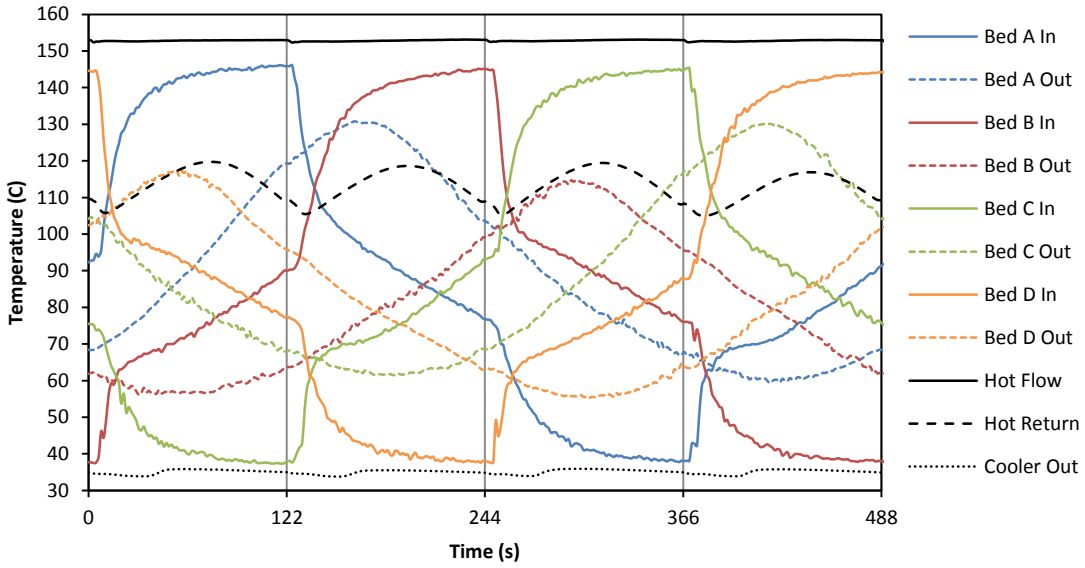

Figure 9.2 – Heat pump water temperature profiles during a complete cycle (cycle time = 480 s, mass flow = 0.01 kg/s)

In Figure 9.3 the pressure of the beds over a cycle are plotted along with the pressure of the evaporator. It can be observed that there is a slight difference in pressure profile between the beds possibly due to small differences in carbon filling or heat transfer in the bed. The graph shows that with this cycle time and mass flow rate combination only one bed desorbs/adsorbs at a time.

It is also possible to observe the effect of the cracking pressure of the evaporator check valves that as mentioned above was 0.345 bar in this case.

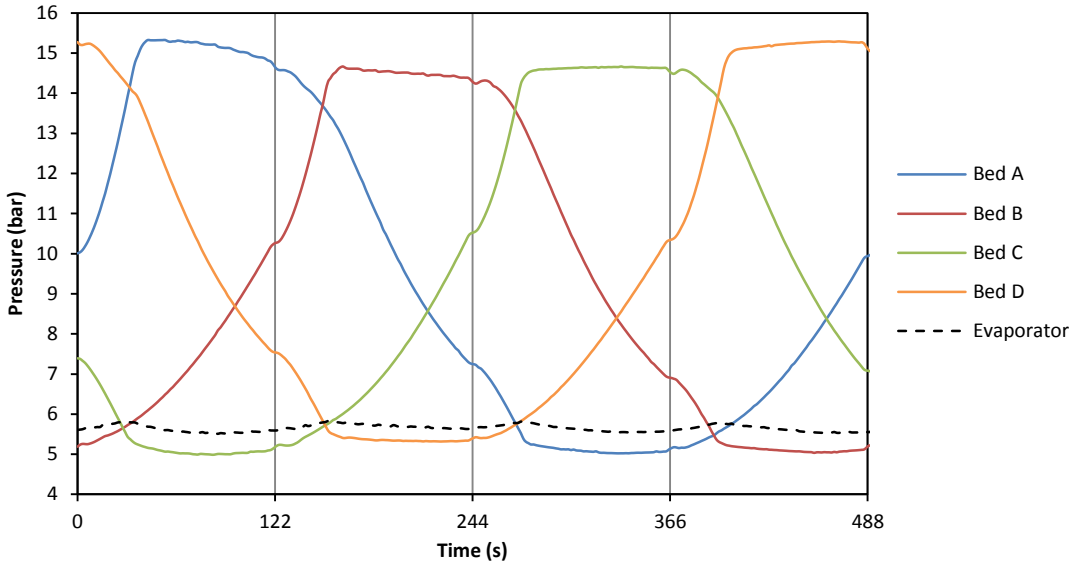

Figure 9.3 – Beds and evaporator pressures during a complete cycle (cycle time = 480 s, mass flow = 0.01 kg/s)

9.2.2.2. Test 1 – Modelling simulation comparison

In the following figures the water temperature and ammonia pressure of this test are plotted along with the values obtained in the computer simulation for the same testing conditions.

Figure 9.4 shows both experimental and simulation profiles of water in and out of Bed A, hot water driving temperature, return temperature of water to the boiler and temperature of the water leaving the cooler.

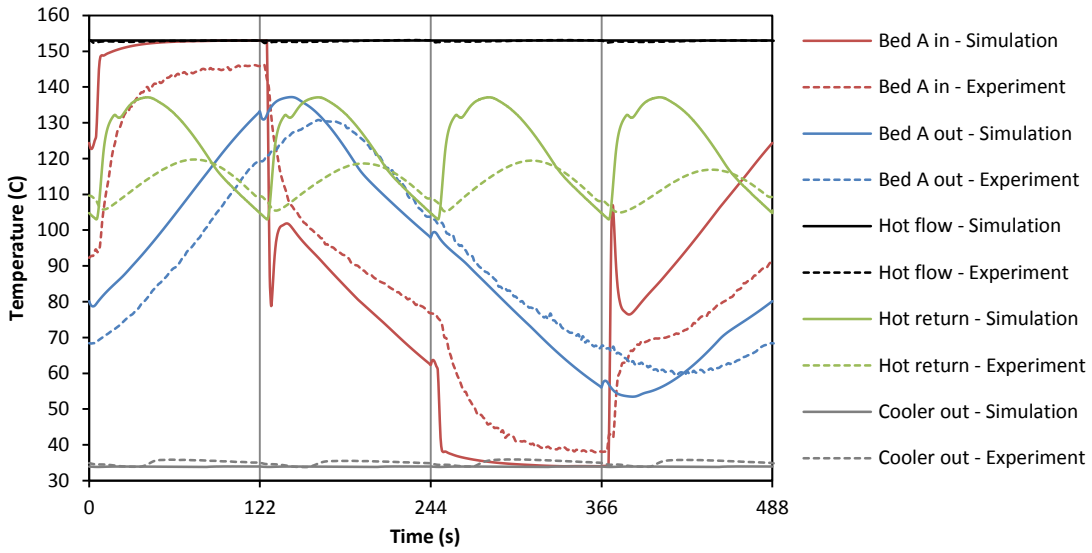

Figure 9.4 – Experimental and simulation comparison heat pump water temperature profiles during a complete cycle (cycle time = 480 s, mass flow = 0.01 kg/s)

It can be observed that the water temperature entering the bed in phases 1 and 3 does not reach the hot or the cooler driving temperatures. In phases 2 and 4 the temperature of the water does not match perfectly the simulation results, being higher and lower in different phases, showing temperature differences of up to 30 °C. This could be due to heat losses to the environment, heat losses between components of the machine and poor performance of the water valves.

The temperature profile of the water exiting the bed in the experiment is very similar to the predicted simulation results but it shows an offset of the results. This could be due to the delay that exists between the experiment and simulation when the water reaches the hot and the cooler driving temperatures.

The temperature profiles of the water return to the boiler show important differences, being much higher in the simulation results. This could be due to the poor thermal properties of the generators and heat losses of the machine.

Figure 9.5 shows both experimental and simulation profiles of ammonia pressure in Bed A, condenser and evaporators.

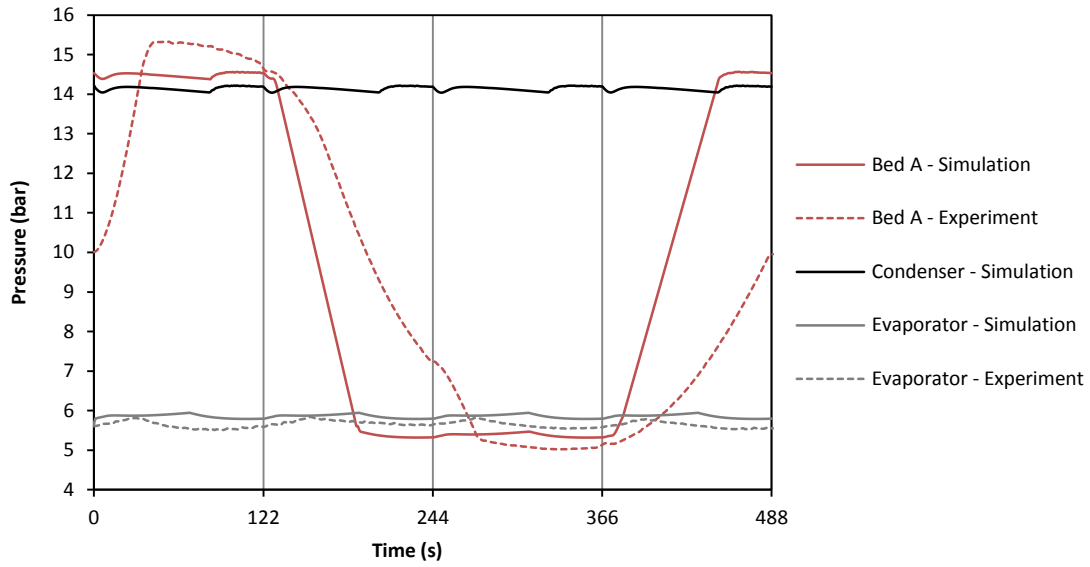

Figure 9.5 – Experimental and simulation comparison of beds, evaporators and condenser pressures during a complete cycle (cycle time = 480 s, mass flow = 0.01 kg/s)

It can be observed that the profiles of the experiment and simulation of the bed pressure show important differences. There exists a delay of pressurisation and depressurisation of the bed and the length of time that the check valves of the bed remain open is much shorter during the experiment. This could be due to poor thermal properties of the generators and lower or higher water driving temperatures (as seen in Figure 9.4).

9.2.2.3. Test 2 – Experimental results

In the second case (Figure 9.6) the hot driving temperature was 156 °C, the condensing temperature 39 °C, the evaporating temperature 10.5 °C, the heat pump mass flow rate 0.019 kg/s and the cycle time 480 s (488 s). This case was chosen to be displayed as its cycle time is the same as the previous example but the mass flow rate is double. This creates different water profiles in and out of the beds and different return temperatures to the electric heater.

With these conditions the heating COP obtained was 1.06 (no heat losses were taken into account for the small generator testing results as there is no data available for them) and the power output was 4.59 kW without heat losses. These values are lower to those obtained by the simulation, the heating COP and output power were 1.23 and 6.02 kW respectively.

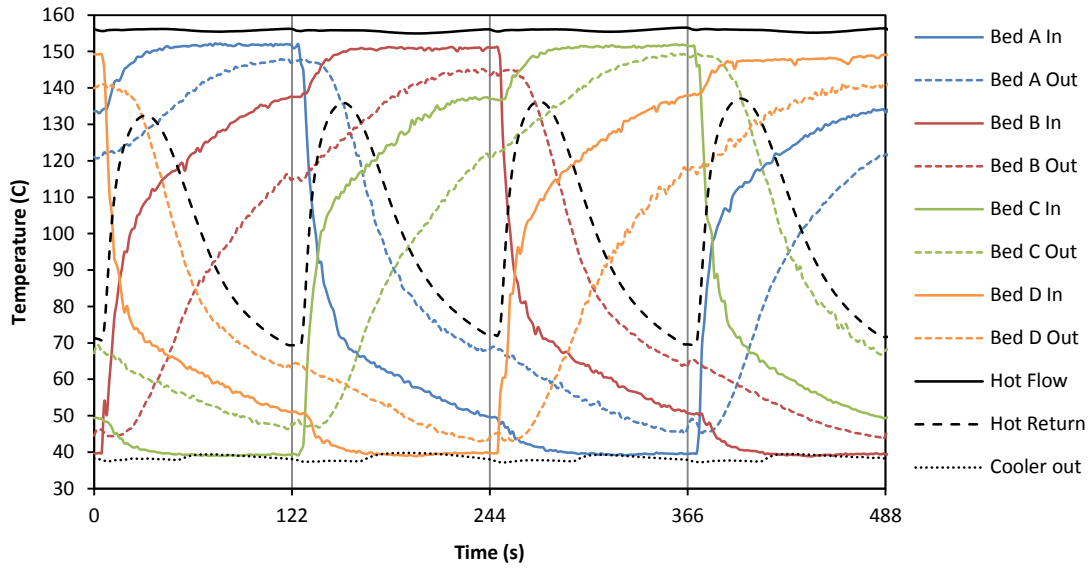

Figure 9.6 – Heat pump water temperature profiles during a complete cycle (cycle time = 480 s, mass flow = 0.019 kg/s)

In Figure 9.7 the pressures of the beds over a cycle are plotted along with the pressure of the evaporator. The graph shows that with this cycle time and mass flow rate combination up to two beds can desorb/adsorb at a time. This happens as the mass flow rate is much higher than the previous example and the beds start to desorb/adsorb during the preheating/cooling stages.

It is also possible to observe the effect of the cracking pressure of the evaporator check valves (0.345 bar).

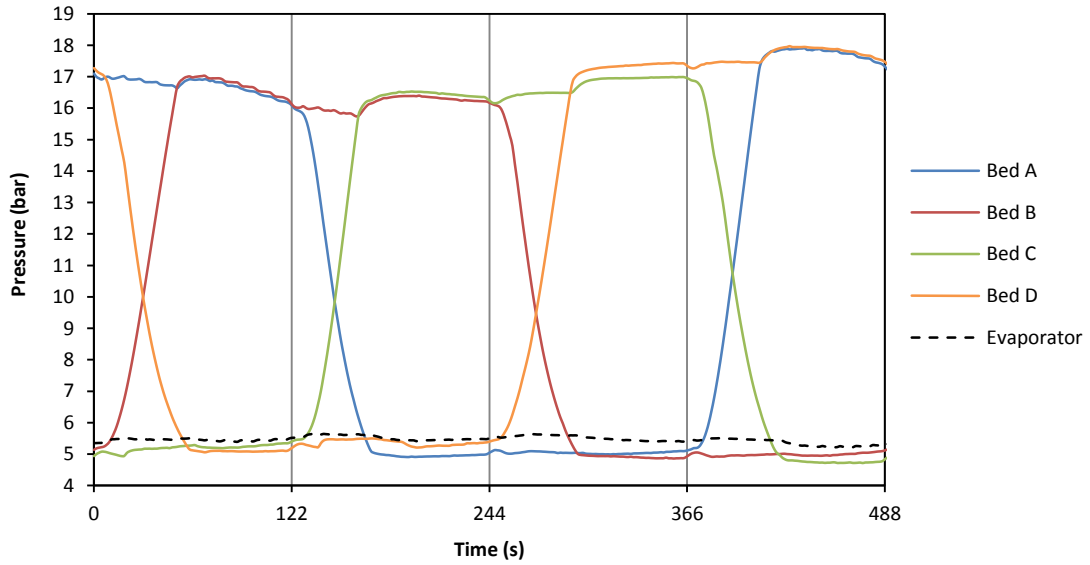

Figure 9.7 – Beds and evaporator pressures during a complete cycle (cycle time = 480 s, mass flow = 0.019 kg/s)

9.2.2.4. Test 2 – Modelling simulation comparison

Figure 9.8 shows both experimental and simulation profiles of water in and out of Bed A, hot water driving temperature, return temperature of water to the boiler and temperature of the water leaving the cooler.

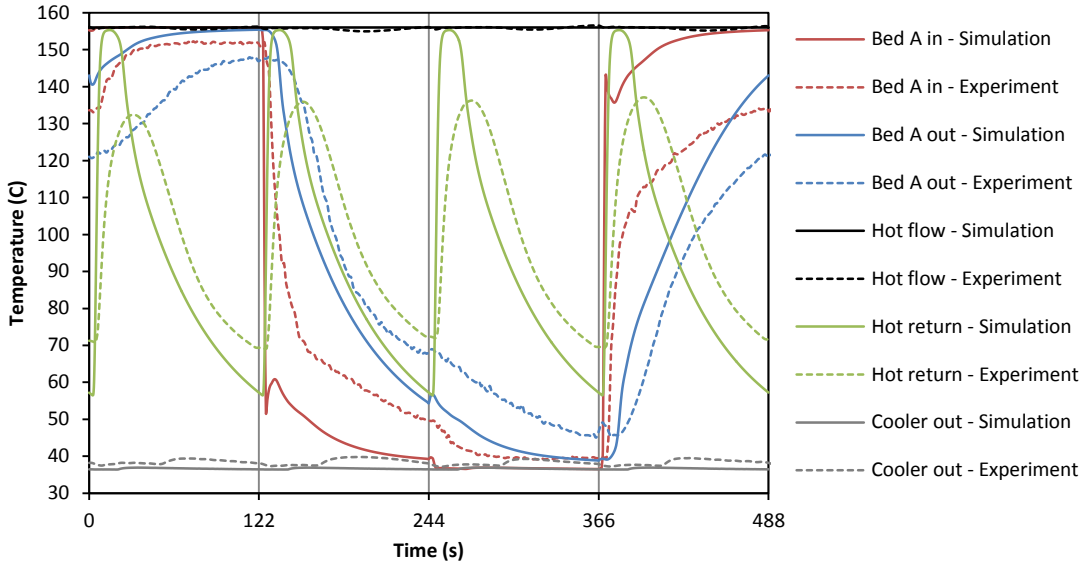

Figure 9.8 – Experimental and simulation comparison heat pump water temperature profiles during a complete cycle (cycle time = 480 s, mass flow = 0.019 kg/s)

It can be observed that the water temperature entering the bed in phases 1 and 3 does not reach the hot or the cooler driving temperatures. In phases 2 and 4 the temperature of the water does not match perfectly the simulation results, being higher and lower in different phases, showing temperature differences of up to 20 °C. This could be due to heat losses to the environment, heat losses between components of the machine and poor performance of the water valves.

The temperature profile of the water exiting the bed in the experiment does not match perfectly the simulation results, being higher and lower in different phases, showing temperature differences of up to 20 °C.

The temperature profiles of the water return to the boiler do not match perfectly but look very similar. This mismatch could be due to the poor thermal properties of the generators and heat losses of the machine.

Figure 9.9 shows both experimental and simulation profiles of ammonia pressure in Bed A, condenser and evaporators.

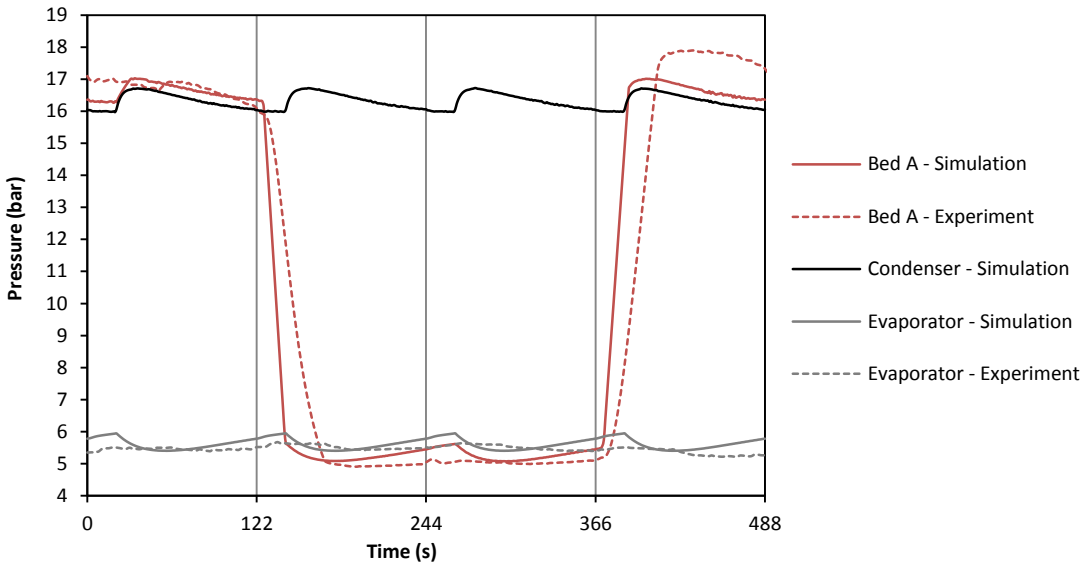

Figure 9.9 – Experimental and simulation comparison of beds, evaporators and condenser pressures during a complete cycle (cycle time = 480 s, mass flow = 0.019 kg/s)

It can be observed that the profiles of the experiment and simulation of the bed pressure show very little differences. There exists a small delay of pressurisation and depressurisation of the bed and length of time that the check valves of the bed remain open.

9.2.3. Tests of large generators

The large generators, described in Chapter 4, were tested after the small generators heat pump system as they were redesigned, manufactured and filled with a different carbon mixture during the length of the project.

A few challenges (water valves and ammonia salts) explained in Chapter 8 were encountered during the testing stage and a complete cycle time-mass flow rate performance map could not be obtained for these generators.

In this section two experiments run at two different conditions are shown. For each tested condition the machine was run for at least 5 cycles until equilibrium and repeatability was reached.

9.2.3.1. Test 1 – Experimental results

In the first case (Figure 9.10) the hot driving temperature was 123 °C, the condensing temperature 30 °C, the evaporating temperature 11.5 °C, the heat pump mass flow rate 0.032 kg/s and the cycle time 400 s. The cycle time indicated in the graph is 404 s due to the fact that every time the stage of

the cycle changes the water pump is stopped and the water valves change position. This takes approximately 1 s per cycle stage, 4 s in total in a cycle.

With these conditions the heating COP obtained was 1.31 if taking into account the heat losses (1.18 without heat losses) and the power output was 4.51 kW if taking into account the heat losses (4.30 kW without heat losses). These values were lower than those obtained by the simulation, the heating COP and output power were 1.67 and 4.84 kW respectively.

In this case poppet style check valves were used in the system.

It is possible to observe the improvement achieved in the inlet temperature profile to the beds. Their temperature is much closer to the driving hot and cold temperatures than in the small generators system.

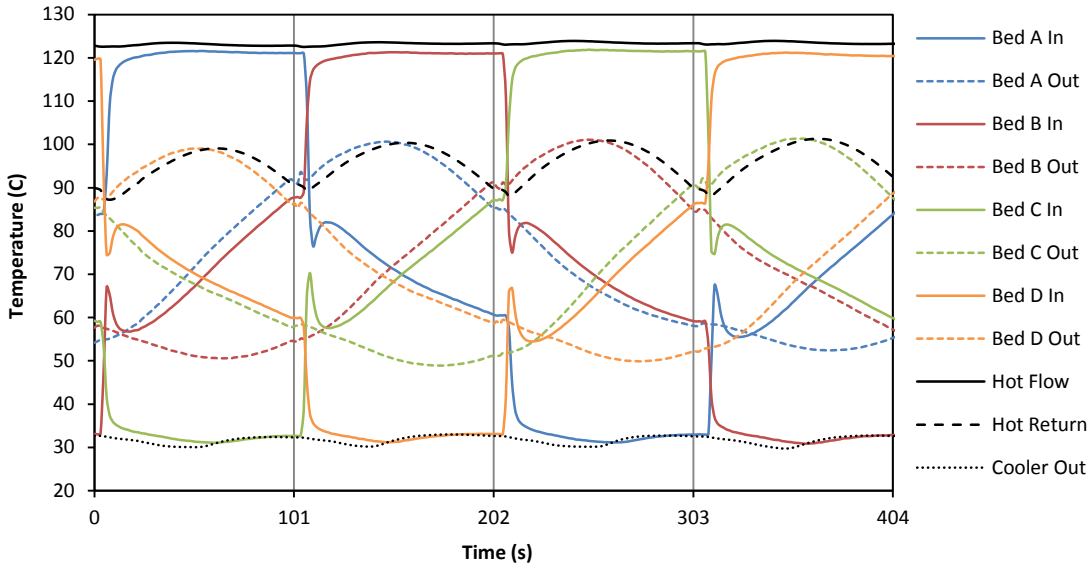

Figure 9.10 – Heat pump water temperature profiles during a complete cycle (cycle time = 400 s, mass flow = 0.032 kg/s)

In Figure 9.11 the pressures of the beds over a cycle are plotted along with the pressure of the condenser and evaporators. It can be observed that there is a slight difference in pressure profile between the beds possibly due to small differences in carbon filling, heat transfer in the bed or problems with the sealing of the check valves. The graph shows that with this cycle time and mass flow rate combination only one bed desorbs/adsorbs at a time. The cracking pressure of the condenser/evaporators check valves can be observed in the graph.

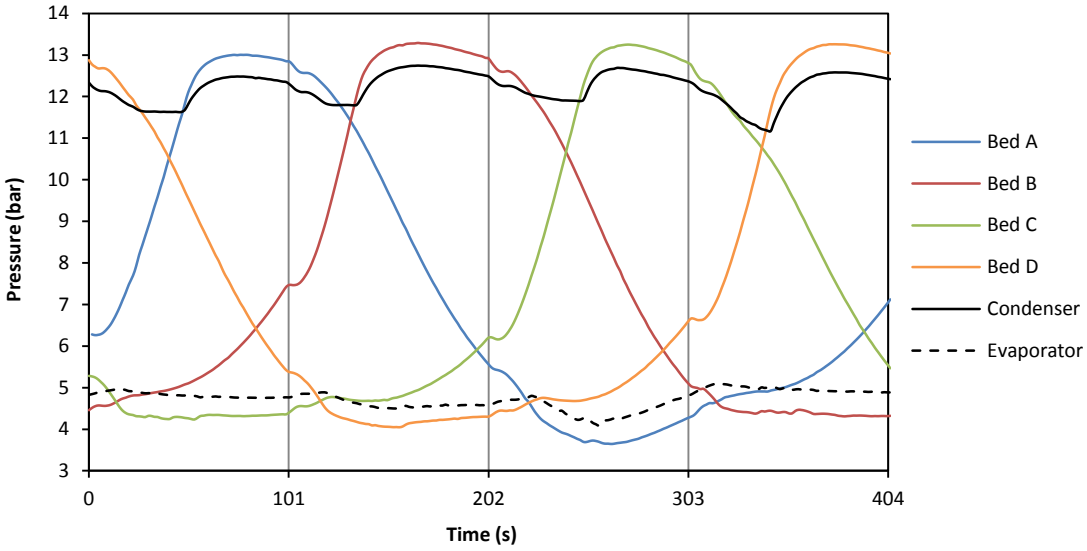

Figure 9.11 – Beds, evaporators and condenser pressures during a complete cycle (cycle time = 400s, mass flow = 0.032 kg/s)

9.2.3.2. Test 1 – Modelling simulation comparison

Figure 9.12 shows both experimental and simulation profiles of water in and out of Bed A, hot water driving temperature, return temperature of water to the boiler and temperature of the water leaving the cooler.

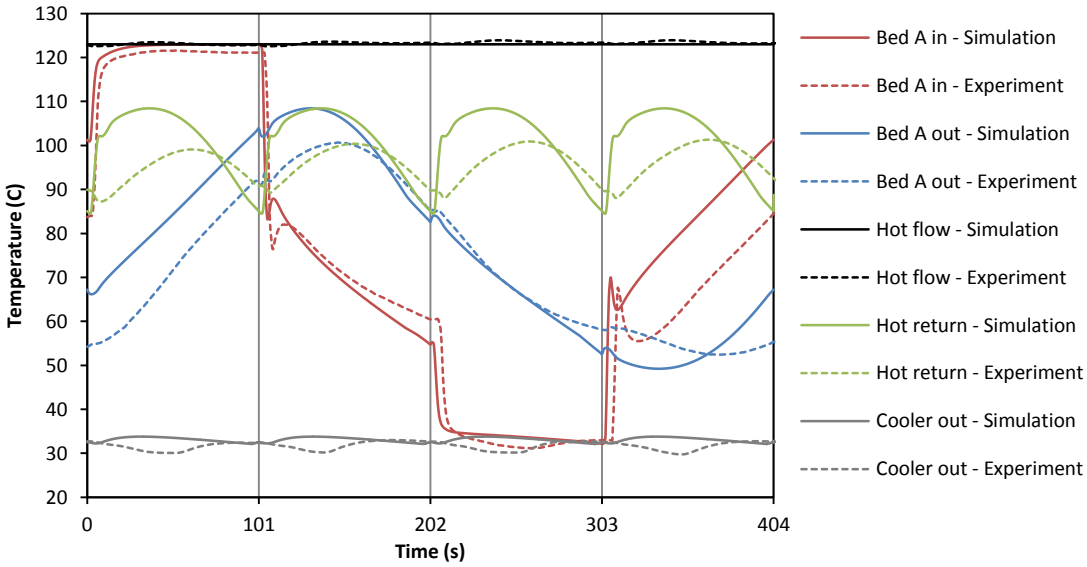

Figure 9.12 – Experimental and simulation comparison heat pump water temperature profiles during a complete cycle (cycle time = 400 s, mass flow = 0.032 kg/s)

It can be observed that the temperature of the water entering the bed in the experiment and in the simulation show very similar results, except for phase 4 where the experimental values are lower.

This could be due to heat losses to the environment or heat losses between components of the machine.

The temperature profile of the water exiting the bed in the experiment is lower to the one predicted by simulation. This could be due to poor thermal properties of the generators.

The temperature profiles of the water return to the boiler show differences, being higher in the simulation results. This could be due to the poor thermal properties of the generators and heat losses of the machine.

Figure 9.13 shows both experimental and simulation profiles of ammonia pressure in Bed A, condenser and evaporators.

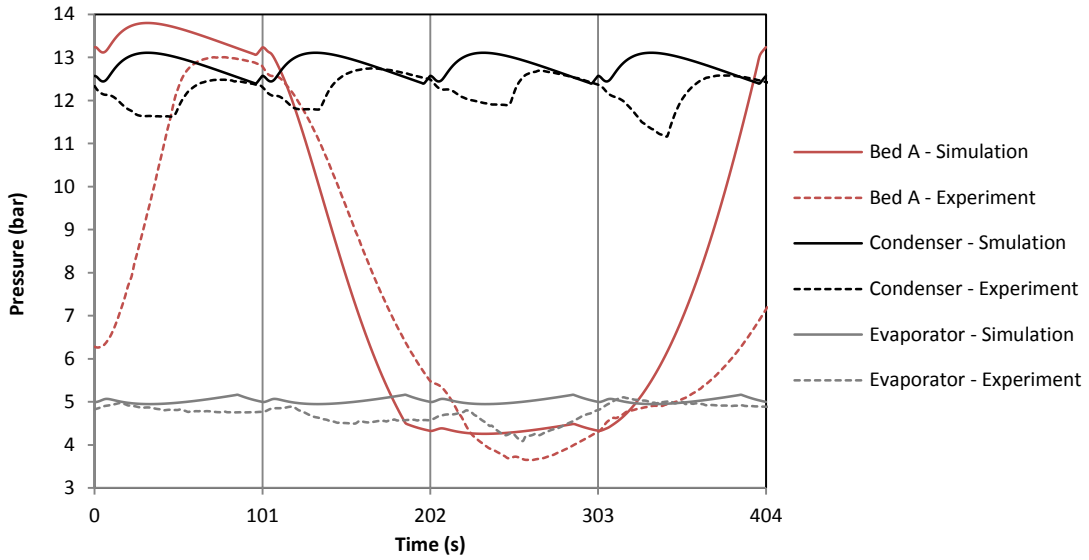

Figure 9.13 – Experimental and simulation comparison of beds, evaporators and condenser pressures during a complete cycle (cycle time = 400 s, mass flow = 0.032 kg/s)

It can be observed that the profiles of the experiment and simulation of the bed pressure show important differences. There exists an important delay of pressurisation and depressurisation of the bed and the length of time that the check valves of the bed remain open is much shorter during the experiment. This could be due to poor thermal properties of the generators and poor performance of the check valves.

This Figure also shows differences between the condenser and evaporator pressures. This is due to irregular behaviour of the four beds (A, B, C and D) during the testing as they were influenced by the poor performance of the check valves.

9.2.3.3. Test 2 – Experimental results

In the second case (Figure 9.14) shown here the hot driving temperature was 148 °C, the condensing temperature 42 °C, the evaporating temperature 10 °C, the heat pump mass flow rate 0.032 kg/s and the cycle time 480 s (488s).

With these conditions the heating COP obtained was 1.26 if taking into account the heat losses (1.13 without heat losses) and the power output was 5.19 kW if taking into account the heat losses (4.92 kW without heat losses). These values were lower than those obtained by the simulation, the heating COP and output power were 1.48 and 5.73 kW respectively.

In this case regular pneumatic ball valves were used in the system in order to avoid blockage with ammonia salts as occurred with the poppet type check valves used previously. The valves were opened and closed by the computer that controlled the whole system, based on pressure signals on both sides of the valve.

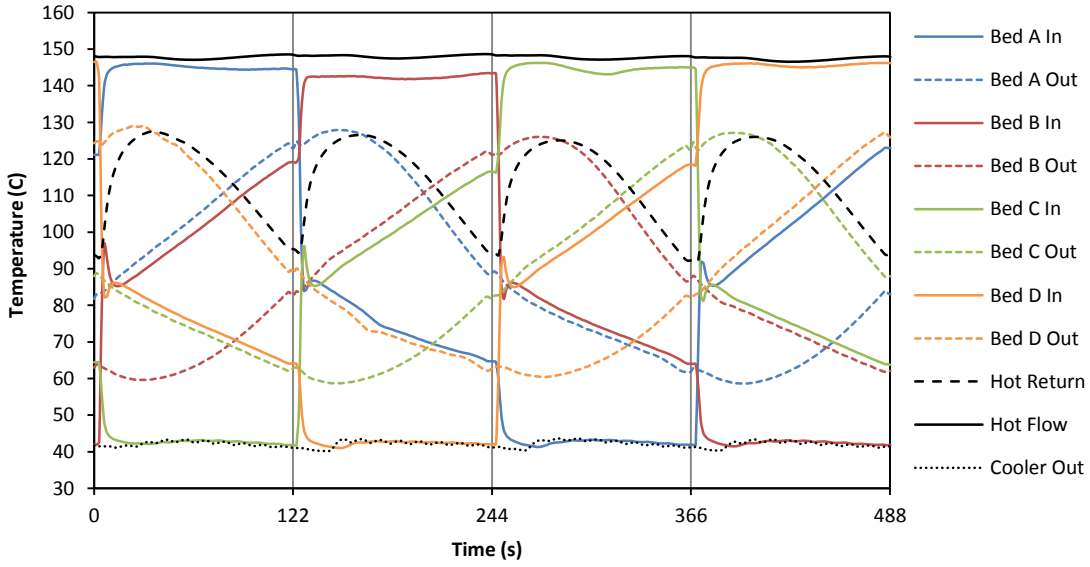

Figure 9.14 – Heat pump water temperature profiles during a complete cycle (cycle time = 480 s, mass flow = 0.032 kg/s)

In Figure 9.15 the pressures of the beds over a cycle are plotted along with the pressure of the condenser and evaporators. The graph shows that with this cycle time and mass flow rate combination only one bed desorbs/adsorbs at a time. In this case there is no cracking pressure in the valves but what it is observed is the opening/closing routine of the pneumatic ball valves. If the pressure of the bed was higher than the condenser one or lower than the evaporator one the ball

valves would open for 6 s. After this time the valves would close for 2 s and the bed would be evaluated again.

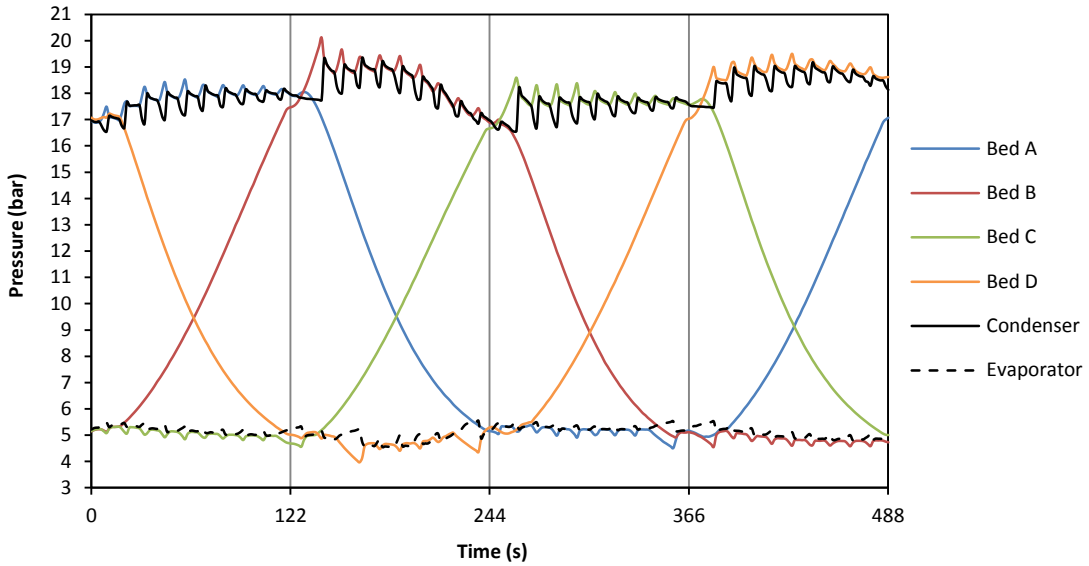

Figure 9.15 – Beds, evaporators and condenser pressures during a complete cycle (cycle time = 480s, mass flow = 0.032 kg/s)

9.2.3.4. Test 2 – Modelling simulation comparison

Figure 9.16 shows both experimental and simulation profiles of water in and out of Bed A, hot water driving temperature, return temperature of water to the boiler and temperature of the water leaving the cooler.

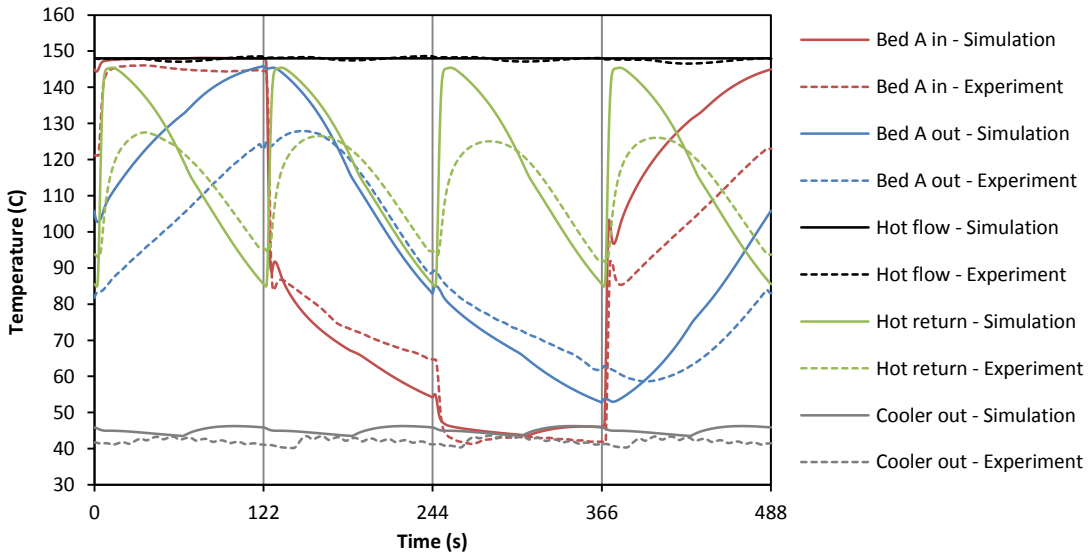

Figure 9.16 – Experimental and simulation comparison heat pump water temperature profiles during a complete cycle (cycle time = 480s, mass flow = 0.032 kg/s)

It can be observed that the temperature of the water entering the bed in the experiment and in the simulation show very similar results, except for phase 4 where the experimental values are lower. This could be due to heat losses to the environment or heat losses between components of the machine.

The temperature profile of the water exiting the bed in the experiment is quite lower to the one predicted by simulation. This could be due to poor thermal properties of the generators.

The temperature profiles of the water return to the boiler show important differences, being higher in the simulation results. This could be due to the poor thermal properties of the generators and heat losses of the machine.

Figure 9.17 shows both experimental and simulation profiles of ammonia pressure in Bed A, condenser and evaporators.

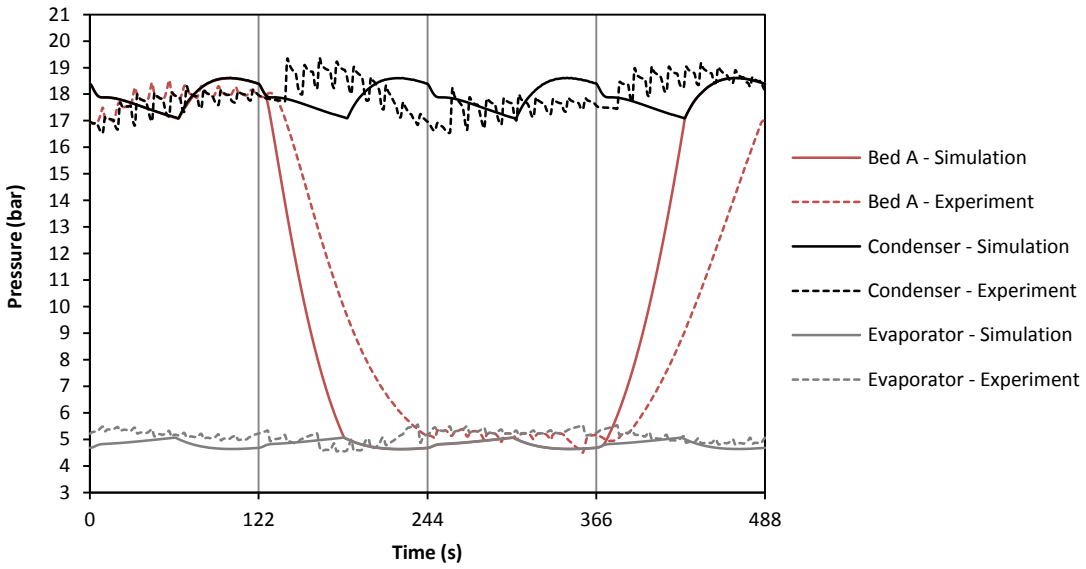

Figure 9.17 – Experimental and simulation comparison of beds, evaporators and condenser pressures during a complete cycle (cycle time = 480s, mass flow = 0.032 kg/s)

It can be observed that the profiles of the experiment and simulation of the bed pressure do not show important differences. There exists a small delay of pressurisation and depressurisation of the bed and the length of time that the check valves of the bed remain open is a bit shorter during the experiment. This could be due to poor thermal properties of the generators and poor performance of the check valves.

This Figure also shows small differences between the condenser and evaporator pressures. This is due to irregular behaviour of the four beds (A, B, C and D) and due to the use of ball valves mechanically operated instead of check valves.

9.3. Challenges

After the testing of the machine with the large generators it was dismantled in order to be examined. It was discovered that the water distributors described in Chapter 4 located at each end of the beds were completely damaged and degradated. It can be seen in Figure 9.18 that due to the high temperature of the water the distributors partially melted and got distorted and as well they were pushed against the tubes blocking most of them (Figure 9.19).

Figure 9.18 – (a, b) Damaged water distributors after testing

This blocking and distortion meant that only a fraction of the beds was being heated and cooled by the hot and cold transfer fluid affecting very negatively the adsorption/desorption performance of the machine. This explained the poor performance of the machine.

The poor experimental performance of the machine due to the blocked tubes can be quantified with a modified version of the computer simulation programme.

The heating COP of Test 1 of the large generators (as shown previously in this Chapter) is 1.67 (heating power is 4.84 kW). If half of the tubes were blocked the heating COP would be 1.45 (heating power is 5.20 kW), with two thirds of the tubes blocked the heating COP would be 1.30 (heating power 6.68 kW) and with three fourths of the tubes blocked the heating COP would drop to 1.23 (heating power 7.21 kW).

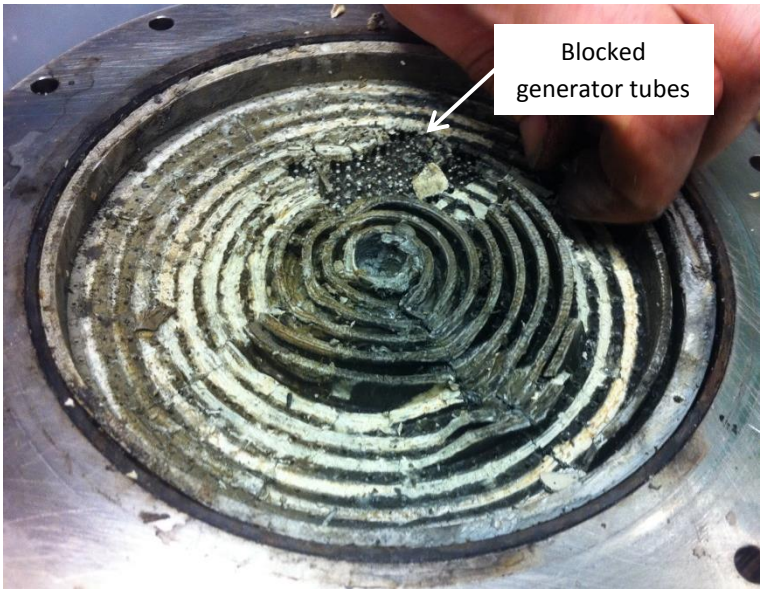

Figure 9.19 – Fragile water distributor after testing

9.4. Conclusions

The laboratory system designed described in Chapter 8 was tested for both size of generators, small and large, both described in Chapter 4.

The performance results obtained with the small generators was very poor and as a result new generators with a larger size (in order to obtain more power output) were manufactured and filled with a different mixture of active carbon.

The testing of the larger generators showed better performance results due to the better heat transfer in the beds, improved water valves and better insulation in the system but the results were still lower than the simulation prediction.

After the testing of the large generators the beds were opened and it was discovered that the installed water distributors were completely distorted and deformed blocking most of the tubes of the heat exchanger. This was the main reason for the low performance of the machine.

Chapter 10

Conclusions and future work

10.1. Introduction

In this chapter, conclusions from the work carried out in this thesis are presented and future work recommendations are made.

10.2. Conclusions

The objectives of the project were:

- To carry out the computational modelling of a four-bed thermal wave heat pump cycle.
- To carry out a heat transfer study of the active carbon available for the heat pump in order to identify the best sorbent sample.
- To develop an efficient way of filling the sorption bed with the chosen carbon sample.
- To design, manufacture and test the modelled heat pump cycle in order to validate the computational modelling.

All the project objectives presented above were met:

The design and manufacturing process of two low thermal mass and high density power sorption shell and tube heat exchangers was presented. Both were made of nickel brazed stainless steel being the large one triple in size of the small one. The sorbent material, active carbon, filling techniques were presented and developed.

The performance of the four-bed thermal wave heat pump cycle was analysed through computational modelling and compared for many different sets of conditions in order to understand its behaviour and the effect these conditions have on the heating COP and heat output power.

The measurement of the heat transfer properties of the active carbon were carried out. The intrinsic thermal conductivity of different carbon samples was tested by two methods, steady state flat plate and transient hot tube technique, along with the measurement of their wall contact resistance by the transient hot tube technique.

The intrinsic thermal conductivities of the steady state flat plate experiments were very similar to the ones corresponding with the transient hot tube technique which indicates that both experiments are comparable and achieve the same results.

Binary mixtures of grains and powder were tested and it was found that they could achieve much higher densities, higher thermal conductivities and lower contact resistances at the same vibration or compression rates than grains on their own.

The laboratory heat pump system was designed and constructed to test the adsorption generators and cycle. The laboratory system designed was tested for both sizes of generators, small and large.

The performance results obtained with the small generators was very poor and as a result new generators with a larger size (in order to obtain more power output) were manufactured and filled with a different mixture of active carbon.

The testing of the larger generators showed better performance results due to the better heat transfer in the beds, improved water valves and better insulation of the system but the results obtained were still lower than the simulation predictions.

After the testing of the large generators the beds were opened and it was discovered that the installed water distributors were completely distorted and deformed blocking most of the tubes of the heat exchanger. This was the main reason for the low performance of the machine.

10.3. Future work

More work is still needed to be done in order to develop further the system in order to make it marketable. The generators manufacturing technique should be developed in order to being able to mass produce them at a low cost.

The generators spiral water distributors should be remanufactured in a material that does not deteriorate at the heat pump driving water temperature (around 170 °C). A proposed material to use would be aluminium due to its high thermal conductivity, high fusion temperature and easy machinability.

A better positioning of the water valves and the generators could be achieved in order to reduce the dead volumes of water that affect the efficiency of the system.

A carbon pre-treatment should be developed in order to remove the impurities that react with the ammonia creating the ammonia salts presented in Chapter 8. These ammonia salts were the cause of pipes blockage and check valves jamming that forced their change to bulky pneumatic actuated ball valves, and that cannot be used in a commercially viable heat pump system.

More research on heat transfer in carbon beds should be carried out in order to find a way to reduce the wall contact resistance in the generators. This would make possible to reduce the size of the adsorption generators and make the system more compact and marketable.

Bibliography

Aristov, Yu. I., Tokarev, M. M., Sharonov, V. E., Universal relation between the boundary temperatures of a basic cycle of sorption heat machines, Chemical engineering science, 63, pp. 2907-2912, 2008.

Ben Amar, N., Sun, L. M., Meunier, F., Numerical analysis of adsorptive temperature wave regenerative heat pump, Applied thermal engineering, 16, pp. 405-418, 1996.

Cooper, M. G., Mikic, B. B., Yovanovich, M. M., Thermal contact conductance, International journal of heat and mass transfer, 12, pp. 279-300, 1969.

Critoph, R. E., Modular regenerative adsorption cycles with fixed beds, applied to trigeneration, Proceedings IMechE, Vol. 219 Part E, Journal of process mechanical engineering, 2005.

Critoph, R. E., Zhong, Y., Review of trends in solid sorption refrigeration and heat pumping technologies, Proceedings IMechE, Vol. 219 Part E, Journal of process mechanical engineering, 2005.

Critoph, R. E., Metcalf, S. J., Specific cooling power intensification limits in ammonia-carbon adsorption refrigeration systems, Applied thermal engineering, 24, pp. 661-678, 2004.

Critoph, R. E., Simulation of a continuous multiple-bed regenerative adsorption cycle, International journal of refrigeration, 24, pp. 428-437, 2001.

Dubinin, M. M., Modern state of the theory of gas and vapour adsorption by microporous adsorbents, Pure applied chemistry, 10, pp. 309-322, 1965.

Gordeeva, L. G., Restuccia, G., Freni, A., Aristov, Yu. I., Water sorption on composites “LiBr in a porous carbon”, Fuel processing technology, 79, pp. 225-231, 2002.

Jones, J. A., Refrigeration technology transfer at JPL/NASA, 32nd Space congress, Florida, 1995.

Kawakita, K., Ludde, K. H., Some considerations on powder compression equations, Powder technology, 4, pp. 61-68, 1970/71.

Metcalf, S. J., Tamainot-Telto, Z., Critoph, R. E., Application of a compact sorption generator to solar refrigeration: Case study of Dakar (Senegal), Applied thermal engineering, 31, pp. 2197-2204, 2011.

Miles, D. J., Shelton, S. V., Design and testing of a solid-sorption heat-pump system, Applied thermal engineering, 16, pp. 389-394, 1996.

Saha, B. B., El-Sharkawy, I. I., Chakraborty, A., Koyama, S., Study on an activated carbon fiber-ethanol adsorption chiller: Part II – performance evaluation, International journal of refrigeration, 30, pp. 96-102, 2007.

Saha, B. B., Koyama, S., Ng, K. C., Hamamoto, Y., Akisawa, A., Kashiwagi, T., Study on a dual-mode, muti-stage, multi-bed regenerative adsorption chiller, Renewable energy, 31, pp. 2076-2090, 2006.

Shelton, S. V., Wepfer, W., Miles, D. J., Square wave analysis of the solid-vapor adsorption heat pump, Heat recovery systems & CHP, 9, pp. 233-247, 1989.

Sun, L. M., Feng, Y., Pons, M., Numerical investigation of adsorptive heat pump systems with thermal wave heat regeneration under uniform-pressure conditions, International journal of heat and mass transfer, 40, pp. 281-293, 1997.

Stovall, T., Larrard, F. de, Buil, M., Linear packing density model of grain mixtures, Powder technology, 48, pp. 1-12, 1986.

Tamainot-Telto, Z., Metcalf, S. J., Critoph, R. E., Zhong, Y., Thorpe, R. N., Carbon-ammonia pairs for adsorption refrigeration applications: ice making, air conditioning and heat pumping, International journal of refrigeration, 32, pp. 1212-1229, 2009.

Tamainot-Telto, Z., Critoph, R. E., Advanced solid sorption air conditioning modules using monolithic carbon-ammonia pair, Applied thermal engineering, 23, pp. 659-674, 2003.

Tamainot-Telto, Z., Critoph, R. E., Screening of low concepts for thermal conductivity enhancements in sorption generators, Technical report: RTDF/01/02No ZTT/REC-1, 2003.

Tamainot-Telto, Z., Critoph, R. E., Thermophysical properties of monolithic carbon, International journal of heat and mass transfer, 43, pp. 2053-2058, 2000.

Taylan, O., Baker, D., Kaftanoglu, B., COP trends for ideal thermal wave adsorption cooling cycles with enhancements, International journal of refrigeration, 35, pp. 562-570, 2012.

Tierney, M. J., Feasibility of driving convective thermal wave chillers with low-grade heat, Renewable energy, 33, pp. 2097-2108, 2008.

Tokarev, M. M., Veselovskaya, J. V., Yanagi, H., Aristov, Yu. I., Novel ammonia sorbents “porous matrix modified by active salt” for adsorptive heat transformation: 2. Calcium chloride in ACF felt, Applied thermal engineering, 30, pp. 845-849, 2010.

Tsotsas, E., Martin, H., Thermal conductivity of packed beds: a review, Chemical engineering processes, 22, pp. 19-37, 1987.

Veselovskaya, J. V., Critoph, R. E., Thorpe, R. N., Metcalf, S. J., Tokarev, M. M., Aristov, Yu. I., Novel ammonia sorbents “porous matrix modified by active salt” for adsorptive heat transformation: 3. Testing of “$BaCl_2$/vermiculite” composite in a lab-scale adsorption chiller, Applied thermal engineering, 30, pp. 118-1192, 2010.

Wang, L. W., Metcalf, S. J., Critoph, R. E., Thorpe, R., Tamainot-Telto, Z., Development of thermal conductive consolidated activated carbon for adsorption refrigeration, Carbon, 50, pp. 977-986, 2012.

Wang, L. W., Metcalf, S. J., Critoph, R. E., Thorpe, R., Tamainot-Telto, Z., Thermal conductivity and permeability of consolidated expanded natural graphite treated with sulphuric acid, Carbon, 49, pp. 4812-4819, 2011.

Wang, L. W., Metcalf, S. J., Critoph, R. E., Thorpe, R., Tamainot-Telto, Z., Two types of natural graphite host matrix for composite activated carbon, Applied thermal engineering, pp. 1-6, 2011.

Wang, L. W., Tamainot-Telto, Z., Metcalf, S. J., Critoph, Wang, R. Z., Anisotropic thermal conductivity and permeability of compacted natural graphite, Applied thermal engineering, 30, pp. 1805-1811, 2010.

Zhong, Y., Critoph, R. E., Thorpe, R. N., Tamainot-Telto, Z., Dynamics of $BaCl_2$-NH_3 adsorption pair, Applied thermal engineering, 29, pp. 1180-1186, 2009.

Zhong, Y., Critoph, R. E., Thorpe, R. N., Evaluation of the performance of solid sorption refrigeration systems using carbon dioxide as refrigerant, Applied thermal engineering, 26, pp. 1807-1811, 2006.

Appendix A

MATLAB models

A1. Ideal 4-bed thermal wave cycle

```
global As Ac UAc UAw UAev UAcond UAcooler Kvcond Kvev Ks Kw Cpw Cpa Cps cpcond cpev Cvw Dw
global Tw Ts Tc Tsat Tgas Twinlet Twcondin Tairevin Tcond Tev Trec Tairevout Twcondout Thot Xin t
global TwoutB TwinC Twoutcooler hw dQsupcond jdQsupcond Mcondg Mevgold pevold pcondold
global AuxTsat AuxTgas AuxTc AuxTs AuxTw AuxX AuxXX Auxp AuxMcte AuxMAMMG Tin Tsatin Kc
global N Ntub dL dt nL nt mwcond j Mcond Mev Mw Ms Mc C k x0 n NTUev NTUcond VoidVol Vev
global Qw Qs Qc Qheat Qcool Qsupcond dMammcond dMammev jdMammev jdMammcond Mctein
global X XX CPC Rgas A B D LMTDev LMTDcond Cpair mairev Vcond NTUcooler Cr Ecooler Mammlin
global Mammcond Mammev MAMMG Mamml Mcte Mliqcond Mliqev MAMMGin Mrec Mevg mw
global  pev pcond p Tcondold Mliqcondnew dQheat Mcondgold Tevold Trecold Mliqevnew dQcool

% Radius
rw= 0.4*10^(-3); % Radius of water (m)
rs= 0.6*10^(-3); % Radius of steel (m)
rc= 1.5*10^(-3); % Radius of carbon (m)
ShellD= 144.5*10^(-3); % Shell diameter (m)

% Areas
Aw= pi*rw^2; % Transversal area of water per tube (m^2)
As= pi*(rs^2-rw^2); % Transversal area of steel per tube (m^2)
Aws= pi*rs^2; % Transversal area of water and steel per tube (m^2)
Ac= sqrt(3)/2*(2*rc)^2-pi*rs^2; % Transversal area of carbon per tube (m^2)
At= sqrt(3)/2*(2*rc)^2; % Transversal total area per tube (m^2)

Ntub= 1777; % Number of tubes in the generator
L= 396*10^(-3); % Length of the generator (m)

Nus= 4; % Nusselt number

% Water
Dw= 958; % Density of the water (kg/m^3)
Cpw= 4219; % Specific heat of the water (J/kg*K)
Cvw= 4178; % Specific heat at constant volume of the water (J/kg*K)
Mw= Aw*Ntub*L*Dw; % Mass of water in the control volume (kg)
Kw= 0.68; % Conductivity of the water (W/K*m)
hw= Kw*Nus/(2*rw); % Convective heat transfer coefficient (W/m^2*K)
Awi= L*pi*2*rw; % Area of the internal surface OF ONE steel tube (m^2)
UAw= hw*Awi*Ntub; % W/K TOTAL HEX, WATER TO STEEL

% Steel
Ds= 8000; % Density of the steel (kg/m^3)
Cps= 460; % Specific heat of the steel (J/kg*K)
Ks= 16; % Thermal conductivity of the stainless steel (W/m*K)
Ms= As*Ntub*L*Ds; % Mass of steel in the control volume (kg)
Volshell= (pi()/4*ShellD^2-Ntub*Aws)*L;
Volhex= Ntub*Ac*L; % Volume inside the generator (without tubes) (m^3)

% Carbon
Dcs= 1000; % Density of solid carbon (kg/m^3)

% Ammonia
Dal= 681.97; % Density of ammonia liquid (kg/m^3)
Cpa= 6677; % Specific heat of the ammonia liquid (J/kg*K)
```

```
C= 2823.4; % Slope of saturated line for Ammonia

% Generator length
N= 40; % Number of transversal parts of the tube
dL= L/N; % Differential of length of the model (m)
nL= N;

% Condenser
Tcondin= 41+273; % Initial temperature of the condenser (K) 50
pcondin= psatamm(Tcondin); % Initial pressure of the condenser (bar)
Vcond= 0.002; % Volume of the condenser (m^3)
Mcond= 4.5; % Mass of the condenser (kg)
cpcond= 460; % Specific heat of condenser (steel) (J/kg*K)
Mcondgin= pcondin*10^5*Vcond/(ramms(pcondin,Tcondin-273)*Tcondin); % Condenser gmass (kg)
UAcond= 1360.8; % Condenser overall heat transfer coefficient (W/K)
mwcond= 0.1582; % Water mass flow in the condenser (kg/s)
Twcondin= 40+273; % Temperature water inlet in the condenser (K);
NTUcond= UAcond/(mwcond*Cpw);

% Evaporator
Tevin= 1+273; % Initial temperature of the evaporator (K)
pevin= psatamm(Tevin); % Initial pressure of the evaporator (bar)
Vev= 0.002; % Volume of the evaporator (m^3)
Mev= 10; % Mass of the evaporator (kg)
cpev= 460; % Specific heat of evaporator (steel) (J/kg*K)
Mevgin= pevin*10^5*Vev/(ramms(pevin,Tevin-273)*Tevin); % Evaporator gas mass (kg)
UAev= 739.8; % Evaporator overall heat transfer coefficient (W/K)
Tairevin= 0+273; % Temperature air inlet in the evaporator (K);
mairev= 1000/3600; % Air mass flow in the evaporator (kg/s) 0.2778
Cpair= 1000; % Specific heat of air (J/kg*K)
NTUev= UAev/(mairev*Cpair);

% Cooler
UAcooler= 3460;

% Receiver
Trecin= Tcondin; % Receiver temperature (K)
Mrecin= 1; % Initial mass in the receiver (kg)

% Check valves
Kvcond= 0.01; % Condenser check valve coefficient
Kvev= 0.01; % Evaporator check valve coefficient

ncycles= 10; % Number of cycles to run
dt= 1/20; % Differential of time in the model (s)

contador= 0;

THOT= 170+273;

Kc= 0.3;
Mc= 3;
Dcb= Mc/Volhex; % DENSITY OF CARBON BED (kg/m^3)
k= 3.9615; x0= 0.2551; n= 1.227; % Data for the carbon used
VoidVol= Volhex-Mc/Dcs; % Volume of gas space (m^3)
R= sqrt((Ac/2+Aws)/pi()); % Equivalent radius of carbon (m)
```

```
UAcarb= 2*pi*Kc*L/log(R/rs)*Ntub; % W/K FOR TOTAL HEAT EXCHANGER, STEEL TO CARBON
UAc= UAcarb;
UAtotal= 1/(1/UAc+1/UAw);

t= 65; % 1/4 of a cycle

mw= 0.0375;

    nt= t/dt+1;

    Tin= 90+273; % Initial temperature of the beds (K)
    Tsatin= Tin-60; % MAKE SATURATION TEMPERATURE 60C LOWER THAN CARBON TEMPERATURE

    % Water
    Tw1= zeros(nL,4*t+1); % Matrix that contains on lengths and times the water temperature
    Tw1(:,1)= Tin;
    Tw2= Tw1; Tw3= Tw1; Tw4= Tw1;
    Tw1f= zeros(nL,1); % Vector flotante
    Tw1f(:)= Tin;
    Tw2f= Tw1f; Tw3f= Tw1f; Tw4f= Tw1f; % Vector flotante

    % Steel
    Ts1= zeros(nL,4*t+1); % Matrix that contains on lengths and times the steel temperature
    Ts1(:,1)= Tin;
    Ts2= Ts1; Ts3= Ts1; Ts4= Ts1;
    Ts1f= zeros(nL,1); % Vector flotante
    Ts1f(:)= Tin;
    Ts2f= Ts1f; Ts3f= Ts1f; Ts4f= Ts1f; % Vector flotante

    % Carbon
    Tc1= zeros(nL,4*t+1); % Matrix that contains on lengths and times the steel temperature
    Tc1(:,1)= Tin;
    Tc2= Tc1; Tc3= Tc1; Tc4= Tc1;
    Tc1f= zeros(nL,1); % Vector flotante
    Tc1f(:)= Tin;
    Tc2f= Tc1f; Tc3f= Tc1f; Tc4f= Tc1f; % Vector flotante

    % Increment in adsorption
    XX1= zeros(nL,4*t); % Matrix that contains on lengths and times the steel temperature %
    XX2= XX1; XX3= XX1; XX4= XX1;
    XX1f= zeros(nL,1); % Vector flotante
    XX2f= XX1f; XX3f= XX1f; XX4f= XX1f;

    % Carbon heat
    Qc1= zeros(nL,4*t);
    Qc2= Qc1; Qc3= Qc1; Qc4= Qc1;

    % Pressure
    pin= psatamm(Tsatin);
    p1= zeros(1,4*t+1); % Matrix GAS PRESSURE (BAR)
    p1(1)= pin;
    p2= p1; p3= p1; p4= p1;
    p1f= pin; p2f= pin; p3f= pin; p4f= pin;

    % Gas temperature
    Tgas1= zeros(1,4*t+1); % Vector with initial gas temperature (K)
    Tgas1(1)= Tin;
```

```
Tgas2= Tgas1; Tgas3= Tgas1; Tgas4= Tgas1;
Tgas1f= Tin; Tgas2f= Tin; Tgas3f= Tin; Tgas4f= Tin;

% Saturation gas temperature
Tsat1= zeros(1,4*t+1); % Vector with initial gas temperature (K)
Tsat1(1)= Tsatin;
Tsat2= Tsat1; Tsat3= Tsat1; Tsat4= Tsat1;
Tsat1f= Tsatin; Tsat2f= Tsatin; Tsat3f= Tsatin; Tsat4f= Tsatin;

Xin= dub2(Tsatin,Tin,x0,k,n); % INITIAL CONCENTRATION
MAMMGin= pin*100000*VoidVol/(Tin*ramms(pin,Tin-273)); % Initial ammonia gas (kg)
Mammlin= Mc*Xin/N;
Mctein= Mc*Xin+MAMMGin; % INITIAL MASS OF AMMONIA IN BED (kg)

% Adsorption
X1= zeros(nL,4*t+1);
X1(:,1)= Xin;
X2= X1; X3= X1; X4= X1;
X1f= zeros(nL,1); % Vector flotante
X1f(:)= Xin;
X2f= X1f; X3f= X1f; X4f= X1f; % Vector flotante

% Ammonia gas mass
MAMMG1= zeros(1,4*t+1);
MAMMG1(1)= MAMMGin;
MAMMG2= MAMMG1; MAMMG3= MAMMG1; MAMMG4= MAMMG1;
MAMMG1f= MAMMGin;
MAMMG2f= MAMMG1f; MAMMG3f= MAMMG1f; MAMMG4f= MAMMG1f; % Vector flotante

% Ammonia adsorbed mass
Mamml1= zeros(nL,4*t+1);
Mamml1(:,1)= Mammlin;
Mamml2= Mamml1; Mamml3= Mamml1; Mamml4= Mamml1;
Mamml1f= zeros(nL,1);
Mamml1f(:)= Mammlin;
Mamml2f= Mamml1f; Mamml3f= Mamml1f; Mamml4f= Mamml1f; % Vector flotante

% Total mass of ammonia
Mcte1= zeros(1,4*t+1);
Mcte1(1)= Mctein;
Mcte2= Mcte1; Mcte3= Mcte1; Mcte4= Mcte1;
Mcte1f= Mctein;
Mcte2f= Mcte1f; Mcte3f= Mcte1f; Mcte4f= Mcte1f; % Vector flotante

% Evaporator
pev= zeros(1,4*t+1); pev(1)= pevin; pevold= pevin;
Tev= zeros(1,4*t+1); Tev(1)= Tevin; Tevold= Tevin;
Mevg= zeros(1,4*t+1); Mevg(1)= Mevgin; Mevgold= Mevgin;
Tairevout= zeros(1,4*t+1); Tairevout(1)= Tevin+(Tairevin-Tevin)/exp(NTUev);
Mliqev= zeros(1,4*t+1);

% Condenser
pcond= zeros(1,4*t+1); pcond(1)= pcondin; pcondold= pcondin;
Tcond= zeros(1,4*t+1); Tcond(1)= Tcondin; Tcondold= Tcondin;
Mcondg= zeros(1,4*t+1); Mcondg(1)= Mcondgin; Mcondgold= Mcondgin;
Twcondout= zeros(1,4*t+1); Twcondout(1)= Tcondin+(Twcondin-Tcondin)/exp(NTUcond);
Mliqcond= zeros(1,4*t+1);
```

```
% Receiver
Trec= zeros(1,4*t+1); Trec(1)= Trecin; Trecold= Trecin;
Mrec= zeros(1,4*t+1); Mrec(1)= Mrecin; Mrecold= Mrecin;

% Water flow
TwoutB= zeros(1,4*t+1); TwoutB(1)= Tin;
TwinC= zeros(1,4*t+1);
TwoutD= zeros(1,4*t+1); TwoutD(1)= Tin;
Twoutcooler= zeros(1,4*t+1);

% Boiler
Thot= zeros(1,4*t+1);
Thot= Thot+THOT; % Vector
Qboiler= (THOT-Tin)*Cpw*dt*mw; % Initial in Joules

% Evaporator
LMTDev= (Tairevin-Tairevout(1))/(log((Tairevin-Tevin)/(Tairevout(1)-Tevin)));
Qcool= 0;
dQcool=UAev*dt*LMTDev;
Qcool= Qcool+dQcool;
Latent= hgamm(Tevin-273)-hfamm(Trecin-273);
Mliqev(1)=dQcool/Latent;

% Condenser
LMTDcond= (Twcondout(1)-Twcondin)/(log((Tcondin-Twcondin)/(Tcondin-Twcondout(1))));
Qheat= 0;
dQheat= UAcond*dt*LMTDcond;
Qheat= Qheat+dQheat;
Latent= hgamm(Tcondin-273)-hfamm(Tcondin-273);
Mliqcond(1)=dQheat/Latent;

% Cooler
NTUcooler= UAcooler/min([Cpw*mw Cpw*mwcond]);
Cr= min([Cpw*mw Cpw*mwcond])/max([Cpw*mw Cpw*mwcond]);
Ecooler= (1-exp(-NTUcooler*(1-Cr)))/(1-Cr*exp(-NTUcooler*(1-Cr)));
Qcooler= 0;
dQcooler= Ecooler*min([Cpw*mw Cpw*mwcond])*(TwoutB(1)-Twcondout(1))*dt;
Qcooler= dQcooler+Qcooler;
TwinC(1)= TwoutB(1)-dQcooler/(mw*Cpw*dt);
TwinCnew= TwinC(1);
Twoutcooler(1)= Twcondout(1)+dQcooler/(mwcond*Cpw*dt);

for c= 1:ncycles
disp(c)
Qsupcond= 0;
Mammev= 0;
Mammcond= 0;

    % Phase 1

    for j=1:t/dt

    jdMammev= 0;
    jdMammcond= 0;
    jdQsupcond= 0;
```

```
            generatorWATER
(THOT,Tw1f(:),Ts1f(:),Tc1f(:),X1f(:),XX1f(:),p1f,Tgas1f,Tsat1f,Mcte1f,MAMMG1f);
            p1f= p;
            Tsat1f= Tsat;
            Tgas1f= Tgas;
            Mcte1f= Mcte;
            MAMMG1f= MAMMG;
            Tw1f= Tw;
            Ts1f= Ts;
            Tc1f= Tc;
            Mamml1f= Mamml;
            XX1f= XX;
            X1f= X;
            if rem(j*dt,1)==0
               p1((j*dt)+1)= p;
               Tsat1((j*dt)+1)= Tsat;
               Tgas1((j*dt)+1)= Tgas;
               Mcte1((j*dt)+1)= Mcte;
               MAMMG1((j*dt)+1)= MAMMG;
               Tw1(:,(j*dt)+1)= Tw;
               Ts1(:,(j*dt)+1)= Ts;
               Tc1(:,(j*dt)+1)= Tc;
               X1(:,(j*dt)+1)= X;
               Mamml1(:,(j*dt)+1)= Mamml;
               Qc1(:,(j*dt))= Qc;
               XX1(:,(j*dt))= XX;
            end

            generatorWATER
(Tw(nL),Tw2f(:),Ts2f(:),Tc2f(:),X2f(:),XX2f(:),p2f,Tgas2f,Tsat2f,Mcte2f,MAMMG2f);
            p2f= p;
            Tsat2f= Tsat;
            Tgas2f= Tgas;
            Mcte2f= Mcte;
            MAMMG2f= MAMMG;
            Tw2f=Tw;
            Ts2f=Ts;
            Tc2f=Tc;
            Mamml2f= Mamml;
            XX2f= XX;
            X2f= X;
            if rem(j*dt,1)==0
               p2((j*dt)+1)= p;
               Tsat2((j*dt)+1)= Tsat;
               Tgas2((j*dt)+1)= Tgas;
               Mcte2((j*dt)+1)= Mcte;
               MAMMG2((j*dt)+1)= MAMMG;
               Tw2(:,(j*dt)+1)= Tw;
               Ts2(:,(j*dt)+1)= Ts;
               Tc2(:,(j*dt)+1)= Tc;
               X2(:,(j*dt)+1)= X;
               Mamml2(:,(j*dt)+1)= Mamml;
               Qc2(:,(j*dt))= Qc;
               XX2(:,(j*dt))= XX;
            end

            TwoutBnew= Tw(nL);
```

```
        if rem(j*dt,1)==0
           TwoutB((j*dt)+1)= Tw(nL);
        end

        generatorWATER
(TwinCnew,Tw3f(:),Ts3f(:),Tc3f(:),X3f(:),XX3f(:),p3f,Tgas3f,Tsat3f,Mcte3f,MAMMG3f);
        p3f= p;
        Tsat3f= Tsat;
        Tgas3f= Tgas;
        Mcte3f= Mcte;
        MAMMG3f= MAMMG;
        Tw3f= Tw;
        Ts3f= Ts;
        Tc3f= Tc;
        Mamml3f= Mamml;
        XX3f= XX;
        X3f= X;
        if rem(j*dt,1)==0
           p3((j*dt)+1)= p;
           Tsat3((j*dt)+1)= Tsat;
           Tgas3((j*dt)+1)= Tgas;
           Mcte3((j*dt)+1)= Mcte;
           MAMMG3((j*dt)+1)= MAMMG;
           Tw3(:,(j*dt)+1)= Tw;
           Ts3(:,(j*dt)+1)= Ts;
           Tc3(:,(j*dt)+1)= Tc;
           X3(:,(j*dt)+1)= X;
           Mamml3(:,(j*dt)+1)= Mamml;
           Qc3(:,(j*dt))= Qc;
           XX3(:,(j*dt))= XX;
        end

        generatorWATER
(Tw(nL),Tw4f(:),Ts4f(:),Tc4f(:),X4f(:),XX4f(:),p4f,Tgas4f,Tsat4f,Mcte4f,MAMMG4f);
        p4f= p;
        Tsat4f= Tsat;
        Tgas4f= Tgas;
        Mcte4f= Mcte;
        MAMMG4f= MAMMG;
        Tw4f= Tw;
        Ts4f= Ts;
        Tc4f= Tc;
        Mamml4f= Mamml;
        XX4f= XX;
        X4f= X;
        if rem(j*dt,1)==0
           p4((j*dt)+1)= p;
           Tsat4((j*dt)+1)= Tsat;
           Tgas4((j*dt)+1)= Tgas;
           Mcte4((j*dt)+1)= Mcte;
           MAMMG4((j*dt)+1)= MAMMG;
           Tw4(:,(j*dt)+1)= Tw;
           Ts4(:,(j*dt)+1)= Ts;
           Tc4(:,(j*dt)+1)= Tc;
           X4(:,(j*dt)+1)= X;
           Mamml4(:,(j*dt)+1)= Mamml;
           Qc4(:,(j*dt))= Qc;
```

```
        XX4(:,(j*dt))= XX;
    end

    TwoutDnew= Tw(nL);
    if rem(j*dt,1)==0
        TwoutD((j*dt)+1)= Tw(nL);
    end

    dQboiler= (THOT-TwoutDnew)*Cpw*dt*mw; % in Joules
    Qboiler= dQboiler+Qboiler;

    Mammcond1= Mammcond;
    Mammev1= Mammev;
    Qsupcond1= Qsupcond;

    % evaporator
    Tairevoutnew= Tevold+(Tairevin-Tevold)/exp(NTUev);
    LMTDev= (Tairevin-Tairevoutnew)/(log((Tairevin-Tevold)/(Tairevoutnew-Tevold)));
    dQcool= UAev*dt*LMTDev;
    Qcool= Qcool+dQcool;
    pevnew= fzero(@dPevapCREB,pevold);
    Tevnew= Tsatamm(pevnew);
    Mevgnew= pevnew*100000*Vev/(Tevnew*ramms(pevnew,Tevnew-273));
    if rem(j*dt,1)==0
        Tairevout((j*dt)+1)= Tairevoutnew;
        pev((j*dt)+1)= pevnew;
        Tev((j*dt)+1)= Tevnew;
        Mevg((j*dt)+1)= Mevgnew;
        Mliqev((j*dt)+1)= Mliqevnew;
    end
    pevold= pevnew;
    Tevold= Tevnew;
    Mevgold= Mevgnew;

    % condenser
    Twcondoutnew= Tcondold+(Twcondin-Tcondold)/exp(NTUcond);
    LMTDcond= (Twcondoutnew-Twcondin)/(log((Tcondold-Twcondin)/(Tcondold-
Twcondoutnew)));
    dQheat= UAcond*dt*LMTDcond;
    Qheat= Qheat+dQheat;
    pcondnew= fzero(@dPcondCREB,pcondold);
    Tcondnew= Tsatamm(pcondnew);
    Mcondgnew= pcondnew*100000*Vcond/(Tcondnew*ramms(pcondnew,Tcondnew-273));
    if rem(j*dt,1)==0
        Twcondout((j*dt)+1)= Twcondoutnew;
        pcond((j*dt)+1)= pcondnew;
        Tcond((j*dt)+1)= Tcondnew;
        Mcondg((j*dt)+1)= Mcondgnew;
        Mliqcond((j*dt)+1)= Mliqcondnew;
    end
    pcondold= pcondnew;
    Tcondold= Tcondnew;
    Mcondgold= Mcondgnew;

    % receiver
    Trecnew= (Trecold*(Mrecold-Mliqevnew)+Tcondnew*Mliqcondnew)/(Mrecold-
Mliqevnew+Mliqcondnew);
```

```
        Mrecnew= Mrecold-Mliqevnew+Mliqcondnew;
        if rem(j*dt,1)==0
          Trec((j*dt)+1)= Trecnew;
          Mrec((j*dt)+1)= Mrecnew;
        end
        Mrecold= Mrecnew;
        Trecold= Trecnew;

        % cooler
        dQcooler= Ecooler*min([Cpw*mw Cpw*mwcond])*(TwoutBnew-Twcondoutnew)*dt;
        Qcooler= Qcooler+dQcooler;
        TwinCnew= TwoutBnew-dQcooler/(mw*Cpw*dt);
        Twoutcoolernew= dQcooler/(mwcond*Cpw*dt)+Twcondoutnew;
        if rem(j*dt,1)==0
          TwinC((j*dt)+1)= TwinCnew;
          Twoutcooler((j*dt)+1)= Twoutcoolernew;
          Twcondout((j*dt)+1)= Twcondoutnew;
        end
      end

      % Phase 2

      for j=t/dt+1:2*t/dt

        jdMammev= 0;
        jdMammcond= 0;
        jdQsupcond= 0;

        generatorWATER
(THOT,Tw2f(:),Ts2f(:),Tc2f(:),X2f(:),XX2f(:),p2f,Tgas2f,Tsat2f,Mcte2f,MAMMG2f);
        p2f= p;
        Tsat2f= Tsat;
        Tgas2f= Tgas;
        Mcte2f= Mcte;
        MAMMG2f= MAMMG;
        Tw2f= Tw;
        Ts2f= Ts;
        Tc2f= Tc;
        Mamml2f= Mamml;
        XX2f= XX;
        X2f= X;
        if rem(j*dt,1)==0
          p2((j*dt)+1)= p;
          Tsat2((j*dt)+1)= Tsat;
          Tgas2((j*dt)+1)= Tgas;
          Mcte2((j*dt)+1)= Mcte;
          MAMMG2((j*dt)+1)= MAMMG;
          Tw2(:,(j*dt)+1)=  Tw;
          Ts2(:,(j*dt)+1)= Ts;
          Tc2(:,(j*dt)+1)= Tc;
          X2(:,(j*dt)+1)= X;
          Mamml2(:,(j*dt)+1)= Mamml;
          Qc2(:,(j*dt))= Qc;
          XX2(:,(j*dt))= XX;
        end
```

```
        generatorWATER
(Tw(nL),Tw3f(:),Ts3f(:),Tc3f(:),X3f(:),XX3f(:),p3f,Tgas3f,Tsat3f,Mcte3f,MAMMG3f);
        p3f= p;
        Tsat3f= Tsat;
        Tgas3f= Tgas;
        Mcte3f= Mcte;
        MAMMG3f= MAMMG;
        Tw3f= Tw;
        Ts3f= Ts;
        Tc3f= Tc;
        Mamml3f= Mamml;
        XX3f= XX;
        X3f= X;
        if rem(j*dt,1)==0
           p3((j*dt)+1)= p;
           Tsat3((j*dt)+1)= Tsat;
           Tgas3((j*dt)+1)= Tgas;
           Mcte3((j*dt)+1)= Mcte;
           MAMMG3((j*dt)+1)= MAMMG;
           Tw3(:,(j*dt)+1)= Tw;
           Ts3(:,(j*dt)+1)= Ts;
           Tc3(:,(j*dt)+1)= Tc;
           X3(:,(j*dt)+1)= X;
           Mamml3(:,(j*dt)+1)= Mamml;
           Qc3(:,(j*dt))= Qc;
           XX3(:,(j*dt))= XX;
        end

        TwoutBnew= Tw(nL);
        if rem(j*dt,1)==0
           TwoutB((j*dt)+1)= Tw(nL);
        end

        generatorWATER
(TwinCnew,Tw4f(:),Ts4f(:),Tc4f(:),X4f(:),XX4f(:),p4f,Tgas4f,Tsat4f,Mcte4f,MAMMG4f);
        p4f= p;
        Tsat4f= Tsat;
        Tgas4f= Tgas;
        Mcte4f= Mcte;
        MAMMG4f= MAMMG;
        Tw4f= Tw;
        Ts4f= Ts;
        Tc4f= Tc;
        Mamml4f= Mamml;
        XX4f= XX;
        X4f= X;
        if rem(j*dt,1)==0
           p4((j*dt)+1)= p;
           Tsat4((j*dt)+1)= Tsat;
           Tgas4((j*dt)+1)= Tgas;
           Mcte4((j*dt)+1)= Mcte;
           MAMMG4((j*dt)+1)= MAMMG;
           Tw4(:,(j*dt)+1)= Tw;
           Ts4(:,(j*dt)+1)= Ts;
           Tc4(:,(j*dt)+1)= Tc;
           X4(:,(j*dt)+1)= X;
           Mamml4(:,(j*dt)+1)= Mamml;
```

```
    Qc4(:,(j*dt))= Qc;
    XX4(:,(j*dt))= XX;
end

generatorWATER
(Tw(nL),Tw1f(:),Ts1f(:),Tc1f(:),X1f(:),XX1f(:),p1f,Tgas1f,Tsat1f,Mcte1f,MAMMG1f);
p1f= p;
Tsat1f= Tsat;
Tgas1f= Tgas;
Mcte1f= Mcte;
MAMMG1f= MAMMG;
Tw1f= Tw;
Ts1f= Ts;
Tc1f= Tc;
Mamml1f= Mamml;
XX1f= XX;
X1f= X;
if rem(j*dt,1)==0
    p1((j*dt)+1)= p;
    Tsat1((j*dt)+1)= Tsat;
    Tgas1((j*dt)+1)= Tgas;
    Mcte1((j*dt)+1)= Mcte;
    MAMMG1((j*dt)+1)= MAMMG;
    Tw1(:,(j*dt)+1)=Tw;
    Ts1(:,(j*dt)+1)=Ts;
    Tc1(:,(j*dt)+1)=Tc;
    X1(:,(j*dt)+1)= X;
    Mamml1(:,(j*dt)+1)= Mamml;
    Qc1(:,(j*dt))=Qc;
    XX1(:,(j*dt))= XX;
end

TwoutDnew= Tw(nL);
if rem(j*dt,1)==0
    TwoutD((j*dt)+1)= Tw(nL);
end

dQboiler= (THOT-TwoutDnew)*Cpw*dt*mw; % in Joules
Qboiler= dQboiler+Qboiler;

Mammcond2= Mammcond-Mammcond1;
Mammev2= Mammev-Mammev1;
Qsupcond2= Qsupcond-Qsupcond1;

% evaporator
Tairevoutnew= Tevold+(Tairevin-Tevold)/exp(NTUev);
LMTDev= (Tairevin-Tairevoutnew)/(log((Tairevin-Tevold)/(Tairevoutnew-Tevold)));
dQcool= UAev*dt*LMTDev;
Qcool= Qcool+dQcool;
pevnew= fzero(@dPevapCREB,pevold);
Tevnew= Tsatamm(pevnew);
Mevgnew= pevnew*100000*Vev/(Tevnew*ramms(pevnew,Tevnew-273));
if rem(j*dt,1)==0
    Tairevout((j*dt)+1)= Tairevoutnew;
    pev((j*dt)+1)= pevnew;
    Tev((j*dt)+1)= Tevnew;
    Mevg((j*dt)+1)= Mevgnew;
```

```
            Mliqev((j*dt)+1)= Mliqevnew;
        end
        pevold= pevnew;
        Tevold= Tevnew;
        Mevgold= Mevgnew;

        % condenser
        Twcondoutnew= Tcondold+(Twcondin-Tcondold)/exp(NTUcond);
        LMTDcond= (Twcondoutnew-Twcondin)/(log((Tcondold-Twcondin)/(Tcondold-
Twcondoutnew)));
        dQheat= UAcond*dt*LMTDcond;
        Qheat= Qheat+dQheat;
        pcondnew= fzero(@dPcondCREB,pcondold);
        Tcondnew= Tsatamm(pcondnew);
        Mcondgnew= pcondnew*100000*Vcond/(Tcondnew*ramms(pcondnew,Tcondnew-273));
        if rem(j*dt,1)==0
            Twcondout((j*dt)+1)= Twcondoutnew;
            pcond((j*dt)+1)= pcondnew;
            Tcond((j*dt)+1)= Tcondnew;
            Mcondg((j*dt)+1)= Mcondgnew;
        end
        pcondold= pcondnew;
        Tcondold= Tcondnew;
        Mcondgold= Mcondgnew;

        % receiver
        Trecnew= (Trecold*(Mrecold-Mliqevnew)+Tcondnew*Mliqcondnew)/(Mrecold-
Mliqevnew+Mliqcondnew);
        Mrecnew= Mrecold-Mliqevnew+Mliqcondnew;
        if rem(j*dt,1)==0
            Trec((j*dt)+1)= Trecnew;
            Mrec((j*dt)+1)= Mrecnew;
        end
        Mrecold= Mrecnew;
        Trecold= Trecnew;

        % cooler
        dQcooler= Ecooler*min([Cpw*mw Cpw*mwcond])*(TwoutBnew-Twcondoutnew)*dt;
        Qcooler= Qcooler+dQcooler;
        TwinCnew= TwoutBnew-dQcooler/(mw*Cpw*dt);
        Twoutcoolernew= dQcooler/(mwcond*Cpw*dt)+Twcondoutnew;
        if rem(j*dt,1)==0
            TwinC((j*dt)+1)= TwinCnew;
            Twoutcooler((j*dt)+1)= Twoutcoolernew;
            Twcondout((j*dt)+1)= Twcondoutnew;
            Mliqcond((j*dt)+1)= Mliqcondnew;
        end
    end

    % Phase 3

    for j=2*t/dt+1:3*t/dt

        jdMammev= 0;
        jdMammcond= 0;
        jdQsupcond= 0;
```

```
        generatorWATER
(THOT,Tw3f(:),Ts3f(:),Tc3f(:),X3f(:),XX3f(:),p3f,Tgas3f,Tsat3f,Mcte3f,MAMMG3f);
        p3f= p;
        Tsat3f= Tsat;
        Tgas3f= Tgas;
        Mcte3f= Mcte;
        MAMMG3f= MAMMG;
        Tw3f= Tw;
        Ts3f= Ts;
        Tc3f= Tc;
        Mamml3f= Mamml;
        XX3f= XX;
        X3f= X;
        if rem(j*dt,1)==0
           p3((j*dt)+1)= p;
           Tsat3((j*dt)+1)= Tsat;
           Tgas3((j*dt)+1)= Tgas;
           Mcte3((j*dt)+1)= Mcte;
           MAMMG3((j*dt)+1)= MAMMG;
           Tw3(:,(j*dt)+1)= Tw;
           Ts3(:,(j*dt)+1)= Ts;
           Tc3(:,(j*dt)+1)= Tc;
           X3(:,(j*dt)+1)= X;
           Mamml3(:,(j*dt)+1)= Mamml;
           Qc3(:,(j*dt))= Qc;
           XX3(:,(j*dt))= XX;
        end

        generatorWATER
(Tw(nL),Tw4f(:),Ts4f(:),Tc4f(:),X4f(:),XX4f(:),p4f,Tgas4f,Tsat4f,Mcte4f,MAMMG4f);
        p4f= p;
        Tsat4f= Tsat;
        Tgas4f= Tgas;
        Mcte4f= Mcte;
        MAMMG4f= MAMMG;
        Tw4f= Tw;
        Ts4f= Ts;
        Tc4f= Tc;
        Mamml4f= Mamml;
        XX4f= XX;
        X4f= X;
        if rem(j*dt,1)==0
           p4((j*dt)+1)= p;
           Tsat4((j*dt)+1)= Tsat;
           Tgas4((j*dt)+1)= Tgas;
           Mcte4((j*dt)+1)= Mcte;
           MAMMG4((j*dt)+1)= MAMMG;
           Tw4(:,(j*dt)+1)= Tw;
           Ts4(:,(j*dt)+1)= Ts;
           Tc4(:,(j*dt)+1)= Tc;
           X4(:,(j*dt)+1)= X;
           Mamml4(:,(j*dt)+1)= Mamml;
           Qc4(:,(j*dt))= Qc;
           XX4(:,(j*dt))= XX;
        end

        TwoutBnew= Tw(nL);
```

```
        if rem(j*dt,1)==0
           TwoutB((j*dt)+1)= Tw(nL);
        end

        generatorWATER
(TwinCnew,Tw1f(:),Ts1f(:),Tc1f(:),X1f(:),XX1f(:),p1f,Tgas1f,Tsat1f,Mcte1f,MAMMG1f);
        p1f= p;
        Tsat1f= Tsat;
        Tgas1f= Tgas;
        Mcte1f= Mcte;
        MAMMG1f= MAMMG;
        Tw1f= Tw;
        Ts1f= Ts;
        Tc1f= Tc;
        Mamml1f= Mamml;
        XX1f= XX;
        X1f= X;
        if rem(j*dt,1)==0
           p1((j*dt)+1)= p;
           Tsat1((j*dt)+1)= Tsat;
           Tgas1((j*dt)+1)= Tgas;
           Mcte1((j*dt)+1)= Mcte;
           MAMMG1((j*dt)+1)= MAMMG;
           Tw1(:,(j*dt)+1)= Tw;
           Ts1(:,(j*dt)+1)= Ts;
           Tc1(:,(j*dt)+1)= Tc;
           X1(:,(j*dt)+1)= X;
           Mamml1(:,(j*dt)+1)= Mamml;
           Qc1(:,(j*dt))=Qc;
           XX1(:,(j*dt))= XX;
        end

        generatorWATER
(Tw(nL),Tw2f(:),Ts2f(:),Tc2f(:),X2f(:),XX2f(:),p2f,Tgas2f,Tsat2f,Mcte2f,MAMMG2f);
        p2f= p;
        Tsat2f= Tsat;
        Tgas2f= Tgas;
        Mcte2f= Mcte;
        MAMMG2f= MAMMG;
        Tw2f= Tw;
        Ts2f= Ts;
        Tc2f= Tc;
        Mamml2f= Mamml;
        XX2f= XX;
        X2f= X;
        if rem(j*dt,1)==0
           p2((j*dt)+1)= p;
           Tsat2((j*dt)+1)= Tsat;
           Tgas2((j*dt)+1)= Tgas;
           Mcte2((j*dt)+1)= Mcte;
           MAMMG2((j*dt)+1)= MAMMG;
           Tw2(:,(j*dt)+1)= Tw;
           Ts2(:,(j*dt)+1)= Ts;
           Tc2(:,(j*dt)+1)= Tc;
           X2(:,(j*dt)+1)= X;
           Mamml2(:,(j*dt)+1)= Mamml;
           Qc2(:,(j*dt))= Qc;
```

```
        XX2(:,(j*dt))= XX;
    end

    TwoutDnew= Tw(nL);
    if rem(j*dt,1)==0
        TwoutD((j*dt)+1)= Tw(nL);
    end

    dQboiler= (THOT-TwoutDnew)*Cpw*dt*mw; % in Joules
    Qboiler= dQboiler+Qboiler;

    Mammcond3= Mammcond-Mammcond1-Mammcond2;
    Mammev3= Mammev-Mammev1-Mammev2;
    Qsupcond3= Qsupcond-Qsupcond1-Qsupcond2;

    % evaporator
    Tairevoutnew= Tevold+(Tairevin-Tevold)/exp(NTUev);
    LMTDev= (Tairevin-Tairevoutnew)/(log((Tairevin-Tevold)/(Tairevoutnew-Tevold)));
    dQcool= UAev*dt*LMTDev;
    Qcool= Qcool+dQcool;
    pevnew= fzero(@dPevapCREB,pevold);
    Tevnew= Tsatamm(pevnew);
    Mevgnew= pevnew*100000*Vev/(Tevnew*ramms(pevnew,Tevnew-273));
    if rem(j*dt,1)==0
        Tairevout((j*dt)+1)= Tairevoutnew;
        pev((j*dt)+1)= pevnew;
        Tev((j*dt)+1)= Tevnew;
        Mevg((j*dt)+1)= Mevgnew;
        Mliqev((j*dt)+1)= Mliqevnew;
    end
    pevold= pevnew;
    Tevold= Tevnew;
    Mevgold= Mevgnew;

    % condenser
    Twcondoutnew= Tcondold+(Twcondin-Tcondold)/exp(NTUcond);
    LMTDcond= (Twcondoutnew-Twcondin)/(log((Tcondold-Twcondin)/(Tcondold-
Twcondoutnew)));
    dQheat= UAcond*dt*LMTDcond;
    Qheat= Qheat+dQheat;
    pcondnew= fzero(@dPcondCREB,pcondold);
    Tcondnew= Tsatamm(pcondnew);
    Mcondgnew= pcondnew*100000*Vcond/(Tcondnew*ramms(pcondnew,Tcondnew-273));
    if rem(j*dt,1)==0
        Twcondout((j*dt)+1)= Twcondoutnew;
        pcond((j*dt)+1)= pcondnew;
        Tcond((j*dt)+1)= Tcondnew;
        Mcondg((j*dt)+1)= Mcondgnew;
    end
    pcondold= pcondnew;
    Tcondold= Tcondnew;
    Mcondgold= Mcondgnew;

    % receiver
    Trecnew= (Trecold*(Mrecold-Mliqevnew)+Tcondnew*Mliqcondnew)/(Mrecold-
Mliqevnew+Mliqcondnew);
    Mrecnew= Mrecold-Mliqevnew+Mliqcondnew;
```

```
        if rem(j*dt,1)==0
            Trec((j*dt)+1)= Trecnew;
            Mrec((j*dt)+1)= Mrecnew;
        end
        Mrecold= Mrecnew;
        Trecold= Trecnew;

        % cooler
        dQcooler= Ecooler*min([Cpw*mw Cpw*mwcond])*(TwoutBnew-Twcondoutnew)*dt;
        Qcooler= Qcooler+dQcooler;
        TwinCnew= TwoutBnew-dQcooler/(mw*Cpw*dt);
        Twoutcoolernew= dQcooler/(mwcond*Cpw*dt)+Twcondoutnew;
        if rem(j*dt,1)==0
            TwinC((j*dt)+1)= TwinCnew;
            Twoutcooler((j*dt)+1)= Twoutcoolernew;
            Twcondout((j*dt)+1)= Twcondoutnew;
            Mliqcond((j*dt)+1)= Mliqcondnew;
        end
    end

    % Phase 4

    for j=3*t/dt+1:4*t/dt

        jdMammev= 0;
        jdMammcond= 0;
        jdQsupcond= 0;

        generatorWATER
(THOT,Tw4f(:),Ts4f(:),Tc4f(:),X4f(:),XX4f(:),p4f,Tgas4f,Tsat4f,Mcte4f,MAMMG4f);
        p4f= p;
        Tsat4f= Tsat;
        Tgas4f= Tgas;
        Mcte4f= Mcte;
        MAMMG4f= MAMMG;
        Tw4f= Tw;
        Ts4f= Ts;
        Tc4f= Tc;
        Mamml4f= Mamml;
        XX4f= XX;
        X4f= X;
        if rem(j*dt,1)==0
            p4((j*dt)+1)= p;
            Tsat4((j*dt)+1)= Tsat;
            Tgas4((j*dt)+1)= Tgas;
            Mcte4((j*dt)+1)= Mcte;
            MAMMG4((j*dt)+1)= MAMMG;
            Tw4(:,(j*dt)+1)= Tw;
            Ts4(:,(j*dt)+1)= Ts;
            Tc4(:,(j*dt)+1)= Tc;
            X4(:,(j*dt)+1)= X;
            Mamml4(:,(j*dt)+1)= Mamml;
            Qc4(:,(j*dt))= Qc;
            XX4(:,(j*dt))= XX;
        end
```

```
        generatorWATER
(Tw(nL),Tw1f(:),Ts1f(:),Tc1f(:),X1f(:),XX1f(:),p1f,Tgas1f,Tsat1f,Mcte1f,MAMMG1f);
        p1f= p;
        Tsat1f= Tsat;
        Tgas1f= Tgas;
        Mcte1f= Mcte;
        MAMMG1f= MAMMG;
        Tw1f= Tw;
        Ts1f= Ts;
        Tc1f= Tc;
        Mamml1f= Mamml;
        XX1f= XX;
        X1f= X;
        if rem(j*dt,1)==0
           p1((j*dt)+1)= p;
           Tsat1((j*dt)+1)= Tsat;
           Tgas1((j*dt)+1)= Tgas;
           Mcte1((j*dt)+1)= Mcte;
           MAMMG1((j*dt)+1)= MAMMG;
           Tw1(:,(j*dt)+1)= Tw;
           Ts1(:,(j*dt)+1)= Ts;
           Tc1(:,(j*dt)+1)= Tc;
           X1(:,(j*dt)+1)= X;
           Mamml1(:,(j*dt)+1)= Mamml;
           Qc1(:,(j*dt))= Qc;
           XX1(:,(j*dt))= XX;
        end

        TwoutBnew= Tw(nL);
        if rem(j*dt,1)==0
           TwoutB((j*dt)+1)= Tw(nL);
        end

        generatorWATER
(TwinCnew,Tw2f(:),Ts2f(:),Tc2f(:),X2f(:),XX2f(:),p2f,Tgas2f,Tsat2f,Mcte2f,MAMMG2f);
        p2f= p;
        Tsat2f= Tsat;
        Tgas2f= Tgas;
        Mcte2f= Mcte;
        MAMMG2f= MAMMG;
        Tw2f= Tw;
        Ts2f= Ts;
        Tc2f= Tc;
        Mamml2f= Mamml;
        XX2f= XX;
        X2f= X;
        if rem(j*dt,1)==0
           p2((j*dt)+1)= p;
           Tsat2((j*dt)+1)= Tsat;
           Tgas2((j*dt)+1)= Tgas;
           Mcte2((j*dt)+1)= Mcte;
           MAMMG2((j*dt)+1)= MAMMG;
           Tw2(:,(j*dt)+1)= Tw;
           Ts2(:,(j*dt)+1)= Ts;
           Tc2(:,(j*dt)+1)= Tc;
           X2(:,(j*dt)+1)= X;
           Mamml2(:,(j*dt)+1)= Mamml;
```

```
    Qc2(:,(j*dt))= Qc;
    XX2(:,(j*dt))= XX;
end

generatorWATER
(Tw(nL),Tw3f(:),Ts3f(:),Tc3f(:),X3f(:),XX3f(:),p3f,Tgas3f,Tsat3f,Mcte3f,MAMMG3f);
p3f= p;
Tsat3f= Tsat;
Tgas3f= Tgas;
Mcte3f= Mcte;
MAMMG3f= MAMMG;
Tw3f= Tw;
Ts3f= Ts;
Tc3f= Tc;
Mamml3f= Mamml;
XX3f= XX;
X3f= X;
if rem(j*dt,1)==0
    p3((j*dt)+1)= p;
    Tsat3((j*dt)+1)= Tsat;
    Tgas3((j*dt)+1)= Tgas;
    Mcte3((j*dt)+1)= Mcte;
    MAMMG3((j*dt)+1)= MAMMG;
    Tw3(:,(j*dt)+1)= Tw;
    Ts3(:,(j*dt)+1)= Ts;
    Tc3(:,(j*dt)+1)= Tc;
    X3(:,(j*dt)+1)= X;
    Mamml3(:,(j*dt)+1)= Mamml;
    Qc3(:,(j*dt))= Qc;
    XX3(:,(j*dt))= XX;
end

TwoutDnew= Tw(nL);
if rem(j*dt,1)==0
    TwoutD((j*dt)+1)= Tw(nL);
end

dQboiler= (THOT-TwoutDnew)*Cpw*dt*mw; % in Joules
Qboiler= dQboiler+Qboiler;

Mammcond4= Mammcond-Mammcond1-Mammcond2-Mammcond3;
Mammev4= Mammev-Mammev1-Mammev2-Mammev3;
Qsupcond4= Qsupcond-Qsupcond1-Qsupcond2-Qsupcond3;

% evaporator
Tairevoutnew= Tevold+(Tairevin-Tevold)/exp(NTUev);
LMTDev= (Tairevin-Tairevoutnew)/(log((Tairevin-Tevold)/(Tairevoutnew-Tevold)));
dQcool= UAev*dt*LMTDev;
Qcool= Qcool+dQcool;
pevnew= fzero(@dPevapCREB,pevold);
Tevnew= Tsatamm(pevnew);
Mevgnew= pevnew*100000*Vev/(Tevnew*ramms(pevnew,Tevnew-273));
if rem(j*dt,1)==0
    Tairevout((j*dt)+1)= Tairevoutnew;
    pev((j*dt)+1)= pevnew;
    Tev((j*dt)+1)= Tevnew;
    Mevg((j*dt)+1)= Mevgnew;
```

```
            Mliqev((j*dt)+1)= Mliqevnew;
        end
        pevold= pevnew;
        Tevold= Tevnew;
        Mevgold= Mevgnew;

        % condenser
        Twcondoutnew= Tcondold+(Twcondin-Tcondold)/exp(NTUcond);
        LMTDcond= (Twcondoutnew-Twcondin)/(log((Tcondold-Twcondin)/(Tcondold-
Twcondoutnew)));
        dQheat= UAcond*dt*LMTDcond;
        Qheat= Qheat+dQheat;
        pcondnew= fzero(@dPcondCREB,pcondold);
        Tcondnew= Tsatamm(pcondnew);
        Mcondgnew= pcondnew*100000*Vcond/(Tcondnew*ramms(pcondnew,Tcondnew-273));
        if rem(j*dt,1)==0
            Twcondout((j*dt)+1)= Twcondoutnew;
            pcond((j*dt)+1)= pcondnew;
            Tcond((j*dt)+1)= Tcondnew;
            Mcondg((j*dt)+1)= Mcondgnew;
        end
        pcondold= pcondnew;
        Tcondold= Tcondnew;
        Mcondgold= Mcondgnew;

        % receiver
        Trecnew= (Trecold*(Mrecold-Mliqevnew)+Tcondnew*Mliqcondnew)/(Mrecold-
Mliqevnew+Mliqcondnew);
        Mrecnew= Mrecold-Mliqevnew+Mliqcondnew;
        if rem(j*dt,1)==0
            Trec((j*dt)+1)= Trecnew;
            Mrec((j*dt)+1)= Mrecnew;
        end
        Mrecold= Mrecnew;
        Trecold= Trecnew;

        % cooler
        dQcooler= Ecooler*min([Cpw*mw Cpw*mwcond])*(TwoutBnew-Twcondoutnew)*dt;
        Qcooler= Qcooler+dQcooler;
        TwinCnew= TwoutBnew-dQcooler/(mw*Cpw*dt);
        Twoutcoolernew= dQcooler/(mwcond*Cpw*dt)+Twcondoutnew;
        if rem(j*dt,1)==0
            TwinC((j*dt)+1)= TwinCnew;
            Twoutcooler((j*dt)+1)= Twoutcoolernew;
            Twcondout((j*dt)+1)= Twcondoutnew;
            Mliqcond((j*dt)+1)= Mliqcondnew;
        end
    end

MADS= Mammev;
MDES= Mammcond;
QHEAT= Qheat;
QCOOLER= Qcooler;
QCOOL= Qcool;
QBOILER= Qboiler;
PBOILER= QBOILER/(4*t);
COPC= Qcool/QBOILER;
```

```
    COPH= (Qheat+Qcooler)/QBOILER;
    SCP= Qcool/1000/(4*t)/(4*Mc);
    SHP= (Qheat+Qcooler)/1000/(4*t)/(4*Mc);
    globalerror= min(abs(QCOOL+QBOILER-QHEAT-QCOOLER)/(QCOOL+QBOILER)*100,
abs(QCOOL+QBOILER-QHEAT-QCOOLER)/(QHEAT+QCOOLER)*100);
    THOTAVR= THOT-273;
    TWOUTB= sum(TwoutB)/length(TwoutB)-273;
    TWINC= sum(TwinC)/length(TwinC)-273;
    TWOUTD= sum(TwoutD)/length(TwoutD)-273;
    TWCONDOUT= sum(Twcondout)/length(Twcondout)-273;
    TWOUTCOOLER= sum(Twoutcooler)/length(Twoutcooler)-273;
    PCONDAVR= sum(pcond)/length(pcond);
    PEVAVR= sum(pev)/length(pev);
    TREC= sum(Trec)/length(Trec)-273;

      Tw1(:,1)= Tw1(:,4*t+1); Tw2(:,1)= Tw2(:,4*t+1); Tw3(:,1)= Tw3(:,4*t+1); Tw4(:,1)=
Tw4(:,4*t+1);
      Ts1(:,1)= Ts1(:,4*t+1); Ts2(:,1)= Ts2(:,4*t+1); Ts3(:,1)= Ts3(:,4*t+1); Ts4(:,1)= Ts4(:,4*t+1);
      Tc1(:,1)= Tc1(:,4*t+1); Tc2(:,1)= Tc2(:,4*t+1); Tc3(:,1)= Tc3(:,4*t+1); Tc4(:,1)= Tc4(:,4*t+1);
      X1(:,1)= X1(:,4*t+1); X2(:,1)= X2(:,4*t+1); X3(:,1)= X3(:,4*t+1); X4(:,1)= X4(:,4*t+1);
      Mamml1(:,1)= Mamml1(:,4*t+1); Mamml2(:,1)= Mamml2(:,4*t+1); Mamml3(:,1)=
Mamml3(:,4*t+1); Mamml4(:,1)= Mamml4(:,4*t+1);

      XX1(:,1)= XX1(:,4*t); XX2(:,1)= XX2(:,4*t); XX3(:,1)= XX3(:,4*t); XX4(:,1)= XX4(:,4*t);

      Tsat1(1)= Tsat1(4*t+1); Tsat2(1)= Tsat2(4*t+1); Tsat3(1)= Tsat3(4*t+1); Tsat4(1)=
Tsat4(4*t+1);
      Tgas1(1)= Tgas1(4*t+1); Tgas2(1)= Tgas2(4*t+1); Tgas3(1)= Tgas3(4*t+1); Tgas4(1)=
Tgas4(4*t+1);
      p1(1)= p1(4*t+1); p2(1)= p2(4*t+1); p3(1)= p3(4*t+1); p4(1)= p4(4*t+1);
      MAMMG1(1)= MAMMG1(4*t+1); MAMMG2(1)= MAMMG2(4*t+1); MAMMG3(1)=
MAMMG3(4*t+1); MAMMG4(1)= MAMMG4(4*t+1);
      Mcte1(1)= Mcte1(4*t+1); Mcte2(1)= Mcte2(4*t+1); Mcte3(1)= Mcte3(4*t+1); Mcte4(1)=
Mcte4(4*t+1);

      pev(1)= pev(4*t+1);
      Tev(1)= Tev(4*t+1);
      Mevg(1)= Mevg(4*t+1);
      Mliqev(1)= Mliqev(4*t+1);

      pcond(1)= pcond(4*t+1);
      Tcond(1)= Tcond(4*t+1);
      Mcondg(1)= Mcondg(4*t+1);
      Mliqcond(1)= Mliqcond(4*t+1);

      Trec(1)= Trec(4*t+1);
      Mrec(1)= Mrec(4*t+1);

      Tairevout(1)= Tairevout(4*t+1);
      Twcondout(1)= Twcondout(4*t+1);
      Twoutcooler(1)= Twoutcooler(4*t+1);

      TwinC(1)= TwinC(4*t+1);
      TwoutB(1)= TwoutB(4*t+1);
      TwoutD(1)= TwoutD(4*t+1);
      Thot(1)= Thot(4*t+1);
```

```
    Qcooler=0;
    Qcool=0;
    Qheat=0;
    Qboiler= 0;

end
```

A2. 4-bed thermal wave cycle with 'real effects'

```
global As Ac UAc UAw UAev UAcond UAcooler Kvcond Kvev Ks Kw Cpw Cpa Cps cpcond cpev Dw Vev
global Tw Ts Tc Tsat Tgas Twinlet Twcondin Tairevin Tcond Tev Trec Tairevout Twcondout Thot Cvw
global AuxTsat AuxTgas AuxTc AuxTs AuxTw AuxX AuxXX Auxp AuxMcte AuxMAMMG Tin Tsatin hw
global N Ntub dL dt nL nt mwcond j Mcond Mev Mw Ms Mc C k x0 n NTUev NTUcond VoidVol Mevg
global Qc Qheat Qcool Qsupcond dMammcond dMammev jdMammev jdMammcond dQsupcond
global X XX CPC Rgas A B D LMTDev LMTDcond Cpair mairev jdQsupcond Mammlin Mctein Xin Mrec
global Mammcond Mammev MAMMG Mamml Mcte Mliqcond Mliqev MAMMGin TwoutcoolerLOAD
global  pev pcond p Tcondold Mliqcondnew dQheat Mcondgold Tevold Trecold Mliqevnew dQcool
global Kc THOT t mw MW Mevgold pevold pcondold Mcondg Vcond NTUcooler Cr Ecooler Tspiral
global Twout Twhose Twpipe Vhose Vvalve Vpipe nPIPE nHOSE Twnew nSPIRAL TwoutcoolerBED

% Radius
rw= 0.4*10^(-3); % Radius of water (m)
rs= 0.6*10^(-3); % Radius of steel (m)
rc= 1.5*10^(-3); % Radius of carbon (m)
ShellD= 144.5*10^(-3); % Shell diameter (m)

% Areas
Aw= pi*rw^2; % Transversal area of water per tube (m^2)
As= pi*(rs^2-rw^2); % Transversal area of steel per tube (m^2)
Aws= pi*rs^2; % Transversal area of water and steel per tube (m^2)
Ac= sqrt(3)/2*(2*rc)^2-pi*rs^2; % Transversal area of carbon per tube (m^2)
At= sqrt(3)/2*(2*rc)^2; % Transversal total area per tube (m^2)

Ntub= 1777; % Number of tubes in the generator
L= 396*10^(-3); % Length of the generator (m)

Nus= 4; % Nusselt number

% Water
Dw= 958; % Density of the water (kg/m^3)
Cpw= 4219; % Specific heat of the water (J/kg*K)
Cvw= 4178; % Specific heat at constant volume of the water (J/kg*K)
Mw= Aw*Ntub*L*Dw; % Mass of water in the control volume (kg)
Kw= 0.68; % Conductivity of the water (W/K*m)
hw= Kw*Nus/(2*rw); % Convective heat transfer coefficient (W/m^2*K)

Awi= L*pi*2*rw; % Area of the internal surface OF ONE steel tube (m^2)
UAw= hw*Awi*Ntub; % W/K TOTAL HEX, WATER TO STEEL

% Steel
Ds= 8000; % Density of the steel (kg/m^3)
Cps= 460; % Specific heat of the steel (J/kg*K)
Ks= 16; % Thermal conductivity of the stainless steel (W/m*K)
Ms= As*Ntub*L*Ds; % Mass of steel in the control volume (kg)

Volshell= (pi()/4*ShellD^2-Ntub*Aws)*L;
Volhex= Ntub*Ac*L; % Volume inside the generator (without tubes) (m^3)

% Carbon
Dcs= 1000; % Density of solid carbon (kg/m^3)
```

```
% Ammonia
Dal= 681.97; % Density of ammonia liquid (kg/m^3)
Cpa= 6677; % Specific heat of the ammonia liquid (J/kg*K)
C= 2823.4; % Slope of saturated line for Ammonia

% Generator lenght
N= 40; % Number of transversal parts of the tube
dL= L/N; % Differential of length of the model (m)
nL= N;

% Condenser
Tcondin= 41+273; % Initial temperature of the condenser (K) 50
pcondin= psatamm(Tcondin); % Initial pressure of the condenser (bar)
Vcond= 0.002; % Volume of the condenser (m^3)
Mcond= 4.5; % Mass of the condenser (kg)
cpcond= 460; % Specific heat of condenser (steel) (J/kg*K)
Mcondgin= pcondin*10^5*Vcond/(ramms(pcondin,Tcondin-273)*Tcondin); % Condenser gmass (kg)
UAcond= 1360.8; % Condenser overall heat transfer coefficient (W/K)
mwcond= 0.1582; % Water mass flow in the condenser (kg/s)
Twcondin= 40+273; % Temperature water inlet in the condenser (K);
NTUcond= UAcond/(mwcond*Cpw);

% Evaporator
Tevin= 1+273; % Initial temperature of the evaporator (K)
pevin= psatamm(Tevin); % Initial pressure of the evaporator (bar)
Vev= 0.002; % Volume of the evaporator (m^3)
Mev= 10; % Mass of the evaporator (kg)
cpev= 460; % Specific heat of evaporator (steel) (J/kg*K)
Mevgin= pevin*10^5*Vev/(ramms(pevin,Tevin-273)*Tevin); % Evaporator gas mass (kg)
UAev= 739.8; % Evaporator overall heat transfer coefficient (W/K)
Tairevin= 0+273; % Temperature air inlet in the evaporator (K);
mairev= 1000/3600; % Air mass flow in the evaporator (kg/s) 0.2778
Cpair= 1000; % Specific heat of air (J/kg*K)
NTUev= UAev/(mairev*Cpair);

% Cooler
UAcooler= 3460;

% Receiver
Trecin= Tcondin; % Receiver temperature (K)
Mrecin= 1; % % Initial mass in the receiver (kg)

% Check valves
Kvcond= 0.01; % Condenser check valve coefficient
Kvev= 0.01; % Evaporator check valve coefficient

ncycles= 10; % Number of cycles to run
dt= 1/20; % Time step (s)

contador= 0;

THOT= 170+273;

Kc= 0.3;

Mc= 3;
Dcb= Mc/Volhex; % DENSITY OF CARBON BED (kg/m^3)
```

```
k= 3.9615; x0= 0.2551; n= 1.227; % Data for the carbon used
VoidVol= Volhex-Mc/Dcs; % Volume of gas space (m^3)
R= sqrt((Ac/2+Aws)/pi()); % Equivalent radius of carbon (m)

Kamm= 0.06; % Ammonia thermal conductivity (W/mK)
tr= 0.026/1000; % Contact layer thickness (m)

UAcarb= 2*pi*Kc*L/log(R/rs)*Ntub; % W/K FOR TOTAL HEAT EXCHANGER, STEEL TO CARBON
UAamm= 2*pi*Kamm*L/log((2*rs+2*tr)/(2*rs))*Ntub; % W/K FOR TOTAL HEAT EXCHANGER, STEEL
TO CARBON

UAc= 1/(1/UAcarb+1/UAamm);

UAtotal= 1/(1/UAc+1/UAw);

MW= 0.0375; % Water mass flow
t= 65; % 1/4th cycle time

    tspeedpump= 7; % seconds

    nt= t/dt+1;

    Tin= (THOT+Twcondin)/2; % Initial temperature of the beds (K)
    Tsatin= Tin-60; % MAKE SATURATION TEMPERATURE 60C LOWER THAN CARBON TEMPERATURE

    % Volume delays
    Vhose= 0.05; % kg / l
    Vpipe= 0.023;
    Vvalve= 0.023; % kg / l
    Vspiral= 0.075;
    those= Vhose/MW; % s
    tpipe= Vpipe/MW;
    tspiral= Vspiral/MW;
    nHOSE= round(those/dt);
    nPIPE= round(tpipe/dt);
    nSPIRAL= round(tspiral/dt);

    % Water
    Tw1= zeros(nL,4*t+1); % Matrix that contains on lengths and times the water temperature %
    Tw1(:,1)= Tin;
    Tw2= Tw1; Tw3= Tw1; Tw4= Tw1;
    Tw1f= zeros(nL,1); % Vector flotante
    Tw1f(:)= Tin;
    Tw2f= Tw1f; Tw3f= Tw1f; Tw4f= Tw1f; % Vector flotante

    % Steel
    Ts1= zeros(nL,4*t+1); % Matrix that contains on lengths and times the steel temperature %
    Ts1(:,1)= Tin;
    Ts2= Ts1; Ts3= Ts1; Ts4= Ts1;
    Ts1f= zeros(nL,1); % Vector flotante
    Ts1f(:)= Tin;
    Ts2f= Ts1f; Ts3f= Ts1f; Ts4f= Ts1f; % Vector flotante

    % Carbon
    Tc1= zeros(nL,4*t+1); % Matrix that contains on lengths and times the steel temperature %
    Tc1(:,1)= Tin;
    Tc2= Tc1; Tc3= Tc1; Tc4= Tc1;
```

```
Tc1f= zeros(nL,1); % Vector flotante
Tc1f(:)= Tin;
Tc2f= Tc1f; Tc3f= Tc1f; Tc4f= Tc1f; % Vector flotante

% Increment in adsorption
XX1= zeros(nL,4*t); % Matrix that contains on lengths and times the steel temperature %
XX2= XX1; XX3= XX1; XX4= XX1;
XX1f= zeros(nL,1); % Vector flotante
XX2f= XX1f; XX3f= XX1f; XX4f= XX1f;

% Carbon heat
Qc1= zeros(nL,4*t);
Qc2= Qc1; Qc3= Qc1; Qc4= Qc1;

% Pressure
pin= psatamm(Tsatin);
p1= zeros(1,4*t+1); % Matrix GAS PRESSURE (BAR)
p1(1)= pin;
p2= p1; p3= p1; p4= p1;
p1f= pin; p2f= pin; p3f= pin; p4f= pin;

% Gas temperature
Tgas1= zeros(1,4*t+1); % Vector with initial gas temperature (K)
Tgas1(1)= Tin;
Tgas2= Tgas1; Tgas3= Tgas1; Tgas4= Tgas1;
Tgas1f= Tin; Tgas2f= Tin; Tgas3f= Tin; Tgas4f= Tin;

% Saturation gas temperatura
Tsat1= zeros(1,4*t+1); % Vector with initial gas temperature (K)
Tsat1(1)= Tsatin;
Tsat2= Tsat1; Tsat3= Tsat1; Tsat4= Tsat1;
Tsat1f= Tsatin; Tsat2f= Tsatin; Tsat3f= Tsatin; Tsat4f= Tsatin;
Xin= dub2(Tsatin,Tin,x0,k,n); % INITIAL CONCENTRATION
MAMMGin= pin*100000*VoidVol/(Tin*ramms(pin,Tin-273)); % Initial ammonia gas (kg)
Mammlin= Mc*Xin/N;
Mctein= Mc*Xin+MAMMGin; % INITIAL MASS OF AMMONIA IN BED (kg)

% Adsorption
X1= zeros(nL,4*t+1);
X1(:,1)= Xin;
X2= X1; X3= X1; X4= X1;
X1f= zeros(nL,1); % Vector flotante
X1f(:)= Xin;
X2f= X1f; X3f= X1f; X4f= X1f; % Vector flotante

% Ammonia gas mass
MAMMG1= zeros(1,4*t+1);
MAMMG1(1)= MAMMGin;
MAMMG2= MAMMG1; MAMMG3= MAMMG1; MAMMG4= MAMMG1;
MAMMG1f= MAMMGin;
MAMMG2f= MAMMG1f; MAMMG3f= MAMMG1f; MAMMG4f= MAMMG1f; % Vector flotante

% Ammonia adsorbed mass
Mamml1= zeros(nL,4*t+1);
Mamml1(:,1)= Mammlin;
Mamml2= Mamml1; Mamml3= Mamml1; Mamml4= Mamml1;
Mamml1f= zeros(nL,1);
```

```
Mamml1f(:)= Mammlin;
Mamml2f= Mamml1f; Mamml3f= Mamml1f; Mamml4f= Mamml1f; % Vector flotante

% Total mass of ammonia
Mcte1= zeros(1,4*t+1);
Mcte1(1)= Mctein;
Mcte2= Mcte1; Mcte3= Mcte1; Mcte4= Mcte1;
Mcte1f= Mctein;
Mcte2f= Mcte1f; Mcte3f= Mcte1f; Mcte4f= Mcte1f; % Vector flotante

% Evaporator
pev= zeros(1,4*t+1); pev(1)= pevin; pevold= pevin;
Tev= zeros(1,4*t+1); Tev(1)= Tevin; Tevold= Tevin;
Mevg= zeros(1,4*t+1); Mevg(1)= Mevgin; Mevgold= Mevgin;
Tairevout= zeros(1,4*t+1); Tairevout(1)= Tevin+(Tairevin-Tevin)/exp(NTUev);
Mliqev= zeros(1,4*t+1);

% Condenser
pcond= zeros(1,4*t+1); pcond(1)= pcondin; pcondold= pcondin;
Tcond= zeros(1,4*t+1); Tcond(1)= Tcondin; Tcondold= Tcondin;
Mcondg= zeros(1,4*t+1); Mcondg(1)= Mcondgin; Mcondgold= Mcondgin;
Twcondout= zeros(1,4*t+1); Twcondout(1)= Tcondin+(Twcondin-Tcondin)/exp(NTUcond);
Mliqcond= zeros(1,4*t+1);

% Receiver
Trec= zeros(1,4*t+1); Trec(1)= Trecin; Trecold= Trecin;
Mrec= zeros(1,4*t+1); Mrec(1)= Mrecin; Mrecold= Mrecin;

% Water flow
TwoutcoolerLOAD= zeros(1,4*t+1);
TwoutcoolerBED= zeros(1,4*t+1);
Twincooler= zeros(1,4*t/dt);
Twoutcooler= zeros(1,4*t/dt);
Twinboiler= zeros(1,4*t/dt);

TwV1Aold= zeros(1,nHOSE)+(THOT+Twcondin)/2;
TwV2Aold= zeros(1,nHOSE)+(THOT+Twcondin)/2;
TwV1Bold= zeros(1,nHOSE)+(THOT+Twcondin)/2;
TwV2Bold= zeros(1,nHOSE)+(THOT+Twcondin)/2;
TwV1Cold= zeros(1,nHOSE)+(THOT+Twcondin)/2;
TwV2Cold= zeros(1,nHOSE)+(THOT+Twcondin)/2;
TwV1Dold= zeros(1,nHOSE)+(THOT+Twcondin)/2;
TwV2Dold= zeros(1,nHOSE)+(THOT+Twcondin)/2;

Twspiral1old= zeros(1,nSPIRAL)+(THOT+Twcondin)/2;
Twspiral2old= zeros(1,nSPIRAL)+(THOT+Twcondin)/2;
Twspiral3old= zeros(1,nSPIRAL)+(THOT+Twcondin)/2;
Twspiral4old= zeros(1,nSPIRAL)+(THOT+Twcondin)/2;

Twp12old= zeros(1,nPIPE)+(THOT+Twcondin)/2;
Twp21old= zeros(1,nPIPE)+(THOT+Twcondin)/2;

TwpCinold= zeros(1,nHOSE)+(THOT+Twcondin)/2;
TwpCoutold= zeros(1,nHOSE)+(THOT+Twcondin)/2;
TwpHinold= zeros(1,nHOSE)+(THOT+Twcondin)/2;
TwpHoutold= zeros(1,nHOSE)+THOT;
```

```
TwV1bold= THOT;
TwV1mbold= (THOT+Twcondin)/2;
TwV1mtold= (THOT+Twcondin)/2;
TwV1told= (THOT+Twcondin)/2;
TwV2bold= (THOT+Twcondin)/2;
TwV2mbold= (THOT+Twcondin)/2;
TwV2mtold= (THOT+Twcondin)/2;
TwV2told= (THOT+Twcondin)/2;

Twoutp12= (THOT+Twcondin)/2;
Twoutp21=(THOT+Twcondin)/2;

Twout1= zeros(1,4*t/dt)+(THOT+Twcondin)/2;
Twout2= zeros(1,4*t/dt)+(THOT+Twcondin)/2;
Twout3= zeros(1,4*t/dt)+(THOT+Twcondin)/2;
Twout4= zeros(1,4*t/dt)+(THOT+Twcondin)/2;

Twout1s= zeros(1,4*t/dt)+(THOT+Twcondin)/2;
Twout2s= zeros(1,4*t/dt)+(THOT+Twcondin)/2;
Twout3s= zeros(1,4*t/dt)+(THOT+Twcondin)/2;
Twout4s= zeros(1,4*t/dt)+(THOT+Twcondin)/2;

TwoutpHin= zeros(1,4*t/dt)+(THOT+Twcondin)/2;
TwoutpHout= zeros(1,4*t/dt)+THOT;
TwoutpCin= zeros(1,4*t/dt)+(THOT+Twcondin)/2;
TwoutpCout= zeros(1,4*t/dt)+(THOT+Twcondin)/2;

TwoutV1t= zeros(1,4*t/dt)+(THOT+Twcondin)/2;
TwoutV1mt= zeros(1,4*t/dt)+(THOT+Twcondin)/2;
TwoutV1mb= zeros(1,4*t/dt)+(THOT+Twcondin)/2;
TwoutV1b= zeros(1,4*t/dt)+THOT;
TwoutV2t= zeros(1,4*t/dt)+(THOT+Twcondin)/2;
TwoutV2mt= zeros(1,4*t/dt)+(THOT+Twcondin)/2;
TwoutV2mb= zeros(1,4*t/dt)+(THOT+Twcondin)/2;
TwoutV2b= zeros(1,4*t/dt)+(THOT+Twcondin)/2;

TwoutV1A= zeros(1,4*t/dt)+(THOT+Twcondin)/2;
TwoutV2A= zeros(1,4*t/dt)+(THOT+Twcondin)/2;
TwoutV1B= zeros(1,4*t/dt)+(THOT+Twcondin)/2;
TwoutV2B= zeros(1,4*t/dt)+(THOT+Twcondin)/2;
TwoutV1C= zeros(1,4*t/dt)+(THOT+Twcondin)/2;
TwoutV2C= zeros(1,4*t/dt)+(THOT+Twcondin)/2;
TwoutV1D= zeros(1,4*t/dt)+(THOT+Twcondin)/2;
TwoutV2D= zeros(1,4*t/dt)+(THOT+Twcondin)/2;

% Boiler
Thot= zeros(1,4*t+1)+THOT;

Qboiler= (THOT-Tin)*Cpw*dt*MW; % Inicial in Joules

LMTDev= (Tairevin-Tairevout(1))/(log((Tairevin-Tevin)/(Tairevout(1)-Tevin)));
Qcool= 0;
dQcool=UAev*dt*LMTDev;
Qcool= Qcool+dQcool;
Latent= hgamm(Tevin-273)-hfamm(Trecin-273);
Mliqev(1)=dQcool/Latent;
```

```
LMTDcond= (Twcondout(1)-Twcondin)/(log((Tcondin-Twcondin)/(Tcondin-Twcondout(1))));
Qheat= 0;
dQheat= UAcond*dt*LMTDcond;
Qheat= Qheat+dQheat;
Latent= hgamm(Tcondin-273)-hfamm(Tcondin-273);
Mliqcond(1)=dQheat/Latent;

% Cooler
NTUcooler= UAcooler/min([Cpw*MW Cpw*mwcond]);
Cr= min([Cpw*MW Cpw*mwcond])/max([Cpw*MW Cpw*mwcond]);
Ecooler= (1-exp(-NTUcooler*(1-Cr)))/(1-Cr*exp(-NTUcooler*(1-Cr)));
Qcooler= 0;
dQcooler= Ecooler*min([Cpw*MW Cpw*mwcond])*(((THOT+Twcondin)/2)-Twcondout(1))*dt;
Qcooler= dQcooler+Qcooler;
TwoutcoolerBED(1)= ((THOT+Twcondin)/2)-dQcooler/(MW*Cpw*dt);
TwoutcoolerLOAD(1)= Twcondout(1)+dQcooler/(mwcond*Cpw*dt);

for c= 1:ncycles
   disp(c)
   Qsupcond= 0;
   Mammev= 0;
   Mammcond= 0;
   Mammev1= 0; Mammev2= 0; Mammev3= 0; Mammev4= 0;
   Mammcond1= 0; Mammcond2= 0; Mammcond3= 0; Mammcond4= 0;

   % Phase 1

   for j=1:t/dt

      if j < tspeedpump/dt
         mw= MW/(tspeedpump/dt)*j;
      else mw= MW;
      end

      jdMammev= 0;
      jdMammcond= 0;
      jdQsupcond= 0;

      hose(THOT,TwV1Aold)
      TwoutV1A(j)= Twout; TwV1Aold= Twhose;

      generatorWATER
(TwoutV1A(j),Tw1f(:),Ts1f(:),Tc1f(:),X1f(:),XX1f(:),p1f,Tgas1f,Tsat1f,Mcte1f,MAMMG1f);
      p1f= p;
      Tsat1f= Tsat;
      Tgas1f= Tgas;
      Mcte1f= Mcte;
      MAMMG1f= MAMMG;
      Tw1f= Tw;
      Ts1f= Ts;
      Tc1f= Tc;
      Mamml1f= Mamml;
      XX1f= XX;
      X1f= X;
      if rem(j*dt,1)==0
         p1((j*dt)+1)= p;
         Tsat1((j*dt)+1)= Tsat;
```

```
        Tgas1((j*dt)+1)= Tgas;
        Mcte1((j*dt)+1)= Mcte;
        MAMMG1((j*dt)+1)= MAMMG;
        Tw1(:,(j*dt)+1)= Tw;
        Ts1(:,(j*dt)+1)= Ts;
        Tc1(:,(j*dt)+1)= Tc;
        X1(:,(j*dt)+1)= X;
        Mamml1(:,(j*dt)+1)= Mamml;
        Qc1(:,(j*dt))= Qc;
        XX1(:,(j*dt))= XX;
    end

    Twout1(j)= Tw(nL);
    pdt1(j)=p;

    spiral(Twout1(j),Twspiral1old);
    Twout1s(j)= Twout; Twspiral1old= Tspiral;

    hose(Twout1s(j),TwV2Aold);
    TwoutV2A(j)= Twout; TwV2Aold= Twhose;

    valve(TwoutV2A(j),TwV2bold)
    TwoutV2b(j)= Twnew(1); TwV2bold= Twnew(2);

    pipe(TwoutV2b(j),Twp12old)
    Twoutp12(j)= Twout; Twp12old= Twhose;

    valve(Twoutp12(j),TwV1mbold)
    TwoutV1mb(j)= Twnew(1); TwV1mbold= Twnew(2);

    hose(TwoutV1mb(j),TwV1Bold)
    TwoutV1B(j)= Twout; TwV1Bold= Twhose;

    generatorWATER
(TwoutV1B(j),Tw2f(:),Ts2f(:),Tc2f(:),X2f(:),XX2f(:),p2f,Tgas2f,Tsat2f,Mcte2f,MAMMG2f);
    p2f= p;
    Tsat2f= Tsat;
    Tgas2f= Tgas;
    Mcte2f= Mcte;
    MAMMG2f= MAMMG;
    Tw2f=Tw;
    Ts2f=Ts;
    Tc2f=Tc;
    Mamml2f= Mamml;
    XX2f= XX;
    X2f= X;
    if rem(j*dt,1)==0
        p2((j*dt)+1)= p;
        Tsat2((j*dt)+1)= Tsat;
        Tgas2((j*dt)+1)= Tgas;
        Mcte2((j*dt)+1)= Mcte;
        MAMMG2((j*dt)+1)= MAMMG;
        Tw2(:,(j*dt)+1)= Tw;
        Ts2(:,(j*dt)+1)= Ts;
        Tc2(:,(j*dt)+1)= Tc;
        X2(:,(j*dt)+1)= X;
        Mamml2(:,(j*dt)+1)= Mamml;
```

```
    Qc2(:,(j*dt))= Qc;
    XX2(:,(j*dt))= XX;
  end

  Twout2(j)= Tw(nL);
  pdt2(j)=p;

  spiral(Twout2(j),Twspiral2old);
  Twout2s(j)= Twout; Twspiral2old= Tspiral;

  hose(Twout2s(j),TwV2Bold)
  TwoutV2B(j)= Twout; TwV2Bold= Twhose;

  valve(TwoutV2B(j),TwV2mbold)
  TwoutV2mb(j)= Twnew(1); TwV2mbold= Twnew(2);

  hose(TwoutV2mb(j),TwpCinold)
  TwoutpCin(j)= Twout; TwpCinold= Twhose;


  % condenser
  Twcondoutnew= Tcondold+(Twcondin-Tcondold)/exp(NTUcond);
  LMTDcond= (Twcondoutnew-Twcondin)/(log((Tcondold-Twcondin)/(Tcondold-
Twcondoutnew)));
  dQheat= UAcond*dt*LMTDcond;
  Qheat= Qheat+dQheat;
  pcondnew= fzero(@dPcondCREB,pcondold);
  Tcondnew= Tsatamm(pcondnew);
  Mcondgnew= pcondnew*100000*Vcond/(Tcondnew*ramms(pcondnew,Tcondnew-273));
  if rem(j*dt,1)==0
    Twcondout((j*dt)+1)= Twcondoutnew;
    pcond((j*dt)+1)= pcondnew;
    Tcond((j*dt)+1)= Tcondnew;
    Mcondg((j*dt)+1)= Mcondgnew;
    Mliqcond((j*dt)+1)= Mliqcondnew;
  end
  pcondold= pcondnew;
  Tcondold= Tcondnew;
  Mcondgold= Mcondgnew;

  % cooler
  Twincooler(j)= TwoutpCin(j);
  dQcooler= Ecooler*min([Cpw*mw Cpw*mwcond])*(Twincooler(j)-Twcondoutnew)*dt;
  Qcooler= Qcooler+dQcooler;
  ToutcoolerBEDnew= Twincooler(j)-dQcooler/(mw*Cpw*dt);
  TwoutcoolerLOADnew= dQcooler/(mwcond*Cpw*dt)+Twcondoutnew;
  if rem(j*dt,1)==0
    TwoutcoolerBED((j*dt)+1)= ToutcoolerBEDnew;
    TwoutcoolerLOAD((j*dt)+1)= TwoutcoolerLOADnew;
  end
  Twoutcooler(j)= ToutcoolerBEDnew;

  hose(Twoutcooler(j),TwpCoutold)
  TwoutpCout(j)= Twout; TwpCoutold= Twhose;

  valve(TwoutpCout(j),TwV1mtold)
  TwoutV1mt(j)= Twnew(1); TwV1mtold= Twnew(2);
```

```
        hose(TwoutV1mt(j),TwV1Cold)
        TwoutV1C(j)= Twout; TwV1Cold= Twhose;

        generatorWATER
(TwoutV1C(j),Tw3f(:),Ts3f(:),Tc3f(:),X3f(:),XX3f(:),p3f,Tgas3f,Tsat3f,Mcte3f,MAMMG3f);
        p3f= p;
        Tsat3f= Tsat;
        Tgas3f= Tgas;
        Mcte3f= Mcte;
        MAMMG3f= MAMMG;
        Tw3f= Tw;
        Ts3f= Ts;
        Tc3f= Tc;
        Mamml3f= Mamml;
        XX3f= XX;
        X3f= X;
        if rem(j*dt,1)==0
           p3((j*dt)+1)= p;
           Tsat3((j*dt)+1)= Tsat;
           Tgas3((j*dt)+1)= Tgas;
           Mcte3((j*dt)+1)= Mcte;
           MAMMG3((j*dt)+1)= MAMMG;
           Tw3(:,(j*dt)+1)= Tw;
           Ts3(:,(j*dt)+1)= Ts;
           Tc3(:,(j*dt)+1)= Tc;
           X3(:,(j*dt)+1)= X;
           Mamml3(:,(j*dt)+1)= Mamml;
           Qc3(:,(j*dt))= Qc;
           XX3(:,(j*dt))= XX;
        end

        Twout3(j)= Tw(nL);
        pdt3(j)=p;

        spiral(Twout3(j),Twspiral3old);
        Twout3s(j)= Twout; Twspiral3old= Tspiral;

        hose(Twout3s(j),TwV2Cold)
        TwoutV2C(j)= Twout; TwV2Cold= Twhose;

        valve(TwoutV2C(j),TwV2mtold)
        TwoutV2mt(j)= Twnew(1); TwV2mtold= Twnew(2);

        pipe(TwoutV2mt(j),Twp21old)
        Twoutp21(j)= Twout; Twp21old= Twhose;

        valve(Twoutp21(j),TwV1told)
        TwoutV1t(j)= Twnew(1); TwV1told= Twnew(2);

        hose(TwoutV1t(j),TwV1Dold)
        TwoutV1D(j)= Twout; TwV1Dold= Twhose;

        generatorWATER
(TwoutV1D(j),Tw4f(:),Ts4f(:),Tc4f(:),X4f(:),XX4f(:),p4f,Tgas4f,Tsat4f,Mcte4f,MAMMG4f);
        p4f= p;
        Tsat4f= Tsat;
```

```
Tgas4f= Tgas;
Mcte4f= Mcte;
MAMMG4f= MAMMG;
Tw4f= Tw;
Ts4f= Ts;
Tc4f= Tc;
Mamml4f= Mamml;
XX4f= XX;
X4f= X;
if rem(j*dt,1)==0
   p4((j*dt)+1)= p;
   Tsat4((j*dt)+1)= Tsat;
   Tgas4((j*dt)+1)= Tgas;
   Mcte4((j*dt)+1)= Mcte;
   MAMMG4((j*dt)+1)= MAMMG;
   Tw4(:,(j*dt)+1)= Tw;
   Ts4(:,(j*dt)+1)= Ts;
   Tc4(:,(j*dt)+1)= Tc;
   X4(:,(j*dt)+1)= X;
   Mamml4(:,(j*dt)+1)= Mamml;
   Qc4(:,(j*dt))= Qc;
   XX4(:,(j*dt))= XX;
end

Twout4(j)= Tw(nL);
pdt4(j)=p;

spiral(Twout4(j),Twspiral4old);
Twout4s(j)= Twout; Twspiral4old= Tspiral;

hose(Twout4s(j),TwV2Dold)
TwoutV2D(j)= Twout; TwV2Dold= Twhose;

valve(TwoutV2D(j),TwV2told)
TwoutV2t(j)= Twnew(1); TwV2told= Twnew(2);

hose(TwoutV2t(j),TwpHinold)
TwoutpHin(j)= Twout; TwpHinold= Twhose;

% boiler
Twinboiler(j)= TwoutpHin(j);
dQboiler= (THOT-Twinboiler(j))*Cpw*dt*mw; % in Joules
Qboiler= dQboiler+Qboiler;

Mammev1= Mammev;
Mammcond1= Mammcond;
Qsupcond1= Qsupcond;

% evaporator
Tairevoutnew= Tevold+(Tairevin-Tevold)/exp(NTUev);
LMTDev= (Tairevin-Tairevoutnew)/(log((Tairevin-Tevold)/(Tairevoutnew-Tevold)));
dQcool= UAev*dt*LMTDev;
Qcool= Qcool+dQcool;
pevnew= fzero(@dPevapCREB,pevold);
Tevnew= Tsatamm(pevnew);
Mevgnew= pevnew*100000*Vev/(Tevnew*ramms(pevnew,Tevnew-273));
if rem(j*dt,1)==0
```

```
            Tairevout((j*dt)+1)= Tairevoutnew;
            pev((j*dt)+1)= pevnew;
            Tev((j*dt)+1)= Tevnew;
            Mevg((j*dt)+1)= Mevgnew;
            Mliqev((j*dt)+1)= Mliqevnew;
          end
          pevold= pevnew;
          Tevold= Tevnew;
          Mevgold= Mevgnew;

          % receiver
          Trecnew= (Trecold*(Mrecold-Mliqevnew)+Tcondnew*Mliqcondnew)/(Mrecold-
Mliqevnew+Mliqcondnew);
          Mrecnew= Mrecold-Mliqevnew+Mliqcondnew;
          if rem(j*dt,1)==0
            Trec((j*dt)+1)= Trecnew;
            Mrec((j*dt)+1)= Mrecnew;
          end
          Mrecold= Mrecnew;
          Trecold= Trecnew;
        end

        % Phase 2
        for j=t/dt+1:2*t/dt

          if j < (t+tspeedpump)/dt
            mw= MW/(tspeedpump/dt)*(j-t/dt);
          else mw= MW;
          end

          jdMammev= 0;
          jdMammcond= 0;
          jdQsupcond= 0;

          hose(THOT,TwV1Bold)
          TwoutV1B(j)= Twout; TwV1Bold= Twhose;

          generatorWATER
(TwoutV1B(j),Tw2f(:),Ts2f(:),Tc2f(:),X2f(:),XX2f(:),p2f,Tgas2f,Tsat2f,Mcte2f,MAMMG2f);
          p2f= p;
          Tsat2f= Tsat;
          Tgas2f= Tgas;
          Mcte2f= Mcte;
          MAMMG2f= MAMMG;
          Tw2f= Tw;
          Ts2f= Ts;
          Tc2f= Tc;
          Mamml2f= Mamml;
          XX2f= XX;
          X2f= X;
          if rem(j*dt,1)==0
            p2((j*dt)+1)= p;
            Tsat2((j*dt)+1)= Tsat;
            Tgas2((j*dt)+1)= Tgas;
            Mcte2((j*dt)+1)= Mcte;
            MAMMG2((j*dt)+1)= MAMMG;
            Tw2(:,(j*dt)+1)=  Tw;
```

```
    Ts2(:,(j*dt)+1)= Ts;
    Tc2(:,(j*dt)+1)= Tc;
    X2(:,(j*dt)+1)= X;
    Mamml2(:,(j*dt)+1)= Mamml;
    Qc2(:,(j*dt))= Qc;
    XX2(:,(j*dt))= XX;
  end

  Twout2(j)= Tw(nL);
  pdt2(j)=p;

  spiral(Twout2(j),Twspiral2old);
  Twout2s(j)= Twout; Twspiral2old= Tspiral;

  hose(Twout2s(j),TwV2Bold)
  TwoutV2B(j)= Twout; TwV2Bold= Twhose;

  valve(TwoutV2B(j),TwV2bold)
  TwoutV2b(j)= Twnew(1); TwV2bold= Twnew(2);

  pipe(TwoutV2b(j),Twp12old)
  Twoutp12(j)= Twout; Twp12old= Twhose;

  valve(Twoutp12(j),TwV1mbold)
  TwoutV1mb(j)= Twnew(1); TwV1mbold= Twnew(2);

  hose(TwoutV1mb(j),TwV1Cold)
  TwoutV1C(j)= Twout; TwV1Cold= Twhose;

  generatorWATER
(TwoutV1C(j),Tw3f(:),Ts3f(:),Tc3f(:),X3f(:),XX3f(:),p3f,Tgas3f,Tsat3f,Mcte3f,MAMMG3f);
  p3f= p;
  Tsat3f= Tsat;
  Tgas3f= Tgas;
  Mcte3f= Mcte;
  MAMMG3f= MAMMG;
  Tw3f= Tw;
  Ts3f= Ts;
  Tc3f= Tc;
  Mamml3f= Mamml;
  XX3f= XX;
  X3f= X;
  if rem(j*dt,1)==0
    p3((j*dt)+1)= p;
    Tsat3((j*dt)+1)= Tsat;
    Tgas3((j*dt)+1)= Tgas;
    Mcte3((j*dt)+1)= Mcte;
    MAMMG3((j*dt)+1)= MAMMG;
    Tw3(:,(j*dt)+1)= Tw;
    Ts3(:,(j*dt)+1)= Ts;
    Tc3(:,(j*dt)+1)= Tc;
    X3(:,(j*dt)+1)= X;
    Mamml3(:,(j*dt)+1)= Mamml;
    Qc3(:,(j*dt))= Qc;
    XX3(:,(j*dt))= XX;
  end
```

```
        Twout3(j)= Tw(nL);
        pdt3(j)=p;

        spiral(Twout3(j),Twspiral3old);
        Twout3s(j)= Twout; Twspiral3old= Tspiral;

        hose(Twout3s(j),TwV2Cold)
        TwoutV2C(j)= Twout; TwV2Cold= Twhose;

        valve(TwoutV2C(j),TwV2mbold)
        TwoutV2mb(j)= Twnew(1); TwV2mbold= Twnew(2);

        hose(TwoutV2mb(j),TwpCinold)
        TwoutpCin(j)= Twout; TwpCinold= Twhose;


        % condenser
        Twcondoutnew= Tcondold+(Twcondin-Tcondold)/exp(NTUcond);
        LMTDcond= (Twcondoutnew-Twcondin)/(log((Tcondold-Twcondin)/(Tcondold-
Twcondoutnew)));
        dQheat= UAcond*dt*LMTDcond;
        Qheat= Qheat+dQheat;
        pcondnew= fzero(@dPcondCREB,pcondold);
        Tcondnew= Tsatamm(pcondnew);
        Mcondgnew= pcondnew*100000*Vcond/(Tcondnew*ramms(pcondnew,Tcondnew-273));
        if rem(j*dt,1)==0
           Twcondout((j*dt)+1)= Twcondoutnew;
           pcond((j*dt)+1)= pcondnew;
           Tcond((j*dt)+1)= Tcondnew;
           Mcondg((j*dt)+1)= Mcondgnew;
           Mliqcond((j*dt)+1)= Mliqcondnew;
        end
        pcondold= pcondnew;
        Tcondold= Tcondnew;
        Mcondgold= Mcondgnew;

        % cooler
        Twincooler(j)= TwoutpCin(j);
        dQcooler= Ecooler*min([Cpw*mw Cpw*mwcond])*(Twincooler(j)-Twcondoutnew)*dt;
        Qcooler= Qcooler+dQcooler;
        ToutcoolerBEDnew= Twincooler(j)-dQcooler/(mw*Cpw*dt);
        TwoutcoolerLOADnew= dQcooler/(mwcond*Cpw*dt)+Twcondoutnew;
        if rem(j*dt,1)==0
           TwoutcoolerBED((j*dt)+1)= ToutcoolerBEDnew;
           TwoutcoolerLOAD((j*dt)+1)= TwoutcoolerLOADnew;
        end
        Twoutcooler(j)= ToutcoolerBEDnew;

        hose(Twoutcooler(j),TwpCoutold)
        TwoutpCout(j)= Twout; TwpCoutold= Twhose;

        valve(TwoutpCout(j),TwV1mtold)
        TwoutV1mt(j)= Twnew(1); TwV1mtold= Twnew(2);

        hose(TwoutV1mt(j),TwV1Dold)
        TwoutV1D(j)= Twout; TwV1Dold= Twhose;
```

```
        generatorWATER
(TwoutV1D(j),Tw4f(:),Ts4f(:),Tc4f(:),X4f(:),XX4f(:),p4f,Tgas4f,Tsat4f,Mcte4f,MAMMG4f);
        p4f= p;
        Tsat4f= Tsat;
        Tgas4f= Tgas;
        Mcte4f= Mcte;
        MAMMG4f= MAMMG;
        Tw4f= Tw;
        Ts4f= Ts;
        Tc4f= Tc;
        Mamml4f= Mamml;
        XX4f= XX;
        X4f= X;
        if rem(j*dt,1)==0
           p4((j*dt)+1)= p;
           Tsat4((j*dt)+1)= Tsat;
           Tgas4((j*dt)+1)= Tgas;
           Mcte4((j*dt)+1)= Mcte;
           MAMMG4((j*dt)+1)= MAMMG;
           Tw4(:,(j*dt)+1)= Tw;
           Ts4(:,(j*dt)+1)= Ts;
           Tc4(:,(j*dt)+1)= Tc;
           X4(:,(j*dt)+1)= X;
           Mamml4(:,(j*dt)+1)= Mamml;
           Qc4(:,(j*dt))= Qc;
           XX4(:,(j*dt))= XX;
        end

        Twout4(j)= Tw(nL);
        pdt4(j)=p;

        spiral(Twout4(j),Twspiral4old);
        Twout4s(j)= Twout; Twspiral4old= Tspiral;

        hose(Twout4s(j),TwV2Dold)
        TwoutV2D(j)= Twout; TwV2Dold= Twhose;

        valve(TwoutV2D(j),TwV2mtold)
        TwoutV2mt(j)= Twnew(1); TwV2mtold= Twnew(2);

        pipe(TwoutV2mt(j),Twp21old)
        Twoutp21(j)= Twout; Twp21old= Twhose;

        valve(Twoutp21(j),TwV1told)
        TwoutV1t(j)= Twnew(1); TwV1told= Twnew(2);

        hose(TwoutV1t(j),TwV1Aold)
        TwoutV1A(j)= Twout; TwV1Aold= Twhose;

        generatorWATER
(TwoutV1A(j),Tw1f(:),Ts1f(:),Tc1f(:),X1f(:),XX1f(:),p1f,Tgas1f,Tsat1f,Mcte1f,MAMMG1f);
        p1f= p;
        Tsat1f= Tsat;
        Tgas1f= Tgas;
        Mcte1f= Mcte;
        MAMMG1f= MAMMG;
        Tw1f= Tw;
```

```
Ts1f= Ts;
Tc1f= Tc;
Mamml1f= Mamml;
XX1f= XX;
X1f= X;
if rem(j*dt,1)==0
   p1((j*dt)+1)= p;
   Tsat1((j*dt)+1)= Tsat;
   Tgas1((j*dt)+1)= Tgas;
   Mcte1((j*dt)+1)= Mcte;
   MAMMG1((j*dt)+1)= MAMMG;
   Tw1(:,(j*dt)+1)=Tw;
   Ts1(:,(j*dt)+1)=Ts;
   Tc1(:,(j*dt)+1)=Tc;
   X1(:,(j*dt)+1)= X;
   Mamml1(:,(j*dt)+1)= Mamml;
   Qc1(:,(j*dt))=Qc;
   XX1(:,(j*dt))= XX;
end

Twout1(j)= Tw(nL);
pdt1(j)=p;

spiral(Twout1(j),Twspiral1old);
Twout1s(j)= Twout; Twspiral1old= Tspiral;

hose(Twout1s(j),TwV2Aold)
TwoutV2A(j)= Twout; TwV2Aold= Twhose;

valve(TwoutV2A(j),TwV2told)
TwoutV2t(j)= Twnew(1); TwV2told= Twnew(2);

hose(TwoutV2t(j),TwpHinold)
TwoutpHin(j)= Twout; TwpHinold= Twhose;

% boiler
Twinboiler(j)= TwoutpHin(j);
dQboiler= (THOT-Twinboiler(j))*Cpw*dt*mw; % in Joules
Qboiler= dQboiler+Qboiler;

Mammcond2= Mammcond-Mammcond1;
Mammev2= Mammev-Mammev1;
Qsupcond2= Qsupcond-Qsupcond1;

% evaporator
Tairevoutnew= Tevold+(Tairevin-Tevold)/exp(NTUev);
LMTDev= (Tairevin-Tairevoutnew)/(log((Tairevin-Tevold)/(Tairevoutnew-Tevold)));
dQcool= UAev*dt*LMTDev;
Qcool= Qcool+dQcool;
pevnew= fzero(@dPevapCREB,pevold);
Tevnew= Tsatamm(pevnew);
Mevgnew= pevnew*100000*Vev/(Tevnew*ramms(pevnew,Tevnew-273));
if rem(j*dt,1)==0
   Tairevout((j*dt)+1)= Tairevoutnew;
   pev((j*dt)+1)= pevnew;
   Tev((j*dt)+1)= Tevnew;
   Mevg((j*dt)+1)= Mevgnew;
```

```
            Mliqev((j*dt)+1)= Mliqevnew;
        end
        pevold= pevnew;
        Tevold= Tevnew;
        Mevgold= Mevgnew;

        % receiver
        Trecnew= (Trecold*(Mrecold-Mliqevnew)+Tcondnew*Mliqcondnew)/(Mrecold-
Mliqevnew+Mliqcondnew);
        Mrecnew= Mrecold-Mliqevnew+Mliqcondnew;
        if rem(j*dt,1)==0
            Trec((j*dt)+1)= Trecnew;
            Mrec((j*dt)+1)= Mrecnew;
        end
        Mrecold= Mrecnew;
        Trecold= Trecnew;
    end

    % Phase 3

    for j=2*t/dt+1:3*t/dt

        if j < (2*t+tspeedpump)/dt
            mw= MW/(tspeedpump/dt)*(j-2*t/dt);
        else mw= MW;
        end

        jdMammev= 0;
        jdMammcond= 0;
        jdQsupcond= 0;

        hose(THOT,TwV1Cold)
        TwoutV1C(j)= Twout; TwV1Cold= Twhose;

        generatorWATER
(TwoutV1C(j),Tw3f(:),Ts3f(:),Tc3f(:),X3f(:),XX3f(:),p3f,Tgas3f,Tsat3f,Mcte3f,MAMMG3f);
        p3f= p;
        Tsat3f= Tsat;
        Tgas3f= Tgas;
        Mcte3f= Mcte;
        MAMMG3f= MAMMG;
        Tw3f= Tw;
        Ts3f= Ts;
        Tc3f= Tc;
        Mamml3f= Mamml;
        XX3f= XX;
        X3f= X;
        if rem(j*dt,1)==0
            p3((j*dt)+1)= p;
            Tsat3((j*dt)+1)= Tsat;
            Tgas3((j*dt)+1)= Tgas;
            Mcte3((j*dt)+1)= Mcte;
            MAMMG3((j*dt)+1)= MAMMG;
            Tw3(:,(j*dt)+1)= Tw;
            Ts3(:,(j*dt)+1)= Ts;
            Tc3(:,(j*dt)+1)= Tc;
            X3(:,(j*dt)+1)= X;
```

```
    Mamml3(:,(j*dt)+1)= Mamml;
    Qc3(:,(j*dt))= Qc;
    XX3(:,(j*dt))= XX;
  end

  Twout3(j)= Tw(nL);
  pdt3(j)=p;

  spiral(Twout3(j),Twspiral3old);
  Twout3s(j)= Twout; Twspiral3old= Tspiral;

  hose(Twout3s(j),TwV2Cold)
  TwoutV2C(j)= Twout; TwV2Cold= Twhose;

  valve(TwoutV2C(j),TwV2bold)
  TwoutV2b(j)= Twnew(1); TwV2bold= Twnew(2);

  pipe(TwoutV2b(j),Twp12old)
  Twoutp12(j)= Twout; Twp12old= Twhose;

  valve(Twoutp12(j),TwV1mbold)
  TwoutV1mb(j)= Twnew(1); TwV1mbold= Twnew(2);

  hose(TwoutV1mb(j),TwV1Dold)
  TwoutV1D(j)= Twout; TwV1Dold= Twhose;

  generatorWATER
(TwoutV1D(j),Tw4f(:),Ts4f(:),Tc4f(:),X4f(:),XX4f(:),p4f,Tgas4f,Tsat4f,Mcte4f,MAMMG4f);
  p4f= p;
  Tsat4f= Tsat;
  Tgas4f= Tgas;
  Mcte4f= Mcte;
  MAMMG4f= MAMMG;
  Tw4f= Tw;
  Ts4f= Ts;
  Tc4f= Tc;
  Mamml4f= Mamml;
  XX4f= XX;
  X4f= X;
  if rem(j*dt,1)==0
    p4((j*dt)+1)= p;
    Tsat4((j*dt)+1)= Tsat;
    Tgas4((j*dt)+1)= Tgas;
    Mcte4((j*dt)+1)= Mcte;
    MAMMG4((j*dt)+1)= MAMMG;
    Tw4(:,(j*dt)+1)= Tw;
    Ts4(:,(j*dt)+1)= Ts;
    Tc4(:,(j*dt)+1)= Tc;
    X4(:,(j*dt)+1)= X;
    Mamml4(:,(j*dt)+1)= Mamml;
    Qc4(:,(j*dt))= Qc;
    XX4(:,(j*dt))= XX;
  end

  Twout4(j)= Tw(nL);
  pdt4(j)=p;
```

```
        spiral(Twout4(j),Twspiral4old);
        Twout4s(j)= Twout; Twspiral4old= Tspiral;

        hose(Twout4s(j),TwV2Dold)
        TwoutV2D(j)= Twout; TwV2Dold= Twhose;

        valve(TwoutV2D(j),TwV2mbold)
        TwoutV2mb(j)= Twnew(1); TwV2mbold= Twnew(2);

        hose(TwoutV2mb(j),TwpCinold)
        TwoutpCin(j)= Twout; TwpCinold= Twhose;

        % condenser
        Twcondoutnew= Tcondold+(Twcondin-Tcondold)/exp(NTUcond);
        LMTDcond= (Twcondoutnew-Twcondin)/(log((Tcondold-Twcondin)/(Tcondold-
Twcondoutnew)));
        dQheat= UAcond*dt*LMTDcond;
        Qheat= Qheat+dQheat;
        pcondnew= fzero(@dPcondCREB,pcondold);
        Tcondnew= Tsatamm(pcondnew);
        Mcondgnew= pcondnew*100000*Vcond/(Tcondnew*ramms(pcondnew,Tcondnew-273));
        if rem(j*dt,1)==0
          Twcondout((j*dt)+1)= Twcondoutnew;
          pcond((j*dt)+1)= pcondnew;
          Tcond((j*dt)+1)= Tcondnew;
          Mcondg((j*dt)+1)= Mcondgnew;
          Mliqcond((j*dt)+1)= Mliqcondnew;
        end
        pcondold= pcondnew;
        Tcondold= Tcondnew;
        Mcondgold= Mcondgnew;

        % cooler
        Twincooler(j)= TwoutpCin(j);
        dQcooler= Ecooler*min([Cpw*mw Cpw*mwcond])*(Twincooler(j)-Twcondoutnew)*dt;
        Qcooler= Qcooler+dQcooler;
        ToutcoolerBEDnew= Twincooler(j)-dQcooler/(mw*Cpw*dt);
        TwoutcoolerLOADnew= dQcooler/(mwcond*Cpw*dt)+Twcondoutnew;
        if rem(j*dt,1)==0
          TwoutcoolerBED((j*dt)+1)= ToutcoolerBEDnew;
          TwoutcoolerLOAD((j*dt)+1)= TwoutcoolerLOADnew;
        end
        Twoutcooler(j)= ToutcoolerBEDnew;

        hose(Twoutcooler(j),TwpCoutold)
        TwoutpCout(j)= Twout; TwpCoutold= Twhose;

        valve(TwoutpCout(j),TwV1mtold)
        TwoutV1mt(j)= Twnew(1); TwV1mtold= Twnew(2);

        hose(TwoutV1mt(j),TwV1Aold)
        TwoutV1A(j)= Twout; TwV1Aold= Twhose;

        generatorWATER
(TwoutV1A(j),Tw1f(:),Ts1f(:),Tc1f(:),X1f(:),XX1f(:),p1f,Tgas1f,Tsat1f,Mcte1f,MAMMG1f);
        p1f= p;
        Tsat1f= Tsat;
```

```
            Tgas1f= Tgas;
            Mcte1f= Mcte;
            MAMMG1f= MAMMG;
            Tw1f= Tw;
            Ts1f= Ts;
            Tc1f= Tc;
            Mamml1f= Mamml;
            XX1f= XX;
            X1f= X;
            if rem(j*dt,1)==0
               p1((j*dt)+1)= p;
               Tsat1((j*dt)+1)= Tsat;
               Tgas1((j*dt)+1)= Tgas;
               Mcte1((j*dt)+1)= Mcte;
               MAMMG1((j*dt)+1)= MAMMG;
               Tw1(:,(j*dt)+1)= Tw;
               Ts1(:,(j*dt)+1)= Ts;
               Tc1(:,(j*dt)+1)= Tc;
               X1(:,(j*dt)+1)= X;
               Mamml1(:,(j*dt)+1)= Mamml;
               Qc1(:,(j*dt))=Qc;
               XX1(:,(j*dt))= XX;
            end

            Twout1(j)= Tw(nL);
            pdt1(j)=p;

            spiral(Twout1(j),Twspiral1old);
            Twout1s(j)= Twout; Twspiral1old= Tspiral;

            hose(Twout1s(j),TwV2Aold)
            TwoutV2A(j)= Twout; TwV2Aold= Twhose;

            valve(TwoutV2A(j),TwV2mtold)
            TwoutV2mt(j)= Twnew(1); TwV2mtold= Twnew(2);

            pipe(TwoutV2mt(j),Twp21old)
            Twoutp21(j)= Twout; Twp21old= Twhose;

            valve(Twoutp21(j),TwV1told)
            TwoutV1t(j)= Twnew(1); TwV1told= Twnew(2);

            hose(TwoutV1t(j),TwV1Bold)
            TwoutV1B(j)= Twout; TwV1Bold= Twhose;

            generatorWATER
(TwoutV1B(j),Tw2f(:),Ts2f(:),Tc2f(:),X2f(:),XX2f(:),p2f,Tgas2f,Tsat2f,Mcte2f,MAMMG2f);
            p2f= p;
            Tsat2f= Tsat;
            Tgas2f= Tgas;
            Mcte2f= Mcte;
            MAMMG2f= MAMMG;
            Tw2f= Tw;
            Ts2f= Ts;
            Tc2f= Tc;
            Mamml2f= Mamml;
            XX2f= XX;
```

```
X2f= X;
if rem(j*dt,1)==0
   p2((j*dt)+1)= p;
   Tsat2((j*dt)+1)= Tsat;
   Tgas2((j*dt)+1)= Tgas;
   Mcte2((j*dt)+1)= Mcte;
   MAMMG2((j*dt)+1)= MAMMG;
   Tw2(:,(j*dt)+1)= Tw;
   Ts2(:,(j*dt)+1)= Ts;
   Tc2(:,(j*dt)+1)= Tc;
   X2(:,(j*dt)+1)= X;
   Mamml2(:,(j*dt)+1)= Mamml;
   Qc2(:,(j*dt))= Qc;
   XX2(:,(j*dt))= XX;
end

Twout2(j)= Tw(nL);
pdt2(j)=p;

spiral(Twout2(j),Twspiral2old);
Twout2s(j)= Twout; Twspiral2old= Tspiral;

hose(Twout2s(j),TwV2Bold)
TwoutV2B(j)= Twout; TwV2Bold= Twhose;

valve(TwoutV2B(j),TwV2told)
TwoutV2t(j)= Twnew(1); TwV2told= Twnew(2);

hose(TwoutV2t(j),TwpHinold)
TwoutpHin(j)= Twout; TwpHinold= Twhose;

% boiler
Twinboiler(j)= TwoutpHin(j);
dQboiler= (THOT-Twinboiler(j))*Cpw*dt*mw; % in Joules
Qboiler= dQboiler+Qboiler;

Mammcond3= Mammcond-Mammcond1-Mammcond2;
Mammev3= Mammev-Mammev1-Mammev2;
Qsupcond3= Qsupcond-Qsupcond1-Qsupcond2;

% evaporator
Tairevoutnew= Tevold+(Tairevin-Tevold)/exp(NTUev);
LMTDev= (Tairevin-Tairevoutnew)/(log((Tairevin-Tevold)/(Tairevoutnew-Tevold)));
dQcool= UAev*dt*LMTDev;
Qcool= Qcool+dQcool;
pevnew= fzero(@dPevapCREB,pevold);
Tevnew= Tsatamm(pevnew);
Mevgnew= pevnew*100000*Vev/(Tevnew*ramms(pevnew,Tevnew-273));
if rem(j*dt,1)==0
   Tairevout((j*dt)+1)= Tairevoutnew;
   pev((j*dt)+1)= pevnew;
   Tev((j*dt)+1)= Tevnew;
   Mevg((j*dt)+1)= Mevgnew;
   Mliqev((j*dt)+1)= Mliqevnew;
end
pevold= pevnew;
Tevold= Tevnew;
```

```
            Mevgold= Mevgnew;

            % receiver
            Trecnew= (Trecold*(Mrecold-Mliqevnew)+Tcondnew*Mliqcondnew)/(Mrecold-
Mliqevnew+Mliqcondnew);
            Mrecnew= Mrecold-Mliqevnew+Mliqcondnew;
            if rem(j*dt,1)==0
               Trec((j*dt)+1)= Trecnew;
               Mrec((j*dt)+1)= Mrecnew;
            end
            Mrecold= Mrecnew;
            Trecold= Trecnew;

         end

         % Phase 4
         for j= 3*t/dt+1:4*t/dt

            if j < (3*t+tspeedpump)/dt
               mw= MW/(tspeedpump/dt)*(j-3*t/dt);
            else mw= MW;
            end

            jdMammev= 0;
            jdMammcond= 0;
            jdQsupcond= 0;

            hose(THOT,TwV1Dold)
            TwoutV1D(j)= Twout; TwV1Dold= Twhose;

            generatorWATER
(TwoutV1D(j),Tw4f(:),Ts4f(:),Tc4f(:),X4f(:),XX4f(:),p4f,Tgas4f,Tsat4f,Mcte4f,MAMMG4f);
            p4f= p;
            Tsat4f= Tsat;
            Tgas4f= Tgas;
            Mcte4f= Mcte;
            MAMMG4f= MAMMG;
            Tw4f= Tw;
            Ts4f= Ts;
            Tc4f= Tc;
            Mamml4f= Mamml;
            XX4f= XX;
            X4f= X;
            if rem(j*dt,1)==0
               p4((j*dt)+1)= p;
               Tsat4((j*dt)+1)= Tsat;
               Tgas4((j*dt)+1)= Tgas;
               Mcte4((j*dt)+1)= Mcte;
               MAMMG4((j*dt)+1)= MAMMG;
               Tw4(:,(j*dt)+1)= Tw;
               Ts4(:,(j*dt)+1)= Ts;
               Tc4(:,(j*dt)+1)= Tc;
               X4(:,(j*dt)+1)= X;
               Mamml4(:,(j*dt)+1)= Mamml;
               Qc4(:,(j*dt))= Qc;
               XX4(:,(j*dt))= XX;
            end
```

```
        Twout4(j)= Tw(nL);
        pdt4(j)=p;

        spiral(Twout4(j),Twspiral4old);
        Twout4s(j)= Twout; Twspiral4old= Tspiral;

        hose(Twout4s(j),TwV2Dold)
        TwoutV2D(j)= Twout; TwV2Dold= Twhose;

        valve(TwoutV2D(j),TwV2bold)
        TwoutV2b(j)= Twnew(1); TwV2bold= Twnew(2);

        pipe(TwoutV2b(j),Twp12old)
        Twoutp12(j)= Twout; Twp12old= Twhose;

        valve(Twoutp12(j),TwV1mbold)
        TwoutV1mb(j)= Twnew(1); TwV1mbold= Twnew(2);

        hose(TwoutV1mb(j),TwV1Aold)
        TwoutV1A(j)= Twout; TwV1Aold= Twhose;

        generatorWATER
(TwoutV1A(j),Tw1f(:),Ts1f(:),Tc1f(:),X1f(:),XX1f(:),p1f,Tgas1f,Tsat1f,Mcte1f,MAMMG1f);
        p1f= p;
        Tsat1f= Tsat;
        Tgas1f= Tgas;
        Mcte1f= Mcte;
        MAMMG1f= MAMMG;
        Tw1f= Tw;
        Ts1f= Ts;
        Tc1f= Tc;
        Mamml1f= Mamml;
        XX1f= XX;
        X1f= X;
        if rem(j*dt,1)==0
           p1((j*dt)+1)= p;
           Tsat1((j*dt)+1)= Tsat;
           Tgas1((j*dt)+1)= Tgas;
           Mcte1((j*dt)+1)= Mcte;
           MAMMG1((j*dt)+1)= MAMMG;
           Tw1(:,(j*dt)+1)= Tw;
           Ts1(:,(j*dt)+1)= Ts;
           Tc1(:,(j*dt)+1)= Tc;
           X1(:,(j*dt)+1)= X;
           Mamml1(:,(j*dt)+1)= Mamml;
           Qc1(:,(j*dt))= Qc;
           XX1(:,(j*dt))= XX;
        end

        Twout1(j)= Tw(nL);
        pdt1(j)=p;

        spiral(Twout1(j),Twspiral1old);
        Twout1s(j)= Twout; Twspiral1old= Tspiral;

        hose(Twout1s(j),TwV2Aold)
```

```
        TwoutV2A(j)= Twout; TwV2Aold= Twhose;

        valve(TwoutV2A(j),TwV2mbold)
        TwoutV2mb(j)= Twnew(1); TwV2mbold= Twnew(2);

        hose(TwoutV2mb(j),TwpCinold)
        TwoutpCin(j)= Twout; TwpCinold= Twhose;

        % condenser
        Twcondoutnew= Tcondold+(Twcondin-Tcondold)/exp(NTUcond);
        LMTDcond= (Twcondoutnew-Twcondin)/(log((Tcondold-Twcondin)/(Tcondold-
Twcondoutnew)));
        dQheat= UAcond*dt*LMTDcond;
        Qheat= Qheat+dQheat;
        pcondnew= fzero(@dPcondCREB,pcondold);
        Tcondnew= Tsatamm(pcondnew);
        Mcondgnew= pcondnew*100000*Vcond/(Tcondnew*ramms(pcondnew,Tcondnew-273));
        if rem(j*dt,1)==0
           Twcondout((j*dt)+1)= Twcondoutnew;
           pcond((j*dt)+1)= pcondnew;
           Tcond((j*dt)+1)= Tcondnew;
           Mcondg((j*dt)+1)= Mcondgnew;
           Mliqcond((j*dt)+1)= Mliqcondnew;
        end
        pcondold= pcondnew;
        Tcondold= Tcondnew;
        Mcondgold= Mcondgnew;

        % cooler
        Twincooler(j)= TwoutpCin(j);
        dQcooler= Ecooler*min([Cpw*mw Cpw*mwcond])*(Twincooler(j)-Twcondoutnew)*dt;
        Qcooler= Qcooler+dQcooler;
        ToutcoolerBEDnew= Twincooler(j)-dQcooler/(mw*Cpw*dt);
        TwoutcoolerLOADnew= dQcooler/(mwcond*Cpw*dt)+Twcondoutnew;
        if rem(j*dt,1)==0
           TwoutcoolerBED((j*dt)+1)= ToutcoolerBEDnew;
           TwoutcoolerLOAD((j*dt)+1)= TwoutcoolerLOADnew;
        end
        Twoutcooler(j)= ToutcoolerBEDnew;

        hose(Twoutcooler(j),TwpCoutold)
        TwoutpCout(j)= Twout; TwpCoutold= Twhose;

        valve(TwoutpCout(j),TwV1mtold)
        TwoutV1mt(j)= Twnew(1); TwV1mtold= Twnew(2);

        hose(TwoutV1mt(j),TwV1Bold)
        TwoutV1B(j)= Twout; TwV1Bold= Twhose;

        generatorWATER
(TwoutV1B(j),Tw2f(:),Ts2f(:),Tc2f(:),X2f(:),XX2f(:),p2f,Tgas2f,Tsat2f,Mcte2f,MAMMG2f);
        p2f= p;
        Tsat2f= Tsat;
        Tgas2f= Tgas;
        Mcte2f= Mcte;
        MAMMG2f= MAMMG;
        Tw2f= Tw;
```

```
Ts2f= Ts;
Tc2f= Tc;
Mamml2f= Mamml;
XX2f= XX;
X2f= X;
if rem(j*dt,1)==0
   p2((j*dt)+1)= p;
   Tsat2((j*dt)+1)= Tsat;
   Tgas2((j*dt)+1)= Tgas;
   Mcte2((j*dt)+1)= Mcte;
   MAMMG2((j*dt)+1)= MAMMG;
   Tw2(:,(j*dt)+1)= Tw;
   Ts2(:,(j*dt)+1)= Ts;
   Tc2(:,(j*dt)+1)= Tc;
   X2(:,(j*dt)+1)= X;
   Mamml2(:,(j*dt)+1)= Mamml;
   Qc2(:,(j*dt))= Qc;
   XX2(:,(j*dt))= XX;
end

Twout2(j)= Tw(nL);
pdt2(j)=p;

spiral(Twout2(j),Twspiral2old);
Twout2s(j)= Twout; Twspiral2old= Tspiral;

hose(Twout2s(j),TwV2Bold)
TwoutV2B(j)= Twout; TwV2Bold= Twhose;

valve(TwoutV2B(j),TwV2mtold)
TwoutV2mt(j)= Twnew(1); TwV2mtold= Twnew(2);

pipe(TwoutV2mt(j),Twp21old)
Twoutp21(j)= Twout; Twp21old= Twhose;

valve(Twoutp21(j),TwV1told)
TwoutV1t(j)= Twnew(1); TwV1told= Twnew(2);

hose(TwoutV1t(j),TwV1Cold)
TwoutV1C(j)= Twout; TwV1Cold= Twhose;

generatorWATER
(TwoutV1C(j),Tw3f(:),Ts3f(:),Tc3f(:),X3f(:),XX3f(:),p3f,Tgas3f,Tsat3f,Mcte3f,MAMMG3f);
p3f= p;
Tsat3f= Tsat;
Tgas3f= Tgas;
Mcte3f= Mcte;
MAMMG3f= MAMMG;
Tw3f= Tw;
Ts3f= Ts;
Tc3f= Tc;
Mamml3f= Mamml;
XX3f= XX;
X3f= X;
if rem(j*dt,1)==0
   p3((j*dt)+1)= p;
   Tsat3((j*dt)+1)= Tsat;
```

```
    Tgas3((j*dt)+1)= Tgas;
    Mcte3((j*dt)+1)= Mcte;
    MAMMG3((j*dt)+1)= MAMMG;
    Tw3(:,(j*dt)+1)= Tw;
    Ts3(:,(j*dt)+1)= Ts;
    Tc3(:,(j*dt)+1)= Tc;
    X3(:,(j*dt)+1)= X;
    Mamml3(:,(j*dt)+1)= Mamml;
    Qc3(:,(j*dt))= Qc;
    XX3(:,(j*dt))= XX;
end

Twout3(j)= Tw(nL);
pdt3(j)=p;

spiral(Twout3(j),Twspiral3old);
Twout3s(j)= Twout; Twspiral3old= Tspiral;

hose(Twout3s(j),TwV2Cold)
TwoutV2C(j)= Twout; TwV2Cold= Twhose;

valve(TwoutV2C(j),TwV2told)
TwoutV2t(j)= Twnew(1); TwV2told= Twnew(2);

hose(TwoutV2t(j),TwpHinold)
TwoutpHin(j)= Twout; TwpHinold= Twhose;

% boiler
Twinboiler(j)= TwoutpHin(j);
dQboiler= (THOT-Twinboiler(j))*Cpw*dt*mw; % in Joules
Qboiler= dQboiler+Qboiler;

Mammcond4= Mammcond-Mammcond1-Mammcond2-Mammcond3;
Mammev4= Mammev-Mammev1-Mammev2-Mammev3;
Qsupcond4= Qsupcond-Qsupcond1-Qsupcond2-Qsupcond3;

% evaporator
Tairevoutnew= Tevold+(Tairevin-Tevold)/exp(NTUev);
LMTDev= (Tairevin-Tairevoutnew)/(log((Tairevin-Tevold)/(Tairevoutnew-Tevold)));
dQcool= UAev*dt*LMTDev;
Qcool= Qcool+dQcool;
pevnew= fzero(@dPevapCREB,pevold);
Tevnew= Tsatamm(pevnew);
Mevgnew= pevnew*100000*Vev/(Tevnew*ramms(pevnew,Tevnew-273));
if rem(j*dt,1)==0
    Tairevout((j*dt)+1)= Tairevoutnew;
    pev((j*dt)+1)= pevnew;
    Tev((j*dt)+1)= Tevnew;
    Mevg((j*dt)+1)= Mevgnew;
    Mliqev((j*dt)+1)= Mliqevnew;
end
pevold= pevnew;
Tevold= Tevnew;
Mevgold= Mevgnew;

% receiver
```

```
            Trecnew= (Trecold*(Mrecold-Mliqevnew)+Tcondnew*Mliqcondnew)/(Mrecold-
Mliqevnew+Mliqcondnew);
            Mrecnew= Mrecold-Mliqevnew+Mliqcondnew;
            if rem(j*dt,1)==0
               Trec((j*dt)+1)= Trecnew;
               Mrec((j*dt)+1)= Mrecnew;
            end
            Mrecold= Mrecnew;
            Trecold= Trecnew;

         end

         MADS= Mammev;
         MDES= Mammcond;
         QCOND= Qheat;
         QEVAP= Qcool;
         QCOOLER= Qcooler;
         QBOILER= Qboiler;
         PBOILER= QBOILER/(4*t);
         COPC= Qcool/QBOILER;
         COPH= (Qheat+Qcooler)/QBOILER;
         SCP= Qcool/1000/(4*t)/(4*Mc);
         SHP= (Qheat+Qcooler)/1000/(4*t)/(4*Mc);
         globalerror= min(abs(QEVAP+QBOILER-QCOND-QCOOLER)/(QEVAP+QBOILER)*100,
abs(QEVAP+QBOILER-QCOND-QCOOLER)/(QCOND+QCOOLER)*100)

         Tw1(:,1)= Tw1(:,4*t+1); Tw2(:,1)= Tw2(:,4*t+1); Tw3(:,1)= Tw3(:,4*t+1); Tw4(:,1)=
Tw4(:,4*t+1);
         Ts1(:,1)= Ts1(:,4*t+1); Ts2(:,1)= Ts2(:,4*t+1); Ts3(:,1)= Ts3(:,4*t+1); Ts4(:,1)= Ts4(:,4*t+1);
         Tc1(:,1)= Tc1(:,4*t+1); Tc2(:,1)= Tc2(:,4*t+1); Tc3(:,1)= Tc3(:,4*t+1); Tc4(:,1)= Tc4(:,4*t+1);
         X1(:,1)= X1(:,4*t+1); X2(:,1)= X2(:,4*t+1); X3(:,1)= X3(:,4*t+1); X4(:,1)= X4(:,4*t+1);
         Mamml1(:,1)= Mamml1(:,4*t+1); Mamml2(:,1)= Mamml2(:,4*t+1); Mamml3(:,1)=
Mamml3(:,4*t+1); Mamml4(:,1)= Mamml4(:,4*t+1);

         XX1(:,1)= XX1(:,4*t); XX2(:,1)= XX2(:,4*t); XX3(:,1)= XX3(:,4*t); XX4(:,1)= XX4(:,4*t);

         Tsat1(1)= Tsat1(4*t+1); Tsat2(1)= Tsat2(4*t+1); Tsat3(1)= Tsat3(4*t+1); Tsat4(1)=
Tsat4(4*t+1);
         Tgas1(1)= Tgas1(4*t+1); Tgas2(1)= Tgas2(4*t+1); Tgas3(1)= Tgas3(4*t+1); Tgas4(1)=
Tgas4(4*t+1);
         p1(1)= p1(4*t+1); p2(1)= p2(4*t+1); p3(1)= p3(4*t+1); p4(1)= p4(4*t+1);
         MAMMG1(1)= MAMMG1(4*t+1); MAMMG2(1)= MAMMG2(4*t+1); MAMMG3(1)=
MAMMG3(4*t+1); MAMMG4(1)= MAMMG4(4*t+1);
         Mcte1(1)= Mcte1(4*t+1); Mcte2(1)= Mcte2(4*t+1); Mcte3(1)= Mcte3(4*t+1); Mcte4(1)=
Mcte4(4*t+1);

         pev(1)= pev(4*t+1);
         Tev(1)= Tev(4*t+1);
         Mevg(1)= Mevg(4*t+1);
         Mliqev(1)= Mliqev(4*t+1);

         pcond(1)= pcond(4*t+1);
         Tcond(1)= Tcond(4*t+1);
         Mcondg(1)= Mcondg(4*t+1);
         Mliqcond(1)= Mliqcond(4*t+1);

         Trec(1)= Trec(4*t+1);
```

```
    Mrec(1)= Mrec(4*t+1);

    Tairevout(1)= Tairevout(4*t+1);
    Twcondout(1)= Twcondout(4*t+1);
    TwoutcoolerLOAD(1)= TwoutcoolerLOAD(4*t+1);
    TwoutcoolerBED(1)= TwoutcoolerBED(4*t+1);

    TwoutV1A(1)= TwoutV1A(4*t/dt);

    Qcooler=0;
    Qcool=0;
    Qheat=0;
    Qboiler= 0;

  for j=1:4*t/dt
    if rem(j*dt,1)==0
        Twinb((j*dt))= Twinboiler(j);
        Twinc((j*dt))= Twincooler(j);
        TwoutV1a((j*dt))= TwoutV1A(j);
        TwoutV1b((j*dt))= TwoutV1B(j);
        TwoutV1c((j*dt))= TwoutV1C(j);
        TwoutV1d((j*dt))= TwoutV1D(j);
        Twout1spiral((j*dt))= Twout1s(j);
        Twout2spiral((j*dt))= Twout2s(j);
        Twout3spiral((j*dt))= Twout3s(j);
        Twout4spiral((j*dt))= Twout4s(j);
        TwOUT1((j*dt))= Twout1(j);
    end
  end
  Twinb= Twinb'-273;
  Twinc= Twinc'-273;
  TwoutV1a= TwoutV1a'-273;
  TwoutV1b= TwoutV1b'-273;
  TwoutV1c= TwoutV1c'-273;
  TwoutV1d= TwoutV1d'-273;
  Twout1spiral= Twout1spiral'-273;
  Twout2spiral= Twout2spiral'-273;
  Twout3spiral= Twout3spiral'-273;
  Twout4spiral= Twout4spiral'-273;

  end
```

A3. Other functions

```
function generatorWATER (TWI,TW,TS,TC,AX,AXX,P,TGAS,TSAT,MCTE,MAG)
global Mamml  Mammcond Mammev MAMMG Ms Mc Mw Mcte mw Tcondold dQsupcond
global Twinlet Tairevout Tw Ts Tc Tsat Tweight Tgas Tcond pcondold pevold jdQsupcond
global As Ac UAc  N dL dt Ntub Ks Kc UAw Cpw Cpa Cps C k x0 n nL nt VoidVol Kvcond Kvev COSA
global i j Rgas A B D CPC HSUPAMMG  HSUPAMMC X XX p Qc Qsupcond jdMammcond jdMammev
global AuxXX AuxTc AuxTs AuxTw AuxX Auxp AuxTgas AuxTsat AuxMcte AuxMAMMG dMammcond
dMammev
Twinlet= TWI;
AuxTw= TW;
AuxTs= TS;
AuxTc= TC;
AuxX= AX;
AuxXX= AXX;
Auxp= P;
AuxTgas= TGAS;
AuxTsat= TSAT;
AuxMcte= MCTE;
AuxMAMMG= MAG;
Tw= zeros(nL,1);
Ts= zeros(nL,1);
Tc= zeros(nL,1);
Qc= zeros(nL,1);
A= zeros(nL,1);
B= zeros(nL,1);
D= zeros(nL,1);
CPC= zeros(nL,1);
XX= zeros(nL,1);
X= zeros(nL,1);
Mamml= zeros(nL,1);
HSUPAMMC= zeros(nL,1);
p=0;
Tsat= 0;
Tgas= 0;
Tweight=0;
Rgas= 0;
HSUPAMMG= 0;
MAMMG= 0;
Tw(1)=dt*N/(Mw*Cpw)*(UAw/N*(AuxTs(1)-AuxTw(1))-mw*Cpw/2*(AuxTw(2)-Twinlet))+AuxTw(1);
Ts(1)=dt*N/(Ms*Cps)*(Ks*As*Ntub/dL*(AuxTs(2)-AuxTs(1))+UAc/N*(AuxTc(1)-AuxTs(1))-
UAw/N*(AuxTs(1)-AuxTw(1)))+AuxTs(1);
Qc(1)= dt*(UAc/N*(AuxTs(1)-AuxTc(1))+Ntub*Kc*Ac/dL*(AuxTc(2)-AuxTc(1)));% HEAT INTO
CARBON, i=1 (J)
for i=2:nL-1
   Tw(i)=dt*N/(Mw*Cpw)*(UAw/N*(AuxTs(i)-AuxTw(i))-mw*Cpw/2*(AuxTw(i+1)-AuxTw(i-
1)))+AuxTw(i);
   Ts(i)=dt*N/(Ms*Cps)*(Ks*As*Ntub/(2*dL)*(AuxTs(i-1)-2*AuxTs(i)+AuxTs(i+1))+UAc/N*(AuxTc(i)-
AuxTs(i))-UAw/N*(AuxTs(i)-AuxTw(i)))+AuxTs(i);
   Qc(i)= dt*(UAc/N*(AuxTs(i)-AuxTc(i))+Ntub*Kc*Ac/(2*dL)*(AuxTc(i-1)-
2*AuxTc(i)+AuxTc(i+1)));%HEAT INTO CARBON (J)
end
Tw(nL)=dt*N/(Mw*Cpw)*(UAw/N*(AuxTs(nL)-AuxTw(nL))-mw*Cpw*(AuxTw(nL)-AuxTw(nL-
1)))+AuxTw(nL);
```

```
Ts(nL)=dt*N/(Ms*Cps)*(Ks*As*Ntub/dL*(AuxTs(nL-1)-AuxTs(nL))+UAc/N*(AuxTc(nL)-AuxTs(nL))-
UAw/N*(AuxTs(nL)-AuxTw(nL)))+AuxTs(nL);
Qc(nL)= dt*(UAc/N*(AuxTs(nL)-AuxTc(nL))+Ntub*Kc*Ac/dL*(AuxTc(nL-1)-AuxTc(nL)));%HEAT INTO
CARBON i=nL-1(J)
Rgas= ramms(Auxp,AuxTgas-273);
HSUPAMMG= hsupamm(AuxTsat-273,AuxTgas-273);
for a=1:nL
   CPC(a)= cpc(AuxTc(a));
   HSUPAMMC(a)= hsupamm(AuxTsat-273,AuxTc(a)-273);
end
p= fzero(@fCREB,Auxp); % p(j+1)
Tsat= Tsatamm(p); % Tsat(j+1)
Tgas= fzero(@tempfutCREB,AuxTgas); % Tgas(j+1)
% Update CPC HSUPAMMC HSUPAMMG Rgas
Rgas= ramms(p,Tgas-273);
HSUPAMMG= hsupamm(Tsat-273,Tgas-273);
for a=1:nL
   CPC(a)= cpc(Tc(a));
   HSUPAMMC(a)= hsupamm(Tsat-273,Tc(a)-273);
end
% End update
if p >= pcondold
   dMammcond= Kvcond*dt*sqrt(p-pcondold);
   jdMammcond=dMammcond+jdMammcond;
   Mammcond= Mammcond+dMammcond;
   Mcte= AuxMcte-dMammcond;
   AuxMcte= Mcte;
   p= fzero(@fauxCREB,Auxp);
   Tsat= Tsatamm(p);
   Tgas= fzero(@tempfutCREB,AuxTgas);
   dQsupcond= dMammcond*(hsupamm(Tsat-273,Tgas-273)-hgamm(Tcondold-273));
   Qsupcond= dQsupcond+Qsupcond;
   jdQsupcond= dQsupcond+jdQsupcond;
elseif p <= pevold
   dMammev= Kvev*dt*sqrt(pevold-p);
   jdMammev= dMammev+jdMammev;
   Mammev= Mammev+dMammev;
   Mcte= AuxMcte+dMammev;
   AuxMcte= Mcte;
   p= fzero(@fauxCREB,Auxp);
   Tsat= Tsatamm(p);
   Tgas= fzero(@tempfutCREB,AuxTgas);
else Mcte= AuxMcte;
end
```

```
function F= fauxCREB(pn)
global AuxX AuxTc AuxXX AuxTsat AuxMAMMG AuxMcte AuxTgas
global VoidVol Cpa N nL Mc C k x0 n CPC Rgas HSUPAMMG HSUPAMMC A B D
global Mamml MAMMG Tweight XX  X Tc Qc
for a=1:nL
   A(a)= Mc/N*(CPC(a)+AuxX(a)*Cpa);
   B(a)= Mc/N*(AuxTc(a)/AuxTsat-1)^(n-1)*Rgas*C*k*n*AuxX(a)*AuxTc(a)/(AuxTsat^2);
   D(a)= AuxTc(a)/AuxTsat*(Tsatamm(pn)-AuxTsat);
   Tc(a)= (Qc(a)+AuxTc(a)*(A(a)+B(a))+B(a)*D(a))/(A(a)+B(a)); % Tc(j+1)
   X(a)= dub2(Tsatamm(pn),Tc(a),x0,k,n); % X(j+1)
   XX(a)= X(a)-AuxX(a); % XX(j+1)
end
MTweightdes=0;
Mweightdes=0;
for a= 1:nL
   if XX(a) < 0
      MTweightdes= MTweightdes-Mc/N*XX(a)*AuxTc(a);
      Mweightdes= Mweightdes-Mc/N*XX(a);
   end
end
Tweight= (MTweightdes+AuxMAMMG*AuxTgas)/(AuxMAMMG+Mweightdes);
for a=1:nL
   B(a)= Mc/N*(AuxTc(a)/AuxTsat-1)^(n-1)*Rgas*C*k*n*AuxX(a)*AuxTc(a)/(AuxTsat^2);

   Tc(a)= (Qc(a)+AuxTc(a)*(A(a)+B(a))+B(a)*D(a))/(A(a)+B(a)); % Tc(j+1)
   X(a)= dub2(Tsatamm(pn),Tc(a),x0,k,n); % X(j+1)
   Mamml(a)= Mc/N*X(a); % Mamml (j+1)
   MAMMG= pn*100000*VoidVol/(Tweight*ramms(pn,Tweight-273)); % MAMMG(j+1)
   XX(a)= X(a)-AuxX(a); % XX(j+1)
end
F= sum(Mamml)+MAMMG-AuxMcte; % Mamml(j+1)+MAMMG(j+1)-Mcte



function H= dPcondCREB (Pn)
global Tcondold Mliqcondnew dQheat jdQsupcond Mcond cpcond Mcondgold Vcond jdMammcond
Latent= hgamm(Tcondold-273)-hfamm(Tcondold-273);
Mliqcondnew=(dQheat-jdQsupcond+Mcond*cpcond*(Tsatamm(Pn)-Tcondold))/Latent; % es el
liquido que entra en el condensador
H= Tsatamm(Pn)*ramms(Pn,Tsatamm(Pn)-273)*(Mcondgold+jdMammcond-Mliqcondnew)-
Pn*Vcond*100000;



function E= dPevapCREB (Pn)
global Tevold Trecold Mliqevnew dQcool Mevgold cpev Mev Vev jdMammev
Latent= hgamm(Tevold-273)-hfamm(Trecold-273);
Mliqevnew=(dQcool-Mev*cpev*(Tsatamm(Pn)-Tevold))/Latent; % es el liquido que entra en el
evaporador debido al cambio en la presion del mismo
E= Tsatamm(Pn)*ramms(Pn,Tsatamm(Pn)-273)*(Mevgold-jdMammev+Mliqevnew)-Pn*Vev*100000;



function G= tempfutCREB (Tn)
global p VoidVol MAMMG
G= Tn*ramms(p,Tn-273)*MAMMG-p*VoidVol*100000;
```

```
function y=cpc(T)
% Specific heat of 208C in J/kg as f(temp. in K)
y=175+2.245*T;


function x= dub(tsat,t,x0,k,n)
% x is conc, tsat is t saturated, t is temp deg K
if tsat>=t
x=x0;
mess='saturation'
x=x0
else
x=x0*exp(-k*((t./tsat-1).^n));
end


function h=hfamm(t)
% returns enthalpy of sat ammonia liquid in J/kg as f(t in deg C)
p=1.0e+002 *[0.00002471878122 0.04584407092907 4.23498846153846];
h=polyval(p,t)*1000;


function h=hgamm(t)
% returns enthalpy of sat ammonia vapour in J/kg as f(t in deg C)
p=1.0e+003 *[-0.00000810606893 0.00101716208791 1.68515907342657];
h=polyval(p,t)*1000;


function h=hsupamm(ts,t)
%returns h of superheated ammonia for t sat, t in deg C.
% -50 < tsat < 60.  Up to 180 C superheat. Joules/kg/K
xx=t-ts;
q1 =[ -0.00000018390464   0.00006799614968  -0.00803818806194];
q2 =[ -0.00002442770771   0.01042121857309   1.02666247502497];
q3 =1.0e+003*[ -0.00000034386776   0.00244406178613   1.68565194143357];
p(1)=polyval(q1,xx);
p(2)=polyval(q2,xx);
p(3)=polyval(q3,xx);
h=polyval(p,ts)*1000;


function y=psatamm(t)
%returns p sat in bar for T in K
y=exp(11.515 - 2748.3 ./t);


function y = ramms(p2,t)
%polynominal approximation of ammonia gas constant for p in bar, t in deg C. Valid -50<tsat<60,
% tsat+10 < t < 250
```

```
tsat =( 2823.4 ./(11.749-log(p2)))-273;
coef1 = 1.0e-009 *[ 0.00000068892947   0.00009565787857   0.00844971035705
0.32843436542347];
coef2 = 1.0e-006 *[-0.00000052403299  -0.00006905794744  -0.00531432390974  -
0.18587792629441];
coef3 = 1.0e-004 *[ 0.00000140592901   0.00017767403458   0.01203459890161
0.37471284774418];
coef4 =[ -0.00000001416664  -0.00000177131542  -0.00010988317152   0.04572946161140];
p(1)=polyval(coef1,tsat)*10000;
p(2)=polyval(coef2,tsat)*10000;
p(3)=polyval(coef3,tsat)*10000;
p(4)=polyval(coef4,tsat)*10000;
y=polyval(p,t);



function y=Tsatamm(p)
%returns T sat in K for p in bar
y= 2748.3./(11.515-log(p));
```

Appendix B

Component specifications

B1. Condenser

AlfaNovaPlate Heat Exchanger

Technical Specification

Model : AlfaNova HP 27-20H (32870 0093 2)
Item Name : 3kW Ammonia Condenser Date : 15/02/2010
Units : 1

		Hot Side Primary side(S4)	Cold side Secondary side
Fluid		Ammonia	Water
Mass flow rate	kg/s	0.002670	0.1666
Fluid Condensed/ Vapourized	kg/s	0.002670	0.000
Inlet temperature	°C	70.0	45.0
Dew p.	°C	50.0	
Outlet temperature(vapor/liquid)	°C	50.0/49.3	49.3
Operating pressure(In/Out)	bara	20.3/20.3	
Pressure drop	kPa	0.0252	2.09
Velocity connection(In/Out)	m/s	0.473/0.0115	0.406/0.406
Heat Exchanged	kW	3.000	
Heat transfer area	m^2	0.45	
O.H.T.C service	$W/(m^2*K)$	3024	
Fouling resistance * 10000	m^2*K/W	0.20	
Margin	%	14.8	
Mean Temperature Difference	K	2.2	
Relative directions of fluids		Countercurrent	
Number of passes		1	1
Materialplate/ bonding		Alloy 316 / SS	
ConnectionS1 (Cold-Out)	Threaded (External)/ 1" ISO 228/1-G (B21) Alloy 316		
ConnectionS2 (Cold-In)	Threaded (External)/ 1" ISO 228/1-G (B21) Alloy 316		
ConnectionS3 (Hot-Out)		Soldering/ 1 1/8" (H21) Alloy 316	
ConnectionS4 (Hot-In)		Soldering/ 1 1/8" (H21) Alloy 316	
Pressure vessel code		PED	
Design pressure at 75.0 Celsius	Bar	40.0	40.0
Design pressure at 225.0 Celsius	Bar	34.0	34.0
Design temperature	°C	-196.0/225.0	
Overall length x width x height	mm	83 x 111 x 310	
Net weight, empty / operating	kg	4.24 / 4.24	
Package length x width x height	mm	280 x 147 x 391	
Package weight	kg	0.000	

Physical Properties

(inlet/outlet)	Hot Side Liquid	Vapour	Cold side Liquid	Vapour
Dens	526.5/561.0	13.58/14.79	988.9/987.0	
Sp.heat	5.355/5.080	3.178/3.820	4.174/4.174	
Visc	0.0869/0.103	0.0117/0.0110	0.596/0.553	
Th.Cond	0.436/0.477	0.0297/0.0276	0.636/0.641	
Bub. p.		50.0/50.0		
Dew p.		50.0/50.0		
Mol.W.		17.03/17.03		
Cr.pr.		113.33/113.33		
Cr.Temp.		132.3/132.3		
Lat.heat		1048.5/1048.5		

B2 Cooler

Plate Heat Exchanger Data Sheet

Model type: SL23TL-AA 30 PLATES

Heat transfer duty (kW):	20
Heat Exchanger circuit - Side 1	
Fluid description:	Water
Fluid flow rate (Kg/sec):	0.33
Inlet temperature (Deg C.):	70.0
Outlet temperature (Deg C.):	55.7
Pressure drop (Kpa):	10.0
Inlet / outlet locations:	F1 / F4
Connection size & type:	0.75 inch BSPT male
Connection material:	Stainless Steel
Max. working pressure (Bar g.):	21.0
Max. working temperature (Deg C.):	120
Heat Exchanger circuit - Side 2	
Fluid description:	Water
Fluid flow rate (Kg/sec):	0.33
Inlet temperature (Deg C.):	50.0
Outlet temperature (Deg C.):	64.3
Pressure drop (Kpa):	8.8
Inlet / outlet locations:	F3 / F2
Connection size & type:	0.75 inch BSPT male
Connection material:	Stainless Steel
Max. working pressure (Bar g.):	21.0
Max. working temperature (Deg C.):	100
Constructional Details	
Channel Arrangement:	1 x 14 / 1 x 15
Plate material:	316 Stainless
Plate type:	Single wall
Braze material:	Copper
Hold up volume (Litres):	.5
Frame length - Dimension L (mm):	81
Weight empty (Kgs):	4

B3 Evaporators

LORDAN

Evaporators- Metric units

Project Name: Heat Pump Evaporator - Stainless tube Al fins
Customer: University of Warwick

Customer Reference: Heat Pump Evaporator
Lordan Reference: Lordan pattern 14

Coil Model: 14 / 4 x 16 x 450 / 11 - 1

Results

Total Capacity (QT):	2.342 kw
Sensible Capacity (QS):	1.555 kw
Leaving Air Dry Bulb Temp. (DBL):	2.61 °C
Leaving Air Wet Bulb Temp. (WBL):	2.44 °C
Air Pressure Drop (WG):	16 Pascal
Face Area:	0.1800 m²
Coil Pressure Drop (COIL DP):	7.0 kPa
Header Pressure Drop (HDR DP):	0.0 kPa
Refrigerant Flow Rate (LB/MIN):	0.1 kg/min
Refrigerant Flow Velocity (FPM):	9.0 m/sec
Refrigerant Charge (CHRG):	0.099 kg
Airflow Velocity:	1.5 m/sec

Input

Coil Construction		Groove Depth (GD)	N/A
Coil Pattern No. (N)	43	Ridge Apex Angle (A)	N/A
Number of Coils (QTY)	1	Number of Ridges (NR)	N/A
No. of Rows Deep (ROWS)	4	Lead Helix Angle (B)	N/A
Fin height(FH)	400 mm	**Operating Conditions**	
Finned Length (FL)	450 mm	Air In Dry Bulb Temp.(TAE)	7 °C
No.of Circuits (CKT)	1	Air In Wet Bulb Temp.(TWB)	6 °C
Circuiting Arrangement (FLO)	Cross	Air Flow (CFM)	1000 m³/h
Fin Spacing (FPI)	11 FPI	Altitude/Air Pressure (P)	Altitude
Fin Material (MTL)	Aluminum	Value (P)	0 Meter Above sea level
Fin Thickness (FIN)	0.15 mm	Standard Air (SA)	Standard
Disributor Orifice Number(NZ)	No Distributor	Liquid Temp. To Expansion Device (LT)	40 °C
Distributor Lines O.D. (OD)	No Distributor mm	Evaporating Temp. (IET)	0 °C
Distributor Lines Length	0 mm	Super Heat (SPHT)	3 °K
		Advanced	

(DL)		Fan to Coil Position (FW)	Coil Only (No Fan)
Header fabricating Technique (HDR)	Extruded	Fan Motor Watts (FW)	N/A
Suction Header Diameter (HDR)	16 mm	Fin Coating Factor (FC)	Bare Fins
Connection O.D.(CON)	16 mm	Fin Coating Thickness (FCT)	0 mm
Refrigerant (FNO)	R-717	Fan – Motor Position (RFW)	No Fan
Tube Wall thickness(T)	Smooth mm	Motor Efficiency (RFW)	N/A
Tube Wall thickness(T)	0.2794 mm		

LORDAN&CO - Kfar Szold 12230 Israel – Phone: 972 4 690 7506 – Fax: 972 4 6907138 – service@lordan.co.il – www.lordan-coils.com

B4 Heater

Technical data according to DIN 12876

Operating temperature range	-60...200 °C
Temperature stability at -10°C	0,01 K
temperature set point / display	5,7" colour Touchscreen
Resolution of display	0,01 K
Internal temperature sensor	Pt100
Sensor external connection	Pt100
Interface digital	Ethernet, USB (Host u. Device), RS232
digital input	ECS ONE
digital output	POKO ONE
Alarm message	optic, acoustic, relay
Safety classification	Class III / FL
Heating power	6 kW
Cooling power with	Thermooil
at 200°C	7 kW
at 100°C	7 kW
Cooling power with	Ethanol
at 0°C	7 kW
at -20°C	6,4 kW
at -40°C	3,3 kW
at -60°C	0,8 kW
Refrigeration machine	water-cooled, CFC- and HCFC-free
Refrigerant	R507
Refrigerant quantity	2,2 kg
Circulation pump:	
max. delivery	60 l/min
max. delivery pressure	1.5 bar
Delivery at 0,4 bar	44 l/min
Delivery at 0,5 bar	40 l/min
Delivery at 1,0 bar	28 l/min
Pump connection	M30x1,5 male
max. permissible kin. viscosity	50 mm²/s
Cooling water connection	G1/2 male
Consumption at water 15°C, flow 0°C	400 l/h
min. cooling water differential pressure	3 bar
max. cooling water pressure	6 bar

Order-No.: 1007.0031.01

Technical data according to DIN 12876

min. filling capacity	5,65 l
Filling capacity expansion tank	26,5 l
Overall dimensions WxDxH **	630x704x1520 mm
Net weight	348 kg
Power supply (3 Phase)	400V 3~N 50Hz
max. current (3 Phase)	16 A
Fuse (3 phase)	3x16 A
alternative power supply (3 phase)	440V 3~N 60Hz
alternative max. current (3 phase)	15 A
alternative fuse (3 phase)	3x16 A
Protection class	IP20
min. ambient temperature	5 °C
max. ambient temperature	40 °C

from Serial-No.: 169819 **1.0/12**

Technical details and dimensions are subject to change. No liability is accepted for errors or omissions.